UNIVERSITA' VITA-SALUTE SAN RAFFAELE

CORSO DI DOTTORATO DI RICERCA INTERNAZIONALE IN MEDICINA MOLECOLARE

CURRICULUM IN CELLULAR AND MOLECULAR BIOLOGY

Unraveling the physiopathological role of sacsin, the protein mutated in autosomal recessive spastic ataxia of Charlevoix–Saguenay (ARSACS)

DoS: Dr. Francesca Maltecca

Second Supervisor: Dr. Smita Saxena

Tesi di DOTTORATO di RICERCA di Daniele De Ritis

matr. 015668

Ciclo di dottorato XXXV

SSD MED/04

Anno Accademico 2021/2022

RELEASE OF PHD THESIS

Il/la sottoscritto/a / *I, the undersigned Daniele De Ritis*

Matricola / *registration number 015668*

nat_ a/ *born in Vimercate (MB)*

il/*on 25/11/1993*

autore della tesi di Dottorato di ricerca dal titolo / *author of the PhD Thesis titled*

Unraveling the physiopathological role of sacsin, the protein mutated in autosomal recessive spastic ataxia of Charlevoix–Saguenay (ARSACS)

☐ AUTORIZZA la Consultazione della tesi / AUTHORIZE *the public release of the thesis*

☑ NON AUTORIZZA la Consultazione della tesi per 12…… mesi /DO NOT AUTHORIZE *the public release of the thesis for* …18… *months*

a partire dalla data di conseguimento del titolo e precisamente */ from the PhD thesis date, specifically*

Dal / *from* ……/……/…… Al / *to* …

Poiché /*because*:

☑ l'intera ricerca o parti di essa sono potenzialmente soggette a brevettabilità/ *The whole project or parts of it may be the subject of a patent application;*

☑ ci sono parti di tesi che sono già state sottoposte a un editore o sono in attesa di pubblicazione/ *Parts of the thesis have been or are being submitted to a publisher or are in the press;*

☐ la tesi è finanziata da enti esterni che vantano dei diritti su di esse e sulla loro pubblicazione/ *the thesis project is financed by external bodies that have rights over it and its publication.*

Si rende noto che parti della tesi sono indisponibili in relazione all'utilizzo di dati tutelati da segreto industriale **(da lasciare solo se applicabile)** /*Please Note: some parts of the thesis are not released due to the law protecting trade secrets* ***(delete if not relevant)***

E' fatto divieto di riprodurre, in tutto o in parte, quanto in essa contenuto / *reproduction of the thesis in whole or in part is forbidden*

Data /Date ..09/02/2023.....Firma /Signature 

DECLARATION

This thesis has been:

- composed by myself and has not been used in any previous application for a degree. Throughout the text I use both 'I' and 'We' interchangeably.
- has been written according to the editing guidelines approved by the University.

Permission to use images and other material covered by copyright has been sought and obtained. For the following image/s (specify), it was not possible to obtain permission and is/are therefore included in thesis under the "fair use" exception (Italian legislative Decree no. 68/2003).

All the results presented here were obtained by myself, except for:

1) Purkinje derivation and immunofluorescences in Results Fig. 12d-e, Purkinje derivation in Results Fig. 13b-c, volumetric analyses in Results Fig. 19 were performed by Dr. Andrea Del Bondio, *Mitochondrial dysfunctions in Neurodegeneration Unit, Division of Neuroscience, San Raffaele Scientific Institute, Milan, Italy.*

2) EM in Results Fig. 17 were performed in collaboration with Dr. Paola Podini and Dr. Angelo Quattrini, *Experimental Neuropathology Unit, Division of Neuroscience and INSPE, San Raffaele Scientific Institute, Milan, Italy.*

3) Immunoprecipitations in Results Fig. 17a,d-f were performed by Dr. Fabiana Longo, *Mitochondrial dysfunctions in Neurodegeneration Unit, Division of Neuroscience, San Raffaele Scientific Institute, Milan, Italy.*

4) AAVs used in Results Fig. 28, Results Fig. 29 and Results Fig. 31 were produced in collaboration with Dr. Vania Broccoli and Dr. Serena Giannelli, *Stem cells and neurogenesis Unit, Division of Neuroscience, San Raffaele Scientific Institute, Milan, Italy.*

I also declare parts of the thesis (exactly Results Section 1, Discussion Section 1, Materials and Methods Section 1) have been already published in our previous paper "Assessment of Sacsin Turnover in Patients With ARSACS. Implications for Molecular Diagnosis and Pathogenesis. Fabiana Longo, Daniele De Ritis, et al, Neurology, Dec 2021, 97 (23) e2315-e2327; DOI: 10.1212/WNL.0000000000012962". Figures from Results Section2 and relative methods and conclusions which I have performed are also being published in (Del Bondio, Longo, De Ritis et al, under review.)

All sources of information are acknowledged by means of reference.

ACKNOWLEDGEMENTS

I am extremely grateful to my mentor and director of studies, Dr. Francesca Maltecca. It would be impossible to resume here last six years in her Lab and thank her for all the invaluable possibilities and opportunities she gave to me, for her scientific guidance, her commitment in teaching me the logic of scientific research and above all for her patience and for always believing in me and supporting me.

I have to thank second supervisor, Dr. Smita Saxena, for her commitment and suggestions on the scientific project.

I am especially grateful to Dr. Fabiana Longo, with whom I have spent much of the time in the Lab, for her total help in previous years and for teaching me to think scientifically everyday in the lab.

I am grateful to all our collaborators. Dr. Marina Scarlato (Department of Neurology, Ospedale San Raffaele, Milan, Italy), Dr. Filippo M Santorelli (IRCCS Fondazione Stella Maris, Pisa, Italy), Dr. Stefano Buffo (Department of Biosciences, University of Milan) for the study on sacsin cotranslational degradation; Dr. Vania Broccoli (Division of Neuroscience, San Raffaele Scientific Institute) and his lab members Dr. Serena Giannelli and Dr. Mirko Luoni, for the AAV gene therapy project and their precious expertise; Dr. Paola Podini and Dr. Angelo Quattrini (San Raffaele Scientific Institute) for EM analyses.

I really have to thank Valentina, Camilla, Erica and Giorgio of the Maltecca's Lab, for their help, scientific, technical and human support and suggestions and for the friendly environment they create every day. In particular, thanks to Erica Spirito, for her big help in the ex vivo part, for her very stimulating discussions also outside science and her great support; Camilla Franchino, for her very precious help in vivo and ex vivo part and great support and moments at any time and day in the Lab; Valentina Gigliucci, for all her help in vivo and ex vivo part, very long scientific and non-scientific discussions and above all for all the coffees together at any time; Giorgio Boschetti for his help, incredible availability and long discussions on neurofilaments; Alessandra Rocco and finally Michela Crotti who recently joined the group but they helped too. I also have to thank former lab member Andrea Del Bondio for all the time spent together, also outside the lab, his precious and invaluable help when I was at the very beginning.

It would be impossible to thank all the people that have helped in some way all these years. In particular, I have to thank Dr. Valeria Berno and ALEMBIC facility for cell imaging and microscopy.

Finally I want to personally thank all my friends, especially Federico for all his incredible human support and help in a lifetime.

Grazie alla mia famiglia tutta, per il loro supportarmi a intraprendere questa strada fin dall'inizio. GRAZIE!

ABSTRACT

Autosomal recessive spastic ataxia of Charlevoix-Saguenay (ARSACS) is a neurodegenerative disorder caused by loss-of-functions mutations in the *SACS* gene encoding for sacsin, a 520-kDa multimodular protein whose function is poorly understood. ARSACS is characterized by early onset cerebellar ataxia, followed by spasticity and sensorimotor neuropathy. ARSACS patients and the *Sacs*$^{-/-}$ mouse model show selective loss of Purkinje neurons (PNs) in anterior lobules. ARSACS patients shows intra- and interfamilial phenotypic variability, with no clear genotype-phenotype correlation. There are currently no treatments available, nor are clinical trials ongoing.

Sacsin is expressed in the central nervous system (CNS) with the highest levels in PNs in the cerebellum. ARSACS is characterized by a peculiar abnormal bundling of neurofilaments (NFs) reported both in ARSACS patients' brain autopsies and *Sacs*$^{-/-}$ mouse brain sections. Other cytopathological hallmarks reported in cellular models of ARSACS were mitochondrial morphology and metabolism impairment. However, the mechanistic link between sacsin function and NFs alterations, and the connection between the mitochondrial alterations, NFs bundling and PNs degeneration, were not deeply assessed, hindering also therapeutic approaches.

By assessing sacsin level and turnover in a panel of ARSACS patients' cells with different mutations, we provided evidence that sacsin is always absent or strikingly reduced regardless of the nature of the *SACS* mutation. For *SACS* missense mutations, which are the vast majority in ARSACS patients, we demonstrated that this is due to preemptive cotranslational degradation of sacsin nascent chains. This mechanism has been observed for the first time as the cause of a human disease and explains lack of genotype-phenotype correlation in ARSACS.

Moreover, we document here an insufficient phosphorylation at the C-tail of NFs subunits that results in more compact NFs fibers in *Sacs*$^{-/-}$ mouse cerebellum. This is an early event in the disease, which causes impairment of organellar trafficking in PNs. I carefully assessed and quantified this phenotype in primary *Sacs*$^{-/-}$ PNs and in cellular models (*SACS*$^{-/-}$ SH-SY5Y cells by CRISPR/Cas9).

Understanding of ARSACS molecular pathology rationalized gene therapy to target NFs bundling. I assessed an engineered miniaturized version of sacsin (minisacsin) suitable for AdenoAssociated Viral (AAV) mediated gene transfer. Using NFs bundling phenotype as a quantitative imaging readout, I have finally demonstrated that minisacsin is not toxic and functional and is able to counteract NFs bundling both in *SACS*$^{-/-}$ SH-SY5Y cells and in *Sacs*$^{-/-}$ PNs, paving the way for a preclinical trial *in vivo*.

TABLE OF CONTENTS

ACKNOWLEDGEMENTS ***3***

ABSTRACT ***5***

TABLE OF CONTENTS ***6***

ACRONYMS AND ABBREVIATIONS ***11***

LIST OF FIGURES AND TABLES ***13***

INTRODUCTION ***17***

1 - *SACS* gene: genomic localization and expression 17

1.1 – Characterization of the SACS gene 17

1.2 – Expression of the SACS gene in mammal tissues 17

1.3 – Subcellular localization of sacsin protein 21

2 - Sacsin protein architecture and domains 23

2.1 - Sacsin architecture 23

2.2 – The N-terminal portion of sacsin contains an ubiquitin-like (UbL) domain 23

2.3 – From the discovery of SRR 1, 2, 3 and XPCB domain to the identification of SIRPT 1, 2, and 3 supra-domains 25

2.4 – The C-terminal portion of sacsin contains a J domain 30

2.5 – The C-terminal end of sacsin contains a HEPN domain 32

2.6 – Concluding remarks on sacsin architecture 34

3 - Autosomal Recessive Spastic Ataxia of Charlevoix-Saguenay (ARSACS) 35

3.1 – Mutations in the SACS gene cause Autosomal Recessive Spastic Ataxia of Charlevoix-Saguenay 35

3.2 – ARSACS clinical manifestations 36

3.3 – Genotype-Phenotype correlation in ARSACS 38

4 - Functional studies of ARSACS pathophysiology in cellular models 41

4.1 - Intermediate filament remodeling 41

4.2 - Altered mitochondrial dynamic, bioenergetic, and transport 45

5 - Mouse models of ARSACS pathophysiology 48

5.1 - The Sacs$^{-/-}$ mouse model 48
5.2 - The Sacs^{R272C} knockin mouse model 55

6 – Ongoing therapeutic approaches in ARSACS 58

6.1 – Approaches aimed at rescuing cellular phenotypes caused by the absence of sacsin 58
6.2 - Rescue of IFs bundling by sacsin domains replacement in vitro 59

AIM OF THE WORK 61

RESULTS 62

1 - Assessment of Sacsin Turnover in Patients With ARSACS 62

1.1 - Clinical features and genetics of ARSACS patients 62
1.2 - Full-Length sacsin protein is dramatically reduced in fibroblasts from patients with ARSACS regardless of the nature of the mutation 65
1.3 - SACS mRNA is reduced in ARSACS fibroblasts carrying frameshift mutations, while it is stable or even increased in those carrying missense mutations 67
1.4 - Inhibition of degradative systems does not rescue sacsin protein full-length sacsin protein in ARSACS patients carrying missense mutations 68
1.5 - Translation of mutant sacsin carrying missense mutations is not blocked in ARSACS patients 72
1.6 - Nascent mutant sacsin products are cotranslationally ubiquitinated and degraded 73
1.7 - Assessment of sacsin protein level in human peripheral blood mononuclear cells (PBMCs) 76

2 - Dissection of sacsin physiopathological function in neurofilaments dynamics 79

2.1 - SACS$^{-/-}$ SH-SY5Y neuronal like cells and Sacs$^{-/-}$ primary PNs show abnormal hypo-phosphorylated neurofilaments bundles 79
2.2 – Integrated OMICS analyses show that NFH phosphorylation dynamics is impaired in Sacs$^{-/-}$ mice. 87
2.3 - Sacsin physically interacts with NF proteins and other cytolinker proteins in SH-SY5Y neuronal-like cells 93
2.4 - Neurofilaments impairment causes defective organelle trafficking in Sacs$^{-/-}$ PNs 97
2.5 – ARSACS pathogenesis model 101

3 - Investigation of novel engineered minisacsin in ARSACS preclinical models 103

3.1 - A novel miniaturized version of sacsin – minisacsin - is stable in vitro 103

3.2 – Minisacsin is functional and rescues NF bundling in vitro in SACS$^{-/-}$ SH-SY5Y neuronal cells 108

3.3 – Minisacsin is stable ex vivo in PNs upon AAV-mediated delivery 112

3.4 – Minisacsin is functional and rescues NF bundling ex vivo in Sacs$^{-/-}$ PNs 116

DISCUSSION 120

1 – Assessment of sacsin turnover in patients with ARSACS 120

1.1 - Effect of missense mutations on sacsin protein level explains lack of genotype-phenotype correlation 120

1.2 – Cotranslational degradation as a novel pathophysiological general mechanism in protein quality control 123

1.3 – Implications for ARSACS diagnosis and therapy 124

2 – NFH accumulation in ARSACS and implications for ARSACS pathogenesis and therapy 126

2.1 – NF remodeling in ARSACS is a primary event in the absence of sacsin 126

2.2 – Mechanistic explanation of NF remodeling in ARSACS 128

2.3 – Neurofilaments accumulation in ARSACS is different from other common neurodegenerative diseases 129

2.4 – Sacsin interacts with NF cytoskeleton linker proteins 131

2.5 – NF remodeling in ARSACS and implications for therapy 134

3 – Minisacsin gene therapy in ARSACS 135

3.1 – Minisacsin in the context of ongoing therapeutic approaches 135

3.2 – Sacsin protein and miniaturized gene strategy 136

3.3 – AAV recombinant capsids for systemic gene therapy 138

MATERIALS AND METHODS 140

1 – Sacsin protein level quantification and turnover assessment in ARSACS patients' cells (Results Section 1) 140

1.1 - Subjects' consent 140

1.2 - Human primary fibroblast derivation from skin biopsies 140

1.3 - Antibodies, drugs and reagents 140

1.4 - Anti N-terminal sacsin antibody (AbN) generation 141
1.5 - SACS deletion by CRISPR/Cas9 141
1.6 – Standard WB analyses 141
1.7 - RNA extraction and Real Time-PCR (qRT- PCR) 142
1.8 - Aggregate detection methods (Results Fig. 5) 142
1.9 - Polysomal profile analysis 143
1.10 - Immunoprecipitation of N-terminal sacsin fragments 143
1.11 - Peripheral blood mononuclear cells 144
1.12 – Statistical analyses 144

2 – NF molecular dissection in ARSACS (Results Section 2 and 3) ... 145

2.1 – Animals 145
2.2 - Antibodies used in WB 145
2.3 - Antibodies used in immunofluorescence 145
2.4 – Primary PNs cultures preparation 145
2.5 - SH-SY5YS cells 146
2.6 - SH-SY5Y differentiation (Results Fig 11, 14 and 18a-b) 146
2.7 - Immunofluorescence in primary PNs and SH-SY5Y cells 146
2.8 - Cerebellar sections immunostaining (Results Fig. 19e) 146
2.9 - Cell imaging 147
2.10 - Mitochondrial live imaging in primary PNs cultures (Results Fig. 21) 147
2.11 - Pipeline for max-NFH quantification 148
2.12 - LFQ proteomics and Phosphoproteomics analyses 148
2.13 - RNAseq analysis 149
2.14 - Sacsin immunoprecipitation and co-IP 149
2.15 - Interactomics 150
2.16 - Functional profiling and enrichments analyses (G-profiler, STRING, GSEA) 150
2.17 - PSD extraction and proteomics 150
2.18 – EM analysis 151
2.19 - Insoluble fractions (Results Fig 17b; Results Fig. 19d) 151
2.20 – Total homogenates (Results Fig. 19c) 151
2.21 - Immunoprecipitation of endogenous NFL in SH-SY5Y cells (Results Fig. 18d). 151
2.22 - Statistical analyses 152

3 – Minisacsin molecular analysis (Results Section 3) 153

3.1 - Plasmid cloning and cell transfection 153
3.2 - Primers used for cloning, sequencing and mutagenesis 153
3.3 - Minisacsin mutagenesis 153
3.4 - V5 immunoprecipitation 154
3.5 - Phosphatase lambda treatment 154
3.6 - Minisacsin AAV production and purification (in collaboration with Dr. Vania Broccoli) 154
3.7 - Primary PNs viral infection 154
3.8 - Sacsin immunostaining in primary PNs 155
3.9 – Statistical Assessment of NF bundling recovery upon minisacsin delivery 155

REFERENCES 156

APPENDIX 1 171

Publications 171

APPENDIX 2 172

Code 172

Pipeline used in Methods Section 2.11 172

ACRONYMS AND ABBREVIATIONS

AD	Alzheimer disease
ALS	Amyotrophic Lateral Sclerosis
ARCA	Autosomal Recessive Cerebellar Ataxia
ARSACS	Autosomal Recessive Spastic Ataxia of Charlevoix-Saguenay
AS	Angelman Syndrome
BDNF	Brain-Derived Neurotrophic Factor
bp	base pair
CA	Cornu Ammonis
CDD	Conserved Domain Database
Cdk5	Cyclin-dependent kinase 5
CNS	Central Nervous System
CPM	Count Per Million
co-IP	co-immunoprecipitation
CSLS	Charlevoix-Saguenay-Lac-Saint-Jean
DCN	Deep Cerebellar Nuclei
DIV	Day In Vitro
DRG	Dorsal Root Ganglia
EM	Electron Microscopy
FRAP	Fluorescence Recovery After Photobleaching
HEPN	Higher Eukaryotes and Prokaryotes Nucleotide-binding domain
HRP	HorseRadish Peroxidase
IFs	Intermediate Filaments
LFQ	Label-Free Quantitative
MOPS	3-(*N*-morpholino)propanesulfonic acid
MS/MS	Tandem mass spectrometry
NER	Nucleotide Excision Repair
NFH	Neurofilament Heavy subunit
NFL	Neurofilament Light subunit
NFM	Neurofilament Medium subunit
NFs	Neurofilaments
npNFH	non-phosphorylated Neurofilament Heavy subunit
OCT	Optical Coherence Tomography
OMM	Outer Mitochondrial Membrane

ORF	Open reading frame
PBMCs	Peripheral Blood Mononuclear Cells
PD	Parkinson disease
PN	Patient
PNs	Purkinje neurons
pNFH	phosphorylated Neurofilament Heavy subunit
PP2A	Protein Phosphatase 2A
PSI-BLAST	Position-Specific Iterative Basic Local Alignment Search Tool
PSORTII	Protein Subcellular Localization Prediction Tool
qRT-PCR	quantitative real-time PCR; quantitative reverse transcription PCR
RNAseq	Bulk RNA sequencing
RPKM	Reads Per Kilobase of exon per Million mapped reads
RQC	Ribosomal Quality Control
RT-PCR	Reverse transcription Polymerase Chain Reaction
SCA	Spinocerebellar Ataxia
SDS-PAGE	Sodium dodecyl-sulfate polyacrylamide gel electrophoresis
SIRPT	sacsin Internal RePeaTs
snRNAseq	single nucleus RNA sequencing
SRR	Sacsin Repeating Region
TD	nucleotidyl transferase domain
UbL	Ubiquitin-Like domain
UTR	Untranslated region
WB	Western Blot
XPCB	Xeroderma Pigmentosum complementation group C binding domain

LIST OF FIGURES AND TABLES

Introduction Figure 1. Sacsin expression in central nervous system by WB..... 18

Introduction Figure 2. Sacsin expression in CNS neurons..... 19

Introduction Figure 3. Sacsin mRNA expression in adult mouse cerebellum..... 20

Introduction Figure 4. Sacsin subcellular localization in immunofluorescence. 22

Introduction Figure 5. Schematic representation of sacsin architecture. 23

Introduction Figure 6. Sacsin possesses an Ubiquitin-Like (UbL) domain at its N-terminal region. 24

Introduction Figure 7. N-terminus of sacsin co-immunoprecipitates with the C8 subunit of the 20S proteasome..... 25

Introduction Figure 8. SRR domain is peculiar of sacsin. 26

Introduction Figure 9. Sacsin is highly conserved in vertebrates..... 28

Introduction Figure 10. Sacsin shares a XPCB domain with the Rad23a protein..... 29

Introduction Figure 11. Sacsin possesses a C-terminal J domain..... 30

Introduction Figure 12. Sacsin J domain crystal structure..... 31

Introduction Figure 13. Sacsin J domain is a functional Hsp40-like co-chaperone in vitro. 32

Introduction Figure 14. Crystal structure of the sacsin HEPN domain... 33

Introduction Figure 15. ARSACS-causing mutations are spread throughout the whole SACS gene. 36

Introduction Figure 16. Genotype-phenotype correlation in ARSACS.... 39

Introduction Figure 17. Overview of IFs proteins in human cells and tissues..... 41

Introduction Figure 18. Intermediate filaments and NF assembly. 43

Introduction Figure 19. Abnormal remodeling of vimentin IFs in ARSACS patients' fibroblasts..... 44

Introduction Figure 20. Abnormal accumulations of vimentin in the absence of sacsin..... 45

Introduction Figure 21. Mitochondria mislocalize at the periphery of vimentin bundles in ARSACS patients-derived fibroblasts. 46

Introduction Figure 22. Improper distribution of mitochondria in neurons in the absence of sacsin..... 47

Introduction Figure 23. Phenotype characterization of $Sacs^{-/-}$ mice. 49

Introduction Figure 24. Progressive PNs loss and axonal swellings in the Sacs-/- mouse. 50

Introduction Figure 25. Accumulation of NFH in immunohistochemistry on $Sacs^{-/-}$ mouse and ARSACS brain. 52

Introduction Figure 26. npNFH accumulates in PNs in $Sacs^{-/-}$ mice..... 53

Introduction Figure 27. NF bundles that form in the absence of sacsin contain all NF subunits. 54

Introduction Figure 28. Molecular characterization of a novel $Sacs^{R272C}$ KI mice..... 55

Introduction Figure 29. Progressive PC loss in $Sacs^{R272C}$ mice. 56

Introduction Figure 30. $Sacs^{R272C}$ exhibit NFH bundles in PNs soma and dendrites. 57

Results Table 1 (from previous page) Table showing cohort of patients used in this work. 64

Results Figure 1. ARSACS mutations used in this study and SACS gene and sacsin protein structures. 64

Results Figure 2 (from previous page). Sacsin protein is drastically reduced in ARSACS fibroblasts carrying different SACS mutations. 66

Results Figure 3. SACS mRNA is stable in patients carrying missense mutations. 67

Results Figure 4 (from previous page). Mutant sacsin is not post-translationally degraded..... 70

Results Figure 5. Mutant sacsin does not aggregate. 71

Results Figure 6. SACS mRNA carrying missense mutations is associated to the polysomal fractions. 73

Results Figure 7. Sacsin protein carrying missense mutations is co-translationally ubiquitinated and degraded. 75

Results Figure 8. Final model explaining why mutant sacsin is almost absent in patients' cells. 76

Results Figure 9. Sacsin is expressed in human peripheral blood mononuclear cells. 77

Results Figure 10 (previous page). Absence of sacsin causes NF bundling in undifferentiated neuronal-like SH-SY5Y cells. 82

Results Figure 11. The absence of sacsin causes NF bundling in differentiated neuronal-like SH-SY5Y cells. 83

Results Figure 12. The npNFH signal increase in Sacs$^{-/-}$ cerebellum is an early event in ARSACS pathogenesis. 84

Results Figure 13. The absence of sacsin causes NFH bundling ex vivo in PNs. 85

Results Figure 14. Microfilament and microtubule cytoskeleton is not impaired in the absence of sacsin in SH-SY5Y cells and primary PNs. 86

Results Figure 15 (from previous page). OMICS analyses from mice cerebellum reveals pathways involved in ARSACS pathogenesis. 89

Results Figure 16 (from previous page). NF subunits levels are not altered while NFH phosphorylation is drastically impaired by OMICS in Sacs$^{-/-}$ mice cerebellum. 91

Results Figure 17. NF fibers form properly in Sacs$^{-/-}$ cerebellum by EM and biochemical analyses. 92

Results Figure 18. Sacsin physically interacts with NFL, plectin and myosin Va. 94

Results Figure 19 (From previous page). Plectin and myosin Va levels are deregulated in sacsin-depleted cells and cerebellum. 97

Results Figure 20. Defective mitochondrial and ER distribution in distal processes of Sacs$^{-/-}$ primary PNs. 98

Results Figure 21. Mitochondrial movement is affected in the absence of sacsin. 99

Results Figure 22. OMICS analyses show reduced abundance of organelles in cerebellar PSD in the absence of sacsin (from previous page)..... 101

Results Figure 23. ARSASC pathogenesis model. 102

Results Figure 24 (from previous page). Minisacsin design and structure. 105

Results Figure 25. Minisacsin is stably expressed in vitro..... 106

Results Figure 26. Analysis of minisacsin double band. 108

Results Figure 27 (from previous page). Minisacsin significantly reduces NF bundling in SACS$^{-/-}$ SH-SY5Y cells..... 111

Results Figure 28. Quantification of NF bundling reduction in SACS$^{-/-}$ SH-SY5Y cells transfected with minisacsin..... 112

Results Figure 29 (from previous page). AAV are able to transduce primary PNs ex vivo..... 114

Results Figure 30. Minisacsin is stable ex vivo in PNs upon AAV-mediated delivery. 115

Results Figure 31. Sacsin endogenous distribution in PNs is similar to minisacsin. 116

Results Figure 32 (from previous page). Minisascin rescues NF bundling in Sacs$^{-/-}$ PNs..... 119

INTRODUCTION

1 - *SACS* gene: genomic localization and expression

1.1 – Characterization of the SACS gene

The SACS gene encodes for the protein sacsin and is mutated in Autosomal Recessive Spastic Ataxia of Charlevoix-Saguenay (ARSACS, OMIM #270550), an early-onset neurodegenerative disease among the most common genetic ataxias. ARSACS disease was already clinically described in 1979 in Canada (Bouchard *et al*, 1979, 1998), in the region of Charlevoix-Saguenay (Quebec); however, the causal gene was discovered only in the year 2000, when Engert et al. identified two mutations in a novel human coding sequence causing ARSACS in the great majority of Canadian patients. The novel gene was on chromosome 13q12.12 (Xiromerisiou *et al*, 2020; Engert *et al*, 2000) and was predicted to encode a single Open reading frame (ORF) of 11500 bp contained in a single giant exon (Engert *et al*, 2000).

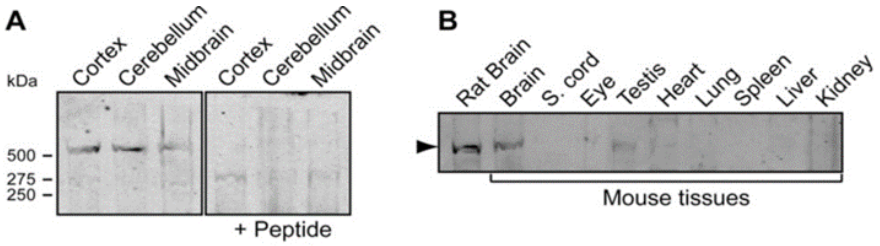
Since then, other nine smaller exons were identified by quantitative retro-transcriptional PCR (qRT-PCR) upstream of the gigantic one (Parfitt *et al*, 2009; Romano *et al*, 2013), for a total transcript of 15600 bp. The gigantic exon is 12868 bp long, the longest exon in the vertebrate genome.

Sacsin protein is 4579 amino acids long, with a molecular weight of 520 kDa. There are no *SACS* paralogue genes in the human genome. Sacsin is highly conserved in vertebrates and in particular in mammals: mice have a single homologue gene which encodes for a protein with length and molecular weight identical to human sacsin. Mouse sacsin shares 93% amino acid identity and 96% similarity to human sacsin. Remarkably, many common invertebrate model organisms lack a sacsin homologue, including *Escherichia coli*, *S. cerevisiae*, *Caenorhabditis elegans* and *Drosophila melanogaster* (Anderson *et al*, 2010; Romano *et al*, 2013).

1.2 – Expression of the SACS gene in mammal tissues

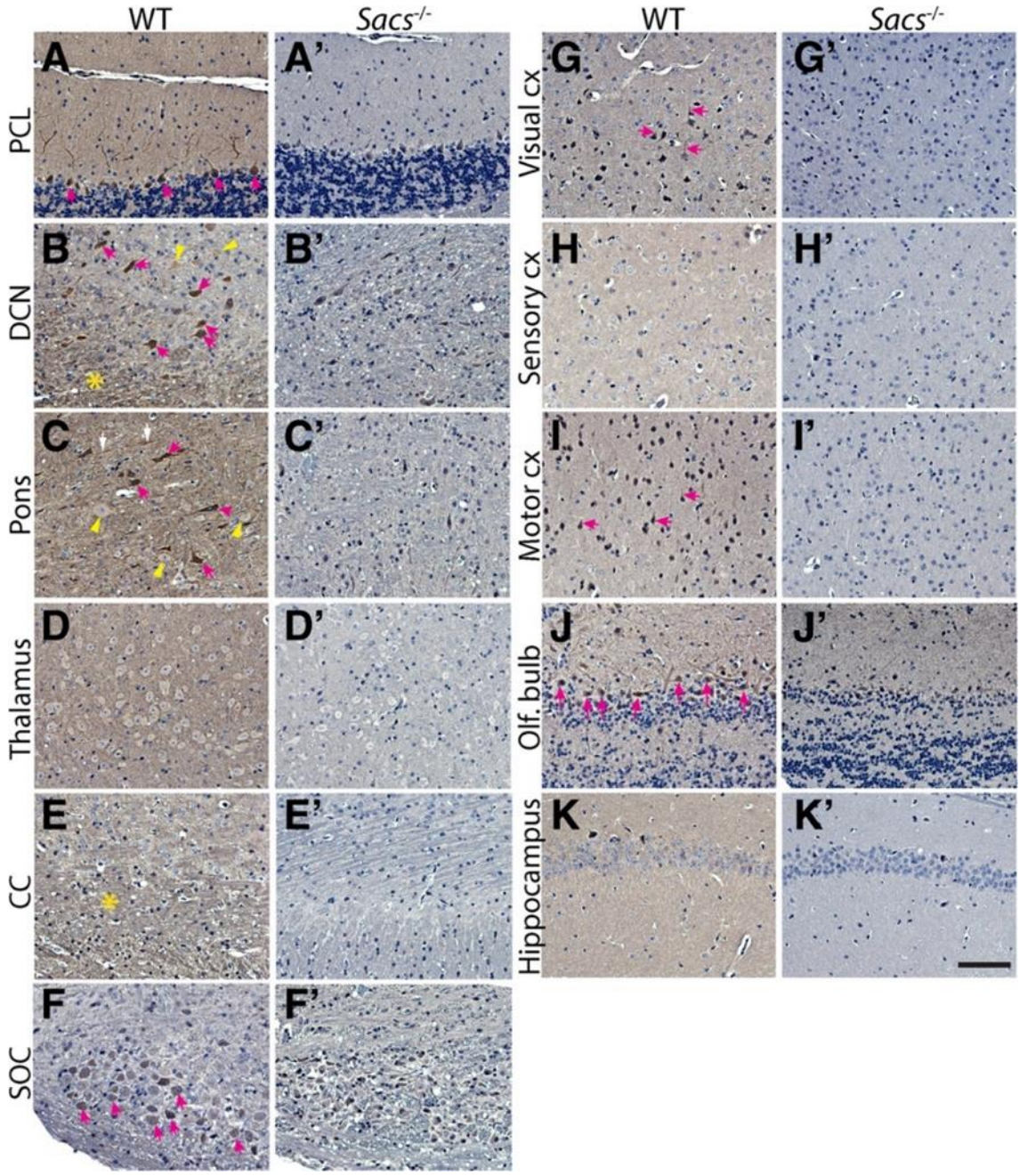
The investigation of *SACS* expression and localization in mammalian tissues was performed at mRNA level by Northern blot analysis, which revealed highest *SACS* expression in postmitotic cells, e.g. human dermal fibroblasts, and tissues, including brain, heart, and skeletal muscle. Low expression was reported in pancreas, and no detection at all in lung, liver, and kidney (Engert *et al*, 2000). Specific analysis of human, rat, and monkey central nervous system (CNS) by mRNA *in situ* hybridization confirmed high expression in all brain regions, with highest levels in pyramidal neurons in Layer V of cerebral cortex, hippocampus, and cerebellum granule cell layer (Engert *et al*, 2000; Parfitt *et al*, 2009). Consistently, first characterization of sacsin protein by Western Blot (WB) on mouse and rat tissue extracts shown that sacsin

protein is specifically expressed in cerebral cortex and cerebellum and at lower level in midbrain; whereas it is much less expressed or not detectable in heart, testis, spinal cord, lung, liver, spleen and kidneys (**Introduction Fig. 1**) (Parfitt *et al*, 2009b), demonstrating that sacsin is mainly a neuronal protein in mammals.



Introduction Figure 1. Sacsin expression in central nervous system by WB. *A-B. WB analysis of different mouse and rat tissue extracts with polyclonal antiserum directed toward sacsin C-terminal region (residues 4489-4503). The band was not detected when the antiserum was pre-incubated with the immunizing peptide. Adapted from* (Parfitt *et al*, 2009) *copyright to Oxford University Press used with permission under the Creative Commons CC-BY-NC license.*

Further characterization of *SACS* expression at protein level was done more recently by another group by immunohistochemistry on brain sections in mice. Here, the *Sacs*$^{-/-}$ mouse model was used in order to demonstrate the specificity of the antibody (Larivière *et al*, 2019). I will discuss thoroughly about this mouse model later. Sacsin was expressed in most areas of the brain (**Introduction Fig. 2**), in particular the highest expression was in soma and neurites (both dendrites and axons) of Purkinje Neurons (PNs) (**Introduction Fig. 2a**), as well as in the deep cerebellar nuclei (DCN) (**Introduction Fig. 2b**). Higher expression in PNs is consistent with the ARSACS ataxic phenotype induced by mutations in the *SACS* gene. However, sacsin was also expressed in several neurons in the pons and the medulla (**Introduction Fig. 2c**), in thalamus (**Introduction Fig. 2d**), in hippocampus in pyramidal cells processes (**Introduction Fig. 2k**) and in the isocortex (**Introduction Fig. 2j**); while in these regions sacsin is especially detected in neurites, in some areas such as the olfactory bulb (**Introduction Fig. 2j**), superior olivary complex neurons (**Introduction Fig. 2f**), visual and motor cerebral cortex areas (**Introduction Fig. 2i**), sacsin appears prevalently expressed in cell bodies (Larivière *et al*, 2019).

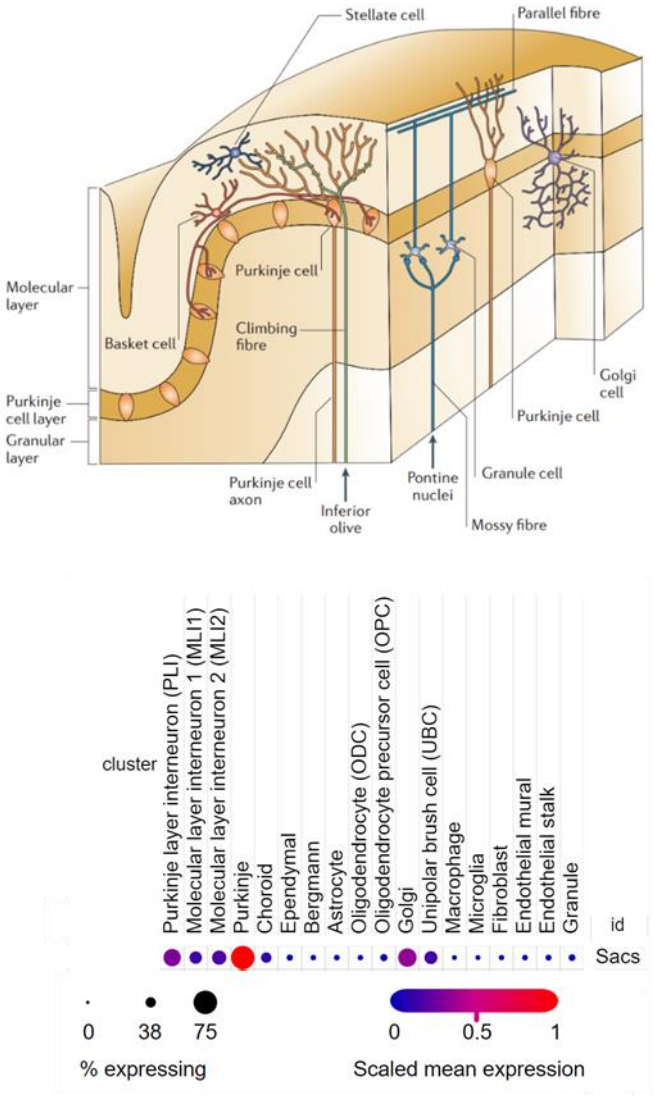


Introduction Figure 2. Sacsin expression in CNS neurons. *A-K. Sacsin immunohistochemistry analysis from sagittal brain sections from wild-type mice (300 days of age). Sacsin is expressed throughout the brain, with highest levels in Purkinje cell bodies and neurites and DCN cell bodies. Sacs$^{-/-}$ mouse model brain sections were used as negative controls. Abbreviations: PCL: Purkinje Cell layer. DCN: Deep Cerebellar Nuclei. CC: Corpus Callosum. SOC: Superior Olivary Complex). Adapted from (Larivière et al, 2019), copyright to John Wiley and Sons, used with permission, license number 5516610607370.*

SACS expression in the cerebellar cortex at single cell resolution

Recently, a comprehensive single-nucleus RNA sequencing (snRNAseq) of the adult mouse cerebellar cortex was published by the Macosko group (Kozareva *et al*, 2021). We used the open access cell atlas data they published to analyze *Sacs*

expression in the cerebellar cortex at single-cell resolution. This analysis revealed that *Sacs* mRNA is expressed at high levels and in a high percentage of PNs, similarly to PNs-specific markers like *Pcp2*. Interestingly, sacsin is also moderately expressed in other GABAergic inhibitory interneurons, both in the Purkinje cell layer and the molecular cell layer, as well as in Golgi cells, which are core components of the cerebellar circuitry. On the other hand, *Sacs* mRNA is almost absent or very lowly expressed in main glutamatergic neurons of the cerebellum – including granule cells, the most numerous cell type in the entire CNS - as well as in non-neuronal cells (**Introduction Fig. 3**) (Kozareva *et al*, 2021). These data suggest that sacsin may be very peculiar to GABAergic neurons, and among them of course of PNs.



Introduction Figure 3. Sacsin mRNA expression in adult mouse cerebellum. *Upper panel: scheme of cerebellar microanatomy (image modified from* (Ramnani, 2006)*, reused under license, license number 5474801356777). Lower panel: Sacs mRNA expression data in different cerebellar cell types obtained through single-cell nucleus RNA sequencing on 60-days-*

old mouse cerebellum. Data from (Kozareva et al, 2021) available at https://singlecell.broadinstitute.org/single_cell/study/SCP795/a-transcriptomic-atlas-of-the-mouse-cerebellum. Used under a Creative Commons Attribution 4.0 International License.

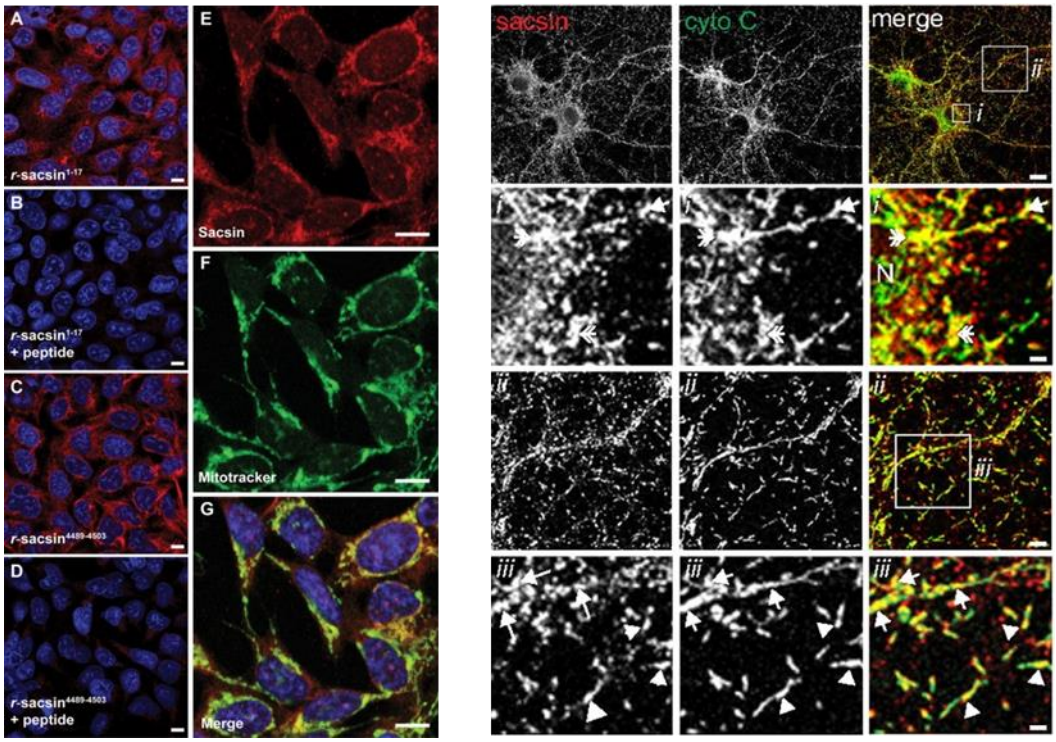
1.3 – Subcellular localization of sacsin protein

Almost 20 years after its discovery, sacsin subcellular localization was still a matter of discussion. Few works assessed experimentally sacsin localization (Parfitt *et al*, 2009; Girard *et al*, 2012), reporting different and contrasting results about its localization in neurons in relation to different organelles, including nuclei and mitochondria. Immunofluorescence analysis in immortalized cell lines shown a diffused cytosolic distribution and some punctate spots in the nucleus (**Introduction Fig. 4**, left panel) (Parfitt *et al*, 2009b); double labelling of sacsin and mitochondrial markers resulted in a partial co-localization to mitochondria in human neuronal-like SH-SY5Y cells and primary hippocampal neurons from rats (**Introduction Fig. 4**, left and right panels) (Parfitt *et al*, 2009b), which was also reported in COS-7 and HeLa cells (Girard *et al*, 2012).

However, these results are undermined by several lines of evidence. First of all, immunofluorescence that we performed exploiting the same antibodies did not reconfirm these data in human healthy-control fibroblasts and human neuronal-like SH-SY5Y cells, as it did not detect any specific sacsin signal in these cells, suggesting that they do not work very efficiently in immunofluorescence. Moreover, these experiments were performed in different cell types than those in which sacsin is physiologically highly expressed and relevant, namely PNs. As I will show in the results, I was indeed able to achieve reliable immunofluorescence staining only with a sacsin C-terminal antibody in primary PNs, where it shown a diffused cytosolic staining pattern, compared to negative controls (see also **Results Section 3.3**). Moreover, subcellular fractionation performed in our lab did not show sacsin co-localization with any organelle (data not shown), and also interactomics data shown only cytosolic interactors (see also **Results section 2.4**). Exclusive cytosolic distribution is consistent with bioinformatics analysis using prediction tools like PSORTII, that show that sacsin does not possess any protein sorting signal.

In particular, the hypothesis of sacsin mitochondrial localization was interesting many years ago, in light of some mitochondrial phenotypes observed in the absence of sacsin (see **Introduction section 1.4**), but it is now outdated. First, it is unlikely that sacsin is translocated inside mitochondria, given its huge dimensions and lack of mitochondrial matrix targeting peptide. Also, sacsin physical interaction with the outer mitochondrial membrane (OMM) remains a controversial point. An interaction between endogenous Drp1 and an exogenous sacsin N-terminal fragment with a

FLAG-tag was reported by co-immunoprecipitation (co-IP) (Girard *et al*, 2012); however, it was not reproduced by co-immunoprecipitating the endogenous sacsin protein with available antibodies, suggesting that it could be a spurious interaction due to overexpression of a recombinant sacsin fragment.



Introduction Figure 4. Sacsin subcellular localization in immunofluorescence. *Left: immunofluorescence of non-human primate COS-7 and human HeLa cells marked with antibodies directed against sacsin's N-terminal or C-terminal residues, noted in superscript, (red) and cytochrome C (green) shows sacsin overlapping to mitochondria. Adapted from (Parfitt et al., 2009) copyright to Oxford University Press used with permission under the Creative Commons CC-BY-NC license.. Right: immunofluorescence of sacsin protein in hippocampal neurons with antibodies directed toward N-terminal (A) and C-terminal (C) portions of sacsin (green), and mitochondria (red) in SH-SY5Y shows sacsin overlapping to mitochondria. Adapted from (Girard et al, 2012) copyright to NATIONAL ACADEMY OF SCIENCES used with permission under the Creative Commons CC-BY-NC license.*

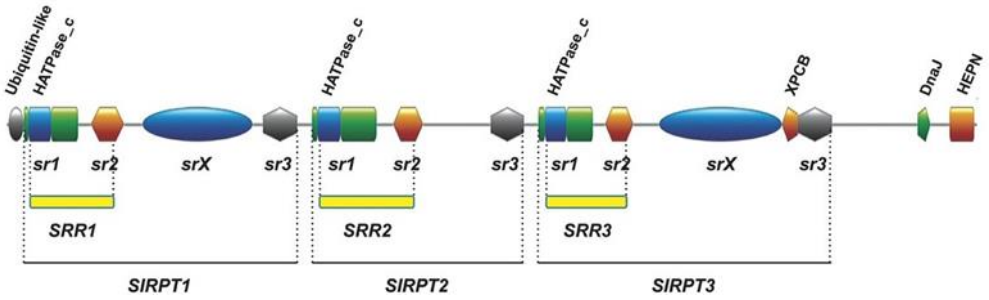
2 - Sacsin protein architecture and domains

2.1 - Sacsin architecture

Human sacsin is a 4579 amino acid-long multimodular protein of 520 kDa. Mice have a sacsin homologous protein of identical length and molecular weight. Its huge dimension has hampered biochemical studies of the protein over the years. The only available information on sacsin functions have been obtained by bioinformatics analyses of the sequence and by the expression of small portions *in vitro*. As shown by the general view of sacsin architecture (**Introduction Fig. 5**), moving from the N-terminal to the C-terminal, sacsin is composed of:

- An Ubiquitin-Like domain (UbL) (Parfitt *et al*, 2009b).
- Three complex domains defined as Sacsin Internal RePeaTs (SIRPT) 1, 2 and 3 (Anderson *et al*, 2010; Romano *et al*, 2013), each containing an H_ATPase_c domain homologous to Hsp90 chaperone family (Engert *et al*, 2000; Romano *et al*, 2013).
- A Xeroderma Pigmentosum complementation group C (XPC) binding domain (XPCB), related to Rad23 protein (Kamionka & Feigon, 2004).
- A J domain, homologous to Hsp40 co-chaperone family (Engert *et al*, 2000; Parfitt *et al*, 2009).
- Finally, a Higher Eukaryotes and Prokaryotes Nucleotide-binding domain (HEPN) (Grynberg *et al*, 2003).

A more detailed description of each domain is provided in the following sections of the thesis.



Introduction Figure 5. Schematic representation of sacsin architecture. *Picture is adapted from (Romano et al, 2013). Details of each depicted domain are reported in the main text. copyright to John Wiley and Sons, used with permission, license number 5516610185928.*

2.2 – The N-terminal portion of sacsin contains an ubiquitin-like (UbL) domain

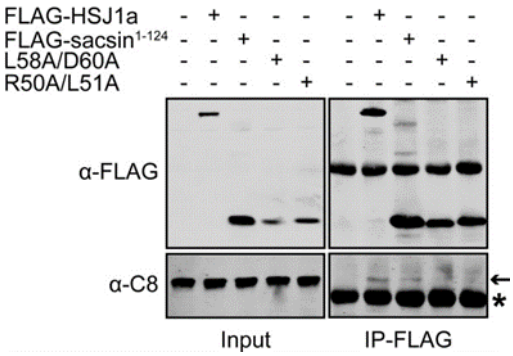
A UbL domain was reported at the N-terminus of sacsin by *in silico* similarity search (**Introduction Fig. 6**) (Parfitt *et al*, 2009b), which makes sacsin an Ubiquitin-like protein. Ubiquitin-like proteins are classified into two groups. The first includes

ubiquitin-like modifiers (such as NEDD8 and SUMO-1), which, similarly to ubiquitin, can be covalently attached to target proteins. The second group, which is the most heterogeneous and to which sacsin belongs, is called *ubiquitin-domain proteins*: these proteins contain a domain homologous to ubiquitin as part of their amino acid sequence and which is neither cleaved nor conjugated to other proteins in the cell. The UbL domain allows ubiquitin-domain proteins to interact with proteasomal components, like the 19S regulatory subunit (Hartmann-Petersen & Gordon, 2004). One of the most characterized ubiquitin-like proteins is the yeast protein Rad23, whose human orthologue is hHR23, which was initially discovered as a player in the nucleotide excision repair process, a vital defense mechanism against UV-derived DNA damage (Dantuma *et al*, 2009). Rad23 acts downstream of other proteins, which recognize ubiquitinated substrates, to target them to the proteasome via its UbL domain (Tsuchiya *et al*, 2017). Interestingly, sacsin UbL domain has a significant homology with the UbL domain of hHR23 (with 43% of identity) (**Introduction Fig. 6**), and contains part of the consensus sequence identified to be essential for interaction of UbL with the proteasome (Parfitt *et al*, 2009b).

```
Sacsin 22  TVAALASWTVRDVKERIFAETG---FPVSEQRLWRGGRELSDWIKIGDLTSKN---CHL
Rad23  19  KIRMEPDETVKVLKEKIEAEKGRDAFPVAGQKLIYAGKILSDDVPIRDYRIDEKNFVVV
Nedd8  14  EVDIEPTDKVERIKERVEEKEG---IPPQQQRLIYSGKQMNDEKTAADYKILGGSVLHL
Ubiqui 14  TLEVEPSDTIENVKAKIQDKEG---IPPDQQRLIFAGKQLEDGRTLSDYNIQKESTLHL
                                      **      *               *
```

Introduction Figure 6. Sacsin possesses an Ubiquitin-Like (UbL) domain at its N-terminal region. *Multiple alignments between the putative UbL domain of sacsin and other ubiquitin-related proteins and the Rad23 UbL domain. Highly conserved residues are illustrated in bold. Residues that play a crucial role in proteasome binding are marked with a star. Adapted from (Parfitt et al, 2009) copyright to Oxford University Press used with permission under the Creative Commons CC-BY-NC license.*

This led to investigate if sacsin could bind the proteasome. The interaction between the 20S proteasome core particle and an exogenous FLAG-tagged N-terminal sacsin fragment (residues 1-124), containing the UbL domain, was reported by co-IP *in vitro* (Parfitt *et al*, 2009b). If residues within the consensus binding site for the proteasome were mutated, the interaction between this N-terminal sacsin fragment and the proteasomal subunit was lost (**Introduction Fig. 7**). However, to our knowledge similar data have not yet been reported for endogenous sacsin in any cellular or animal model.



Introduction Figure 7. N-terminus of sacsin co-immunoprecipitates with the C8 subunit of the 20S proteasome. *The N-terminal sacsin fragment encoding the UbL domain (residues 1-124) with a FLAG-tag at its C-terminus was over-expressed in CHO-1 cells. Cellular lysates were precipitated with an anti-FLAG antibody (IP-FLAG). WB were performed with antibodies directed against the C8 subunit of the 20S proteasome complex (α-C8) and gained FLAG tag (α-FLAG). Input indicates the lysates that were not immunoprecipitated with anti-FLAG antibodies. Interaction with C8 (black arrow) was not detected if the N- terminal sacsin fragment contained two changed residues in the conserved consensus binding site for the proteasome (L58A/D60A and R50A/L51A). FLAG-HSJ1a protein was used as a positive control. Asterisk indicates immunoglobulin chains. Adapted from (Parfitt et al, 2009) copyright to Oxford University Press used with permission under the Creative Commons CC-BY-NC license.*

2.3 – From the discovery of SRR 1, 2, 3 and XPCB domain to the identification of SIRPT 1, 2, and 3 supra-domains

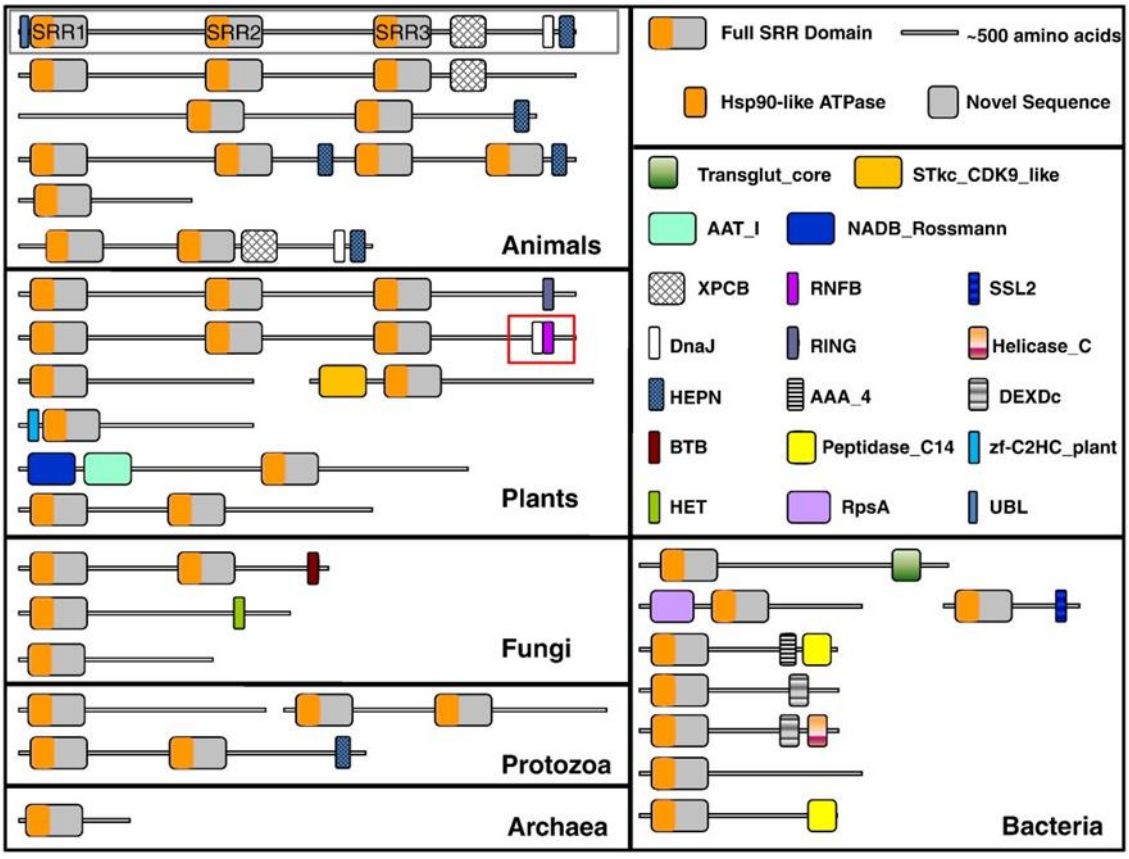
Sacsin has been found to contain three regions, each consisting of approximately 360 amino acids, that are unique to sacsin and highly distinct from other proteins (Engert *et al*, 2000; Anderson *et al*, 2010; Romano *et al*, 2013). The N-terminal portion of each region shares high homology with the Hsp90 N-terminal ATP-binding domain (H_ATPase_c - pfam02518) of *Saccharomyces cerevisiae* (Engert *et al*, 2000). Therefore, these regions seem to be three copies of a novel supra-domain, each in turn containing an ATPase domain, which were called Sacsin Repeating Region (SRR) 1-3, although they share only 22% identity with each other, and are interspersed with less homologous traits (4% identity) (Anderson *et al*, 2010).

Many facts make SRR sacsin domains very peculiar in all kingdoms of life.

- The conserved sequence of the C-terminal portion of the SSR domain is always found, in all genomes analyzed, immediately after the Hsp90-like ATPase domain, i.e. in the SRR itself; it has never been found isolated or in other domains. Due to peculiar combination of its N-terminal ATPase and C-terminal portions, SRR was classified as a novel supra-domain. A supra-domain is defined as a combination of two or more adjacent domains that behave as a functional unit in the evolution of new proteins. Often, a supra-domain displays a novel function beyond that of constituent domains which are usually

found isolated or in different combinations in other proteins. However, this function has yet not been identified for sacsin SRRs.

- SRR domains are present throughout all kingdoms of life. In prokaryotes they are usually isolated proteins or are linked to other unrelated domains. Whereas in eukaryotes they are always in combination with other domains typical of sacsin (UbL, J domain, XPCB and HEPN) (**Introduction Fig. 8**). Furthermore, these domains are always present with the same configuration from N- to C-terminus.
- Many common model organisms lack completely proteins with SSR domains in their genome, including *E. coli*, *S. cerevisiae, D. melanogaster* and *C. elegans*.



Introduction Figure 8. SRR domain is peculiar of sacsin. *Scheme of sacsin repeating region (SRR) domain architecture and phylogenetic distribution and occurrence within other domains, based on the Conserved Domain Database (CDD). Adapted from (Anderson et al, 2010), reused under permission, license number 1317903-1 31-Jan-2023.*

Comparison of the predicted secondary structure of human sacsin SRR ATPase domain with the ATP-binding domain of yeast Hsp90 shown a high structural resemblance too, with consistent position of essential secondary structural elements and amino acid residues involved in ATP binding (Anderson *et al*, 2010). The authors

investigated also the ability of the SRR-ATPase to hydrolyze ATP. A large mouse sacsin fragment containing SRR1 (from 1 to 1456 residues positions) was cloned and tested *in vitro* in a cell-free system. Interestingly, not only the fragment was able to hydrolyse ATP but also the k_{cat} was similar to that of yeast Hsp90. The k_{cat} of Hsp90 is known to be extremely low, and this is functionally relevant to give time to misfolded or unfolded substrates to fold properly before being directed to degradation.

SRR distribution and sacsin evolution

Anderson et al. further divided all the proteins identified by the PSI-BLAST analysis of human SRR into two classes (**Introduction Fig. 8**): (1) proper "sacsin-like proteins" and (2) the broader "SRR-containing proteins". Sacsin-like proteins share the same architecture, namely three SRRs, followed by an XPCB domain, a J domain, and a HEPN domain. These human sacsin homologs have been identified only in animals (Anderson *et al*, 2010; Romano *et al*, 2013); in particular, at least one sacsin-like protein has always been identified in all vertebrate genomes sequenced so far, and only in very few species outside vertebrates. Zebrafish have two sacsin homologue genes, likely due to large genome duplication events that occur in this species. The percentage of amino acid identity is 93-99% in mammals (93% in mice), 83-84% in birds and reptiles, and 68-70% in fish (**Introduction Fig. 9**) (Romano *et al*, 2013). It is worth noting that the UbL domain is much less conserved outside mammals, suggesting that its inclusion may have represented a further complexification of sacsin function in the evolutionary tree. Finally, similar to humans, in rodents' genome (and virtually in all mammals), there is a single gene encoding sacsin and there are no other SRR-containing proteins.



Introduction Figure 9. Sacsin is highly conserved in vertebrates. *Analysis of sacsin sequence among different vertebrates. The similarity scale indicates which homology degree corresponds to each color. Adapted from (Romano et al, 2013) copyright to John Wiley and Sons, used with permission, license number 5516610185928.*

The broader class of "SRR-containing proteins" is composed by all proteins with one or more SRRs. These proteins are spread in all kingdoms of living organisms; they are rarely present in animals, e.g. in fish (Zebrafish have an isolated SRR domain protein in its genome besides the two sacsin-like proteins). The number of SRR repetitions tends to increase with the complexity of organisms. Indeed, prokaryotes have mostly single isolated SRR domains, while higher eukaryotes display tandem repetitions of up to three SRRs as in sacsin (**Introduction Fig. 8**), suggesting recurrent selective pressures that join together SSR domains and in particular exactly three SRRs. Another example of convergent evolution is that, as already mentioned, in eukaryotes SRR are always found together with XPCB or J or HEPN domains, with the same configuration.

Sacsin Internal RePeaTs (SIRPTs)

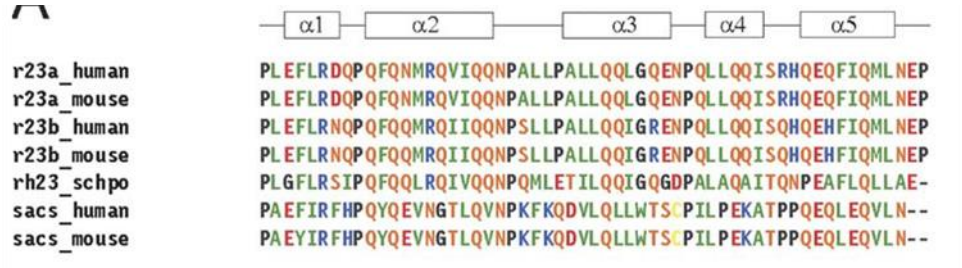
After the discovery of SRRs, Romano et al. identified further regions of self-homology in human sacsin (Romano *et al*, 2013). Combining several bioinformatic tools, authors shown that previously identified SRRs supra-domains are in turn part of three larger modules, named Sacsin Internal RePeaTs 1, 2, and 3 (SIRPT 1, 2 and 3). The three SIRPTs, have low homology between themselves (around 17%) and each display three sub-repeats in the same order, namely sr1, sr2 and sr3. SIRPT1 and SIRPT3 also have a fourth sub-repeat called srX, always between their sr2 and

sr3. The region in each SIRPT which includes sr1 and sr2 corresponds roughly to the SRR supra-domain previously identified by Anderson et al. 2010 (see also **Introduction Fig. 5**). Each SIRPT is very long (about 1100 amino acids); taken together, the SIRPTs cover 84% of all sacsin length. This compositional variability and low homology between the overall SIRPTs may suggest that the three modules are not redundant and may provide additional functions, such as substrate specificity.

Unlike SRRs, PSI-BLAST analysis of the newly discovered sr3 and srX sequences did not reveal homologous sequences in any database in any species. Moreover, SIRPT complex architecture is found only in vertebrates (Romano *et al*, 2013). For this reason, sacsin may be involved in some new and complex processes that emerged with vertebrates, likely explaining sacsin's high expression in the central nervous system (see **Introduction section 1.2**).

The XPCB domain

Between the srX and sr3 motifs of SIRPT3, an XPCB domain is present (see **Introduction Fig. 5**). XPCB is present in human homologs of yeast proteins Rad23A and Rad23B - hHR23A and hHR23B, respectively. Through the XPCB domain, these proteins interact with the Xeroderma pigmentosum, complementation group C (XPC) protein, which is involved in the early stages of a DNA repair pathway known as nucleotide excision repair (NER) (Kamionka & Feigon, 2004). Out of these proteins, XPCB domains have only been found in animals together with SRR domains, almost always in sacsin-like homologues (Anderson *et al*, 2010) (see also **Introduction Fig. 8**). Similar to the respective UbL domains, hHR23 and sacsin XPCB domain shares 35% identity (**Introduction Fig. 10**) (Kamionka & Feigon, 2004).



Introduction Figure 10. Sacsin shares a XPCB domain with the Rad23a protein. *Multiple sequence alignment between human and mouse sacsin XPCB domain and Rad23 proteins from different species. Hydrophobic amino acids are shown in green (F, A, M, I, L, Y, V, W), negatively charged amino acids in red (D, E), positively charged amino acids in blue (H, K, R), polar amino acids in orange (N, Q, S, T), and cysteine in yellow. Above: schematics of the five XPCB α-helices of hHR23A (α1-5) aligned with corresponding amino acid residues below. Adapted from (Kamionka & Feigon, 2004) copyright to John Wiley and Sons used with permission.*

The XPCB domain of hHR23A has been shown to interact with the ubiquitin ligase Ube3A2, encoded by the *UBE3A2* gene, whose mutations cause Angelman syndrome (AS, OMIM #105830). AS is an autosomal dominant disorder affecting mainly neurodevelopment, with features related to autism and seizures, but it has been also associated to ataxia symptoms and ataxic-like movement disorders. In one work (Greer *et al*, 2010), they demonstrated indirectly that Ube3a2 in mice interacts with sacsin. They crossed transgenic mice expressing ubiquitin-HA with wild-type or *Ube3a2* knockout mice. Then, they immunoprecipitated all HA-ubiquitinated brain proteins and performed mass spectrometry analysis and found sacsin only in wild-type mice, and not in Ube3a2 knockout mice, suggesting that sacsin is ubiquitinated in the brain by Ube3a2 and is no longer ubiquitinated upon loss of Ube3a2. In light of the similarity of XPCB region between hHR23 and sacsin, they speculated that the XPCB domain might work as Ube3A binding site. The authors also speculated that interaction with sacsin would explain ataxic components in AS; however, these data have not been reconfirmed by co-IP yet.

2.4 – The C-terminal portion of sacsin contains a J domain

By sequence similarity search, sacsin also possesses a J domain in the C-terminal region (Engert *et al*, 2000). The J domain is typical of Hsp40 co-chaperone family, which encompasses a large set of proteins, expressed in all organisms, that interact with the chaperone family of Hsp70 proteins. Sacsin putative J domain shares 60% identity with different Hsp40 proteins, included E. coli DnaJ (**Introduction Fig. 11**) (Parfitt *et al*, 2009b); strikingly, sacsin presents also the HPD amino acid sequence (histidine, proline, aspartate), which is a highly conserved motif in all members of the Hsp40 family and mediates the interaction with the Hsp70 counterpart (Qiu *et al*, 2006).

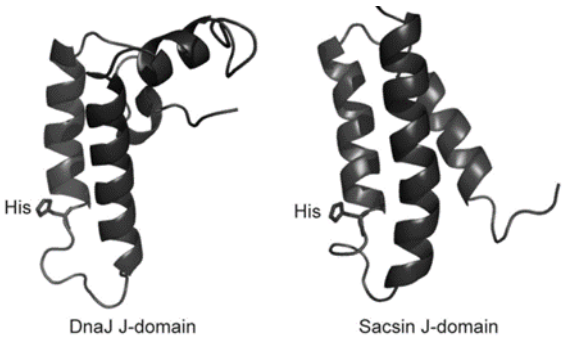
```
Sacsin 4295 -----KKLKVNSLPEILKEVTSVVEQAWKLPESERKKIIRRLYLKWHPDK
Hsj1   1    -------MAS--YYEILDVPR-------SASADDIKKAYRRKALQWHPDK
DnaJ   1    -------MAKQDYYEILGVSK-------TAEEREIRKAYKRLAMKYHPDR
HDJ1   1    --------MGKDYYQTLGLAR-------GASDEEIKRAYRRQALRYHPDK
TAg    1    MDRVLSRADKERLLELLKLPR-----QLWGDFGRMQQAYKQQSLLLHPDK
Hsc20  1    ----------MDYFTLFGLPA-----RYQLDTQALSLRFQDLQRQYHPDK
Con         -------------Y-ILG----------AS--DIK-AYR-LA---HPD-

Sacsin 4309 NPEN----HDIANEVFKHLQHEINRL--EKQAFLDQNADRASRRTFSTSA
Hsj1   51   NPDN----KEFAEKKFKE-VAEAYEVLSDKHKREIY--DRYGREG
DnaJ   51   N----QGD-KEAEAKFKE-IKEAYEVLTDSQKRAAY--DQYGHAAFEQ
HDJ1   51   N----K-E-PGAEEKFKE-IAEAYDVLSDPRKREIF--DRYGEEGLKGSG
TAg    51   ---------GGSHALMQE-LNSLWGTFKTEVYNLRM--NLGGTGFQ
Hsc20  51   FASGSQAEQLAAVQQS-ATINQAWQTLRHPLMRAEY--LLSLHGFDLA
Con         --------------F------A---L-D--KR--Y--D----------
```

Introduction Figure 11. Sacsin possesses a C-terminal J domain. *Multiple sequence alignment of sacsin J domain. Alignment with HSJ1 domain of human Hsp40, E. coli DnaJ, Homo sapiens HDJ1, antigen T of murine polyoma virus (Tag) and E. coli Hsc20. Highly*

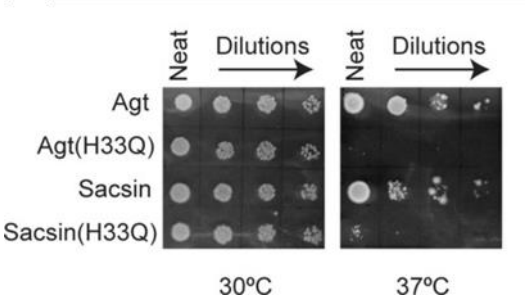
conserved residues are indicated in the line below (Con=consensus). Adapted from (Parfitt et al., 2009) copyright to Oxford University Press used with permission under the Creative Commons CC-BY-NC license.

Sacsin J domain was cloned and crystallized and structural comparison with the J domain of *E. Coli* DnaJ co-chaperone shown the same secondary structure, with the HDP motif in the same spatial orientation (**Introduction Fig. 12**) (Parfitt *et al*, 2009b).



Introduction Figure 12. Sacsin J domain crystal structure. *Scheme of the secondary structure of J domains from sacsin and E. coli DnaJ (Hsp40) protein, made with Pymol. Adapted from (Parfitt et al, 2009). The J domain structure is typical, with four α-helices, with a loop between the second and the third that contains the HPD residues (Histidine, Proline, Aspartate). Copyright to Oxford University Press used with permission under the Creative Commons CC-BY-NC license.*

Sacsin J domain functionality was evaluated in a bacterial complementation assay using an *E. coli* conditional-mutant strain defective for the DnaJ gene, that cannot grow above 37°C. Expression in this strain of an exogenous recombinant DnaJ protein, containing the sacsin J domain sequence, rescued the phenotype, thus suggesting that the domain may be functional (**Introduction Fig. 13**) (Parfitt *et al*, 2009b). In contrast, expression in the same strain of the recombinant DnaJ protein carrying a mutation in the HPD conserved motif, involved in mediating the interaction with *E. coli* Hsp70 chaperone, failed to rescue the mutant phenotype. This result suggests that sacsin J domain function depends on its ability to bind Hsp70 chaperone system (**Introduction Fig. 13**). However, this experiment does not give any evidence on sacsin J domain functionality in the context of mammalian cells and in the full protein.



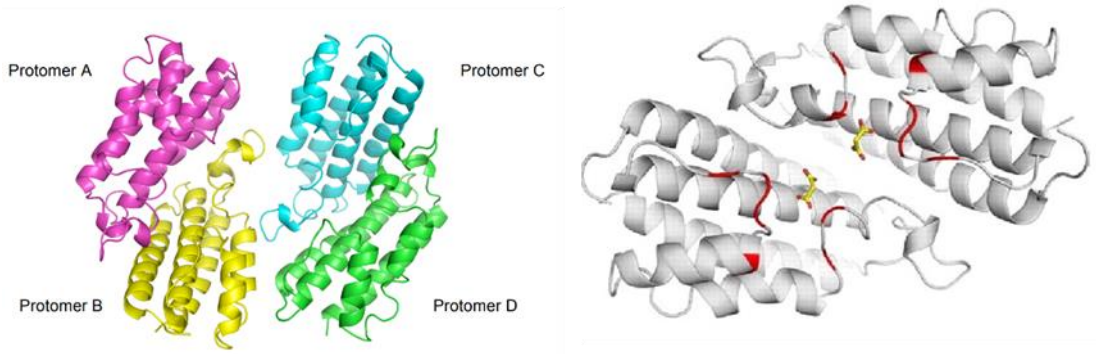
Introduction Figure 13. Sacsin J domain is a functional Hsp40-like co-chaperone in vitro. *Bacterial complementation assay in which E. coli defective for DnaJ gene is unable to grow above 37°C due to accumulation of misfolded and unfolded proteins. Expression of wild type sacsin J domain or Agrobacterium tumefaciens Hsp40 J domain (Agt), rescues the mutant phenotype (bacteria grow at 37°C), while expression of mutant sacsin or mutant Agt J domains in the HPD motif (H33Q), essential for Hsp70 binding, does not. Adapted from (Parfitt et al, 2009) copyright to Oxford University Press used with permission under the Creative Commons CC-BY-NC license.*

2.5 – The C-terminal end of sacsin contains a HEPN domain

PSI-BLAST analysis found that the last 110 amino acids of the sacsin C-terminal portion share homology with the HEPN domain (Grynberg *et al*, 2003). At the beginning, the HEPN domain was found by PSI-BLAST in a large number of archaea and bacterial proteins, whereas in eukaryotes was found only in animals (Li *et al*, 2015; Grynberg *et al*, 2003; Kozlov *et al*, 2011); indeed, no HEPN domains were found in lower eukaryotes, at least by strict sequence similarity. Moreover, in animals the HEPN domain is always contained at the C-terminus of SRR-containing proteins or in sacsin-like proteins (see **Introduction Section 2.3**), frequently after the J domain.

Kozlov et al. cloned and determined the crystal structure of human sacsin HEPN domain (sacsin 4441-4579 residues position) (Kozlov *et al*, 2011). The crystal asymmetric unit is composed of four HEPN domains (here called protomers) that assemble to form two dimers (**Introduction Fig. 14**), suggesting propensity of the HEPN domain to dimerize. Dimerization was also evaluated measuring the molecular weight of HEPN protomers with molecular-exclusion chromatography that gave twice the predicted molecular weight of the HEPN amino acid sequence (~15 kDa). These results show that the HEPN domain has the tendency to dimerize in solution; hence, sacsin protein might dimerize inside the cell through its HEPN domain. The HEPN domains of some bacterial proteins have been structurally characterized too, but their precise function remains unknown. In bacteria, the HEPN domain is often associated with a nucleotidyltransferase (TD) domain, either encoded in the same polypeptide, usually N-terminally to the HEPN, or encoded by a different gene (Li *et al*, 2015; Grynberg *et al*, 2003). The TD domain has been involved in resistance to antibiotics;

kanamycin-TD is an example of a bacterial HEPN-containing enzyme which mediates bacterial resistance to kanamycin by transferring a nucleoside mono-phosphate group from a nucleotide, likely bound to the HEPN domain, to a target antibiotic (Erlandsen *et al*, 2004; Pedersen *et al*, 1995). Since in bacteria the HEPN domain is proposed to be involved in the nucleotide binding, it has been investigated if also sacsin's HEPN domain can bind nucleotides. This role for the HEPN domain may facilitate both the ATP or GTP hydrolysis by the Hsp90-like ATPase domain or ATP or GTP binding by the adjacent Hsp40-like J domains, in agreement with the hypothesis of sacsin being overall a chaperone. Isothermal titration calorimetry and nuclear magnetic resonance shown that the HEPN domain binds indeed GTP with an affinity constant of 1.7 μM (**Introduction Fig. 14**) (Kozlov *et al*, 2011). Moreover, a deeper inspection of the protomers in the crystal shown the presence of negatively charged molecules at the dimer interface, in regions corresponding to the GTP binding sites by nuclear magnetic resonance. Since both protomers within a dimer are involved in this binding, the dimer is likely necessary for the HEPN domain to bind GTP or whatever substrate, and therefore dimerization is likely to be necessary for sacsin HEPN domain to function.



Introduction Figure 14. Crystal structure of the sacsin HEPN domain. *Left: Crystal packing of four HEPN molecules (polypeptide chains A-D) in the asymmetric unit. Each protomer is composed of five α-helices. The physiological dimers are composed of protomers A-B and protomers C-D. Right: nuclear magnetic resonance reconstruction of HEPN dimer bound to GTP molecules. Adapted from (Kozlov et al, 2011) copyright to Elsevier Creative Commons CC-BY.*

Novel identified HEPN domains are linked to RNA binding

An aspect overlooked in ARSACS literature regards the HEPN domain. In fact, novel superfamilies of HEPN domains have been identified with PSI-BLAST by extremely degenerating HEPN sequences and taking into account structural information (Anantharaman *et al*, 2013). This study shown that HEPN sequences are highly divergent, and are spread throughout prokaryotes and eukaryotes genomes, including animals; strikingly, many novel identified HEPN domains were already

independently characterized biochemically as catalytic domains of RNAses involved in different aspects of RNA metabolism, e.g. degradation, splicing, translocation etc. These novel HEPN domains contain conserved motifs and structural elements, shared also in sacsin's HEPN; other HEPN domains likely work as RNA-binding domains with lost catalytic activity. Functionally, they have been involved in many defensive systems both in prokaryotes (noteworthy in CRISPR systems) and in eukaryotes, e.g. in antiviral response and cellular stress, including heat shock and unfolded protein responses. It has been proposed that the HEPN domain in sacsin may couple protein quality control to regulation of mRNA translation in stress conditions (Anantharaman *et al*, 2013). Independently, other studies reported high structural homology between HEPN domains of sacsin and a class of human RNA-binding proteins named roquins (Zhang *et al*, 2015; Srivastava *et al*, 2015). Roquins contain a Ubiquitin ligase E3 domain and bind conserved elements in the 3-'UTR of mRNA targets, usually involved in inflammatory response; roquins contain also two HEPN domains, one of which is C-terminal that mediate intramolecular dimerization, and are actively involved in RNA binding (Srivastava *et al*, 2015). Unlike sacsin, roquin HEPN domains do not contain binding sites for GTP. These studies may suggest novel functions for HEPN and a role for sacsin in linking protein quality control with mRNA regulation or crosstalk with ubiquitination.

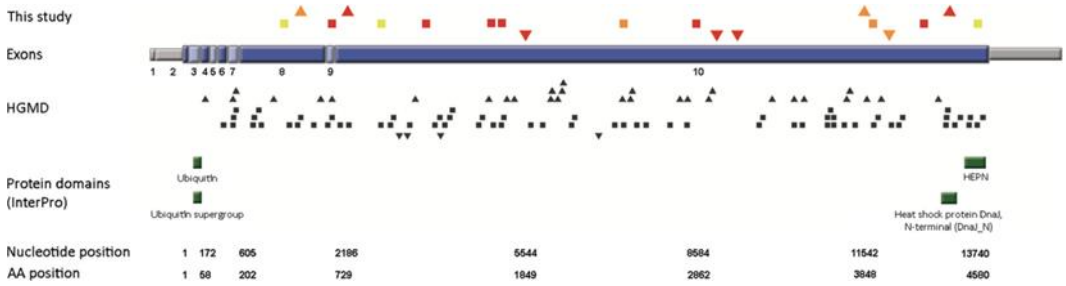
2.6 – Concluding remarks on sacsin architecture

Sacsin is a 520-kDa multimodular protein that contains: an UbL domain that binds to the proteasome; three sacsin repeating regions (SRR) containing an ATPase domain typical of Hsp90 able to hydrolyze ATP; a XPCB binding domain that binds ubiquitin ligase Ube3A; a J domain which can bind Hsp70; a HEPN domain able to bind GTP and analogues substrates. Overall, sacsin may act as a molecular chaperone or co-chaperone. However, since the study of this protein has always been conducted using single regions in conditions far from a physiological state, a complete understanding of how all the domains work in the framework of the endogenous sacsin and its function inside the cell is still missing. Furthermore, sacsin domains may have also acquired novel or cross-talking functions, as supported by (i) extreme distinctiveness of its domains (ii) high sequence divergence of its domains and (iii) convergent evolution in placing these domains in a specific configuration. Such novel functions may correlate with high expression in mammals and in the cerebellum.

3 - Autosomal Recessive Spastic Ataxia of Charlevoix-Saguenay (ARSACS)

3.1 – Mutations in the SACS gene cause Autosomal Recessive Spastic Ataxia of Charlevoix-Saguenay

Autosomal recessive spastic ataxia of Charlevoix-Saguenay (ARSACS - OMIM #270550) is a neurodegenerative disease characterized by early-onset cerebellar ataxia (Vermeer *et al*, 2020). The disease name originates from the region of Charlevoix-Saguenay-Lac-Saint-Jean (CSLS), in Québec (Canada), where the frequency of healthy carriers is 1/22 (Engert *et al*, 2000; Bouhlal *et al*, 2011), likely due to a founder effect, and it is considered the second most common recessive ataxia after Friedreich ataxia (OMIM #229300). Bouchard et al. first described the disease in 1979 in the Québécois patients (Bouchard *et al*, 1979). Later, in 2000, Engert et al. identified two mutations in the *SACS* gene in Québec ARSACS families. One is a single base deletion (g.8844delT) in homozygosis, which represents a major ARSACS haplotype shared by 96% of ARSACS families who descend from an ancestral founder of the population (Engert *et al*, 2000). The second mutation is a nonsense substitution (g.7504C→T), a minor ARSACS haplotype found in six families in heterozygosis with the deletion mentioned above. Both mutations occur in the last gigantic exon of sacsin and should produce a truncated protein. Since then, more than 250 mutations spread all over the *SACS* gene have been identified (**Introduction Fig. 15**) (Synofzik *et al*, 2013). The disease is globally spread and there is no correlation between any ethnicity and disease or specific allele frequency. Many patients are homozygous for *SACS* mutations (45.2%), followed by compound heterozygous (32,9%). Moreover, any type of mutation has been reported, with missense variants being the most represented (37.4%), followed by other truncating point mutations, i.e. small insertion/deletions (indel) and noncoding substitutions (Xiromerisiou *et al*, 2020). Also large gene/chromosomal deletions leading to loss of the *SACS* gene have been described (Terracciano *et al*, 2009).



Introduction Figure 15. ARSACS-causing mutations are spread throughout the whole SACS gene. *Representation of SACS sequence variants. Squares indicate missense; downward triangles indicated insertions/duplications; upward triangles indicate small deletions. Red indicates pathogenic variations; orange indicates likely pathogenic variations; yellow indicates uncertain variations. Adapted from (Synofzik et al, 2013) used under the Creative Commons CC-BY 2.0 license.*

Generally, ARSACS molecular pathology has always been regarded as a loss-of-function mechanism, also given its autosomal recessive pattern. While truncating mutations are expected to lead to loss of sacsin protein, missense mutations have traditionally always been proposed to likely cause instability or misfolding of the protein, reducing its function or half-life, or loss of the function of relevant domains, also based on the evolutionary conservation of the affected residues (Romano *et al*, 2013). However, functional analyses have never been performed to prove these hypotheses, especially in patients' cells. This was a major issue in ARSACS, given both the high prevalence of missense mutations and the lack of clear genotype-phenotype correlation (as detailed below) (Vermeer *et al*, 2020), which I contributed to assess thoroughly in my PhD project. Before dealing with genotype-phenotype correlation in ARSACS, I will briefly describe major clinical manifestations.

3.2 – ARSACS clinical manifestations

From a clinical point of view, ARSACS is characterized by cerebellar ataxia (78.9% of patients), spasticity of lower and upper limbs (78.1%) and sensory-motor peripheral polyneuropathy with demyelinating or axonal degeneration features (73.7%) (Vermeer *et al*, 2020; Xiromerisiou *et al*, 2020); usually the first occurring sign is progressive cerebellar ataxia, which is followed by spasticity and pyramidal signs and finally by peripheral neuropathy. The typical French-Canadian phenotype is much more homogeneous (Bouhlal *et al*, 2011; Xiromerisiou *et al*, 2020), with all patients presenting the triad clinical manifestations, but the discovery of many cases throughout the world has expanded the clinical spectrum, showing much higher phenotype variability. Indeed, outside French-Canadian patients, 71.1% of patients show the characteristic symptoms, but with many cases that present cerebellar ataxia and neuropathy, but no spasticity (Synofzik *et al*, 2013; Aida *et al*, 2021); in some cases, neither spasticity and pyramidal signs, neither neuropathy were

reported (Shimazaki *et al*, 2005); finally, in the most atypical presentations ever reported, the first and main clinical sign is peripheral neuropathy, with no spasticity and pyramidal signs and with mild or even absent ataxia (Vermeer *et al*, 2020; Vill *et al*, 2018).

Other typical ARSACS signs include: distal amyotrophy (likely as consequence of neuropathy), limb weakness, sensory loss, pyramidal signs, cerebellar eye manifestations (i.e., nystagmus) and dysarthria (likely a consequence of ataxia) which results in slurred speech during the childhood which turns incomprehensible by adulthood (Bouchard *et al*, 1979). Additional atypical characteristics are intellectual disability, urinary disfunction, epileptic disorders and hearing loss, present with lower frequency (Xiromerisiou *et al*, 2020). The clinical report by Xiromerisiou based on 222 ARSACS patients outside Canada indicate a mean for the age at onset of three years, ranging between six months and 40 years (the average disease onset in Canadian patients is 1.5 years) (Xiromerisiou *et al*, 2020).

Progressive degeneration of the cerebellar vermis has been commonly documented in patients who underwent magnetic resonance imaging (MRI) (Bouchard *et al*, 1979; Bouhlal *et al*, 2011; Synofzik *et al*, 2013; Vermeer *et al*, 2020; Xiromerisiou *et al*, 2020). Moreover, post-mortem brain analysis from ARSACS patients and MRI studies revealed a remarkable atrophy of superior and middle components of the cerebellar vermis (superior and middle - 60,8% of patients), associated with the early loss of PCs. In contrast, the cerebellar hemispheres are less affected by atrophy. Other examinations revealed bilateral demyelination of both the corticospinal tract (likely accounting for spasticity and pyramidal signs common in ARSACS patients) and the dorsal spinocerebellar tract. Ocular coherence tomography (OCT) permitted also to detect an increased thickness of peripapillary Retinal Nerve Fiber Layer (RNFL) in ARSACS patients, which is uncommon in other forms of ataxia, both autosomal recessive cerebellar ataxia (ARCA) and spinocerebellar ataxia (SCA) (Borruat *et al*, 2017; Desserre *et al*, 2011; Garcia-Martin *et al*, 2013; Pablo *et al*, 2011; Parkinson *et al*, 2018; Ricca *et al*, 2019; van Lint *et al*, 2016; Vingolo *et al*, 2011; Yu-Wai-Man *et al*, 2014; Rezende Filho *et al*, 2021). This feature has been observed, although to a lesser extent, also in carriers of ARSACS mutations (Parkinson *et al*, 2018; van Lint *et al*, 2016). ARSACS diagnosis includes MRI, fundoscopy, OCT, neurological evaluation and sensory and nerve conduction studies. However, in light of the high clinical variability among patients and existence of common symptoms shared by other spinocerebellar ataxia, the ultimate diagnosis is made by genetic testing in order to identify mutations in the *SACS* gene (Pilliod *et al*,

2015). At the moment, no disease-modifying therapies are available for ARSACS patients.

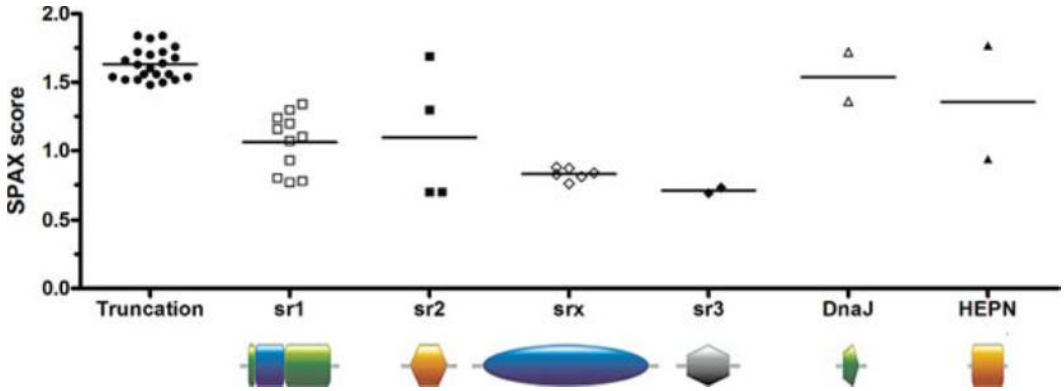
3.3 – Genotype-Phenotype correlation in ARSACS

Given the high clinical variability, especially outside the French-Canadian patients, genotype-phenotype correlation has been a controversial issue in the field. Greater clinical variability is associated with specific characteristics such as age of onset, as well as ocular and retinal manifestations. High variability is also observed in cases where patients exhibit atypical symptoms, that have been sporadically reported and are not deeply explored in clinical reports, for example intellectual disability, hearing impairment, and epilepsy features (Vermeer *et al*, 2020). These variations do not correlate with specific mutations. Variability has been observed even in the presence of the same mutation. As an example, one mutation was found to segregate in two ARSACS Tunisian families: in one family the disease appeared at the age of 3 and was associated with skeletal abnormalities, whereas in the other family the onset was after age 10, and patients did not show skeletal problems. In contrast, a study conducted over 23 German patients from 16 different families that had 16 different mutations, shown a very homogeneous clinical phenotype (Bouhlal *et al*, 2011).

There is not a clear genotype-phenotype correlation also considering the type or the localization of mutations and disease severity, as any type of mutations that have been observed spread randomly all over the *SACS* gene. Patients with large gene/chromosomal deletions (Terracciano *et al*, 2009), that lead to loss of *SACS,* have similar phenotype to those that harbour point mutations - insertion/deletions (indels) or missense-substitutions (**Introduction Fig. 15**) (Synofzik *et al*, 2013). The gigantic exon 10 contains 71% of mutations, then exon 8 followed with 10.8%, exon 9 with 2%, exon 7 with 1.5%, exon 6 with 0.5%, and finally exon 3 with 0.5% (Xiromerisiou *et al*, 2020).

Few systematic reviews tried to assess the issue. In a comprehensive work of all *SACS* mutations known up to 2012, Romano et al. found out that missense mutations in different sacsin domains, in homozygosis or in heterozygosis with truncating mutations (nonsense substitutions or indels or large gene deletions), were associated with differential average clinical severity in the patients bearing them, with the J domain being associated with higher average severity score (**Introduction Fig. 16)**; the average clinical severity in patients carrying these missense mutations was lower than in patients carrying only truncating mutations in both alleles. These results were explained by hypothesizing that truncating mutations are predicted to lead to complete loss of function of sacsin protein; whereas missense mutations would

differentially impact sacsin function based on the domain affected, with the J domain being the most relevant for sacsin function (Romano *et al*, 2013). However, although this work was valuable in providing insights that the novel discovered sacsin-distinctive repeats are functional, it was limited regarding the conclusions on genotype-phenotype correlation. First of all, it was qualitative with no statistical tests reported, and rather confirms the high variability of disease severity associated with missense mutations even in the same domains and inter domains (with very high severe scores also for many missense mutations located in other domains other than the J domain); moreover, the overall impact on sacsin protein stability or amount of each missense mutation was not taken into consideration, not even with bioinformatic pathogenicity score prediction; also, they did not take into account patients with heterozygote missense mutations in different domains.



Introduction Figure 16. Genotype-phenotype correlation in ARSACS. *Composite spastic ataxia (SPAX) score (which evaluates the spasticity and ataxia severity of patients) is reported for patients carrying a missense mutation in charge of different sacsin domains, in homozygosis or in heterozygosis with a truncating mutation (which is expected to lead to protein absence); SPAX scores for patients carrying truncating mutations in both alleles are reported for comparison ("truncation" on the x-axis). Horizontal lines indicate mean values. Adapted from (Romano et al, 2013) copyright to John Wiley and Sons, used with permission, license number 5516610185928.*

In another recent systematic work, Xiromerisiou et al. evaluated all *SACS* mutations known up to 2019 all over the world; they calculated computationally the pathogenicity score of each mutation based on algorithms that account for sequence, structure information and phylogeny. The pathogenicity score was reported to be significantly correlated with the age of onset of the disease, as well as with almost all clinical, radiological and ophthalmological characteristics of the patients, including ataxia. However, this study was limited to computational prediction of mutations' pathogenicity, especially based on conservation parameters, and molecular and functional data were not reported, so that the information on how missense mutations affect sacsin protein levels or functions is still missing. Moreover, in order

to make statistical correlations, the authors arbitrarily subdivided the pathogenicity score into three categories (likely, mild and highly pathogenic), which represents a quantitative limitation in the study (Xiromerisiou *et al*, 2020).

In my thesis project I assessed the issue of genotype-phenotype correlation, quantifying the levels of sacsin protein and investigating sacsin turnover in fibroblasts patients' cells carrying a panel of 19 mutations in different combinations, from large gene deletions to heterozygote compound with two missense mutations (See **Results Section 1**).

4 - Functional studies of ARSACS pathophysiology in cellular models

Introduction Section 2 highlighted the hypothesis that this protein is involved in protein quality control. Moreover, our lab and other labs provided data suggesting that sacsin is involved in the regulation of cytoskeletal remodeling and mitochondrial function, as described below.

4.1 - Intermediate filament remodeling

In cell and animal models of ARSACS, a distinctive abnormal remodeling of intermediate filaments (IFs) has been observed. However, before showing these results, I need to provide some information on IFs biology.

Basic concepts about intermediate filaments (IFs)

IFs are one of the three main cytoskeletal components together with microfilaments and microtubules (Kornreich *et al*, 2015). There are ~70 different human cell type-specific IF proteins divided into six subtypes (IFs Type I-VI) (Snider & Omary, 2014) (**Introduction Fig. 17**), making this class of proteins much more diverse than the other two cytoskeleton branches. IFs are also peculiar as they are only found in metazoans and it is the only cytoskeleton present inside the nucleus (nuclear lamina) (Snider & Omary, 2014).

Cell types (IF type)	IF	Disease associations
All nucleated cells (V)	Lamins (Lamin A, lamin B and lamin C)	Cardiomyopathy, muscular dystrophy, lipodystrophy, leukodystrophy and progeroid syndrome (for example, Hutchinson–Gilford progeria syndrome)
Epithelial cells (I and II) (Type I: K9–K28, K31–K40) (Type II: K1–K8, K71–K86)	Keratins (Hair, epidermal and simple epithelial)	Skin fragility (for example, epidermolysis bullosa simplex) and other skin disorders, hair and nail disorders, corneal dystrophy and predisposition to liver diseases
Mesenchymal cells (III)	Vimentin	Cataract
Glia cells (III)	Glial fibrillary acidic protein	Alexander disease
Neurons (III and IV)	Light, medium and heavy neurofilaments, peripherin and α-internexin	Charcot–Marie–Tooth disease, predisposition to amyotrophic lateral sclerosis and Parkinson's disease
Myocytes (III and IV)	Desmin, synemin and syncoilin	Myopathy and muscular dystrophy
Developing and regenerating cells (IV)	Nestin	None reported
Lens (VI or orphan)	Filensin and phakinin	Cataract

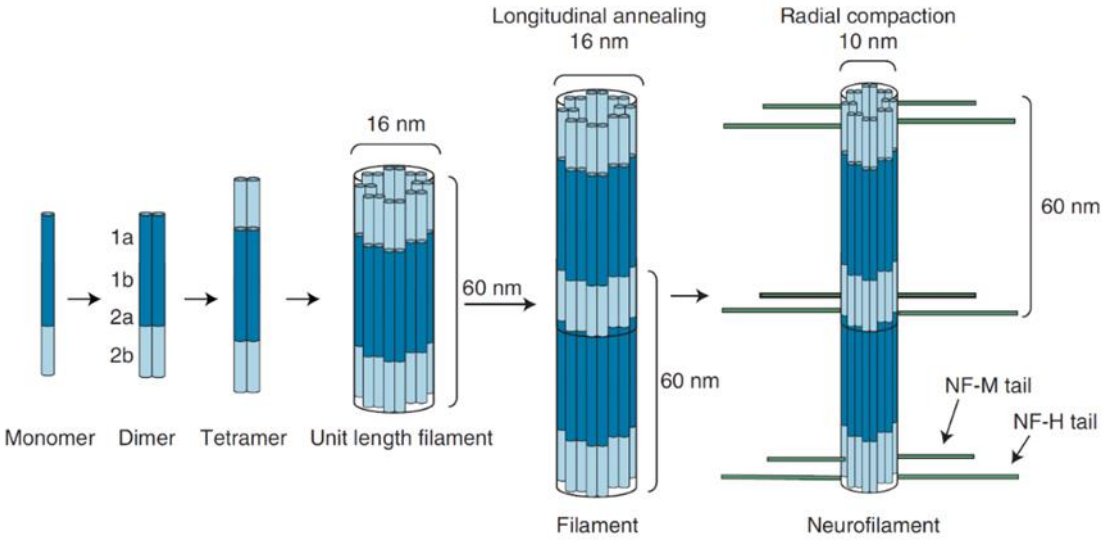
IF, intermediate filament; K, keratin.

Introduction Figure 17. Overview of IFs proteins in human cells and tissues. *Protein subtypes with their expression pattern and involvement in human disease. Adapted from (Snider et al, 2014), reused with permission License number 5472410975789, 19 Jan 2023.*

All IFs proteins share a tripartite structure: a head domain at the N-terminal, a central α-helical rod domain and a tail domain at the C-terminal. The N-terminal and C-terminal domains vary greatly in terms of sequence among different IFs proteins, whereas the central rod domain is conserved (Snider & Omary, 2014). IFs proteins

assemble together to generate IFs through a multi-step process. Initially, two IFs proteins form polar coiled-coil dimers with their rod domains in the same orientation; then two dimers dimerize in antiparallel way to form staggered nonpolar tetramers; up to now, all intermediate structures are generally soluble oligomers; then eight tetramers bind laterally in parallel way into precursors which are not soluble in nonionic detergents and are called unit-length filaments (ULFs). Indeed, these precursors anneal end-to-end forming at first immature long filaments that are 16nm in diameter (elongation). Radial compaction of the immature filament into the canonical 10-nm intermediate filament diameter follows (Gentil *et al*, 2015). However, this process is slightly different for nuclear IFs (lamins) (Snider & Omary, 2014).

Vimentin is the major IF subunit in a variety of cell types, including mesenchymal and undifferentiated neuronal-precursors cells (Snider & Omary, 2014). In particular, while neuronal precursor cells express preferentially vimentin or nestin (Yabe *et al*, 2003; Bernal & Arranz, 2018), mature neurons express mainly neurofilaments (NF). NF subunits form heteropolymers with four subunits: neurofilament light (NFL), neurofilament medium (NFM), and neurofilament heavy (NFH); other subunits are α-internexin in the central nervous system and peripherin in the peripheral nervous system (Bomont, 2021). Dimers form between NFL and itself or between NFL and either NFH or NFM. In turn, tetramers are found to be of two types: those containing NFL and NFH and those containing NFL and NFM (Cohlberg *et al*, 1995). Generally, NFH and NFM do not polymerize between themselves *in vivo*. This is in agreement with the fact that in 10-nm filaments, NFL is the most abundant and forms the core, whereas NFH and NFM are lateral and less abundant, and form typical side arms with their long C-terminal tails that extend radially from the 10-nm filaments (**Introduction Fig. 18**). Recently, it has been discovered that NFL also dimerizes with α-internexin in the CNS (Yuan *et al*, 2017; Bomont, 2021; Gentil *et al*, 2015).



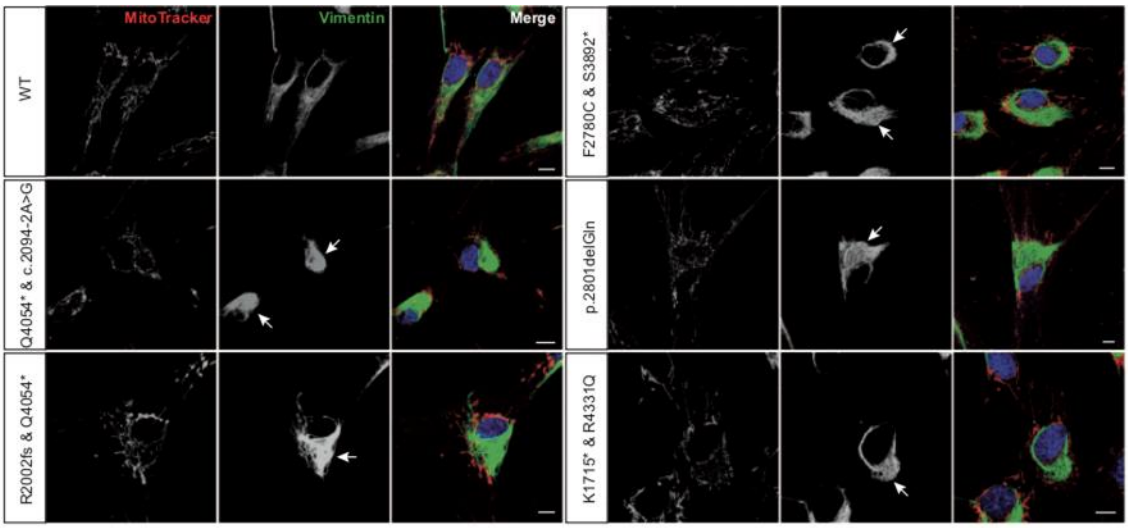
Introduction Figure 18. Intermediate filaments and NF assembly. *Monomers of NF proteins form parallel coiled-coil homo- or hetero-dimers. Two dimers then form staggered antiparallel tetramers. The lateral association of eight tetramers forms unit-length filaments (ULFs) which bind head to head during filament elongation. The resulting filaments are therefore nonpolar. Radial compaction achieves ultimately a 10-nm diameter structure which is distinctive of IFs. NFH and NFM form typical side arms with their long C-terminal tails that extend radially from the 10-nm filament. These radial tails are extremely negatively charged, as they are enriched in Glutamate residues and phosphorylation modifications. Adapted from (Yuan et al, 2017), reused under Permission; copyright to Cold Spring Harbor Laboratory Press.*

NFM and NFH stand out from the other NF subunits due to the exceptional length of their tail domains. These regions contain multiple Lys-Ser-Pro (KSP) repeats undergoing extensive phosphorylation regulated by different kinases and phosphatases (Holmgren *et al*, 2012; Yuan *et al*, 2017). IF proteins undergo different post-translational modifications exerting different effects on IF dynamics. Among them, phosphorylation plays an important role in regulating IF assembly. In this regard, depending on the subunit and the position of modified residues within the IF proteins, phosphorylation may exert opposite effect. For instance, vimentin or NFL head domain phosphorylation is associated with filament disassembly, whereas NFH tail domain phosphorylation is thought to promote interactions of NF subunits with each other and with other cytoskeletal proteins via the NFH tail; this leads to the formation of a lattice that provides structural integrity to mature axons (Paulin *et al*, 2022; Yuan *et al*, 2017).

IF remodeling in ARSACS

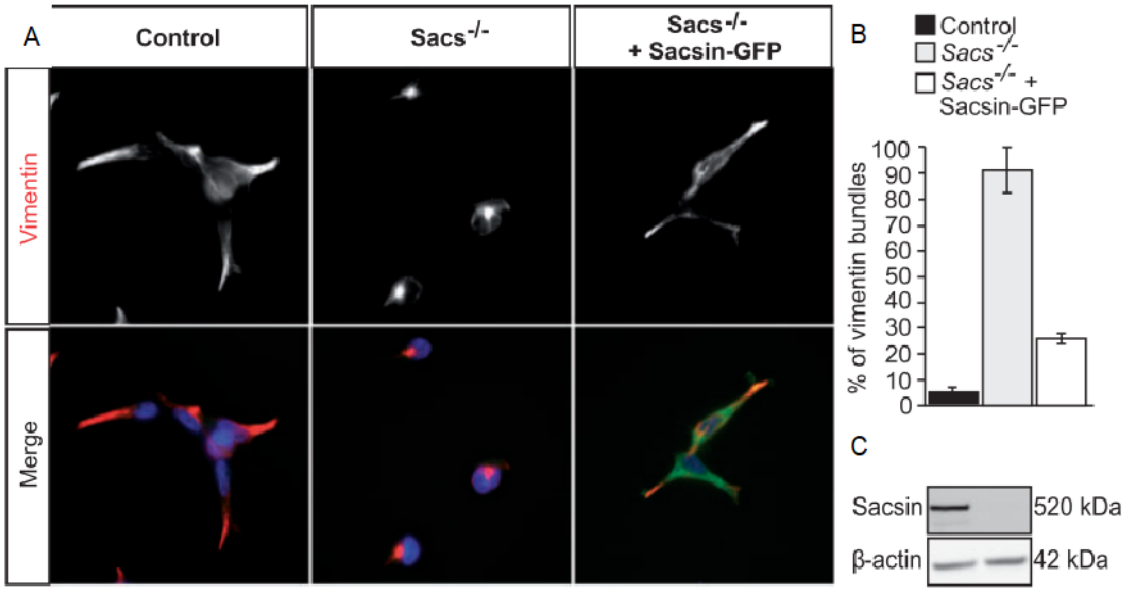
As a collaborative effort with other groups, our lab shown that the absence of sacsin causes a dramatic remodeling of vimentin, the major IF protein expressed in fibroblasts. Confocal imaging revealed that vimentin filaments were bundled in perinuclear accumulations in ARSACS patient fibroblasts, whereas vimentin was

evenly distributed throughout the cytoplasm in control cells (**Introduction Fig. 19**) (Duncan *et al*, 2017).



Introduction Figure 19. Abnormal remodeling of vimentin IFs in ARSACS patients' fibroblasts. *Representative images by confocal microscopy of a mitochondrial-specific dye (MitoTracker, in red) and vimentin (green) in five ARSACS patients' fibroblast cell lines compared to controls from healthy individuals. Cells were counterstained with DAPI. Arrows indicate examples of vimentin remodeling. Adapted from (Duncan et al, 2017) used under Creative Commons CC BY license.*

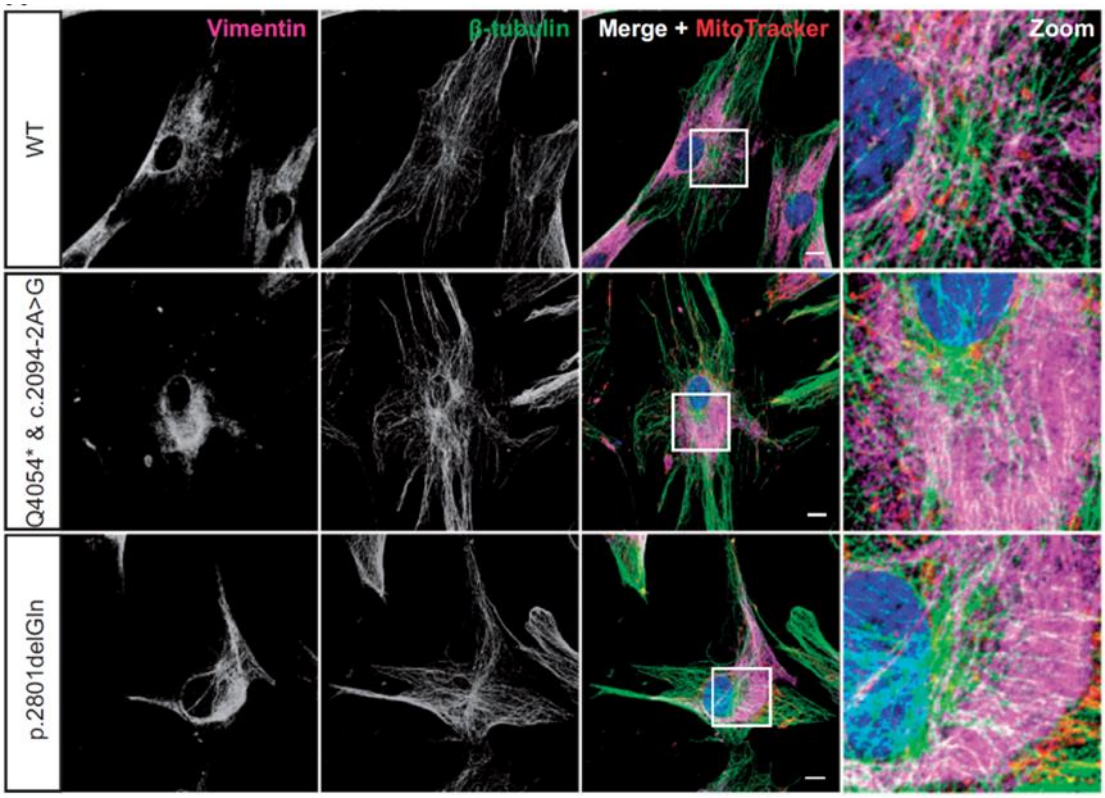
This result was further confirmed in *SACS*$^{-/-}$ HEK293 cell line generated by CRISPR/Cas9; indeed, these cells exhibited perinuclear collapse of the vimentin network as observed in ARSACS patients' fibroblasts. Interestingly, these perinuclear bundles of vimentin were rescued by transfection of a plasmid for expression of full-length sacsin-GFP (**Introduction Fig. 20**) (Duncan *et al*, 2017).



Introduction Figure 20. Abnormal accumulations of vimentin in the absence of sacsin. *A. Representative images by confocal microscopy of vimentin (red) and GFP (green) in SACS$^{-/-}$ HEK293 cells generated by CRISPR/Cas9 and transfected with a plasmid encoding full-length sacsin-GFP. Cells were counterstained with DAPI. B. Quantification of the percentage of cells with abnormal vimentin network (collapsed bundle); results are expressed as mean ± SEM. C. WB analysis of sacsin levels of the SACS$^{-/-}$ clone referred to in A and B. Adapted from (Duncan et al, 2017) used under Creative Commons CC BY license.*

4.2 - Altered mitochondrial dynamic, bioenergetic, and transport

Another interesting evidence emerging from studies in cellular models lacking sacsin is the alteration of mitochondrial dynamics, functionality, and transport in neurons. Concerning mitochondrial dynamics, in siRNA-mediated *SACS* knockdown SH-SY5Y cells and patient fibroblasts, the mitochondrial network appears more fused than in the wild-type control conditions. Patients' fibroblasts display sometimes bulbed mitochondria, which are a typical sign of mitochondrial hyperfusion (Girard *et al*, 2012). In addition, a recent work from our lab shown also that hyperfused mitochondria are mislocalized in areas peripheral to the abnormal accumulations and bundles of vimentin in ARSACS patients' fibroblasts (**Introduction Fig. 21**) (Duncan *et al*, 2017). This alteration in mitochondrial morphology was proposed to occur through the defective recruitment of the fission machinery (and in particular Drp1) to mitochondria in the absence of sacsin (Bradshaw *et al*, 2016); however, interaction between sacsin and Drp1 in physiological conditions remains controversial.

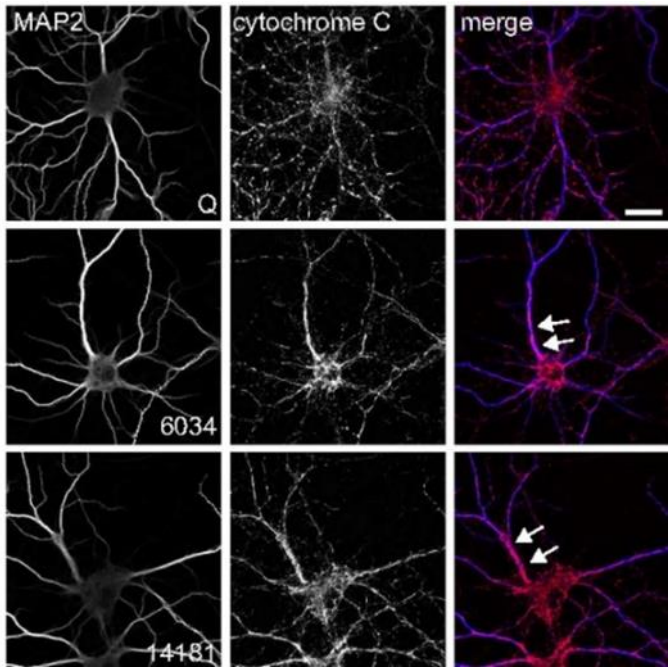


Introduction Figure 21. Mitochondria mislocalize at the periphery of vimentin bundles in ARSACS patients-derived fibroblasts. *Representative images by confocal microscopy of MitoTracker (red), vimentin (pink) and β-tubulin (green) in fibroblasts from ARSACS patients and healthy individuals as control. Right images show magnification of the regions indicated by the white squares, highlighting displaced mitochondria in ARSACS fibroblasts. Adapted from (Duncan et al, 2017) used under Creative Commons CC BY license.*

It has been also shown that the absence of sacsin impacts on mitochondrial bioenergetics. Girard et al. reported first that, at steady state, both siRNA-mediated *SACS* knockdown in human neuronal-like SH-SY5Y cells and ARSACS patients-derived fibroblasts show reduced mitochondrial membrane potential, seen by lower TMRM intensity signal, indicating a general mitochondrial damage and altered functionality (Girard *et al*, 2012). Moreover, Bradshaw et al., demonstrated an impairment of mitochondrial metabolism in the same cellular models, with reduced oxygen consumption rate of basal and maximal respiration, as well as ATP production; by microarray analysis, they also reported a reduction of the expression of genes encoding the oxidative phosphorylation (OXPHOS) complexes and an increase in the expression of genes related to oxidative stress. These results may suggest accumulation of reactive oxygen species (ROS) and oxidative stress as a result of mitochondrial damage (Bradshaw *et al*, 2016).

The absence of sacsin, also affects mitochondrial transport in neurons. Indeed, siRNA-mediated *SACS* knockdown in cultured murine hippocampal neurons shown a

reduced number of mitochondria in distal dendrites and an abnormal accumulation and aggregation of mitochondria in the soma and proximal regions of dendrites (**Introduction Fig. 22**). In these neurons, dendrites' morphology was altered (with lower number and thinner diameter) with respect to controls.



Introduction Figure 22. Improper distribution of mitochondria in neurons in the absence of sacsin. *Representative images by confocal microscopy of immunofluorescence cytochrome C (mitochondrial marker, in red) and Map2 (purple) in siRNA-mediated Sacs knockdown hippocampal neurons. Cultured hippocampal neurons transfected with Sacs siRNAs (6034 and 14181) and scrambled siRNA (Q). Arrows indicate accumulated mitochondria in proximal dendrites. Adapted from (Girard et al, 2012) used under the Creative Commons CC-BY-NC license.*

In conclusion, ARSACS cellular models shown two main pathological phenotypes at cellular level: IF remodeling and altered mitochondrial dynamics, bioenergetics and trafficking. However, how these phenotypes are mechanistically linked with each other and to sacsin function remains an open issue; also their relevance in causing PN death in ARSACS has not been addressed. Mitochondrial functional studies were limited to *in vitro* cellular models, namely ARSACS patients' fibroblasts and SH-SY5Y cells, or *ex vivo* to hippocampal murine *Sacs*$^{-/-}$ neurons, which are not the most and primarily affected neural type in ARSACS.

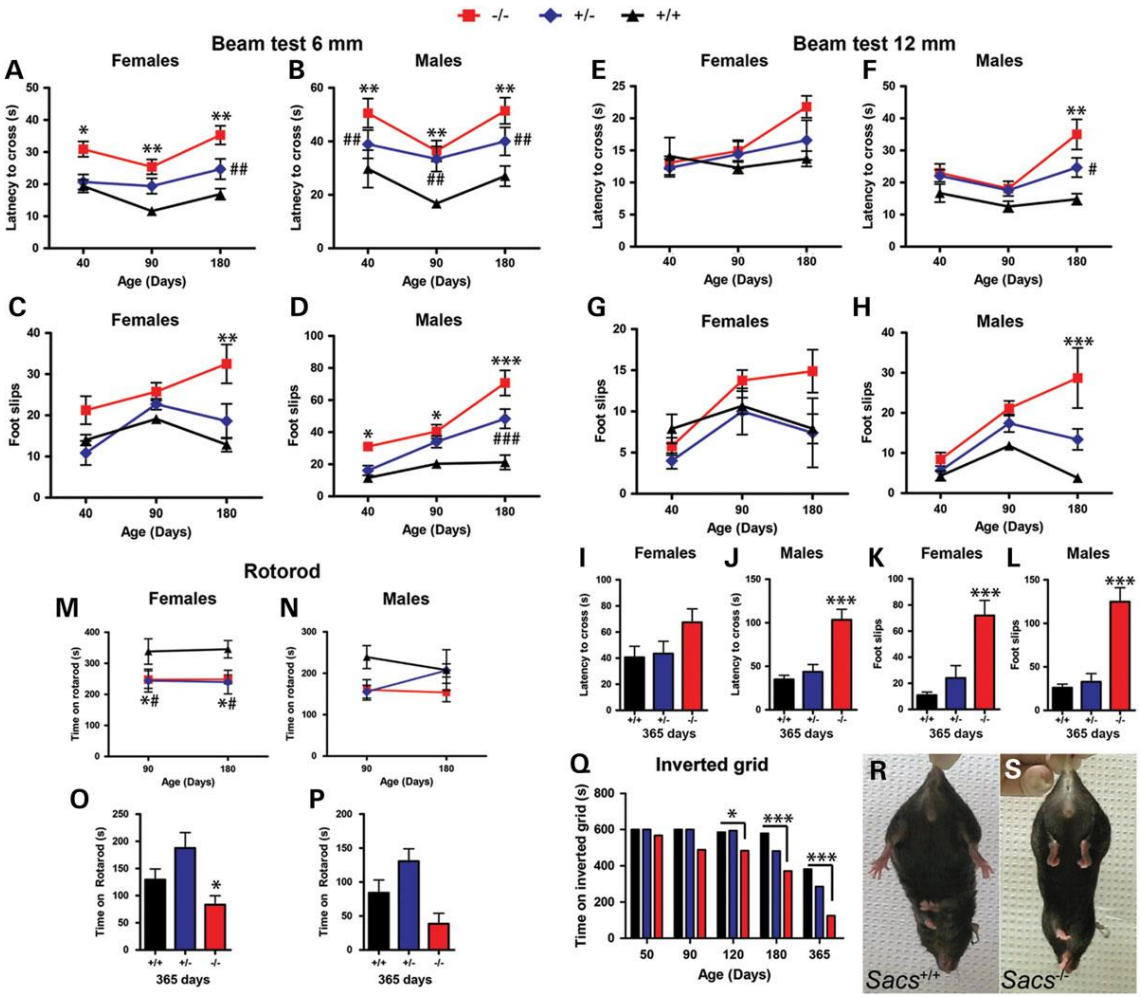
In the **Results Section 2**, I will describe NF bundling observed in the absence of sacsin; this is likely the first event that occurs in the absence of sacsin in PNs and this in turn impairs the transport of mitochondria along the highly extended and arborized dendritic compartment in PNs, thus explaining the link with a mitochondrial component in ARSACS pathogenesis.

5 - Mouse models of ARSACS pathophysiology

Two mouse models that recapitulate the ARSACS phenotype have been generated: the null *Sacs*$^{-/-}$ and the *Sacs*^{R272C} knock-in mouse, which inserts a patient missense mutation into the *Sacs* homologue gene.

5.1 - The Sacs$^{-/-}$ *mouse model*

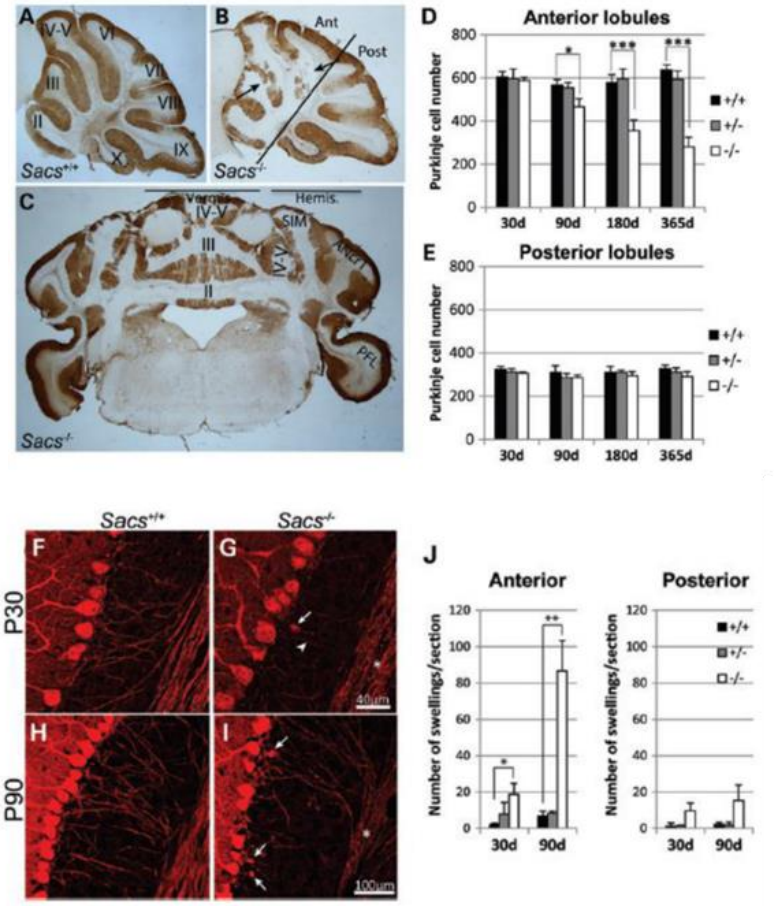
Both bioinformatics and *in vitro* approaches illustrated so far have intrinsic limitations as they cannot assess or predict the function of sacsin protein in the context of a complex living organism. Moreover, studies *in vitro* were performed in cell types that are not primarily affected in ARSACS. Hence, to study sacsin function in a physiological context, *Sacs*$^{-/-}$ mice were generated by traditional gene targeting in embryonic stem cells replacing the last *Sacs* exon with the IRES-βGal cassette. Their characterization was assessed by (Larivière *et al*, 2015). *Sacs*$^{-/-}$ mice start to show early-onset ataxia and motor deficits starting from 40 days of age, which then becomes more evident at three months of age, when the beam walking (BW) and rotarod tests underline balance defects and general motor incoordination, respectively. These deficits progressively worsen, until, between seven and fifteen months of age, the abnormal gait and tremors become typical features of the *Sacs*$^{-/-}$ mice (**Introduction Fig. 23**). At four months of age, these mice also show muscular wasting and weakness, as recorded by inverted grid test, phenocopying ARSACS patients (Larivière *et al*, 2015).



Introduction Figure 23. Phenotype characterization of Sacs$^{-/-}$ mice. *A-P. Results of balance beam and rotarod tests of motor coordination at 40, 90 and 180 days of age. Q. Inverted grid test of mice from 50 to 365 days. R-S. Representative hindlimb clasping reflex exhibited by one year old Sacs$^{-/-}$ (S) and wild-type (R) mice. Adapted from (Larivière et al, 2015) copyright to Oxford University Press, used under permission, license number 5516600912896.*

PN loss begins in *Sacs*$^{-/-}$ mice at three months of age in the anterior medial cerebellum, similarly to ARSACS patients (**Introduction Fig. 24 a-e**) (Larivière *et al*, 2015). In particular, one recent paper shows that cell death occurs predominantly in PNs that do not express aldolase C (aka zebrin) (Toscano Márquez *et al*, 2021). However, unlike patients, PNs loss in *Sacs*$^{-/-}$ mice is not limited to the vermis, but it spreads to cerebellar hemispheres. Moreover, PN axons show progressive swelling starting from one month of age, suggesting that there is an axonal degeneration that precedes the loss of the cell body (**Introduction Fig. 24 f-i**). Although silver staining of the corticospinal tract reveals signs of neurodegeneration implying ongoing spasticity, histological examination does not show morphological alteration or reduction of axon number in mice up to 2 years of age, unlike ARSACS patients. In contrast, peripheral neuropathy is observed in *Sacs*$^{-/-}$ mice as reduction (of about

25% in respect to controls) of spinal motor neurons total number and myelinated axons of diameter larger than 7-10 μm with concomitant increase of number of myelinated axons of smaller dimension (3-4 μm) at 2 years of age. As a consequence, muscle wasting in lower limbs is also observed at later stages. Therefore, these events are observed at later time points, in agreement with the fact that the ataxic phenotype is the primary ARSACS clinical manifestation.

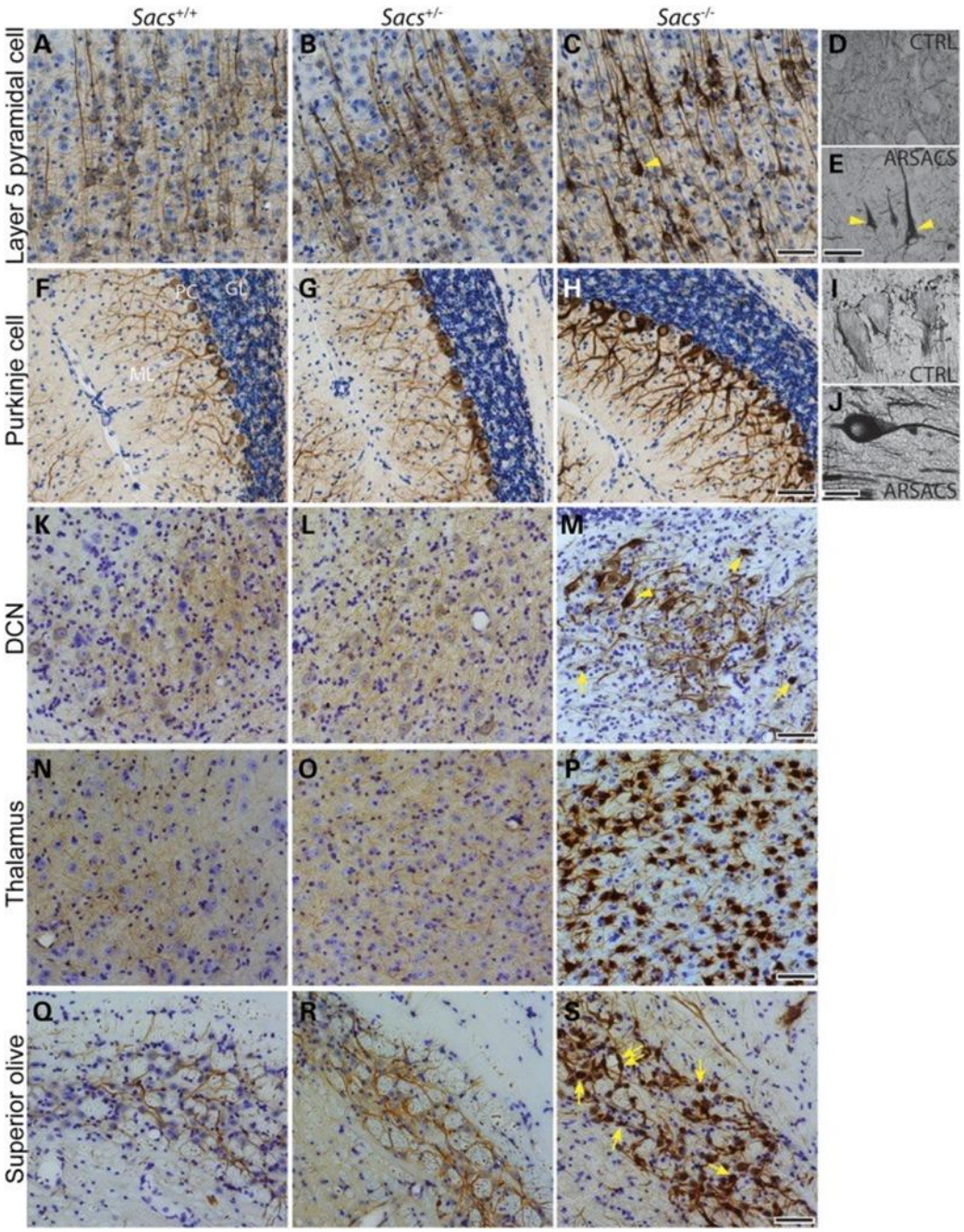


Introduction Figure 24. Progressive PNs loss and axonal swellings in the Sacs-/- mouse. *A-E. Calbindin immunohistochemistry on mid-sagittal brain sections from 365-day-old Sacs$^{+/+}$ (A) and Sacs$^{-/-}$ (B) mice, with PNs number count in the cerebellar anterior (D) and posterior (E) lobules. G-J. Calbindin labelling of cerebellar parasagittal brain sections of 30-day-old Sacs$^{-/-}$ mice show dystrophic axons (asterisk and arrowheads in G) in Sacs$^{-/-}$ mice compared with controls (F-I), and relative quantifications (J). Adapted from (Larivière et al, 2015) copyright to Oxford University Press, used under permission, license number 5516600912896.*

In the Sacs$^{-/-}$ model, IF dynamics were also evaluated focusing on NF which, as mentioned above, are composed by different subunits and can undergo phosphorylation and dephosphorylation. Immunohistochemistry in *Sacs$^{-/-}$* mice compared to wild-type controls at 180 days of age has revealed that they show general and spread accumulation of NFH all over the brain at this late stage, seen

with a pan-NFH antibody that recognizes both phosphorylated and non-phosphorylated NFH subunits; regions in which accumulation was seen include proximal dendrites and soma in many areas of the central nervous system, especially in thalamus, PNs in cerebellum, DCN and superior olivary nucleus (**Introduction Fig. 25 a-c, f-h, k-s,** respectively) (Larivière *et al*, 2015). Strikingly, the alteration of NF distribution has been found also in ARSACS patient neurons after brain autopsies; in particular, accumulation of NFH in proximal dendrites has been observed in corticospinal neurons of layer 5 and in PNs from an ARSACS patient (**Introduction Fig. 25 d-e, i-j,** respectively) (Larivière *et al*, 2015).

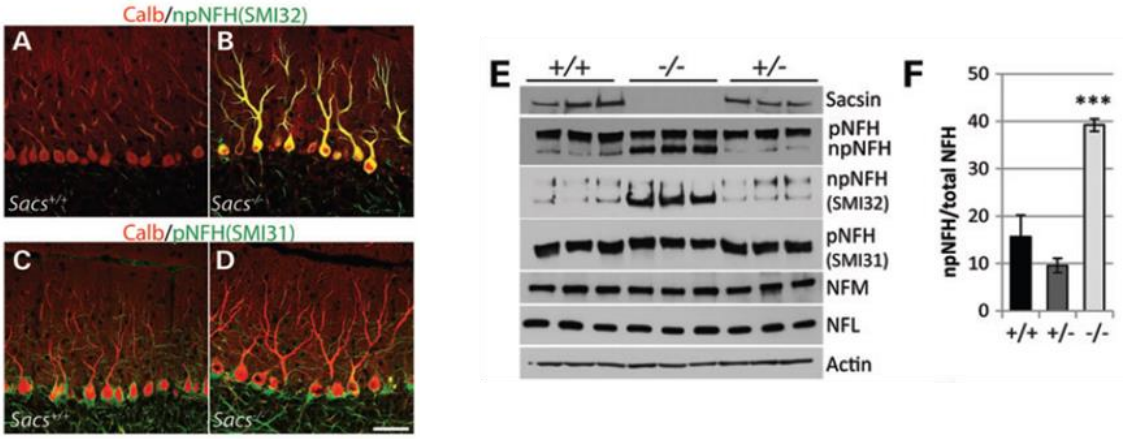
This evidence has been further confirmed by immunolabeling with an antibody against NFH in 4-week-old dissociated spinal cord cultures: bundling of NFH was detected in the soma of $Sacs^{-/-}$ motor and sensory neurons (Duncan *et al*, 2017).



Introduction Figure 25. Accumulation of NFH in immunohistochemistry on Sacs$^{-/-}$ mouse and ARSACS brain. *Immunohistochemistry of sagittal sections of brain from 180 days-old Sacs$^{-/-}$ mice, Sacs$^{+/-}$ mice and controls (A, B, C, F, G, H, K, L, M, N, O, P, Q, R, S) and from the biopsy of an ARSACS patient's brain (E and J) and healthy individuals (D and I), stained with panNFH. Accumulation of NFH is different in several neuronal populations both in Sacs$^{-/-}$ mice and patients relative to control. Adapted from (Larivière et al, 2015) copyright to Oxford University Press, used under permission, license number 5516600912896.*

Additionally, at the same age, immunofluorescence of PNs layer in tissue sections derived from *Sacs$^{-/-}$* mice with antibodies specific for non-phosphorylated NFH (npNFH) (SMI32) shown increased signal in soma and dendrites in respect to WT mice, whereas staining with antibodies specific for phosphorylated forms (pNFH)

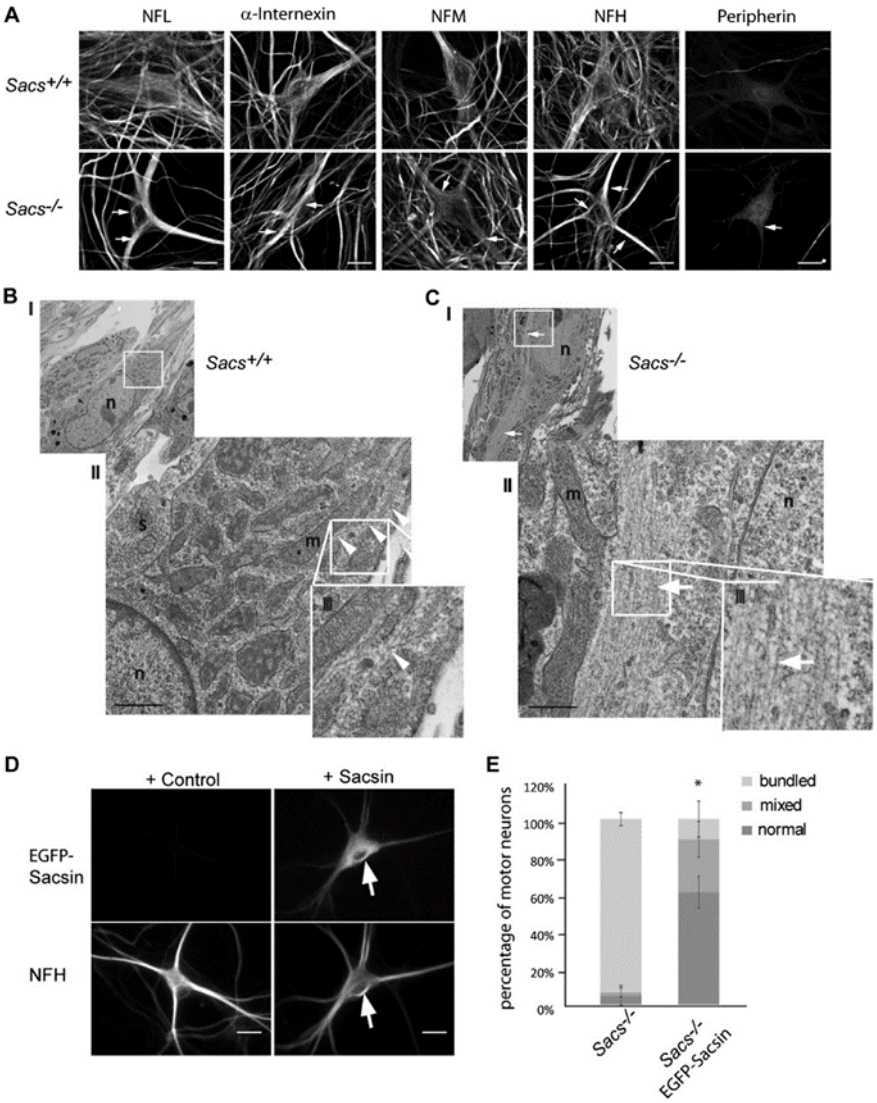
(SMI31) failed to show significant differences (**Introduction Fig. 26**) (Larivière *et al*, 2015). WB on cerebellar extracts probed with pan-NFH, SMI31 and SMI32 confirmed an increased npNFH to total NFH ratio in *Sacs*$^{-/-}$ mice relative to controls, and unchanged levels of pNFH (Larivière *et al*, 2015). In wild-type motor neurons the NF network is distributed uniformly in the soma and dendrites (while in dorsal root ganglia – DRG - sensory neurons lack dendrites). In *Sacs*$^{-/-}$ mice motor neurons, NF fibers fuse into bundles, whereas in DRG sensory neurons they form perinuclear large bundles as described for vimentin in ARSACS patients' fibroblasts (see **Introduction Section 4.1**) (Duncan *et al*, 2017).



Introduction Figure 26. npNFH accumulates in PNs in Sacs$^{-/-}$ mice. *A-D. Immunofluorescence of PNs from 180 days-old Sacs$^{-/-}$ mice and controls with antibodies directed against calbindin (red) and either npNFH (A-B) or pNFH (C-D) (green). E-F. Immunoblots of insoluble cytoskeletal fractions from cerebellum of Sacs$^{+/+}$, Sacs$^{+/-}$ and Sacs$^{-/-}$ mice (180 days-old) with pan-NFH, SMI31, SMI32, NFL and NFM antibodies and relative quantification of the ratio of npNFH over total NFH in different genotypes. Adapted from (Larivière et al, 2015) copyright to Oxford University Press, used under permission, license number 5516600912896.*

Gentil et al. further demonstrated the role of sacsin in regulating NF dynamics in the *Sacs*$^{-/-}$ mouse model (Larivière *et al*, 2015; Gentil *et al*, 2019). After reconfirming the presence of NF bundles in cultured spinal motor neurons from DRGs dissociated from *Sacs*$^{-/-}$ mice, they detected all the NF components in these bundles by immunohistochemistry: NFL, NFM, NFH, peripherin and α-internexin (**Introduction Fig. 27a**). Transmission electron microscopy shown NF bundles extending from around the nucleus and coursing through a dendritic process (**Introduction Fig. 27 b-c**); organelles, including mitochondria, were mislocalized to the periphery (Gentil *et al*, 2019), in line with what is observed in ARSACS patients' fibroblasts (Duncan *et al*, 2017). The microinjection of plasmids encoding full length sacsin GFP-tagged in 6-week-old *Sacs*$^{-/-}$ spinal cord DRG cultures, resolved NF bundles after two days (**Introduction Fig. 27 d-e**). Moreover, EGFP-sacsin was found to be in close

proximity to NF bundles, indicating a strong association. In addition, Fluorescence Recovery After Photobleaching (FRAP) experiments on NFH-GFP in motor neurons shown impaired but not absent turnover of NF bundles, compared to physiologically distributed NF turnover. In contrast, the turnover of normally distributed NF was comparable in *Sacs*$^{+/+}$ and *Sacs*$^{-/-}$ mouse cells, implying a secondary, rather than primary, defect, perhaps due to impaired access of necessary factors involved in the organization of the NF (Gentil *et al*, 2019).

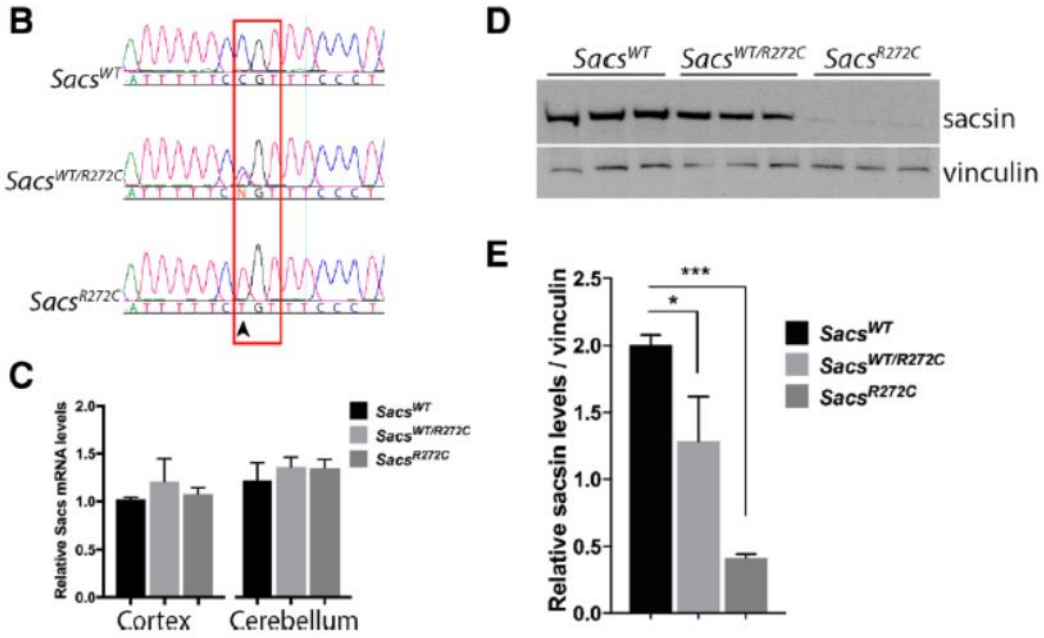


Introduction Figure 27. NF bundles that form in the absence of sacsin contain all NF subunits. *A. Representative images of motor neurons in 3-week-old dissociated spinal cord DRG cultures. B-C. Representative electron microscopy images of motor neurons from 6-week-old spinal cord DRG cultures (Sacs*$^{+/+}$ *and Sacs*$^{-/-}$*). D. Resolution of NF bundles in neurons upon overexpression of full-length sacsin by microinjection. E. Quantitation of the effect of EGFP-sacsin on the percentage of cells showing NF bundles or normal NF network in Sacs*$^{-/-}$ *motor neurons. Adapted from (Gentil et al, 2019) copyright to John Wiley and Sons, used with permission, license number 5516611158641.*

5.2 - The Sacs^{R272C} knockin mouse model

A novel *Sacs^{R272C}* (c.816C>T) knockin (KI) mouse model, that carries patients' R272C missense mutation in homozygosis, has been generated using traditional gene targeting techniques (Larivière *et al*, 2019). This mutation lies at the end of the Hsp90-like ATPase domain in the first sr1 subrepeat (Romano *et al*, 2013) and it was described in homozygosis in two cases in Canada (**Introduction Fig. 28**) (Thiffault *et al*, 2013).

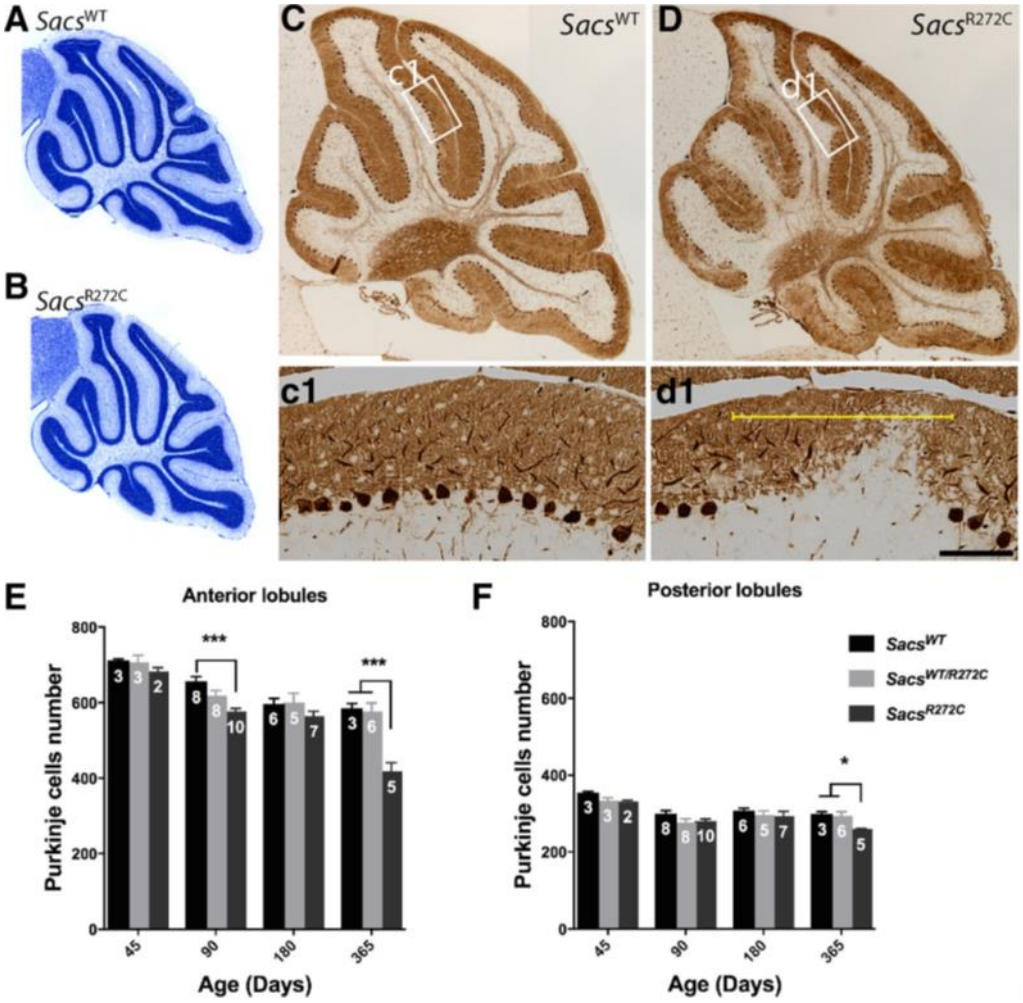
This novel mouse model presents with a strikingly reduced level of sacsin protein in the cerebellum, similarly to the null *Sacs$^{-/-}$* model; this data was argued by the authors likely to be due to effects of the mutation on protein folding, which determines its degradation and loss of function. We indeed provided a mechanistic explanation of sacsin protein reduction supported by data, by our studies of genotype-phenotype correlation in ARSACS patients' cells (See **Results Section 1**).



Introduction Figure 28. Molecular characterization of a novel Sacs^{R272C} KI mice. *B. Genomics analysis. C. qRT-PCR of Sacs mRNA from cortex and cerebellum. D-E. WB analysis of sacsin protein from cerebellum lysates and relative quantification. Adapted from (Larivière et al, 2019) copyright to John Wiley and Sons, used with permission, license number 5516610607370.*

Sacs^{R272C} mice show early balance deficits (mostly males) but milder muscle weakness and no general motor coordination impairments compared to *Sacs$^{-/-}$* mice. Nissl staining in P45 *Sacs^{R272C}* mice shows also normal cerebellar structure and lobulation with respect to age-matched controls (**Introduction Fig. 29 a-b**); strikingly, as in the null *Sacs$^{-/-}$* model, there is a significant PNs loss restricted to the

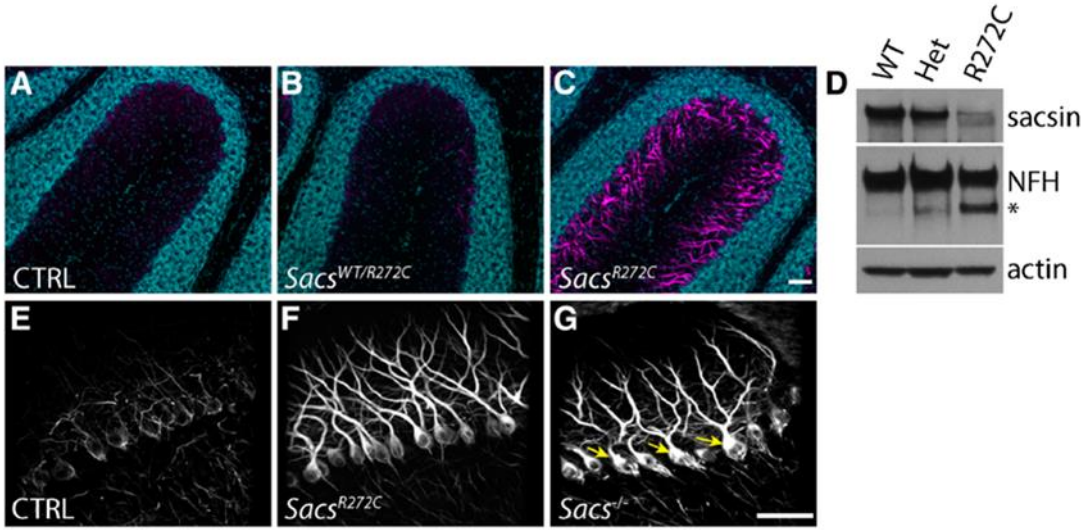
anterior lobules and starting at 90 days of age, which is progressive up to one year of age (**Introduction Fig. 29 c-d**), with the only difference being a slight loss of PNs in posterior lobules observed at one year in *Sacs*^{R272C} mice (Larivière *et al*, 2019).



Introduction Figure 29. Progressive PC loss in Sacs^{R272C} mice. *A-B. Nissl stain of vermal cerebellar sections from P45 Sacs^{R272C} (B) and controls mice (A). C-D. Calbindin immunolabeling on vermal sagittal brain sections from 300-day-old mice. E-F. Neuronal cell counts in the anterior (I to VI) and posterior (VII to X) lobules at different ages. Adapted from (Larivière et al, 2019) copyright to John Wiley and Sons, used with permission, license number 5516610607370.*

Sacs^{R272C} mice also show NF bundling similar to *Sacs*$^{-/-}$ mice, as observed by immunolabeling with pan-NFH antibody on sagittal cerebellar sections at 300 days of age (Larivière *et al*, 2019) (**Introduction Fig. 30 a-c,e-g**). NFH accumulation was observed also in somatodendritic compartments in several CNS neuronal populations, including neurons in layer II-III and V of the isocortex, cornu ammonis 1 (CA1), 2 (CA2) and 3 (CA3) pyramidal neurons of the hippocampal formation and thalamic neurons. Finally, WB analysis from insoluble cytoskeletal fractions from the

cerebellum of 300 days-old mice revealed an increase in the non-phosphorylated form of NFH in *Sacs*^{R272C} too (**Introduction Fig. 30d**).



Introduction Figure 30. Sacs^{R272C} exhibit NFH bundles in PNs soma and dendrites. *A-C. Immunolabelling of cerebellar sections from 300 days-old Sacs$^{+/+}$, Sacs$^{R272C/+}$ and Sacs^{R272C} mice with pan-NFH antibody (magenta); sections were counterstained with Hoechst (cyan blue). D. Immunoblots from insoluble cytoskeletal fractions from the cerebellum of 300 days-old Sacs$^{+/+}$, Sacs$^{R272C/+}$ and Sacs^{R272C} mice with pan-NFH antibody. The asterisk indicates non-phosphorylated NFH. E-G. NFH bundling at the same age in PNs from Sacs$^{+/+}$, Sacs^{R272C} and Sacs$^{-/-}$ mice, showing the same phenotype. Yellow arrows indicate NFH bundling in the soma. Adapted from (Larivière et al, 2019), copyright to John Wiley and Sons, used with permission, license number 5516610607370.*

In conclusion, *Sacs*$^{-/-}$ and *Sacs*^{R272C} mouse models well recapitulate the main alterations of ARSACS, and phenocopy each other. They exhibit ataxia due to cerebellar degeneration and PN loss; they also show neuropathy, and sequential muscle wasting although at a very later stage; also, spasticity seems to be less severe than in patients (Larivière *et al*, 2019). Moreover, both *Sacs*$^{-/-}$ and *Sacs*^{R272C} PNs have npNFH accumulation in their somatodendritic region. For this reason, they are suitable tools to further investigate ARSACS cytopathology and treatments.

In the next section I will discuss ongoing experimental therapeutic approaches in ARSACS and their limitations.

6 – Ongoing therapeutic approaches in ARSACS

So far, there are no drugs available for ARSACS that act on the cause of the pathogenesis, except for symptomatic treatments. Clinical research is also significantly lagging behind, as there are currently no clinical trials or any drugs that have been proven effective in preclinical models in published literature. However, some therapeutic and translational approaches are being experimentally explored.

6.1 – Approaches aimed at rescuing cellular phenotypes caused by the absence of sacsin

In one approach, Naef et al, proposed the null *Sacs*$^{-/-}$ zebrafish generated by genome editing as a tool for high-throughput screening of small molecules, and in particular repurposed drugs, that are known to improve glutamate metabolism, speculating that neurotransmission modulation could recover PNs degeneration; indeed, they tested the effects on locomotor function of specific neuroprotective agents (namely acetyl-DL-leucine and tauroursodeoxycholic acid) in *Sacs*$^{-/-}$ zebrafish larvae, although without any quantitative assessment of ataxic phenotype in this animal model (Naef *et al*, 2021). It is still to be assessed if this model recapitulates the cerebellar degeneration seen in ARSACS patients, as motor assessment as well as treatments were performed at an embryonal-larval stage in which the development of the zebrafish cerebellum is not completed. Also, the presence of NF bundles, which are the hallmark of ARSACS, has not been investigated in this model. Another issue on using this model is that, differently from mammals that express a single *SACS* gene, the Zebrafish genome has two different sacsin-like homologs, as well as another SRR containing protein (see **Introduction Section 2.3**). The authors have silenced only one copy of the gene, albeit the one with the highest homology to human *SACS*.

Other treatments have been reported in literature that aim to act at the main consequences of sacsin loss at the cellular level – mitochondrial alterations and IF bundling.

Based on the impaired mitochondrial metabolism reported in ARSACS patients' fibroblasts and SH-SY5Y cells (Girard *et al*, 2012; Bradshaw *et al*, 2016; Criscuolo *et al*, 2015) (see **Introduction Section 4**), one study explored the antioxidant properties of polydopamine nanoparticles (PDNPs) (Battaglini *et al*, 2022). In this study it was examined PDNPs action on fibroblasts from ARSACS patients, such as the biocompatibility, uptake, and the ability of PDNPs to reduce ROS and protect from cell death and mitochondrial damage induced by stimulation of oxidative stress. The findings suggested that PDNPs may be able to partially alleviate oxidative stress

associated with ARSACS, making them a potential therapeutic agent. However, both this treatment and mitochondrial metabolism and oxidative stress in the absence of sacsin have only been evaluated *in vitro*, and there are no clear data in literature regarding mitochondrial failure *in vivo* in PNs and its contribution to neurodegeneration. This issue has been indeed investigated in this thesis (see **Results Section 2.4** and **Discussion Section 2.5**).

Finally, some approaches are aimed at rescuing IF bundling seen in the absence of sacsin; in particular, these approaches are related to the putative sacsin chaperone function on NF and modulation of cellular chaperone systems to resolve NF bundling. Indeed, overexpression of molecular chaperone *HSPA1A* (Hsp70) or pharmacological induction of heat shock proteins (Hsp70, Hsp27 or co-chaperone Hsp40) with celastrol, was reported to rescue NF bundling in mixed *Sacs*$^{-/-}$ spinal motor neurons and DRG cultures (Gentil *et al*, 2019); since celastrol is also known to inhibit Hsp90 chaperone, one group pharmacologically inhibited Hsp90 chaperone to rescue vimentin bundling in ARSACS patients' fibroblasts (Nethisinghe *et al*, 2021). Although highly valuable, one issue related to these approaches is that there are no data demonstrating that sacsin actually acts as a molecular chaperone or co-chaperone for IF and NF in neurons and that NF subunits folding and filaments assembly are indeed directly involved in ARSACS. Moreover, high evolutionary divergence and the striking peculiarity of sacsin domain combinations suggest that its function *in vivo* may be more complex than the ones forecasted just by bioinformatic analysis of its conserved sequences.

Nevertheless, another noteworthy approach was aimed to rescue IF bundling by means of replacing single sacsin domains, in particular the J domain of sacsin, as I will briefly detail in next section.

6.2 - Rescue of IFs bundling by sacsin domains replacement in vitro

In one study, Gentil et al, tested the effects of injecting plasmids encoding single sacsin domains (SIRPT1, SIRPT2, SIRPT3, UbL, J domain and HEPN) on NF bundling in *Sacs*$^{-/-}$ dissociated spinal cord motor neurons from dissociated DRGs. Indeed, SIRPT1, UbL and J domains were able to reduce the percentage of cells showing NF bundles, in favor to normal filamentous network as observed in control cells, with the J domain showing the highest rescue. Interestingly, HEPN and SIRPT2-3 had no or very minor effect, thus this work was valuable in providing experimental evidence that SIRPTs modules are not just redundant repetitions (Gentil *et al*, 2019). The authors reconfirmed the ability of sacsin J domain alone to reduce bundling in *Sacs*$^{-/-}$ DRG dissociated cultures, in the form of a cell-membrane permeating peptide in

which sacsin J domain amino acidic sequence was fused to a HIV viral-derived penetrating peptide, making it a potential therapeutic agent (Dabbaghizadeh *et al*, 2022).

Although these studies provided a proof of principle of NF rescue by replacing single sacsin domains, a strategy which can be potentially extended to gene therapy, they were undermined by many limitations. The experiments were performed only *in vitro* or in dissociated neurons (mixed spinal motor neurons and DRG cultures) which are not the most affected in ARSACS, or are affected only at later stage (e.g. spinal motor neurons are affected in *Sacs*$^{-/-}$ mice starting at 2 years of age). Another issue was that single domain transfection in control cells had opposite or contrasting effects on NF cytoskeleton formation. Treatment up to 24 hours of fibroblasts or mixed spinal motor neurons from dissociated DRGs (either *Sacs*$^{-/-}$ or control) with the sacsin J domain penetrating peptide, increased proportion of cells with completely diffused or even absent vimentin/NF network, due to their dissolution; prolonged treatment resulted in formation of perinuclear ring-like bundles over time. Also, the sacsin J domain peptide accumulated in the nucleus during this period of time, consistent with its biochemical nature, which is not a subcellular compartment of sacsin localization in normal conditions (Dabbaghizadeh *et al*, 2022). Also, the other individual domains alone shown differential patterns of action on NF network formation and maintenance upon transfection *in vitro* in control cells; for example, all SIRPT domains, in particular SIRPT1, promoted the formation of filamentous NF network, while UbL results in complete disaggregation in many cells and HEPN in bundle formation (Gentil *et al*, 2019). Thus, the J domain (and the UbL domain) alone can result in disruption and dissolution of NF network in control cells, likely due to their aspecific and general biochemical activity. Therefore, it is likely that a combination of different sacsin domains is necessary to rescue NF bundling, while maintaining normal function and avoiding toxicity in control cells. Another great limitation in focusing only on chaperone activity is the absence of data showing that sacsin acts actually as a NF chaperone, and how sacsin is mechanistically linked to NF. Finally, a limitation of both these studies was the quantitative assessment of bundle formation, which was performed by counting cells belonging to arbitrarily defined categories (Gentil *et al*, 2019; Dabbaghizadeh *et al*, 2022).

In my thesis project, I developed a quantitative method to quantify and measure changes in NF bundling in the absence of sacsin. I then explored a novel gene therapy approach aimed at reducing NF bundles in PNs, restoring sacsin function by delivery of a smaller version of sacsin while showing no significant effects on control cells.

AIM OF THE WORK

Autosomal recessive spastic ataxia of Charlevoix-Saguenay (ARSACS) is a neurodegenerative disorder caused by loss-of-functions mutations in the *SACS* gene which encodes for sacsin, a 520-kDa multimodular protein. Sacsin is mainly expressed in the central nervous system (CNS) with the highest levels in PNs in the cerebellum. ARSACS is characterized by a peculiar and abnormal bundling of npNFH that was reported both in ARSACS patients' fibroblasts and at late stages in ARSACS brain autopsies as well as $Sacs^{R272C}$ and $Sacs^{-/-}$ mouse models brain sections.

My work aimed to achieve a better understanding of many open issues in the field which undermine the therapeutic approaches explored so far. These open issues regarded 1) the genotype-phenotype correlation, with particular regard to the effect of *SACS* missense mutations, whether they affect single domain functions or the levels of the protein; 2) the mechanistic link between sacsin function and NF alterations, especially whether sacsin may act as a chaperone regulating NF misfolding, assembly or turnover; 3) the connection between the mitochondrial component, which has also been observed in ARSACS, and npNFH bundling; finally 4) the lack of therapeutic approaches that target efficiently the NF bundling in PNs. Understanding of ARSACS molecular pathology rationalized gene therapy as targeted treatment to counteract NF bundling. In detail:

(i) I assessed the issue of genotype-phenotype correlation by deeply assessing sacsin turnover in a large set of skin fibroblasts derived from ARSACS patients, including 19 mutations of different nature and position along the *SACS* gene.

(ii) I dissected the NFH bundling typical of ARSACS by using integrated biochemical, imaging and cross-species OMICS approaches. I also provided a quantitative algorithm to measure NF remodeling in imaging in ARSACS cell models.

(iii) Finally, I employed the NFH bundling phenotype as a readout to assess the effectiveness of a novel recombinant engineered miniaturized version of sacsin protein that carries a combination of multiple sacsin domains in $SACS^{-/-}$ SH-SY5Y cells and in primary $Sacs^{-/-}$ PNs.

RESULTS

DISCLAIMER

We and I are used here interchangeably. I have achieved all results presented here and performed all the analyses presented here, with the following exceptions: Purkinje derivation and immunofluorescences in Results Fig. 12d-e; Purkinje derivation in Results Fig. 13b-c; EM in Results Fig. 17; immunoprecipitations in Results Fig. 17a,d-f; volumetric analyses in Results Fig. 19.

Section 1 text and figures have been adapted from open access accessible paper previously published (Longo, De Ritis et al., 2021), which I have co-authored and thoroughly contributed to. Some of Section 2 figures which I have performed are being published in Del Bondio, Longo, De Ritis et al., (under final revision). Section 3 text and figures are confidential patented information. All images in this section are used under Creative Commons CC-BY-NC-ND 4.0 license.

1 - Assessment of Sacsin Turnover in Patients With ARSACS

1.1 - Clinical features and genetics of ARSACS patients

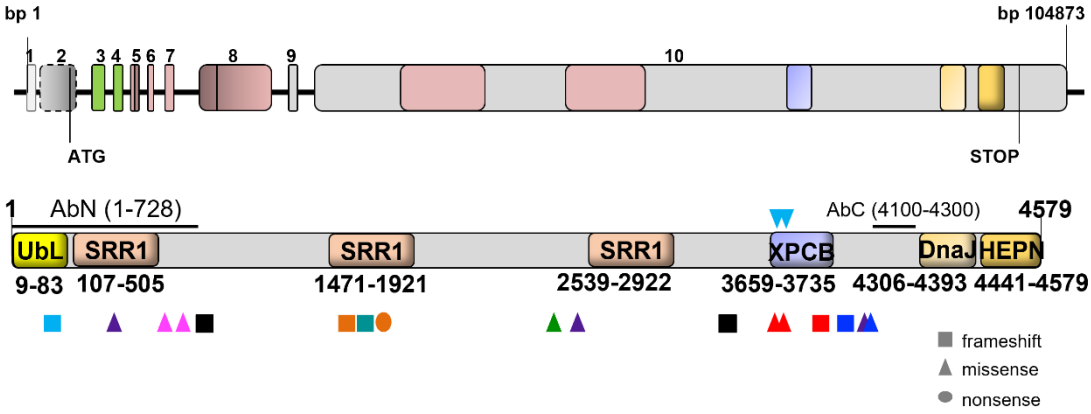
To investigate genotype-phenotype correlation in ARSACS, we collected a patient cohort that resembles the wide ARSACS phenotypic spectrum, both in terms of disease onset (which ranges from 14 months to 25 years of age) and clinical features (**Results Table 1**). Notably, two set of siblings were included (PN6a-b, PN8a-b).

To recapitulate heterogeneous ARSACS genetics, we selected patients carrying mutations of different nature and localized all along the domains of sacsin protein: compound heterozygotes for a missense mutation on one allele and a truncating mutation on the other allele (either frameshift or noncoding) (PN1, PN2, PN7); compound heterozygous for two different truncating mutations (PN3, PN6a, PN6b); compound heterozygous for a missense mutation and a large gene deletion (PN4); compound heterozygous for truncating mutations and a large gene deletion (PN8a, PN8b); and finally compound heterozygous for biallelic missense mutations (PN5, PN9) (**Results Fig. 1**). Mutations carried by PN3 (p.[Glu723fsTer15];[Phe3209fsTer46]), PN6a and PN6b (p.[Ser1531fsTer9];[Arg1645Ter]), PN8a and PN8b (p.[Asn1586fsTer3];[deleted_allele]) and PN9 (p.[Pro536Leu];[Arg632Trp]) were unpublished, at least in compound heterozygosity in the combinations mentioned above. The other mutations were already published (PN1 and PN2; PN4; PN5; PN7) (Baets *et al*, 2010; Terracciano *et al*, 2009; Masciullo *et al*, 2012; Ricca *et al*, 2019).

Patients with ARSACS	*SACS* variations	Age at onset and sex	DSI-ARSACS	Ataxia	Dysarthria	Sensory loss	Walking difficulties/ support/wheelchair	RNFL thickness by OCT	Age at MRI	TCC/cerebral atrophy/WM changes	Cerebellar atrophy (hem/ vermis)	Spinal cord atrophy	Reference
PN1	p.[(Arg3636Gln; Pro3652Thr)]; [Leu3745fsTer1]	15 y M	nv	++	++	+	Wheelchair	nv	35	−/−/−	—	—	4
PN2	p.[Cys72fsTer4]; [(Arg3636Gln; Pro3652Thr)]	>25 y M	nv	+	+	+	Walking with support	nv	58	−/+/−	+	—	4
PN3	p.[Glu723fsTer15]; [Phe3209fsTer46]	5 y M	nv/SARA score: 10/ 40	+	−/+	—	Wheelchair	nv	5	+/−/−	+	nv	Unpublished
PN4	p.[Leu2374Ser];[deleted_allele]	26 mo M	nv/SARA score: 26/ 40	++	++	+++	Walking difficulties	nv	54	−/+−/+−	+++ Vermis	nv	23
PN5	p.[(Gly188Glu; Ser2465Leu)]; [Leu3916Trp]	16 y M	9	+	−/+	+	Walking with support	+	36	−/−/−	+ Vermis	+	24
PN6a	p.[Ser1531fsTer9]; [Arg1645Ter]	18 mo M	17	+	++	+	Walking difficulties	++	24	−/+/+−	++ Vermis	+	Unpublished
PN6b	p.[Ser1531fsTer9]; [Arg1645Ter]	18 mo M	12	++	−/+	+++	Walking with support	++	25	−/−/−	++ Vermis	+	Unpublished
PN7	p.[Ile3755fsTer8]; [Asp3926Gly]	14 mo F	16	++	—	++	Walking with support	++	28	−/−/−	+ Vermis	+	25
PN8a	p.[Asn1586fsTer3]; [deleted_allele]	14 mo F	17	++	—	++	Wheelchair	++	27	−/−/−	++ Vermis	+	Unpublished
PN8b	p.[Asn1586fsTer3]; [deleted_allele]	18 mo F	21	+	—	++	Walking difficulties	++	34	−/+−/−	+ Vermis	+	Unpublished
PN9	p.[Pro536Leu]; [Arg632Trp]	16 y M	nv/SARA score: 17/ 40	—	—	+	Wheelchair	nv	29	−/−/−	+	+	Unpublished

Results Table 1 (from previous page) Table showing cohort of patients used in this work. *For each patient, relative SACS mutations and ARSACS clinical phenotypes are reported. Abbreviations: ARSACS = autosomal recessive spastic ataxia of Charlevoix-Saguenay; y = year; mo = month; DSI = disease severity index; nv = not evaluated; OCT = optical coherence tomography; RNFL = retinal nerve fiber layer; TCC = thin corpus callosum; WM = white matter; - = absent; +- = subtle; + = present; +++=very strongly present.*

ARSACS patients	*SACS* mutations	Reference	Expected truncated sacsin protein
PN1	p[R3636Q; P3652T] + [L3745fsX1]	Baets et al., 2010	412 kDa
PN2	p[C72fsX4] + [R3636Q; P3652T]	Baets et al., 2010	8 kDa
PN3	p[E723fsX15] + [F3209fsX46]	Longo et al., 2021	358 kDa; 81 kDa
PN4	p[L2374S] + [deleted_allele]	Terracciano et al., 2009	
PN5	p[G188E;p.S2465L] + [L3916W]	Ricca et al., 2019	
PN6a	p[S1531fsX9] + [R1645X]	Longo et al., 2021	170 kDa; 180 kDa
PN6b	p[S1531fsX9] + [R1645X]	Longo et al., 2021	170 kDa; 180 kDa
PN7	p[I3755fsX8] + [D3926G]	Masciullo et al., 2012	410 kDa
PN8a	p[N1586fsX3] + [deleted_allele]	Longo et al., 2021	175 kDa
PN8b	p[N1586fsX3] + [deleted_allele]	Longo et al., 2021	175 kDa
PN9	p[P536L] + [R632W]	Longo et al., 2021	



Results Figure 1. ARSACS mutations used in this study and SACS gene and sacsin protein structures. *Above: Table reporting ARSACS patients and their mutations, the literature references and the expected molecular weights of the putative truncated sacsin products deriving from frameshift mutations. Below: Schematics of SACS gene illustrating the identified sacsin functional domains and exons (upper). Sacsin protein reporting patient mutations -unless the large gene deletions- respecting the patient color code in the table above. AbN and AbC antibodies used in this study are shown (bottom). Abbreviations: PN: patient; AbN/C: N/C-terminal anti-sacsin antibody; UbL: Ubiquitin-Like domain; SRR: Sacsin Repeating Region; XPCB: Xeroderma Pigmentosus group C protein Binding domain; HEPN: Higher Eukaryotes and Prokaryotes Nucleotide-binding domain; bp: base pair; aa: aminoacid.*

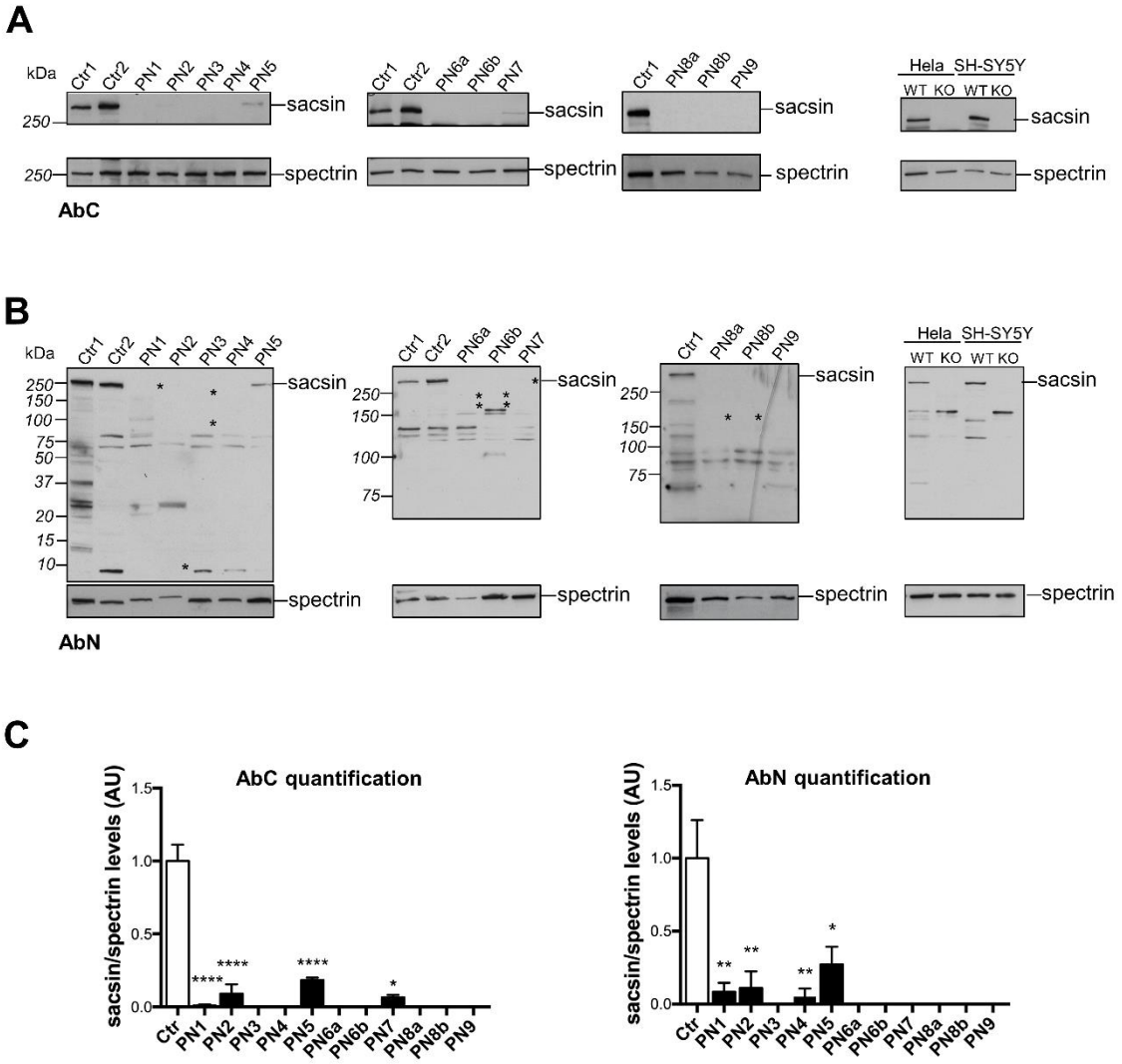
Disease severity did not correlate with the type and position of *SACS* mutations, as there were patients with one or two missense mutations that have similar or more severe ataxia scores or other clinical manifestations compared to patients carrying only truncating mutations or large gene deletion (**Results Table 1**). Also, siblings,

who share the same mutations, had different clinical manifestations; for example, two brothers, with an age difference of three years among them, had different clinical phenotype: one with clear spastic paraparesis and the other with neuropathic/ataxic gait (**Results Table 1**).

1.2 - Full-Length sacsin protein is dramatically reduced in fibroblasts from patients with ARSACS regardless of the nature of the mutation

To further investigate correlation between clinical severity and *SACS* genetic mutations, we studied the impact of these mutations on sacsin protein level in skin fibroblasts derived from the eleven compound heterozygous ARSACS patients described above, for a total of nineteen different mutations analyzed (**Results Fig. 1**). To robustly quantify sacsin protein level, we performed western blot (WB) on patients' cells by using both an available commercial C-terminal anti-sacsin antibody (AbC) (**Results Fig. 2a**) and a novel N-terminal anti-sacsin antibody (AbN) (**Results Fig. 2b** – see also schematics in **Results Fig. 1** for epitopes positions). AbN was designed and generated by our group, as there are no commercial antibodies directed against the sacsin N-terminal region that work efficiently in WB. To validate the specificity of AbN, I generated different *SACS*$^{-/-}$ clonal cell lines by CRISPR/Cas9-mediated genome editing to disrupt the *SACS* gene in multiple human immortalized cell types (HeLa and neuronal-like SH-SY5Y cells). *SACS*$^{-/-}$ clonal cell lines were selected by WB screening with AbC; importantly, sacsin protein was detected by WB at the expected molecular weight of 520 kDa in all *SACS*$^{+/+}$ human cells tested with AbN, while it was absent in all *SACS*$^{-/-}$ negative-control cells (**Results Fig. 2b** – rightmost WB).

With both AbC and AbN antibodies, full-length sacsin protein was revealed to be dramatically reduced or virtually absent in all ARSACS patients' cells, regardless of the nature of *SACS* mutations (**Results Fig. 2a,b** – representative WB and **c** - quantification).



Results Figure 2 (from previous page). Sacsin protein is drastically reduced in ARSACS fibroblasts carrying different SACS mutations. *A. Representative WB showing residual sacsin protein in ARSACS patient-derived primary fibroblasts versus controls by using a C-terminal anti-sacsin antibody (AbC). Spectrin is used as loading control. B. Representative WB showing residual sacsin protein in ARSACS patient-derived primary fibroblasts versus controls by using AbN. Asterisks indicate the molecular weights of the expected truncated sacsin products deriving from frameshift mutations (reported in the table in Results Fig. 1). C. Quantification of sacsin levels relative to spectrin in WB experiments by using AbC and AbN. Data are presented as mean ± SEM. *p≤0.05; **p<0.01; ***p<0.001, ****p<0.0001 (n=at least three, Student's t-test).*

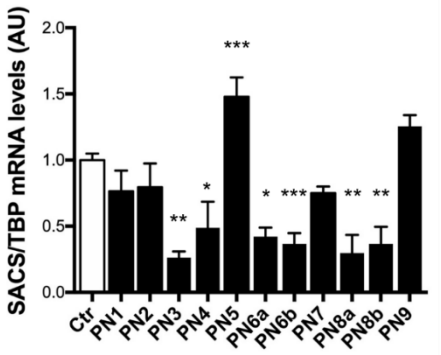
This finding was unexpected for patients carrying monoallelic missense mutations, and even more for those carrying biallelic missense mutations. With AbN we also were not able to identify putative truncated products in patients carrying frameshift or noncoding mutations at any molecular weight (**Results Fig. 2b** – asterisks highlight predicted molecular weight of truncated products based on position of the truncating mutations; see also **Results Fig. 1** for reference). Indeed, all bands

detected in WB by AbN, other than sacsin full-length, were shared both by control and patients' cells, likely due to aspecific binding to proteins that carry an N-terminal Ubl domain which is quite common among proteasome-interacting proteins in human cells.

1.3 - SACS mRNA is reduced in ARSACS fibroblasts carrying frameshift mutations, while it is stable or even increased in those carrying missense mutations

To understand if the absence of full-length sacsin (and of truncated sacsin products) in ARSACS fibroblasts is due to mRNA instability, we analyzed *SACS* mRNA level by real-time PCR (qRT-PCR).

In ARSACS patients carrying only truncating mutations, *SACS* mRNA was evidently reduced compared to controls (PN3, PN8a, PN8b, PN6a and PN6b), suggesting that these mutations may lead to Non-sense Mediated Decay (NMD) of the mRNA, thus also explaining the lack of the total full-length protein and putative truncated products. On the other hand, mRNA resulted to be stable or even increased compared to controls' cells, in patients carrying one or two missense mutations (**Results Fig. 3**). In particular, in ARSACS patients who are compound heterozygous for a missense and a frameshift mutation (PN1, PN2, PN7) or for a missense and large gene deletion (PN4), we found no significant difference in the amount of *SACS* mRNA compared to controls' cells, suggesting that the contribution of the allele carrying the missense determines the conserved amount of *SACS* mRNA. Interestingly, in patients carrying two missense mutations, *SACS* mRNA was increased, although with statistical significancy only in PN9.

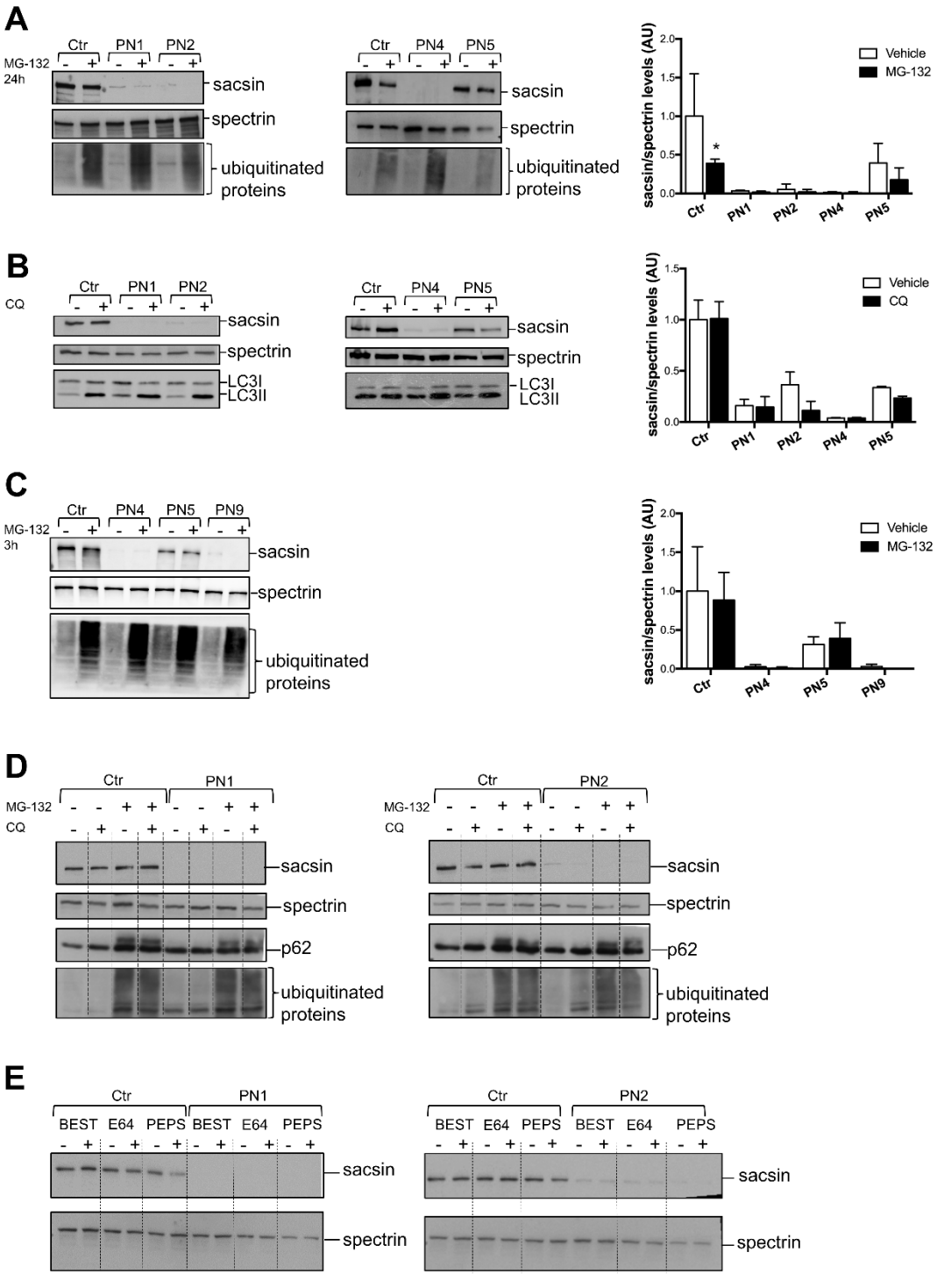


Results Figure 3. SACS mRNA is stable in patients carrying missense mutations. *SACS mRNA quantification by qRT-PCR in ARSACS patient-derived primary fibroblasts versus controls, normalized to TBP mRNA levels. Data are presented as mean ± SEM. *p<0.05; **p<0.01; ***p<0.001, ****p<0.0001 (n=at least 3, Student's t-test).*

1.4 - Inhibition of degradative systems does not rescue sacsin protein full-length sacsin protein in ARSACS patients carrying missense mutations

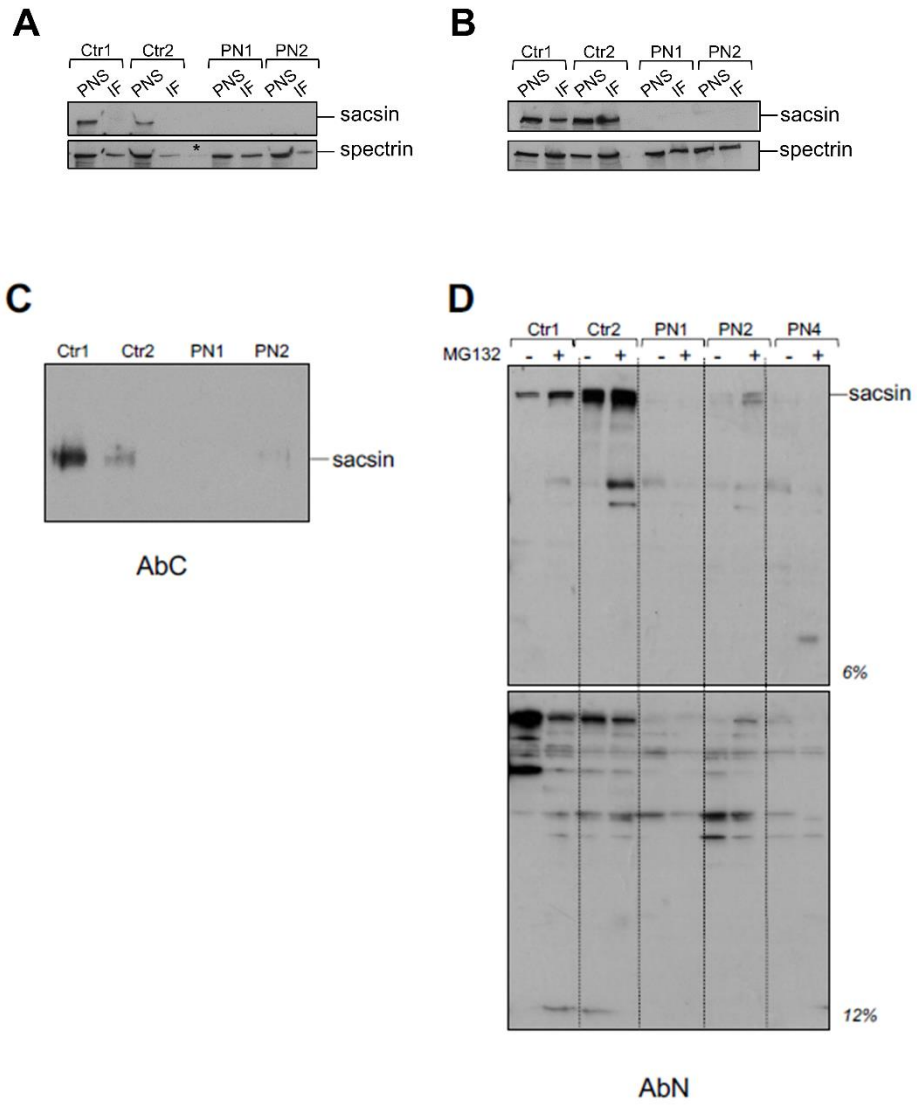
Because *SACS* mRNA is stable and sacsin protein is dramatically reduced in ARSACS patients' fibroblasts carrying missense mutations, we investigated whether mutant sacsin could undergo a faster post-translational degradation in these cells. Unfolded or aberrant proteins are usually targeted by the proteasome system or the autophagic system, the main molecular pathways involved in protein quality control and maintenance of cellular proteostasis (Morimoto & Cuervo, 2014). To test this hypothesis, we blocked cellular degradative systems by treating patient cells carrying one or two missense mutations either with a proteasome inhibitor (MG-132, 1 μM, 24 hours) (**Results Fig. 4a**) or an autophagy inhibitor (Chloroquine – CQ - 20 μM, 24 hours) (**Results Fig. 4b**). Both treatments did not rescue mutant sacsin in treated ARSACS patients' fibroblasts. Since by blocking the proteasomal pathway for 24 hours a statistically significant reduction of sacsin levels was observed in controls (**Results Fig. 4a** – graph), we hypothesized that a prolonged MG-132 treatment and consequent cellular stress induction could possibly lead to global inhibition of protein synthesis (Gandin *et al*, 2010). Thus, we blocked the proteasome reducing the time of treatment to three hours. In this condition, sacsin was stable in controls, but again not rescued in treated patients' cells (**Results Fig. 4c**). Moreover, since blockade of the proteasome or autophagic flux can in turn lead to increased autophagy or proteasome inhibition respectively as adaptation to stress (Kocaturk & Gozuacik, 2018), we also blocked both pathways simultaneously, but also in this case we did not see any increase in the amount of sacsin protein in patients' cells (**Results Fig. 4d**).

Other than proteasome-mediated degradation and autophagy, protein turnover can be mediated by specific proteases in the cytosol, which belong to three major classes: cysteine proteases, amino peptidases and aspartyl proteases. Therefore, we inhibited specific proteases with E64, bestatin and pepstatin respectively, in patients' cells carrying missense mutations. However, also in this case, the low amount of mutant sacsin full-length in ARSACS patients' cells was not increased by any of these treatments (**Results Fig. 4e**).


A
Ctr
PN1
PN2
MG-132
24h
sacsin
spectrin
ubiquitinated
proteins
Ctr
PN4
PN5
sacsin
spectrin
ubiquitinated
proteins
sacsin/spectrin levels (AU)
Vehicle
MG-132
Ctr
PN1
PN2
PN4
PN5
B
Ctr
PN1
PN2
CQ
sacsin
spectrin
LC3I
LC3II
Ctr
PN4
PN5
sacsin
spectrin
LC3I
LC3II
sacsin/spectrin levels (AU)
Vehicle
CQ
Ctr
PN1
PN2
PN4
PN5
C
Ctr
PN4
PN5
PN9
MG-132
3h
sacsin
spectrin
ubiquitinated
proteins
sacsin/spectrin levels (AU)
Vehicle
MG-132
Ctr
PN4
PN5
PN9
D
Ctr
PN1
MG-132
CQ
sacsin
spectrin
p62
ubiquitinated
proteins
Ctr
PN2
MG-132
CQ
sacsin
spectrin
p62
ubiquitinated
proteins
E
Ctr
PN1
BEST
E64
PEPS
BEST
E64
PEPS
sacsin
spectrin
Ctr
PN2
BEST
E64
PEPS
BEST
E64
PEPS
sacsin
spectrin

Results Figure 4 (from previous page). Mutant sacsin is not post-translationally degraded. *A. Representative WB and quantification of sacsin levels in patient and control fibroblasts after proteasome blockage experiments, by using 1uM MG-132 for 24 hours. Ubiquitinated proteins are used as readout of the treatment and spectrin as loading control. B. Representative WB and quantification of sacsin levels in patient and control fibroblasts after autophagy blockage experiments, by using 20uM Chloroquine (CQ) for 24 hours. LC3I conversion in LC3II is used as readout of the treatment. C. Representative WB and quantification of sacsin levels in patient and control fibroblasts after proteasome blockage experiments, by using 1uM MG-132 for three hours. Ubiquitinated proteins are used as readout of the treatment. D. Representative WB of sacsin levels in patient and control fibroblasts upon proteasome plus autophagy blockage, by using 0.5uM MG-132 and 10uM CQ for 18 hours. P62 is used as readout of the CQ treatment and ubiquitinated proteins of the MG-132 treatment. E. Representative WB of sacsin levels in patient and control fibroblasts upon protease inhibition by using different protease inhibitors one by one for 48 hours (repeating the treatment at 24 hours). In (A–C), data are presented as mean ± SEM. n=at least 3, *p<0.05 (Student's t-test).*

Next, we took into consideration that sacsin carrying missense mutations could be translated but undetectable by standard WB procedures, due to its misfolding or aggregation in the detergent-insoluble fraction. To address this hypothesis, we performed different experiments to solve aggregates in biochemical assays. We checked for mutant sacsin aggregation by loading onto sodium dodecyl sulphate–polyacrylamide gel electrophoresis (SDS-PAGE) both the soluble and insoluble fractions of control and patient fibroblasts, where the insoluble fraction was either subjected to pellet sonication (**Results Fig. 5a**) or directly resuspended in Laemmli buffer (**Results Fig. 5b**): in both cases, sacsin full-length was not detected in the insoluble fractions in patients' cells. As further proof, we also loaded total homogenates from control and patients' whole cellular pellets lysed in ionic-detergent Laemmli buffer and loaded onto mixed acrylamide-agarose gels, to detect even higher molecular weight aggregates (**Results Fig. 5c)**. These experiments suggest that sacsin with missense mutations does not aggregate in the nonionic detergent-insoluble fraction at steady state condition. We checked for the hypothesis that blockade of cellular degradative systems, as described above, could lead to rescue of sacsin mutant protein with missense mutations, but in turn would cause its aggregation in the detergent-insoluble fraction due to misfolding, thus preventing detection by standard WB procedure. However, as negative proof, SDS-PAGE of total homogenates from control and patients' cells lysed in 8M urea after repeated treatment with proteasome blocker MG-132, did not reveal either an increase of sacsin full-length protein, nor the presence of aggregated or truncated products by AbN at any molecular weight in patient cells (**Results Fig. 5d**).

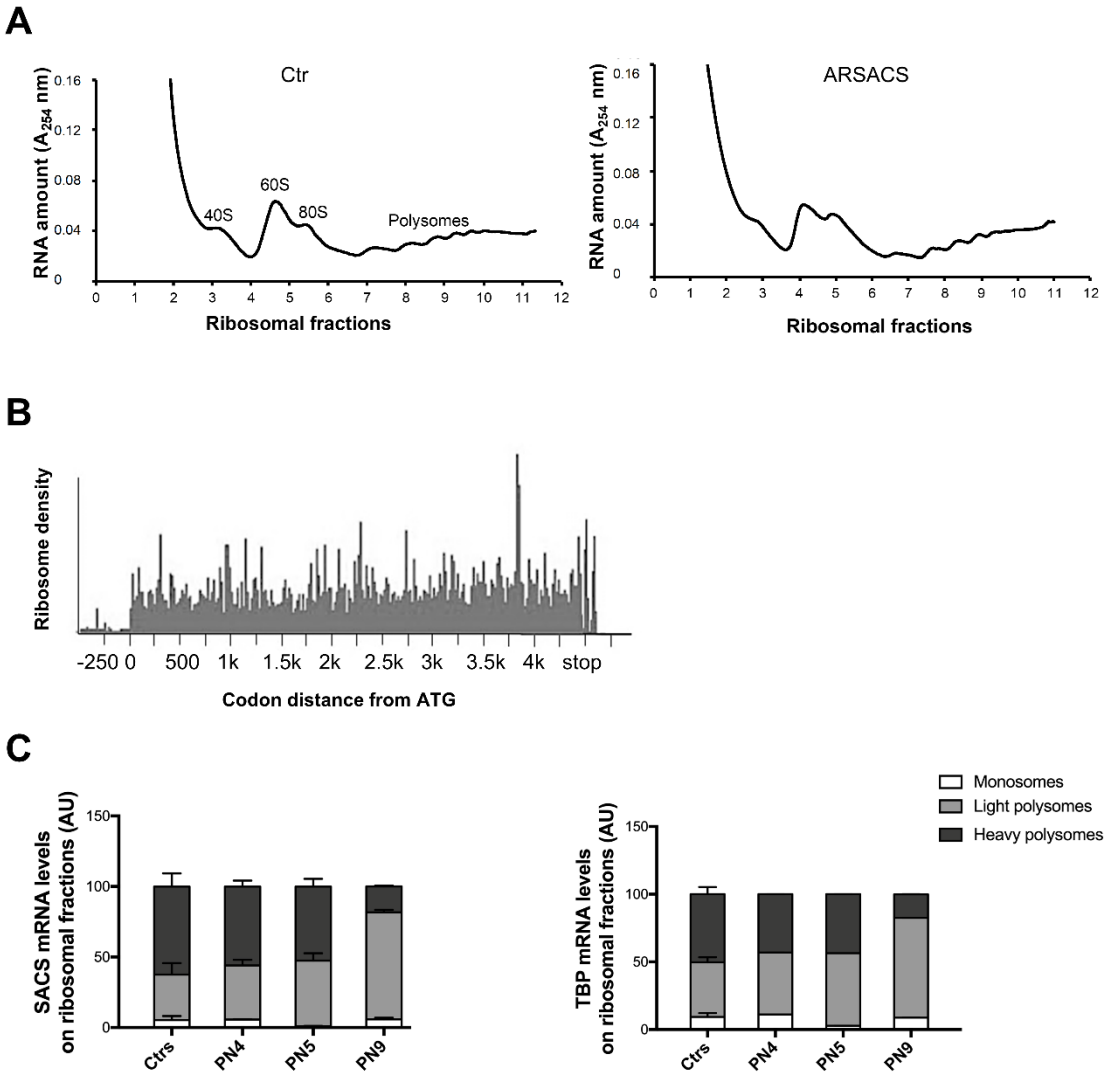


Results Figure 5. Mutant sacsin does not aggregate. *A. Representative WB of sacsin levels in patient and control soluble and insoluble fractions, obtained by pellet sonication. Asterisk represents a leak of material from the adjacent well. PNS: post-nuclear surnatant; IF: insoluble fraction. B. Representative WB of sacsin levels in patient and control soluble and insoluble fractions, each separately resuspended in Laemmli sample buffer. PNS: post-nuclear surnatant; IF: insoluble fraction. C. Total homogenates from control and patient fibroblasts obtained by lysis in Laemmli sample buffer 2X and sonicated, then loaded in an agarose-acrylamide gel at 2.7 %. D. Representative WB of sacsin protein (revealed by using the AbN) in control and patient fibroblasts treated or not with 1μM MG132 and solubilized in 8M Urea and ultrasonicated. The upper panel is a 6% acrylamide gel, the bottom one a 12%, suitable to detect any possible truncated misfolded sacsin proteins.*

Altogether, these results demonstrate that the drastic reduction of mutant sacsin in ARSACS patients with missense mutations is neither caused by a faster post-translational degradation of the protein, nor is due to mutant aggregation.

1.5 - Translation of mutant sacsin carrying missense mutations is not blocked in ARSACS patients

At this point we considered that the absence of sacsin carrying missense mutations could be due to its inefficient translation. We excluded a general problem in translation, as polysomal profiling shown a similar pattern in ARSACS patient and control cells (**Results Fig. 6a**). To investigate if *SACS* mRNA in control cells could be subjected to a translational regulation *per se*, we performed meta-analysis of ribosome profiling data downloaded and analyzed exploiting the GWIPS-viz platform (Michel *et al*, 2014). This analysis shown little accumulation of ribosomes in the 5'UTR of *SACS* mRNA, and a homogenous density of ribosomes across the 13737 nucleotide long mRNA sequence, suggesting the absence of strong regulatory sequences in the 5'UTR (**Results Fig. 6b**). To specifically assess sacsin translation, we investigated if *SACS* mRNA carrying missense mutations was associated to actively translating ribosomes (polysomes) or to single ribosomes (monosomes, which are not coupled to active translation). We thus performed qRT-PCR for sacsin on RNA extracted from the different ribosomal fractions (monosomes, light polysomes, heavy polysomes) obtained from polysomal profiling from ARSACS patients' and controls' cells. We found that *SACS* mRNA was associated with the heavy and light polysomal fractions (the actively translating fractions) in ARSACS patients (PN4, PN5, PN9), as well as in controls (**Results Fig. 6c**, left), demonstrating that there is no impairment of mutant sacsin translation. The same mRNA distribution on the different ribosomal fractions in ARSACS and control cells was observed for an unrelated housekeeping gene encoding TATA-box binding protein (*TBP*) (**Results Fig. 6c**, right).



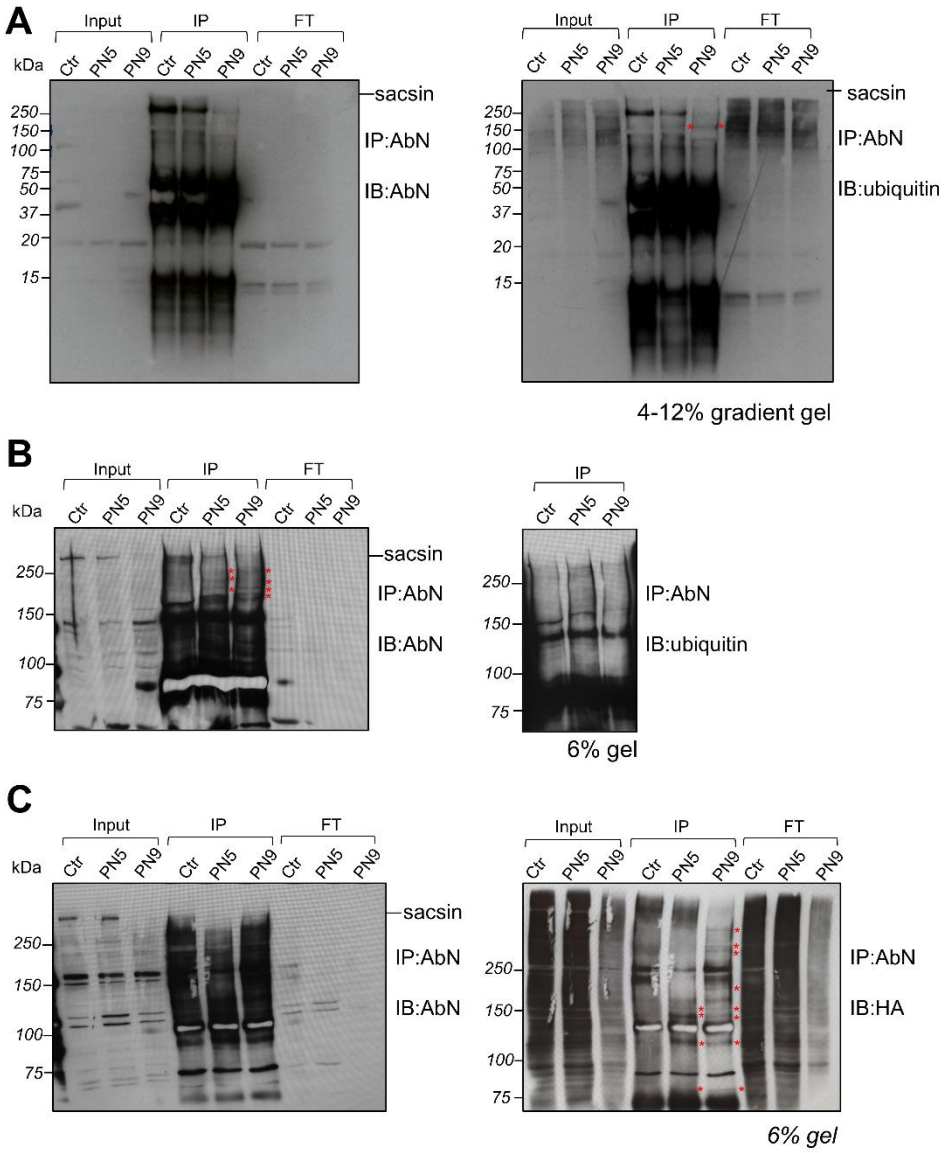
Results Figure 6. SACS mRNA carrying missense mutations is associated to the polysomal fractions. *A. Representative ribosomal profile graphs in control (left) and ARSACS patient fibroblasts (right). B. Ribosomal density on the human sacsin mRNA, retrieved and analyzed from available riboseq datasets. C. qRT-PCR data of the SACS mRNA distribution in different ribosomal fractions: monosomes, light and heavy polysomes in ARSACS patient fibroblasts (PN4, PN5, PN9) compared to 3 different controls (left). TBP mRNA distribution is shown as housekeeping gene analyzed in the same cells (right).*

1.6 - Nascent mutant sacsin products are cotranslationally ubiquitinated and degraded

At this point, having experimentally excluded all the possible molecular mechanisms that could explain the drastic reduction of sacsin observed in ARSACS patient cells carrying missense mutations, we considered that mutant sacsin could be degraded during translation. Two different quality control (QC) mechanisms exist during translation, both leading to the ubiquitination and proteasome-mediated degradation of nascent protein chains. Whereas the ribosomal QC (RQC) is associated

to mRNA degradation and ribosome stalling and splitting (i.e. the NMD, the No-Go Decay etc.) (Inada, 2017), the second pathway, properly called the co-translational QC, senses the correct folding of the nascent chain, promotes the degradation of the protein while it is being actively translated and occurs in the presence of a stable mRNA associated to intact ribosome (Wang *et al*, 2015; Liutkute *et al*, 2020). This pathway is the most plausible in the case of sacsin carrying missense mutations, since we did not detect any reduction of sacsin mRNA and we have demonstrated its association with actively translating polysomes.

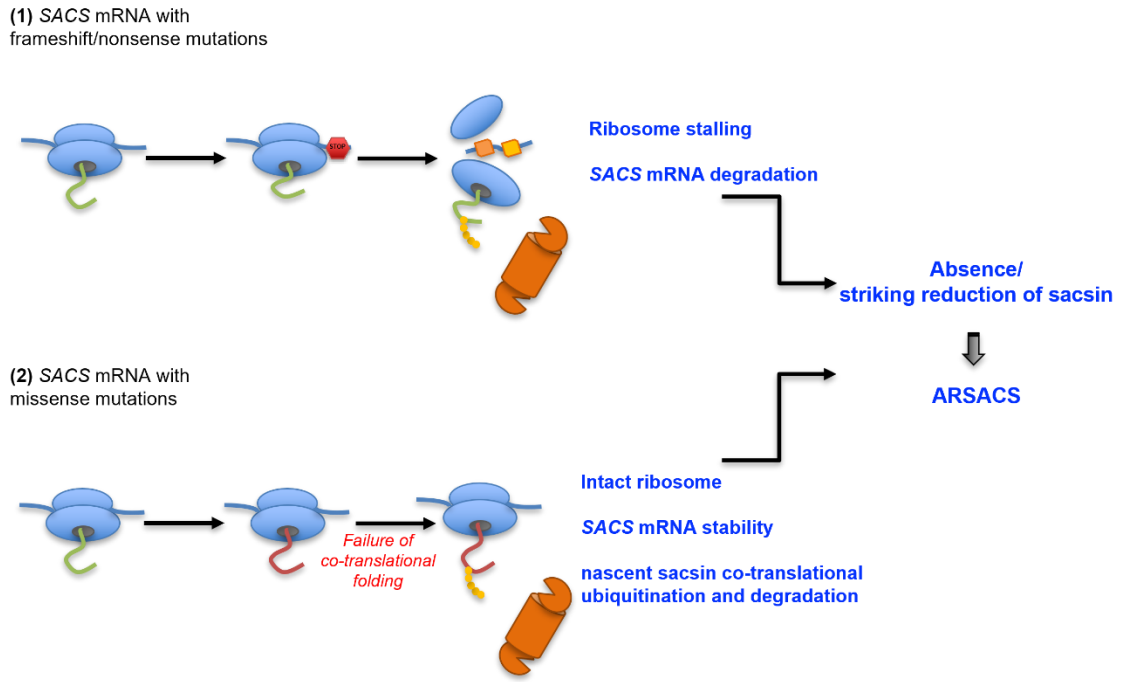
As formal proof of the co-translational degradation of sacsin carrying missense mutations, we looked for the presence of ubiquitinated degradation products of nascent mutant sacsin in ARSACS patient cells, carrying missense mutations only (PN5, PN9). For this purpose, we immunoprecipitated sacsin with AbN (recognizing N-terminal sacsin fragments of any possible molecular weights) in patients' fibroblasts and controls. Since putative mutant sacsin nascent intermediates should be ubiquitinated and degraded by the proteasome, before the immunoprecipitation (IP) we treated the cells with the proteasome inhibitor MG-132 (1μM, 3 hours) to avoid their degradation and improve their detection. We efficiently immunoprecipitated full-length sacsin with AbN in control and (to a lower extent as expected) in patients' cells (**Results Fig. 7a**). Sacsin degradation products were detectable only in the IP from patients' cells, in particular with the anti-ubiquitin immunodecoration (**Results Fig. 7a**, right); these products were especially detected in the higher part of the gel, in agreement with addition of several ubiquitin moieties that would result in increased molecular weight of nascent chains. To better resolve these products, we reloaded an independent sacsin IP in SDS-PAGE at 6% gel (**Results Fig. 7b**). Sacsin degradation products were detected only in the IP of ARSACS patients' cells, especially when immunodecorated with the AbN (**Results Fig. 7b,** left). Finally, to enhance sacsin ubiquitination and detection of mutant sacsin ubiquitinated products, we repeated the previous experiment after transfecting control and patient cells with an exogenous Ubiquitin-HA construct. We confirmed in this condition the detection of sacsin degradation products in ARSACS patients' IP, as revealed by AbN (**Results Fig. 7c,** left); moreover, these differential bands present in the IP samples of patients were strikingly more evident by immunodecoration with anti-HA antibody, definitely demonstrating that these patients-specific products were ubiquitinated (**Results Fig. 7c,** right).



Results Figure 7. Sacsin protein carrying missense mutations is co-translationally ubiquitinated and degraded. *A. Sacsin IP by using AbN in ARSACS patient fibroblasts carrying missense mutations (PN5, PN9) and a control treated with 1uM MG-132 for three hours. 4-12 % gradient gel showing proteins from high molecular weights to 15 kDa, immunodecorated with AbN (left) or ubiquitin (right). B. Independent experiment conducted in the same conditions loaded onto a 6% gel to resolve putative differential N-terminal sacsin bands in patients compared to control. Immunodecoration with AbN (left gel, red asterisks indicate N-terminal sacsin products visible only in the patient IP samples) or ubiquitin (right). C. Sacsin IP by using AbN in ARSACS patient fibroblasts carrying missense mutations (PN5, PN9) and a control upon Ubiquitin-HA overexpression, treated with 1uM MG-132 for 3 hours. 6 % gel showing immunodecoration with AbN (left) and with anti-HA revealing ubiquitinated proteins (right). Red asterisks indicate differential N-terminal sacsin products visible only in the patient IP samples. Abbreviations: IP: immunoprecipitation; FT: Flow through fractions; IB: immunoblotting.*

Altogether all these results support a final model of the first event of ARSACS pathogenesis: in the presence of frameshift or nonsense mutations, *SACS* mRNA is

degraded; whereas in the presence of missense mutations, sacsin fails to fold and constitutively undergoes cotranslational ubiquitination and proteasome-mediated degradation. Thus, the final outcome is the absence/striking reduction of sacsin protein, regardless of the nature of the mutations in *SACS* gene (**Results Fig. 8** - model).

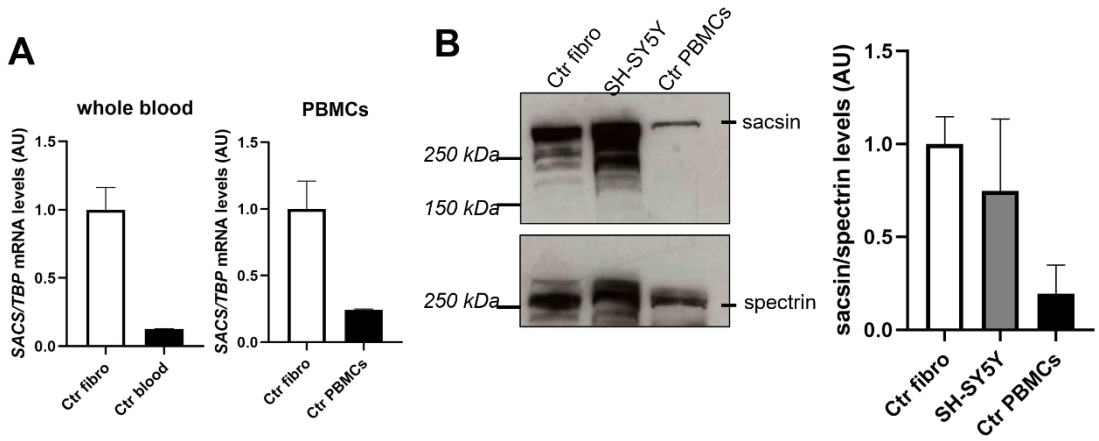


Results Figure 8. Final model explaining why mutant sacsin is almost absent in patients' cells. *In (1) sacsin is prevented to be translated because the SACS mRNA carrying frameshift mutations is degraded by nucleases, while in (2) the SACS mRNA carrying missense mutations is stable and sacsin is cotranslationally degraded. The proteasome is the degradative system implied in these pathways (drawn in orange). Green nascent chain: before sensing the mutation; red nascent chain: after sensing domain misfolding.*

1.7 - Assessment of sacsin protein level in human peripheral blood mononuclear cells (PBMCs)

Cotranslational degradation triggered constitutively by missense mutations in sacsin protein represents a valuable discovery also for i) fast ARSACS molecular diagnostics in suspected patients prior to large *SACS* gene/exome sequencing by looking at the level of the protein from those patients' cells; and ii) for evaluation of missense Variants of Uncertain Significance (VUS). To develop a fast non-invasive ARSASC diagnostic tool, I evaluated if sacsin is physiologically expressed in blood samples from healthy controls, first at mRNA level. By qRT-PCR, *SACS* mRNA was detectable at low level from control whole peripheral blood samples; whereas it was expressed at higher level in peripheral blood mononuclear cells (PBMCs) isolated by medium density gradient (around 25% the expression level in human fibroblasts)

(**Results Fig. 9a**). PBMCs are mainly composed of lymphocytes and monocytes and are much used in immunology and diagnostics research (Riedhammer *et al*, 2016). These data suggest that sacsin should be mainly expressed in PBMCs, in agreement with its general expression in post-mitotic differentiated cells. Therefore, I evaluated sacsin expression at protein level by WB in PBMCs. Fresh obtained human PBMCs are highly prone to protein degradation that was observed upon separating protein lysates in WB, which is very limiting for the detection of very high molecular weight proteins like sacsin, as these proteins are even less stable. Therefore, I set up and optimized a protocol in which PBMCs obtained from fresh human blood were cultured for at least three days in presence of proliferation-stimulating factors. This protocol preferentially expands CD4+ T cells in suspension, while monocytes remain generally attached and do not proliferate at all as they are terminally differentiated. Sacsin protein was well detectable at a reliable level in PBMCs lysates following this protocol with a sharp band by WB and again resulted to be expressed at around 20-25% level compared to control human fibroblasts and human neuronal-like SH-SY5Y cells, corroborating the reproducibility and reliability of this approach (**Results Fig 9b** – representative WB and quantification).



Results Figure 9. Sacsin is expressed in human peripheral blood mononuclear cells. *A. SACS mRNA quantification by qRT-PCR in control healthy fibroblasts and whole blood (left) and PBMCs (right) samples from two healthy subjects (unrelated in respect to control fibroblasts), normalized on TBP mRNA levels. Data are presented as mean ± SEM; n = at least 2. B. Representative WB showing sacsin expression in human PBMCs, compared to control fibroblasts and control human neuronal-like SH-SY5Y cells, by using AbC antibody; spectrin was used as control. C. Quantification of sacsin levels relative to spectrin in WB experiments shown in C; data are shown as mean ± SEM; n=at least 3. Abbreviations: Ctr: healthy controls; RT: retro-transcriptase; PBMCs: Peripheral Blood Mononuclear Cells.*

These results demonstrate that sacsin is physiologically expressed in PBMCs (presumably mainly in T cells), at a level that is quantifiable by WB, making it feasible to diagnose ARSACS based on looking at sacsin protein level in patients' cells. Indeed,

ongoing work is being done in order to translate and test this protocol first in PBMCs from ARSACS patients carrying missense mutations already described in this work and then from patients with novel identified putative missense mutations or VUS, which would definitely prove its diagnostic value, also thanks to continuous close collaboration with clinicians.

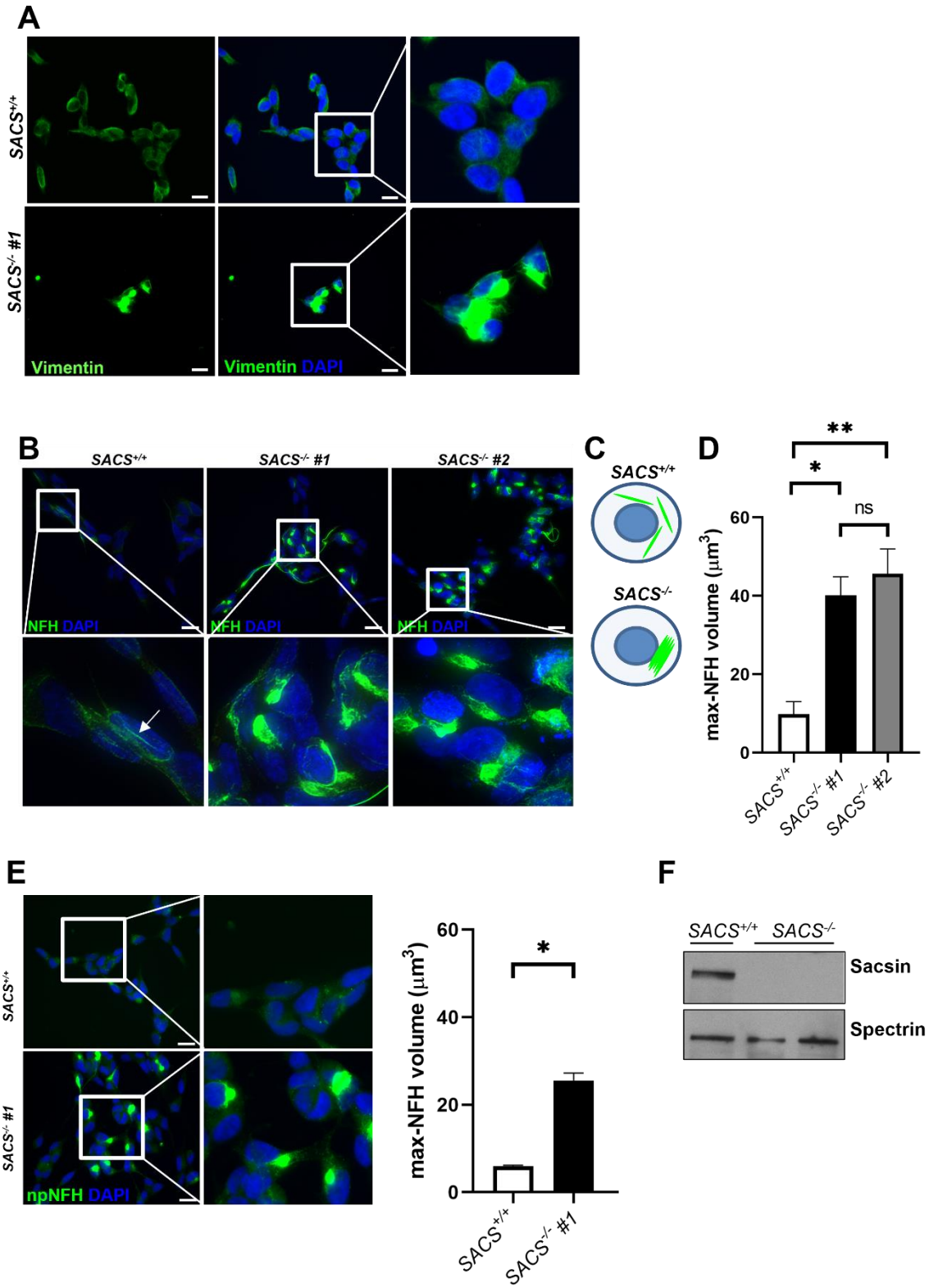
2 - Dissection of sacsin physiopathological function in neurofilaments dynamics

After demonstrating that ARSACS molecular pathology is caused by the absence or striking reduction of sacsin protein, I focused on the physiopathological role of sacsin, investigating cellular and molecular events that underly ARSACS pathogenesis in neurons. The main cytopathological event occurring in ARSACS and reported in the literature is NFs alteration; this was observed clearly in PNs and pyramidal neurons from patients' post mortem brain biopsies and in the *Sacs*$^{-/-}$ mouse model brain sections at ten months of age and in the *Sacs*^{R272C} model at six months of age (Larivière *et al*, 2015, 2019). A systematic dissection of the precise timing and molecular mechanism underlying NF alteration in PNs in ARSACS was missing. We sought to fill this gap by performing integrated cross-species OMICS, biochemical and imaging approaches. I also carefully and quantitatively evaluated and modeled the NF phenotype in two different *in vitro* and *ex vivo* cellular models, namely *SACS*$^{-/-}$ SH-SY5Y cells by CRISPR/Cas9 that I have generated, and *Sacs*$^{-/-}$ primary PNs. Indeed, both these cellular models were further exploited to identify sacsin interactors, to dissect the downstream effects of NFs alteration at cellular and molecular levels and to validate and test therapeutic approaches, as I will report in **Results Section 3** for gene therapy.

2.1 - SACS$^{-/-}$ *SH-SY5Y neuronal like cells and Sacs*$^{-/-}$ *primary PNs show abnormal hypo-phosphorylated neurofilaments bundles*

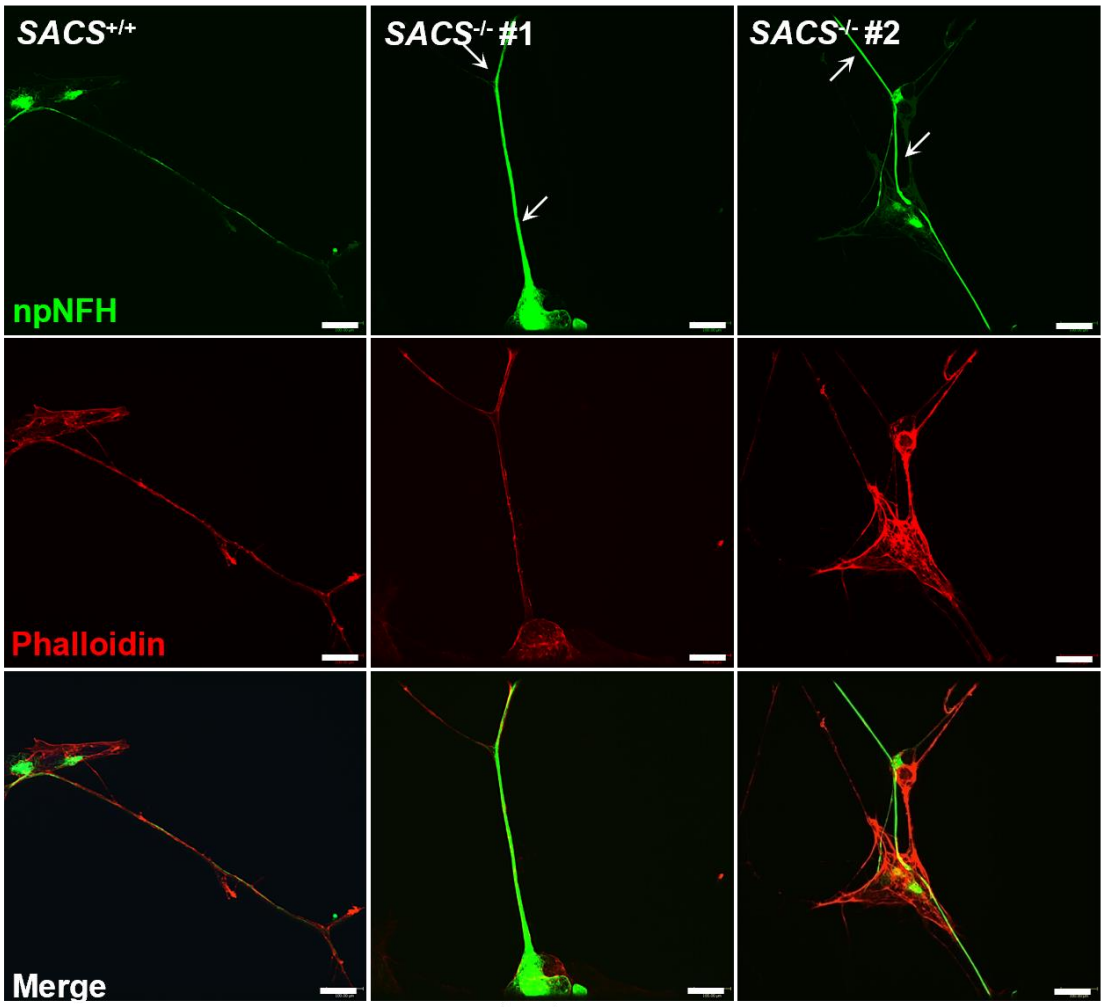
I started studying IFs alteration in two different *SACS*$^{-/-}$ neuronal-like SH-SY5Y clonal cell lines (see **Results Section 1**) to evaluate IF alteration. This cellular model recapitulates the gross IF cytoskeleton alteration which was previously reported in ARSACS patients' fibroblasts cells, by our group and collaborators (Duncan *et al*, 2017). In *SACS*$^{-/-}$ SH-SY5Y cells, vimentin shown to collapse into a single dense bundle, located perinuclearly, instead of being uniformly distributed in the cytoplasm as in the control cells (**Results Fig. 10a**). Also, the NF cytoskeleton was impaired in undifferentiated *SACS*$^{-/-}$ SH-SY5Y cells, as observed by widefield immunofluorescence microscopy of the NFH, at steady state conditions (**Results Fig**. **10b**). Whereas NFH formed distinct and elongated filaments in control cells (**Results Fig. 10b**, white arrows), a single dense bundle, usually located perinuclearly, was detected in most *SACS*$^{-/-}$ cells. To quantitively assess NF remodeling, I set up a bioinformatic pipeline to quantify for each cell the *volume of the largest NF-object* (hence max-NFH volume), by deconvolution and 3D-reconstruction of z-stacks in widefield epifluorescence microscopy. This parameter is directly proportional to the degree of

occurring NF bundling, at this resolution power (**Results Fig. 10c**, schematics model). Indeed max-NFH volume was significantly and reproducibly increased in both *SACS*$^{-/-}$ clones compared to controls at steady state conditions (**Results Fig. 10d**, graph). These results were robustly confirmed by immunofluorescence with SMI32 (an antibody directed against npNFH) in widefield epifluorescence microscopy with deconvolution (**Results Fig. 10e**); suggesting that these NF bundles observed in the absence of sacsin are hypophosphorylated in neuronal-like cells, as will be thoroughly discussed in next section.


A
SACS+/+
SACS-/- #1
Vimentin
Vimentin DAPI
B
SACS+/+
SACS-/- #1
SACS-/- #2
NFH DAPI
C
SACS+/+
SACS-/-
D
**
*
ns
max-NFH volume (µm3)
60
40
20
0
SACS+/+
SACS-/- #1
SACS-/- #2
E
SACS+/+
SACS-/- #1
npNFH DAPI
*
max-NFH volume (µm3)
60
40
20
0
SACS+/+
SACS-/- #1
F
SACS+/+
SACS-/-
Sacsin
Spectrin

Results Figure 10 (previous page). Absence of sacsin causes NF bundling in undifferentiated neuronal-like SH-SY5Y cells. *A. Representative images by 63X widefield microscopy of immunofluorescence with vimentin antibody (green) in steady-state SH-SY5Y cells, showing perinuclear dense bundles in undifferentiated SACS$^{-/-}$ clones compared to controls. Cells were counterstained with DAPI. Rightmost inserts are magnified regions of corresponding white squares. Scale bars = 20μm. B. Representative images by 63X widefield deconvolution microscopy of immunofluorescence with total NFH antibody (green) in steady-state SH-SY5Y cells, showing perinuclear bundling in undifferentiated SACS$^{-/-}$ clones compared to controls. Cells were counterstained with DAPI. Inserts below are magnified regions of corresponding white squares; white arrows indicate normal NF filamentous structures in control cells. Images are shown as max-projections of z-stacks. C. Schematics model of NF bundling quantification: NF fibers (green) became packed in SACS$^{-/-}$ cells and are recognized as a single object at this resolution power, therefore volume of largest NF object in each cell is proportional to bundling; NF objects volume is determined by 3D-reconstruction of z-stacks, in cells defined by dilating nuclei signal (blue circles). D. Quantification of average max-NFH volume (referred to B) after 3D reconstruction of z-stacks. Data are presented as mean ± SEM; n= at least 3 biologically independent experiments (at least 100 cells per experiment); *<0.5,**p<0.01 (ONE-WAY ANOVA with Tukey's test for multiple comparison). E. Representative images by 63X widefield microscopy with deconvolution of immunofluorescence with npNFH antibody (SMI32) (green) and relative average max-NFH volume quantification as in C-D. Staining with DAPI was done to mark nuclei. Rightmost inserts are magnified regions of white squares. Images are shown as max-projections of z-stacks. Data are presented as mean ± SEM; n=3 biologically independent experiments (at least 200 cells per experiment), *p<0.05 (Student's t-test with Welch correction). F. WB analysis to check sacsin levels in both SACS$^{-/-}$ clones used in this study. B-E. Scale bars = 20μm. Images taken with DeltaVision Ultra (G.E. Healthcare).*

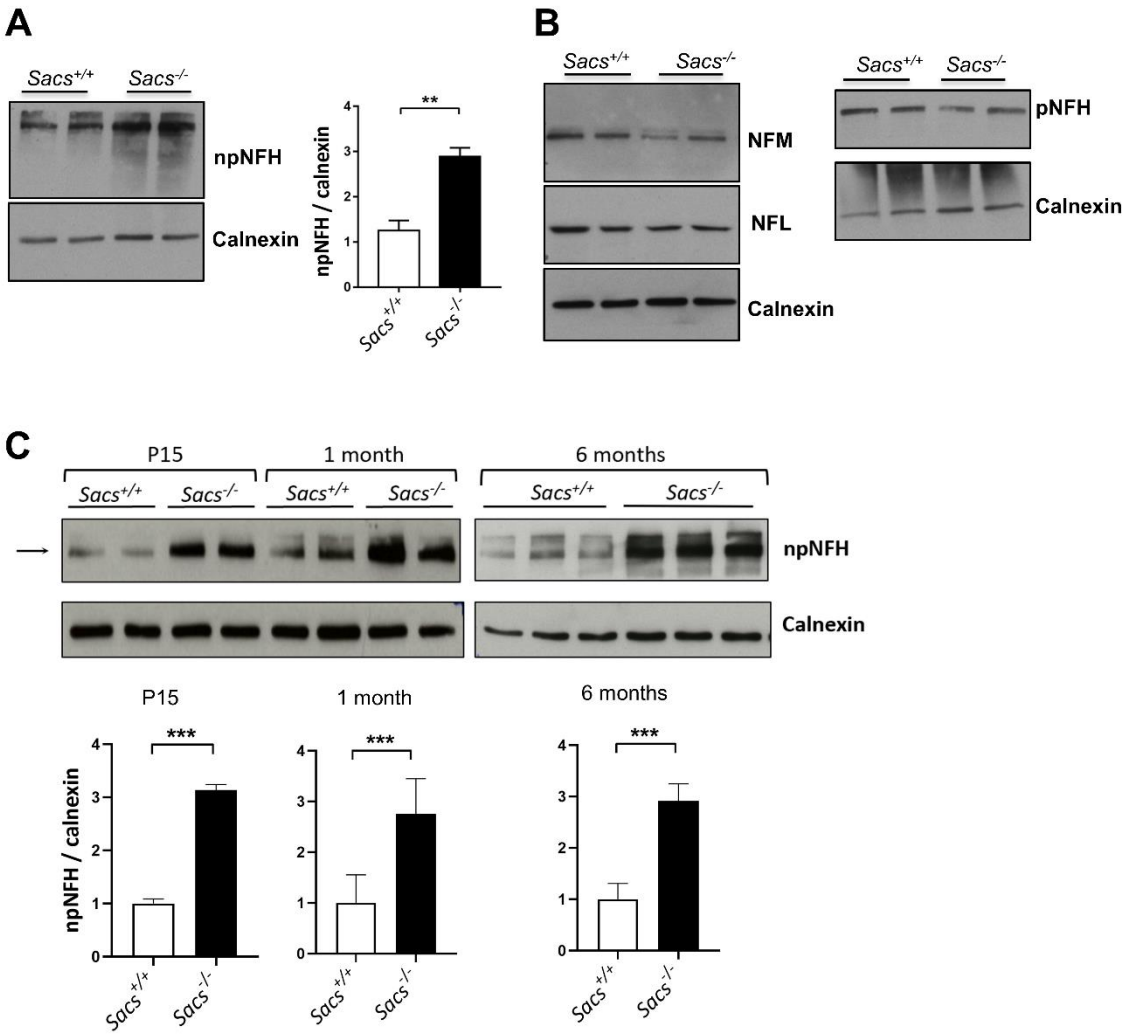
Finally, I treated SH-SY5Y cells with retinoic acid (RA) and BDNF in the absence of serum. In these conditions, proliferation stops, and the cells differentiate toward neuronal-like state, extending long neurites. In differentiated *SACS$^{-/-}$* SH-SY5Y cells, NF distribution was again strikingly altered compared to control differentiated cells, by SMI32 confocal immunofluorescence imaging, showing both bundles in the soma and increased signal in the neurites (**Results Fig. 11**, representative images - white arrows).



Results Figure 11. The absence of sacsin causes NF bundling in differentiated neuronal-like SH-SY5Y cells. *Representative images by 63X confocal microscopy of immunofluorescence with npNFH antibody (green) and phalloidin marking F-actin (red) in two different RA+BDNF differentiated SACS$^{-/-}$ SH-SY5Y clones compared with SACS$^{+/+}$ controls. Controstaining with DAPI was done to mark nuclei. Arrows indicate npNFH accumulation. Images are shown as max projections of z-stacks. Scale bars = 13 µm. Images taken with Ultraview (Perkin Elmer).*

We then focused on sacsin function in cerebellum and PNs. At five months of age (post-symptomatic stage) (Larivière *et al*, 2015), *Sacs*$^{-/-}$ mice displayed increased level of npNFH by WB on cerebellar lysates compared to wild-type control littermates (**Results Fig. 12a**); at the same age, the other NF subunits – NFM and NFL – and pNFH – detected with specific SMI31 antibody - were not increased by WB in cerebellar lysates in *Sacs*$^{-/-}$ mice compared to wild-type controls (**Results. Fig. 12b**), suggesting a specific effect for sacsin on the NFH subunit. Significant drastic increase of npNFH level in *Sacs*$^{-/-}$ cerebellum by WB was already present at pre-symptomatic stages, at one month of age and as early as P15 (**Results Fig. 12c**). This is the

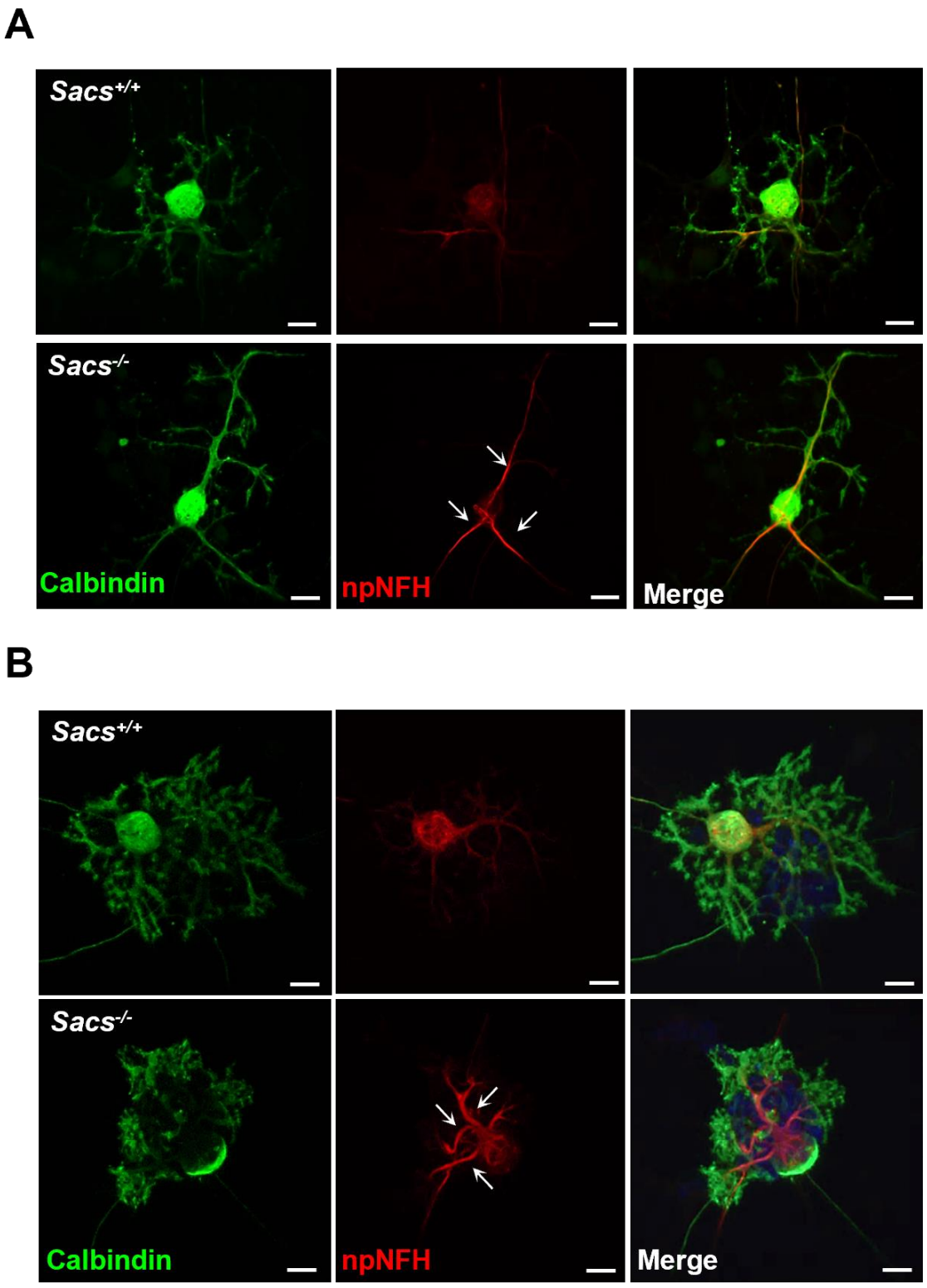
earliest cytopathological event in *Sacs*$^{-/-}$ PN, investigated so far, preceding PNs degeneration.



Results Figure 12. The npNFH signal increase in Sacs$^{-/-}$ cerebellum is an early event in ARSACS pathogenesis. *A. Representative WB of npNFH level (SMI32 antibody) in cerebellar lysates from Sacs$^{-/-}$ and control mice at five months of age with relative quantification normalized on calnexin. Data are reported as mean±SEM; n=at least three biological replicates; ***p<0.001 (Student's t-test with Welch correction). B. Representative WB of NFM and NFL subunits and pNFH isoform (detected with SMI31 antibody) in cerebellar lysates from Sacs$^{-/-}$ and control mice at five months of age. Calnexin shown as normalizer. C. Representative WB of npNFH level in cerebellar lysates from Sacs$^{-/-}$ and control mice in a time course at P15, one month and six months of age, with relative quantification normalized on calnexin on graphs below. Data are mean±SEM; n= at least three biological replicates; ***p<0.001 (Student's t-test with Welch correction). Males or females mice were equally used.*

To investigate NFH distribution at PNs-specific cellular level, we performed confocal imaging of SMI32 immunofluorescence on primary PNs, which revealed in *Sacs*$^{-/-}$ the presence of bundles in the soma and neurites and especially in proximal

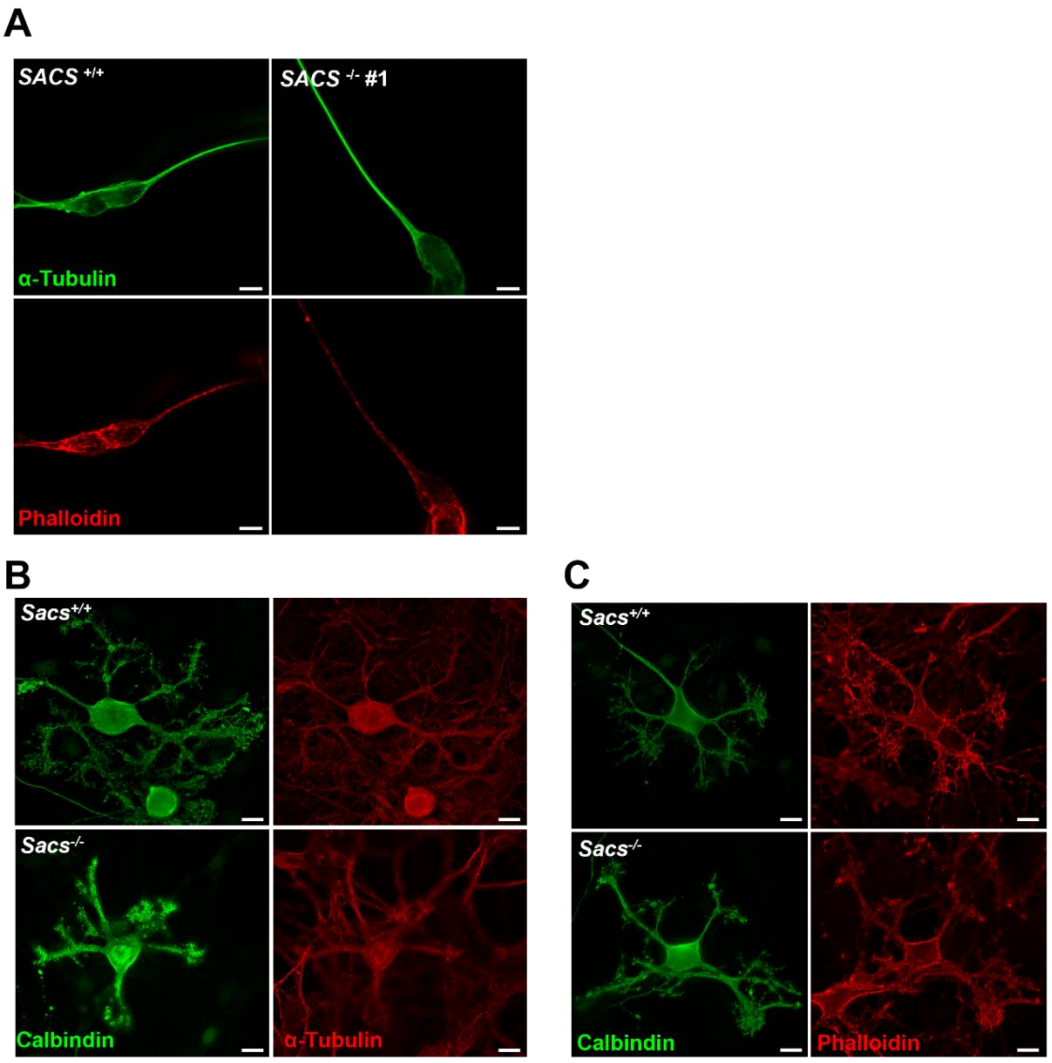
dendrites, already detectable at days in vitro (DIV) 10, when PNs dendritic harbor has already formed, as well as at DIV15 (**Results Fig. 13a-b,** respectively).



Results Figure 13. The absence of sacsin causes NFH bundling ex vivo in PNs. *A-B. Representative images by 63X confocal microscopy of immunofluorescence with calbindin*

(green) and npNFH (red) in DIV10 (A) and DIV15 (B) Sacs$^{-/-}$ and wild-type PNs. Arrows indicate npNFH bundles. Images shown as max projection of z-stacks. Scale bars=13µm. Images taken with Ultraview (Perkin Elmer).

Finally, the other two branches of cytoskeleton – microfilaments and microtubules - did not show gross abnormalities in neurons in the absence of sacsin, as observed by widefield immunofluorescence with deconvolution of tubulin and phalloidin on both neuronally-differentiated *SACS$^{-/-}$* SH-SY5Y cells (**Results Fig. 14a**) and Sacs$^{-/-}$ PNs cultures (**Results Fig. 14b-c**); see also **Results Fig. 11** for phalloidin staining in differentiated SH-SY5Y cells in representative images from an independent experiment).



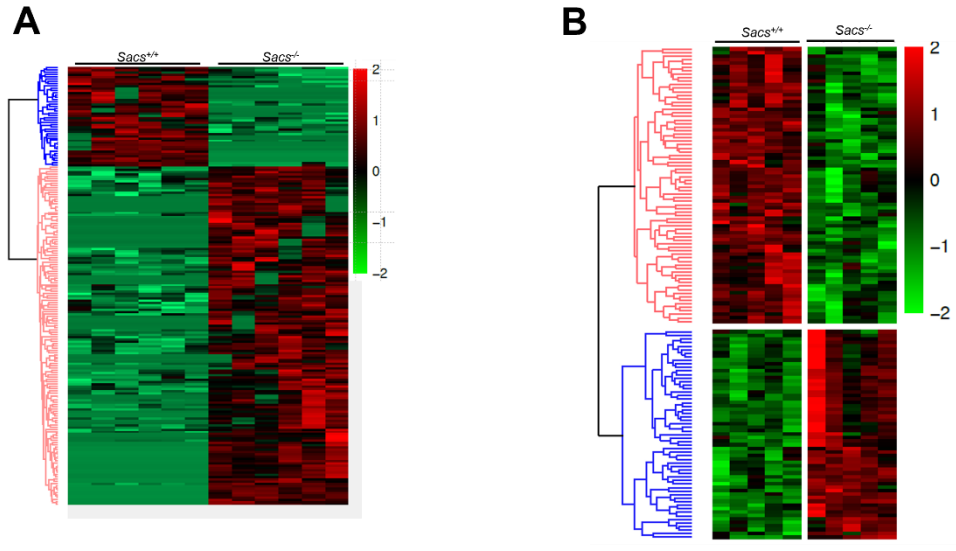
Results Figure 14. Microfilament and microtubule cytoskeleton is not impaired in the absence of sacsin in SH-SY5Y cells and primary PNs. *A. Representative images by widefield microscopy with deconvolution (63X) of immunofluorescence with alpha-tubulin (green) and phalloidin (red) in RA+BDNF neuronally differentiated SACS$^{-/-}$ SH-SY5Y clonal cells and relative controls. Images are shown as max projection of z-stacks. B-C. Representative*

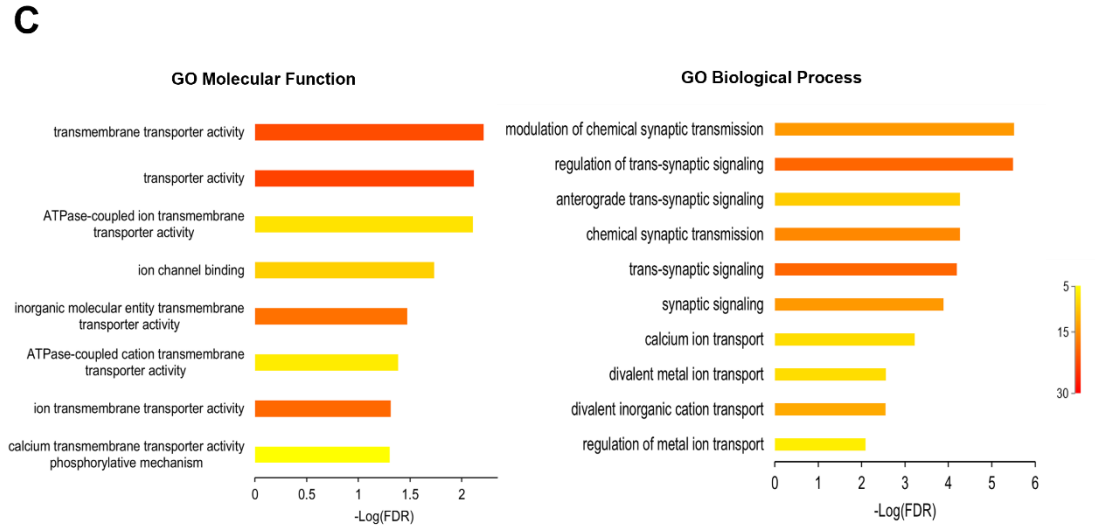
images by widefield microscopy with deconvolution (63X) of immunofluorescence with PNs-specific marker calbindin (green) alpha-tubulin (B) or phalloidin (C) (red) in DIV15 Sacs$^{-/-}$ PNs and relative wild-type controls. Images shown as max projections of z-stacks. A-C. Scale bars = 20µm. Images taken with DeltaVision Ultra (G.E. Healthcare).

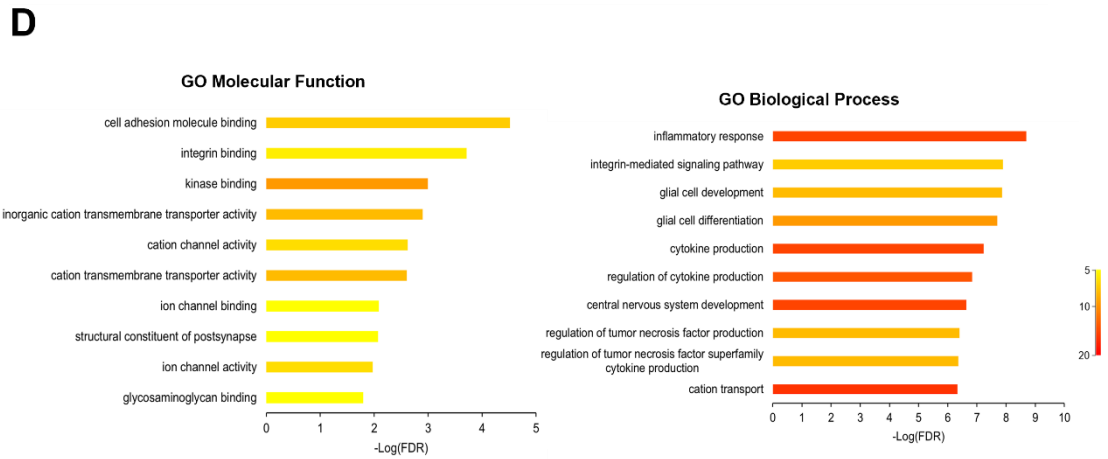
These data suggest a primary role for sacsin in the regulation of IFs cytoskeleton and in particular NFH subunit in neurons. These cellular models also proved to be valuable for examining this phenotype at molecular level and for providing a quantitative readout for therapeutic approaches aimed to rescue NF alteration.

2.2 – Integrated OMICS analyses show that NFH phosphorylation dynamics is impaired in Sacs$^{-/-}$ mice.

The increased amount of npNFH seen by WB in *Sacs*$^{-/-}$ cerebellum could be due to absolute increased level of NFH subunit *per se* or altered phosphorylation dynamics, or both. WB analysis from cerebellar lysates shown a slight decrease of pNFH level (**Results Fig. 12b**), suggesting a dysregulation in phosphorylation dynamics, rather than in expression levels. To assess the issue more quantitatively, we first analyzed data from total cerebellar proteomics by label free quantitative (LFQ) tandem mass-spectrometry (MS/MS) at five months of age. A total of 194 proteins had statistically (FDR<0.05) differential abundance between *Sacs*$^{-/-}$ and *Sacs*$^{+/+}$ littermates (**Results Fig. 15a**), the great majority of which (150) were reduced in *Sacs*$^{-/-}$ cerebellum. I performed functional enrichment – with over-representation analysis (ORA) method of Gene Ontology (GO) pathways – on these proteins, which revealed pathways in calcium homeostasis and synapse functionality as the most affected in the absence of sacsin and which likely underline ongoing neurodegeneration (**Results Fig. 15c**). Bulk RNA sequencing (RNAseq) from *Sacs*$^{-/-}$ and control cerebellum again at five months of age, revealed also 137 significantly (P-adjusted<0.1) differentially expressed genes (59 upregulated and 78 downregulated in *Sacs*$^{-/-}$ cerebellum) (**Results Fig. 15b**). Consistently, GO pathways analysis revealed enrichment of genes involved in ion homeostasis (the majority of which were downregulated, in according with proteomics data), as well as a cluster of genes that belong to transcriptional signature of microglia and astrocytic activation (**Results Fig. 15d**).

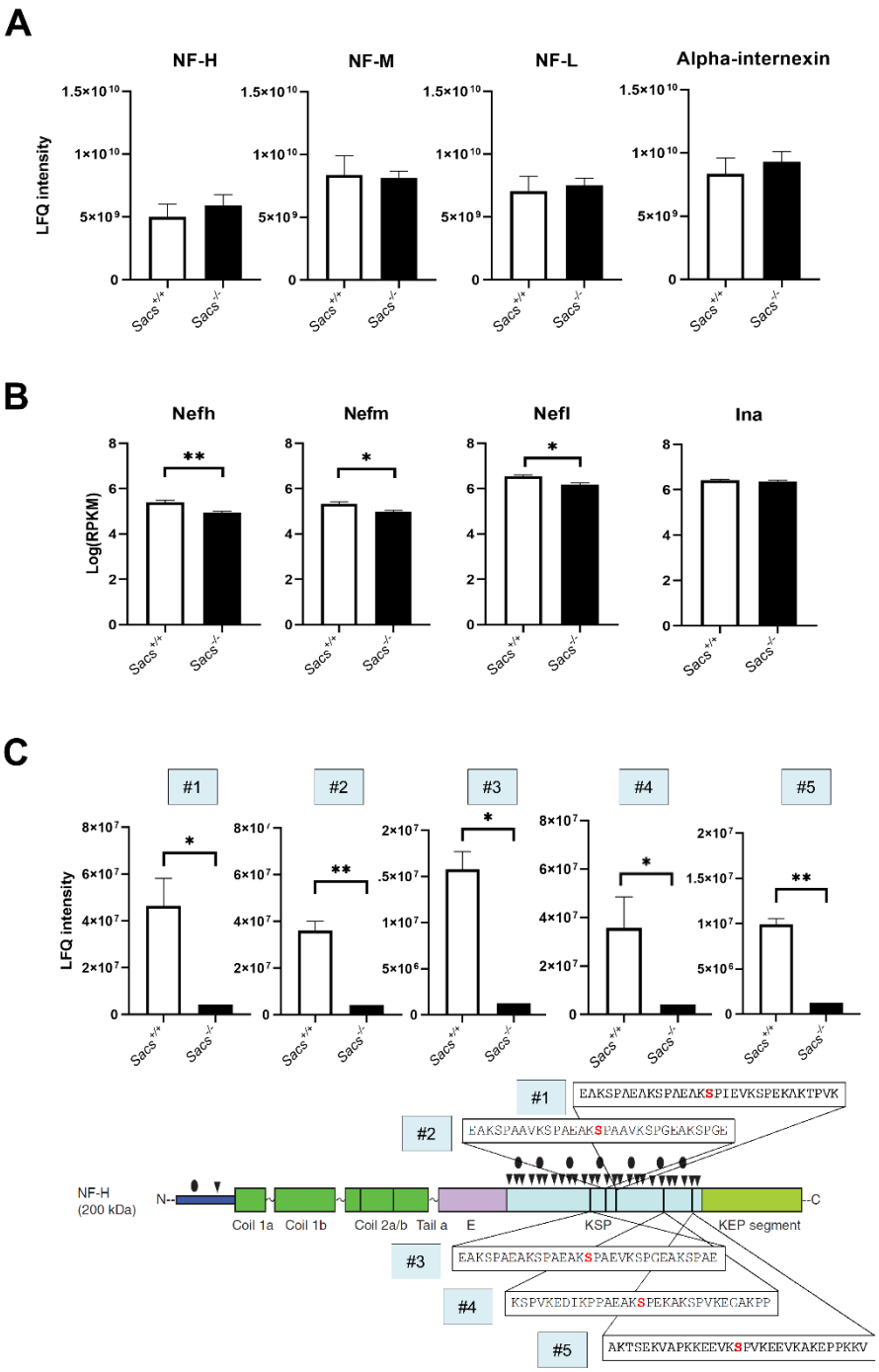

A
Sacs+/+
Sacs-/-
2
1
0
−1
−2
B
Sacs+/+
Sacs-/-
2
1
0
−1
−2


C
GO Molecular Function
transmembrane transporter activity
transporter activity
ATPase-coupled ion transmembrane transporter activity
ion channel binding
inorganic molecular entity transmembrane transporter activity
ATPase-coupled cation transmembrane transporter activity
ion transmembrane transporter activity
calcium transmembrane transporter activity phosphorylative mechanism
0 0.5 1 1.5 2
-Log(FDR)
GO Biological Process
modulation of chemical synaptic transmission
regulation of trans-synaptic signaling
anterograde trans-synaptic signaling
chemical synaptic transmission
trans-synaptic signaling
synaptic signaling
calcium ion transport
divalent metal ion transport
divalent inorganic cation transport
regulation of metal ion transport
0 1 2 3 4 5 6
-Log(FDR)
5
15
30


D
GO Molecular Function
cell adhesion molecule binding
integrin binding
kinase binding
inorganic cation transmembrane transporter activity
cation channel activity
cation transmembrane transporter activity
ion channel binding
structural constituent of postsynapse
ion channel activity
glycosaminoglycan binding
0 1 2 3 4 5
-Log(FDR)
GO Biological Process
inflammatory response
integrin-mediated signaling pathway
glial cell development
glial cell differentiation
cytokine production
regulation of cytokine production
central nervous system development
regulation of tumor necrosis factor production
regulation of tumor necrosis factor superfamily cytokine production
cation transport
0 1 2 3 4 5 6 7 8 9 10
-Log(FDR)
5
10
20

Results Figure 15 (from previous page). OMICS analyses from mice cerebellum reveals pathways involved in ARSACS pathogenesis. *A. Hierarchical clustering comparing 194 differential proteins between Sacs$^{-/-}$ and wild-type controls from maxQUANT analysis of LFQ-MS/MS of total cerebellum at five months of age; n=6 from three independent biological replicates; Student's t-test with permutation test, FDR<0.05. Two control males and one control female, one Sacs$^{-/-}$ male and two Sacs$^{-/-}$ females were used. B. Hierarchical clustering comparing 137 differentially expressed genes between Sacs$^{-/-}$ and wild-type controls from RNAseq data of total cerebellum at five months of age; n=5 independent biological replicates; FDR<0.1, Fisher test. Five control and five Sacs$^{-/-}$ females were used. C. GProfiler enrichment analysis of deregulated proteins showing top ten categories (FDR<0.05, Fisher test) for each GO molecular function (MF) and biological process (BP). Color represents absolute number of genes in each category. D. GProfiler enrichment analysis of differentially expressed genes showing top ten categories (FDR<0.05, Fisher test) for each GO molecular function (MF) and biological process (BP).*

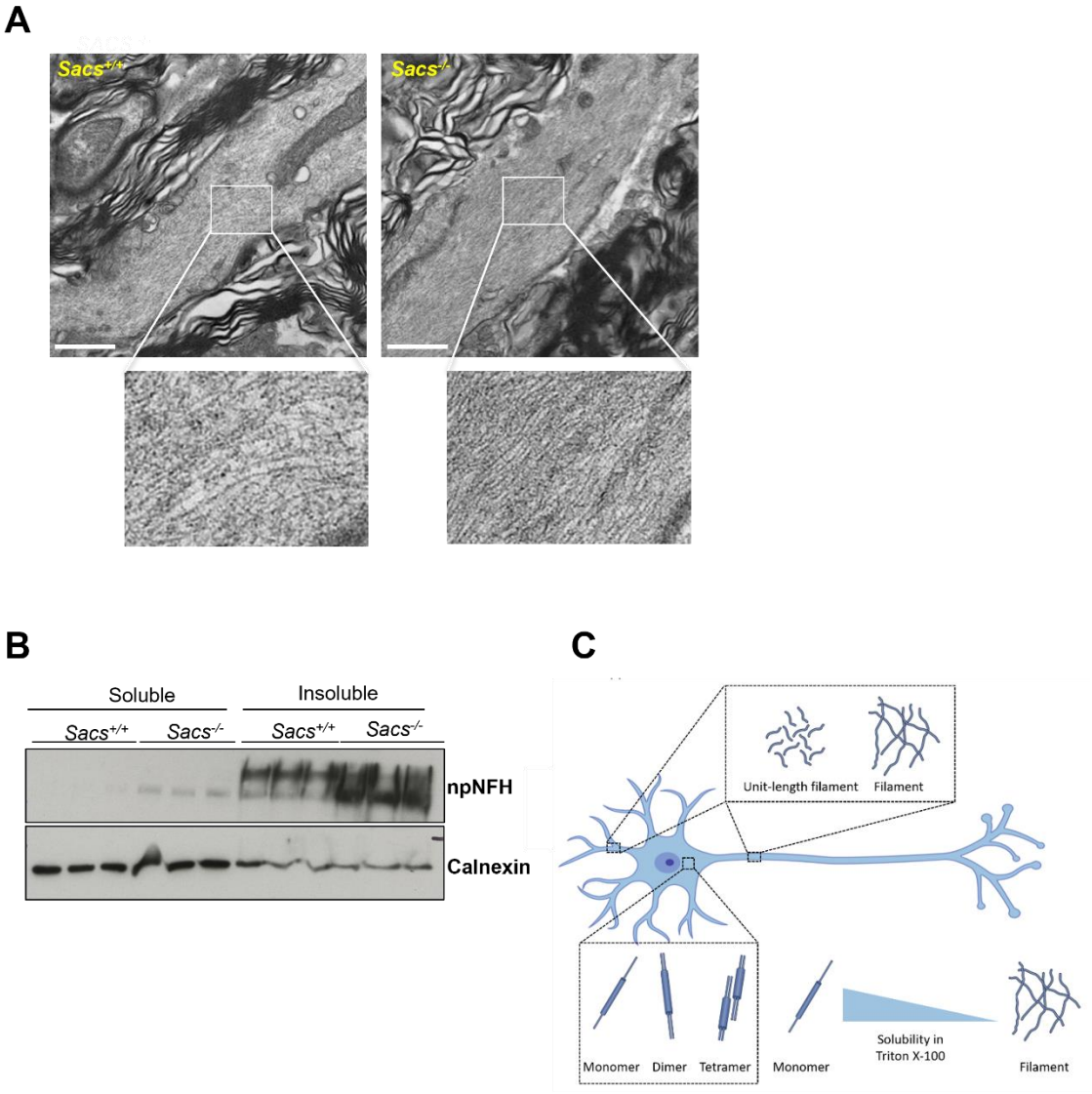
LFQ-MS/MS analysis of total cerebellum shown that all neuronal Type IV IFs proteins expressed in CNS (NF subunits and α-internexin, encoded by *Ina* gene) were not altered by normalized LFQ-intensities (**Results Fig. 16a;** in according with representative WB from **Results Fig. 12b**). In contrast, total mRNA level of each NF subunit was slightly, but significantly, decreased in *Sacs*$^{-/-}$ cerebellum by bulk RNAseq data (**Results Fig. 16b**), which might be suggestive of adaptive downregulation of NF expression to stop their bundling. These data support that npNFH increased level is due to unbalanced proportion between phosphorylated and nonphosphorylated forms of NFH subunit. To resolve precise positions of differential NFH phosphorylation sites, we performed phosphoproteomics on the same cerebellar samples at five months of age, analyzing phospho-peptides by LFQ-MS/MS. Very few proteins resulted to be statistically differentially phosphorylated at any site between *Sacs*$^{-/-}$ and control littermates (data not shown). This number was furtherly reduced by excluding those proteins in which increase of phosphorylated peptides in *Sacs*$^{-/-}$ or control cerebellum may be unreliable due to significant increase of total protein level in the same sample. Among these filtered proteins, NFH subunit was significantly hypo-phosphorylated in *Sacs*$^{-/-}$ at five different phosphosites, all belonging to KSP motifs in the C-terminal tail (**Results Fig. 16c**). Similarly, also one KSP site in C-tail of NFM was statistically hypophosphorylated (data not shown).


A
NF-H
NF-M
NF-L
Alpha-internexin
LFQ intensity
B
Nefh
Nefm
Nefl
Ina
Log(RPKM)
C
#1
#2
#3
#4
#5
LFQ intensity
NF-H
(200 kDa)
N
C
Coil 1a
Coil 1b
Coil 2a/b
Tail a
E
KSP
KEP segment
EAKSPAEAKSPAEAKSPIEVKSPEKAKTPVK
EAKSPAAVKSPAEAKSPAAVKSPGEAKSPGE
EAKSPAEAKSPAEAKSPAEVKSPGEAKSPAE
KSPVKEDIKPPAEAKSPEKAKSPVKEGAKPP
AKTSEKVAPKKEEVKSPVKEEVKAKEPPKKV

Results Figure 16 (from previous page). NF subunits levels are not altered while NFH phosphorylation is drastically impaired by OMICS in Sacs$^{-/-}$ mice cerebellum. *A. LFQ intensity values for all Type IV IFs subunits detected in our LFQ-MS/MS from Sacs$^{-/-}$ and control mice cerebellum at five months of age. Data are reported as mean±SEM with imputation of missing numbers; n=6 from three independent biological replicates; all data were non significant (Student's t-test with Welch correction). B. Log of Reads Per Kilobase of exon per Million mapped reads (RPKM) values for type IV IFs subunits transcripts by RNAseq from Sacs$^{-/-}$ and control mice cerebellum at five months of age. Data are reported as mean±SEM; n=5 independent biological replicates; *p<0.05; **p<0.01 (Student's t-test with Welch correction). C. LFQ intensity values of NFH phosphopeptides by maxquant analysis of LFQ-MS/MS from Sacs$^{-/-}$ and control mice cerebellum at five months of age, showing drastic loss of phosphorylation in the absence of sacsin. Data are reported as mean±SEM with imputation of missing numbers with the lowest value from all the dataset; n=6 from three independent biological replicates; *p<0.05 (Student's t-test with Welch correction). Below: Schematics representation of NFH regions showing the localization of the phosphorylated peptides found as significantly different in Sacs$^{-/-}$ and control mice cerebellum. The phosphorylated aminoacidic residue is highlighted in red. Schematics is adapted from Yuan et al., 2017, reused under Permission, copyright to Cold Spring Harbor Laboratory Press.*

Since phosphorylation of the C-terminal tails of NFH (and to lower extent NFM) is important to maintain mature NF fibers spacing (Yuan *et al*, 2017), we hypothesized that loss of NFH phosphorylation leads to bundling and reduced spacing of structurally normal NF fibers in the absence of sacsin. Electron microscopy of NF fibers in *Sacs*$^{-/-}$ and littermate controls cerebellar slices, at five months of age, confirmed this conclusion, showing normal, ordered, parallel, 10-nm fibers (typical of fully mature IF) in longitudinal sections of PNs axons in *Sacs*$^{-/-}$ samples, which were more densely packed, with less interspace, than in controls (**Results Fig. 17a**, representative images).

Finally, since the various assembly intermediates between monomers and mature filaments are known to be differentially soluble in Triton X-100 detergent, to understand the stage in NF assembly at which NFH phosphorylation status is affected in ARSACS, we extracted Triton-soluble and triton-insoluble fractions from *Sacs*$^{-/-}$ mouse cerebellum and controls, at same age (five months). Indeed, monomers, oligomers and certain polymers are soluble in this non-ionic detergent while mature 10-nm filaments become insoluble after full assembly (Gentil *et al*, 2015; Jung *et al*, 1998). While in the triton-soluble fraction the immunolabelling for npNFH was slightly more intense in *Sacs*$^{-/-}$ mice than in *Sacs*$^{+/+}$ mice, in the triton-insoluble fraction, instead, the npNFH accumulation was strikingly higher in *Sacs*$^{-/-}$ mice (**Results Fig. 17b-c**). These data support that insoluble mature NF fibers are properly assembled and are strongly hypophosphorylated in the absence of sacsin.



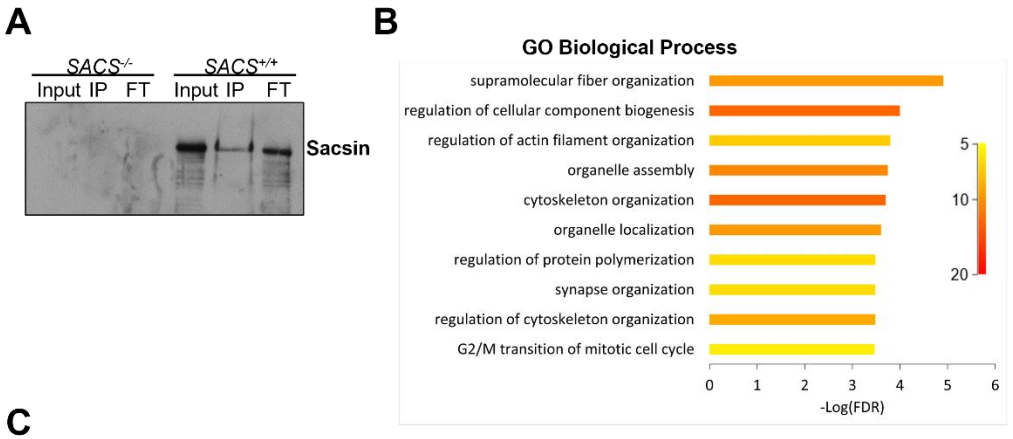
Results Figure 17. NF fibers form properly in Sacs$^{-/-}$ cerebellum by EM and biochemical analyses. *A. Representative electron microscope images (150000X) of longitudinal sections of PN axons from fixed Sacs$^{-/-}$ and control mice cerebellum at five months of age. Scale bars = 500nm. B. WB on Triton-soluble and insoluble fractions from Sacs$^{-/-}$ and control cerebellum lysates at five months of age, normalized on calnexin. Control and Sacs$^{-/-}$ males and females mice were equally used. C. Schematic representation of NF assembly intermediates, with their localization in the neuron and their solubility in Triton X-100. Icon of the neuron was created on Biorender; assembly intermediates were adapted from (Snider & Omary, 2014), copyright Nature publishing group, reused under permission.*

In conclusion, in *Sacs$^{-/-}$* cerebellum, NF subunits abundance is not altered in the absence of sacsin, NF fibers maturate and form properly but are not phosphorylated on NFH subunit C-terminal tails and ultimately they get densely packed, as observed both by light (see also schematics model in **Results Fig. 10c**) and electronic microscopy *in vitro, ex vivo* and *in vivo*.

2.3 - Sacsin physically interacts with NF proteins and other cytolinker proteins in SH-SY5Y neuronal-like cells

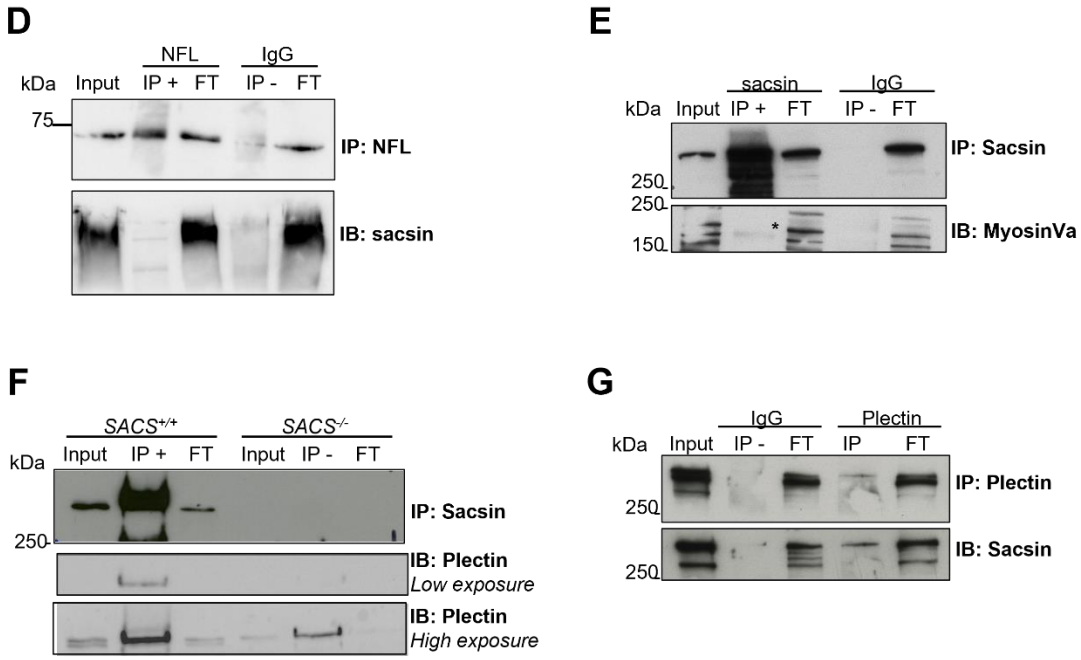
Sacsin may regulate NFH phosphorylation and dynamics directly binding to NF subunits or other cytoskeletal linkers. To study if sacsin and NF subunits physically interact, we performed interactomics by sacsin immunoprecipitation (IP) in neuronally-differentiated SH-SY5Y control cells, followed by LFQ-MS/MS analysis of eluates to identify sacsin interactors (**Results Fig. 18a**). This cellular model was employed as it recapitulates NF bundling, expresses sacsin at high level and is unaffected by contamination and dilution effects by other non-neuronal and non-sacsin-expressing cell types, as may be the case for cerebellar samples or primary PN cultures.

Sixtyseven specific sacsin interactors were identified, which were undetected in control IP from *SACS*$^{-/-}$ SH-SY5Y cells. GO pathways functional analysis with STRING software (a tool for protein-protein interaction analysis) shown enrichment of proteins related to supramolecular fiber organization, actin cytoskeleton organization and organelle localization (**Results Fig. 18b**). NFM and NFL were detected among sacsin interactors, as well as plectin, which is a huge 534-kDa cytoskeletal linker that links NFs to other cellular organelles and structures in a variety of cell types (**Results Fig. 18c**). We were able to validate NFL interaction with sacsin, by reverse co-IP from the detergent-insoluble fraction of SH-SY5Y cells followed by biochemical extraction of NF cytoskeleton, providing further strong evidence of sacsin interaction with NF fibers (**Results Fig. 18d**). Another interesting interactor, belonging to cytoskeleton organization and organelle transport categories, was myosin Va, a 215-kDa neuronal myosin isoform which is involved in anterograde organelle transport along microtubules in dendrites (**Results Fig. 18e**). The physical interactions with myosin Va and plectin were biochemically confirmed by sacsin co-IP from control SH-SY5Y cells lysates (**Results Fig. 18e-f,** respectively) and even from wild-type mice cerebellar lysates by reverse plectin co-IP (**Results Fig. 18g**).



C

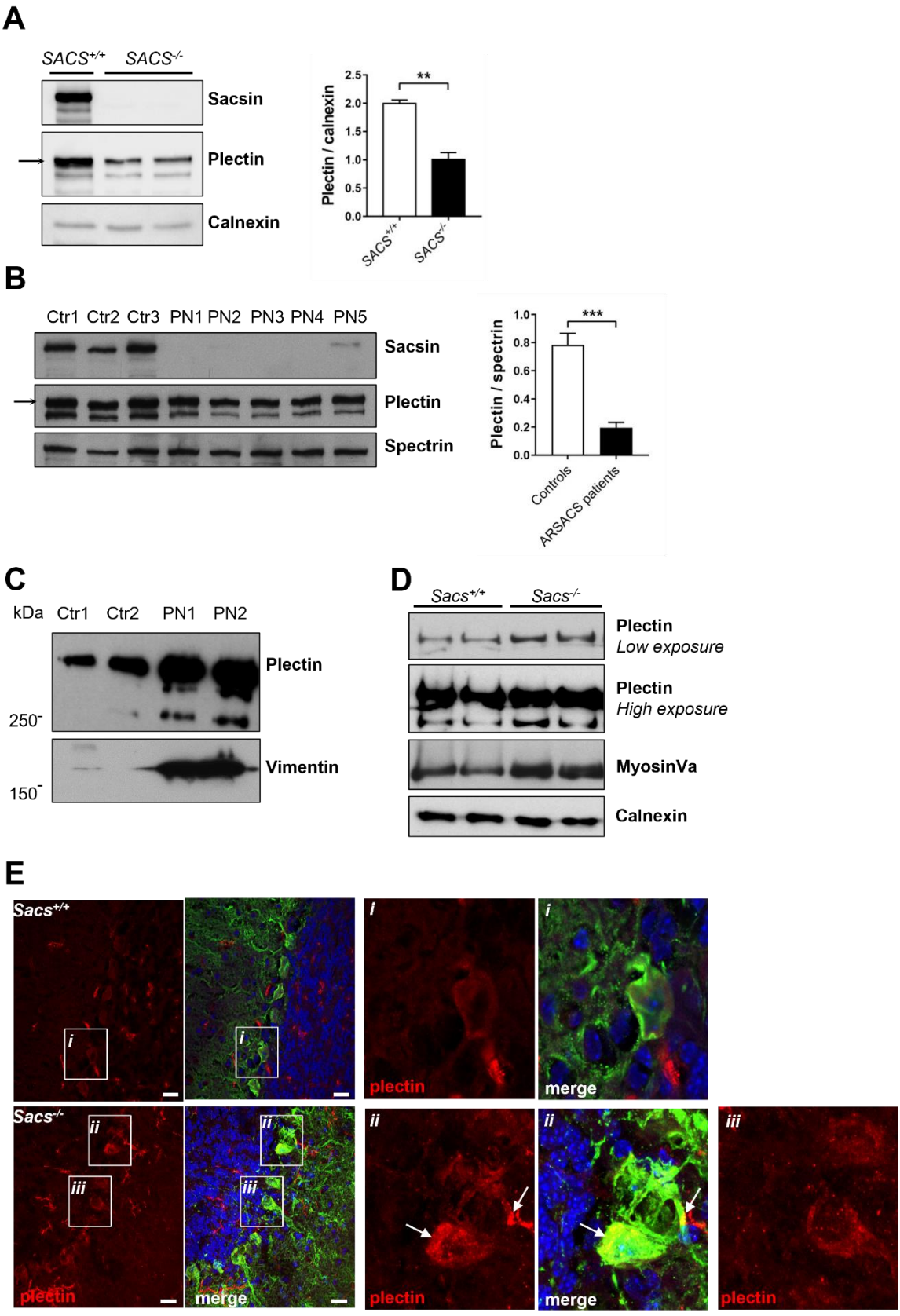
Protein names	Gene names	LFQ intensity WT_01	LFQ intensity WT_01R	LFQ intensity KO_01	LFQ intensity KO_01R
Neurofilament medium polypeptide	NEFM	29,61626	29,46205	NaN	NaN
Neurofilament light polypeptide	NEFL	28,42306	28,3917	NaN	NaN
Plectin	PLEC	28,22972	28,00646	NaN	NaN
Unconventional myosin-Va	MYO5A	28,63903	28,66119	NaN	NaN



Results Figure 18. Sacsin physically interacts with NFL, plectin and myosin Va. *A. Sacsin immunoprecipitation in SACS$^{-/-}$ SH-SY5Y cells (IP=Immunoprecipitation, FT=Flow Through). B. Gene Ontology (Biological Process) STRING enrichment output of sacsin co-immunoprecipated proteins. C. LFQ intensity of selected sacsin cytoskeletal interactors from two biological replicates. D. NFL IP in SACS$^{+/+}$, and SACS$^{-/-}$ as control, SH-SY5Y cells and immunodecoration with anti sacsin. IP was done after NF cytoskeleton extraction form cellular lysates. E-F. Sacsin IP in SACS$^{+/+}$, and SACS$^{-/-}$ as control, SH-SY5Y cells and immunodecoration with anti-myosin Va (E) and anti-plectin (F) antibodies. G. Plectin IP in wild-type cerebellum and immunodecoration with anti-sacsin antibody.*

Next, we investigated if novel sacsin interactors are functionally related in ARSACS pathogenesis. By WB, plectin level was reduced in two neuronal-like *SACS$^{-/-}$* SH-SY5Y monoclonal cell lines (**Results Fig. 19a**). Since plectin is ubiquitously expressed, we

also investigated its level in ARSACS patients' fibroblasts cells. WB in patient cells carrying different mutations (see **Results Fig. 1**), revealed again that plectin is reduced compared to control healthy fibroblasts (**Results Fig. 19b**), suggesting a general role for sacsin in regulating both IFs and plectin in different cell types. To investigate if plectin reduction seen in WB is due to downregulation of its expression, we reperformed WB on total homogenates from ARSACS patients' cells, by lysis of whole cellular pellets in Laemmli buffer 2X and loading on mixed acrylamide-agarose gels, that allows to detect putative aggregates up to 600 kDa complexes (Weiss *et al*, 2008). Importantly, vimentin signal accumulated in total homogenate from patients' cells (**Results Fig. 19c**), similarly to what observed for npNFH in insoluble fractions from *Sacs*$^{-/-}$ cerebellum (**Results Fig. 17b**). Plectin itself increased drastically in total homogenates patients' cells compared to controls (**Results Fig. 19c**), suggesting that the reduction detected by standard WB procedure in triton-soluble fraction was not due to reduction of the protein *per se*, but rather to its redistribution and accumulation in the insoluble-cytoskeletal fraction. Finally, the absence of sacsin impacts on plectin and myosin Va (which is neuronally expressed) *in vivo*, as both proteins increased in the Triton-x100 insoluble fractions from *Sacs*$^{-/-}$ cerebellum, compared to wild-type control littermates (**Results Fig. 19d**). In agreement, in *Sacs*$^{-/-}$ cerebellum sections at five months of age I observed by immunofluorescence plectin accumulation in soma and proximal dendrites of PNs, resembling that of npNFH at the same age, suggesting that its accumulation may undergo a similar pathway in the absence of sacsin *in vivo* (**Results Fig. 19e**).

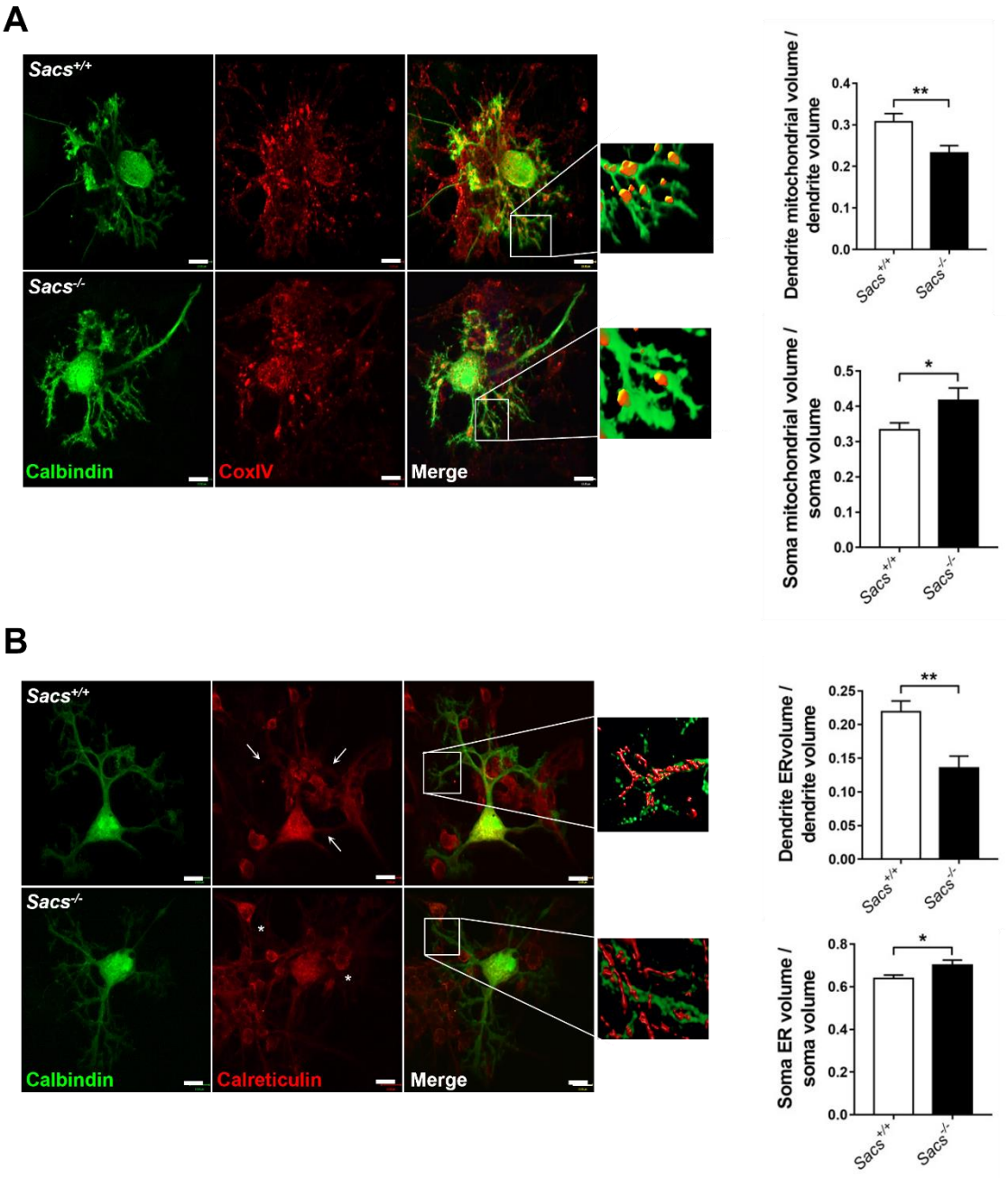

A
SACS+/+
SACS-/-
Sacsin
Plectin
Calnexin
Plectin / calnexin
2.5
2.0
1.5
1.0
0.5
0.0
**
SACS+/+
SACS-/-
B
Ctr1 Ctr2 Ctr3 PN1 PN2 PN3 PN4 PN5
Sacsin
Plectin
Spectrin
Plectin / spectrin
1.0
0.8
0.6
0.4
0.2
0.0
***
Controls
ARSACS patients
C
kDa Ctr1 Ctr2 PN1 PN2
Plectin
250
Vimentin
150
D
Sacs+/+
Sacs-/-
Plectin
Low exposure
Plectin
High exposure
MyosinVa
Calnexin
E
Sacs+/+
i
plectin
merge
Sacs-/-
ii
iii
plectin
merge

Results Figure 19 (From previous page). Plectin and myosin Va levels are deregulated in sacsin-depleted cells and cerebellum. *A-B. WB analysis showing levels of plectin (upper band as indicated by the arrow) in triton-soluble fraction in SACS$^{-/-}$ and SACS$^{+/+}$ SH-SY5Y cells (A) and ARSACS patients' and controls' fibroblasts (B), with relative quantitation (normalized to calnexin). Data are shown as mean±SEM; n= at least four biological replicates; **p<0.01, ***p<0.001 (Student's t-test with Welch correction) C. Acrylamide-agarose gel analysis showing levels of plectin and vimentin in ARSACS patient fibroblasts and relative controls total homogenate (whole cellular pellets directly lysed in Laemmli buffer 2X to include both nonionic detergent soluble and insoluble fractions). D. WB analysis showing levels of plectin and myosin Va in insoluble fractions of Sacs$^{-/-}$ and wild-type cerebellum at five months of age (normalized to calnexin). E. Representative images by confocal microscopy at 63X magnification of immunostaining on sagittal cerebellar slices from Sacs$^{-/-}$ and controls at seven months of age with plectin (red) and PNs-marker calbindin (green). DAPI was used as counterstaining. Sagittal sections close to the midline cut through cerebellar vermis were used for immunostaining; lobules III and IV/V were imaged. White arrows indicate examples of plectin accumulation in soma and proximal dendrites. Inserts are magnified regions of corresponding white squares. Images shown as max projections of z-stacks. Scale bars = 20µm. Images taken with Fluoview (Olympus). D.E. Males and females mice were equally used.*

These data corroborate a mechanistic link between sacsin and NF cytoskeleton subunits, as well as other cytoskeletal linkers involved in organellar trafficking; this led to the question if organelle trafficking is impaired in the absence of sacsin following primary NF cytoskeleton remodeling.

2.4 - Neurofilaments impairment causes defective organelle trafficking in Sacs$^{-/-}$ PNs

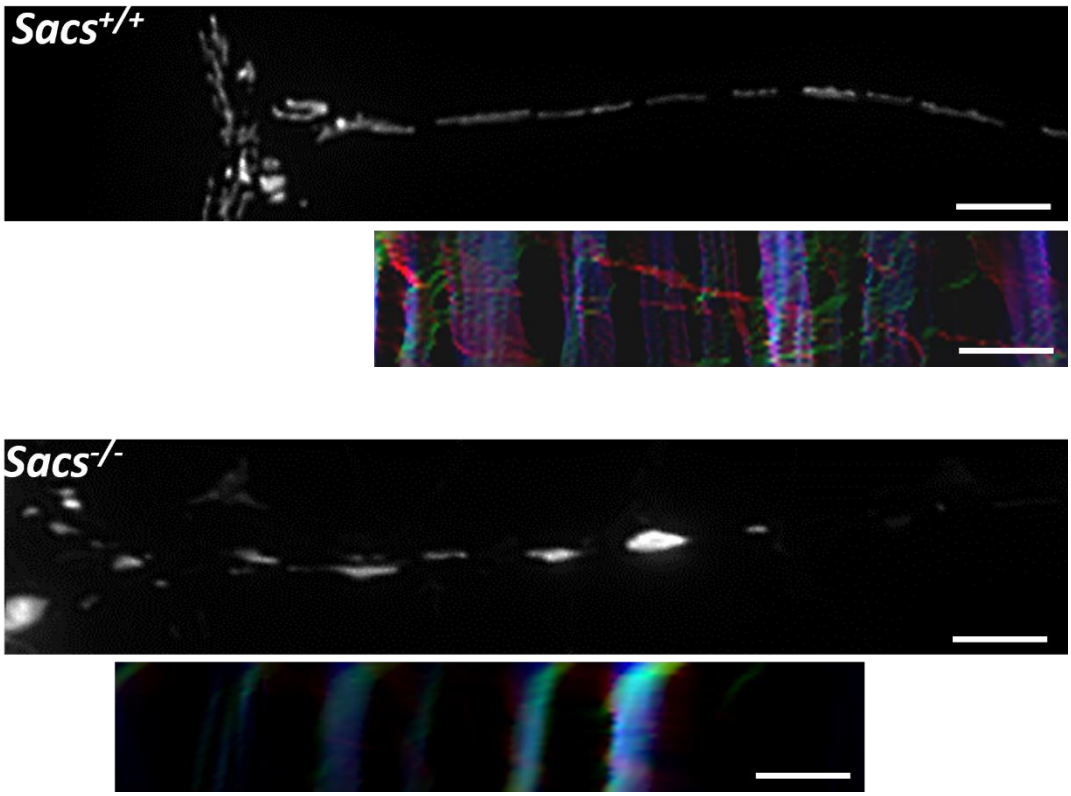
To study if organelle transport is impaired in the absence of sacsin in PNs, we focused mainly on mitochondria and ER transport in dendrites, as i) these organelles are essential for PN survival by buffering post-synaptic calcium influx at distal dendritic sites (Maltecca *et al*, 2015); and ii) proteomics analyses have revealed impairment of both calcium homeostasis and post-synapses in *Sacs$^{-/-}$* cerebellum at five months of age (**Results Fig. 15c**). Confocal immunofluorescence imaging of mitochondria and ER markers in primary *Sacs$^{-/-}$* PNs at DIV15 shown a low number of these organelles in proximal and distal dendrites sites compared to wild-type (**Results Fig. 20a-b**, representative images for mitochondria and ER respectively). This was quantified by volumetric analysis following 3D-reconstruction: while total volume of each organelle in PNs soma (normalized by soma volume) was increased in *Sacs$^{-/-}$* relative to wild-type controls, in the dendritic compartment there was a parallel significant reduction of total volume (normalized by dendritic volume) (**Results Fig. 20b-d**, graphs for mitochondria and ER respectively), demonstrating that both organelles are retained in the soma of PNs at long term stage (DIV15).



Results Figure 20. Defective mitochondrial and ER distribution in distal processes of Sacs$^{-/-}$ primary PNs. *A-B. Representative confocal images (63X) and higher magnification distal dendrites rendering of DIV15 Sacs$^{-/-}$ and wild-type PNs stained in green with calbindin, while in red mitochondrial marker CoxIV (A) and ER marker calreticulin (B). Graphs represent volumetric quantification of dendritic or soma mitochondrial/ER volume (normalized on dendrite/soma volume). Data are shown as mean±SEM; 10 cells quantified from 5 independent experiments; *p<0,05, **p<0.01 (Student's t-test with Welch correction). Scale bars = 13 µm. Images taken with Ultraview (Perkin Elmer).*

To further demonstrate that mitochondria transport is impaired in the absence of sacsin, we performed mitochondria live imaging at DIV10 in primary cultures from cerebellum as above, but infected at DIV0 with a lentivirus carrying MitoDsRed2 (a

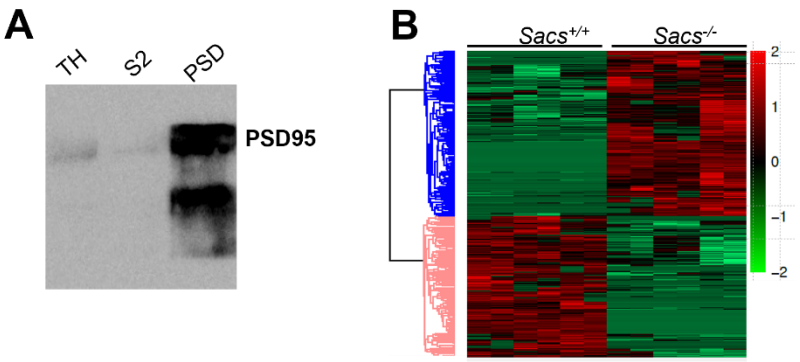
fluorescent protein that localizes in the mitochondrial matrix). This analysis could not be done directly in PNs, as they are not actively transduced by lentiviruses *ex vivo.* Moreover, mitotracker staining is not suitable for time-lapse imaging due to low signal stability. However, we focused on interneurons present in cultures, which are expected to express sacsin (Kozareva *et al*, 2021). Indeed, time-lapse live imaging of MitoDsRed2 in neurites belonging to primary cerebellar interneurons, revealed fewer and more static mitochondria in cultures from *Sacs*$^{-/-}$ mice, compared to wild-type mice (**Results Fig. 21** – representative timeframes and kimographs).

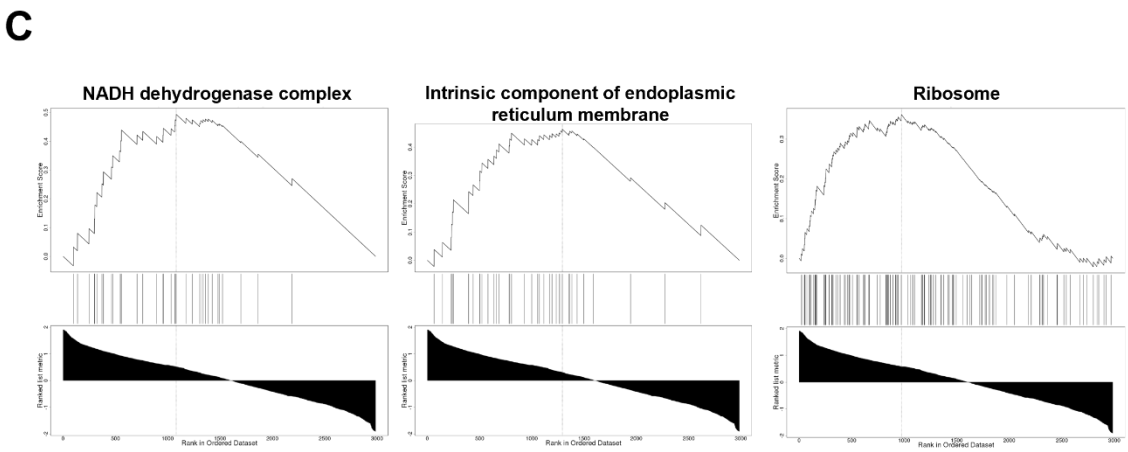


Results Figure 21. Mitochondrial movement is affected in the absence of sacsin. *Mitochondrial live imaging was performed by widefield deconvolution microscopy at 63X in neurites of DIV10 primary cerebellar cultures. Cultures were infected at DIV0 with lentivirus MitoDsred2 (white). For both Sacs*$^{-/-}$ *and wild-type control, one representative time frame is shown (above) with the corresponding kymograph (below). Kymographs show mitochondria trajectories along the corresponding length in x-axis of the representative image, from a time series of 31 images (1 image/minute). Red trajectories: anterograde movement; blue: still mitochondria; green: retrograde movement. Scale bars = 5µm.*

The absence of sacsin and deficient organelle transport to distal sites, in turn detriments synapse proteome in the dendrites, which likely ultimately underlines PNs degeneration (see also **Results Fig. 15a,c**). This was further corroborated by LFQ-MS/MS analysis of the post-synaptic density (PSD) fraction purified from *Sacs*$^{-/-}$ mice cerebellum at one month of age and relative wild-type littermates (**Results Fig. 22a –** representative example of PSD purification by WB analysis). This analysis was

conducted at pre-symptomatic stage to discriminate events in the synapse which were primarily related to the absence of sacsin and early cellular-molecular events, rather than widespread neurodegeneration. We identified 3303 proteins in the mice cerebellar PSD, 455 of which were significantly changed in abundance between *Sacs*$^{-/-}$ and control samples (FDR<0.05) (**Results Fig. 22b**). Gen Set Enrichment Analysis (GSEA) of the entire dataset, revealed, consistent with imaging experiments, significant downregulation (FDR<0.05) of GO cellular core components of different organelles that are known to be transported and associated to PSD sites, including mitochondria Complex I, ER, but also ribosomes and RNA granules (**Results Fig. 22c**), corroborating reduced abundance of these organelles in the absence of sacsin at distal sites.





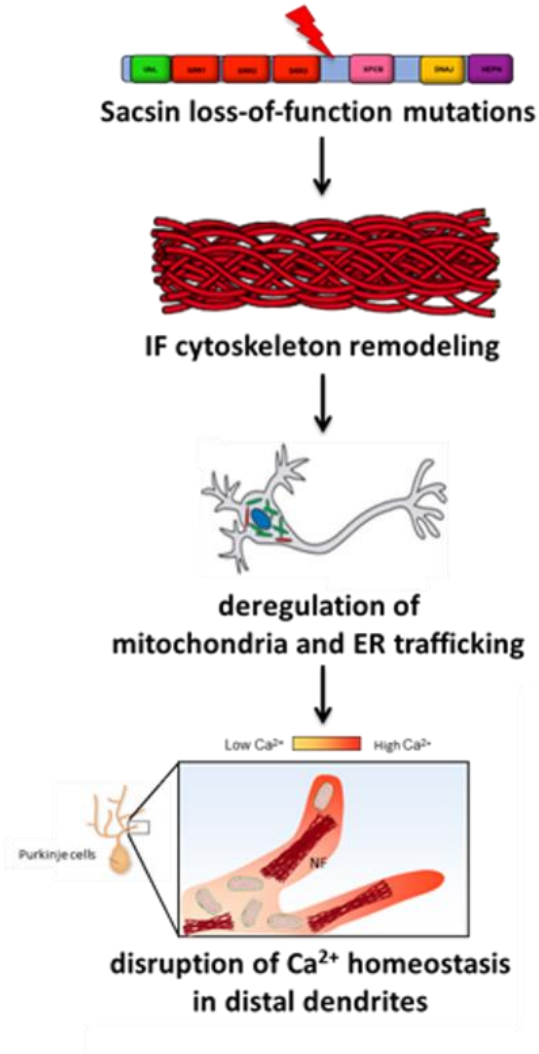
Results Figure 22. OMICS analyses show reduced abundance of organelles in cerebellar PSD in the absence of sacsin (from previous page). *A. representative WB showing PSD enrichment from total cerebellum lysates at one month of age. TH: total cerebellum homogenate; S2:cytosol and light membrane fraction; PSD: triton-X100 insoluble post-synaptic density. B. Hierarchical clustering of 455 differentially abundant proteins from LFQ-MS/MS of Sacs$^{-/-}$ PSD from cerebellum compared to controls; n=6 from three independent biological replicates; Student's t-test with permutation test, FDR<0.05. C. Results of GSEA on total of 3303 proteins detected in cerebellar PSD shows significant downregulation (by normalized enrichment score) of organelle cores proteins. Both control and Sacs$^{-/-}$ males and females pups were equally used.*

These data show that absence of sacsin leads to general impairment of transport in PN dendrites, which may be extended to other organelles and structures other than mitochondria and ER, therefore impacting deeply on synapse functionality and composition.

2.5 – ARSACS pathogenesis model

Sacsin function is primarily relevant for the regulation of IFs cytoskeleton and other related proteins, like plectin, in many cell types. Indeed, loss of sacsin causes remodeling of NF network in human neuronal-like cells and in PNs, consisting of NF fibers dense bundles visible both by electronic and light microscopy. These fibers are ordered and properly assembled, suggesting that sacsin does not affect folding, or NF fibers assembly *per se*. Instead, we provided evidence that NF fibers are hypo-phosphorylated in *Sacs*$^{-/-}$ cerebellum, which indeed may determine the decreased interspacing and therefore lead to formation of the bundles. Moreover, sacsin interacts with NFL, which is the core-forming NF subunit, as well as other cytolinkers as plectin, suggesting that sacsin may scaffold or regulate a macro-complex that regulates NF-network. This function would be primarily relevant for PNs.

We propose a pathogenic cascade in which NF-related cytoskeleton network remodeling causes impairment of organelle transport – mitochondria and ER - to distal dendrites in PNs, leading to impairment of calcium-buffering homeostasis and synapse functionality, as supported by imaging and proteomics analyses, both from whole cerebellar lysates and PSD compartment. Indeed, in a recent work from our group (Del Bondio, Longo, De Ritis et al. manuscript under review), we also directly proved that calcium homeostasis is dysregulated in *Sacs*$^{-/-}$ PNs and causes degeneration of PNs, as *Sacs*$^{-/-}$ mice phenotypes and PNs degeneration are ameliorated and slowed down by administration of the drug ceftriaxone drug, which acts by reducing post-synaptic calcium influx in glutamatergic synapses (**Results Fig. 23**).



Results Figure 23. ARSASC pathogenesis model.

3 - Investigation of novel engineered minisacsin in ARSACS preclinical models

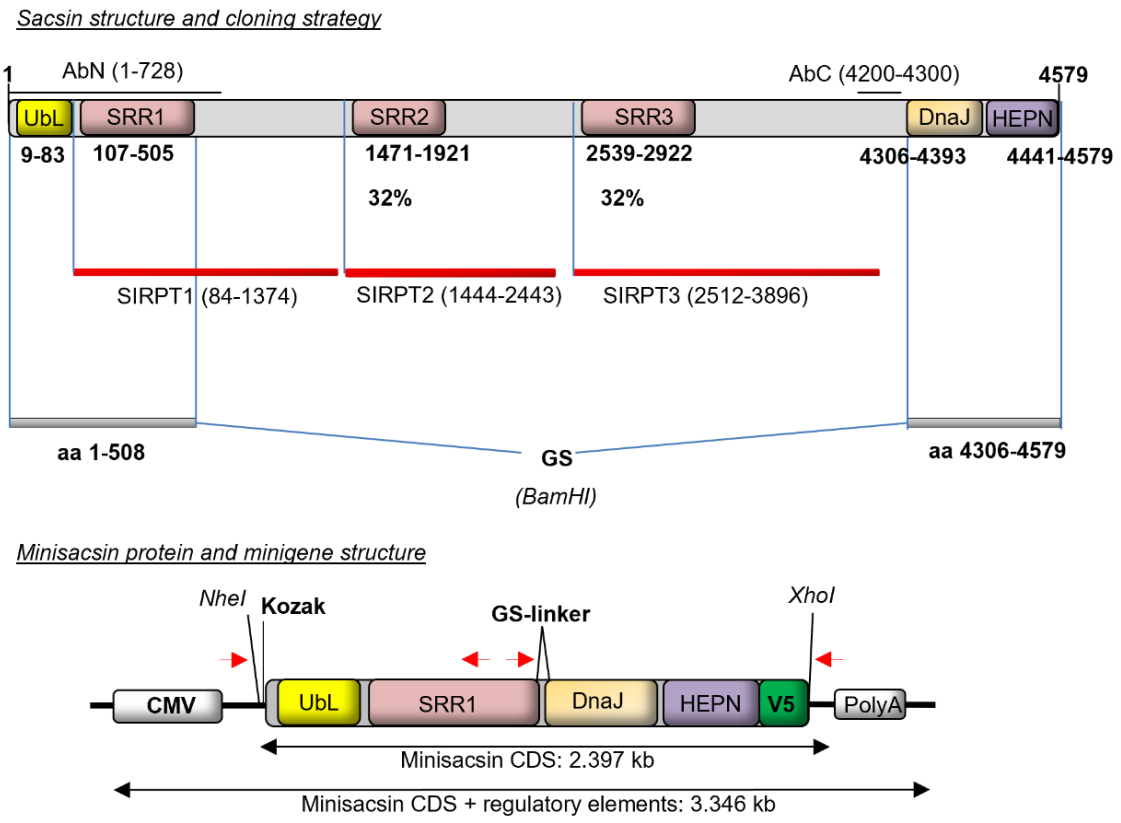
In previous sections I have dissected early molecular events of abnormal NF bundling in *Sacs*$^{-/-}$ PNs and in human neuronal-like *SACS*$^{-/-}$ SH-SY5Y cells. In order to act directly on the first and primary event of ARSACS pathogenesis - NF bundling - and restore sacsin function, I explored the route of gene therapy approach, by assessing sacsin gene replacement into preclinical models. The most promising viral platform for therapeutic delivery of nucleic acids is Adeno-Associated Viral vectors (AAV), due to its non pathogenicity, low immunogenicity and efficient episomal gene transfer in different dividing and non-dividing cell types, included the CNS (Li & Samulski, 2020; Samulski & Muzyczka, 2014; Chan *et al*, 2017; Morabito *et al*, 2017). However, this technology has a strong limitation on the size of the genetic material that can be packaged (4.8 kb), thus it would be impossible for ARSACS, since the *SACS* coding region alone is 15kb in length. Given the multimodularity of sacsin protein, I therefore explored the challenging hypothesis of designing a miniaturized version of sacsin, hence called minisacsin, and studying its functionality, as a proof of concept of AAV gene replacement therapy approach in ARSACS. In this section, minisacsin functionality will be described *in vitro* and *ex vivo* models described in previous section, that best recapitulate the main phenotype occurring in the absence of sacsin.

3.1 - A novel miniaturized version of sacsin – minisacsin - is stable in vitro

I designed a recombinant miniaturized version of sacsin (minisacsin), that combines all different sacsin domains, in a format size suitable for packaging into AAV vectors (4.8 kb). Minisacsin consists of the N-terminal region of human sacsin (aa 1-508), which carries the Ubl and SRR1 domains, linked in frame to the C-terminal region of human sacsin (aa 4306-4579), which carries the DnaJ and HEPN domains (**Results Fig. 24a**, above). Minisacsin carries a single copy of all the sacsin domains that have been singularly cloned and most characterized in literature (Parfitt *et al*, 2009; Ménade *et al*, 2018; Kozlov *et al*, 2011; Anderson *et al*, 2010); in particular, it carries only the first copy of the three SRR domains (SRR1), which is the only one that has been cloned in heterologous systems to assess its biochemical function as molecular chaperone. Although it has been reported that each SRR domain is part of a larger Sacsin Internal Repeat (SIRPT) which encompasses other subdomains besides SRR, the function of these subregions remains completely unknown (Romano 2013); moreover, the size of SIRPT1 alone is too huge (3.8 kb)

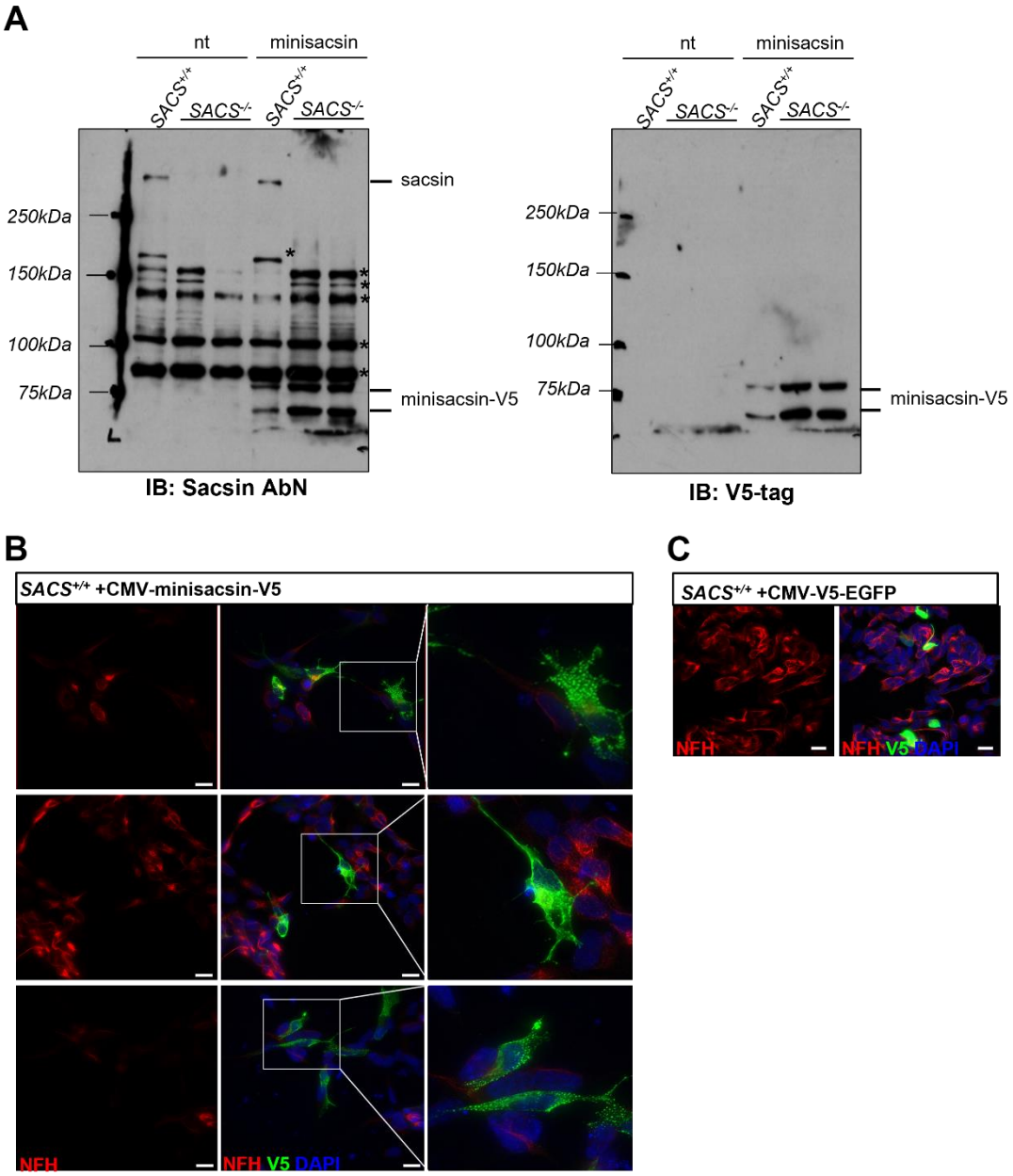
to allow for inserting other domains and regulatory sequences for AAV-based delivery. For these reasons we decided to include only SRR1 in the final minisacsin construct.

I cloned the N-terminal and C-terminal sacsin regions from human cDNA and linked together with a sequence encoding Gly-Ser flexible linker; moreover, I put a V5-tag in frame at the C-terminus of minisacsin. The C-terminal localization was preferred as I had already been able to successfully tag endogenous sacsin at C-terminus with HA-tag by CRISPR/Cas9 mediated homologous recombination (data not shown). In that case, a stable tagged protein was detectable by WB, demonstrating that likely tagging the C-terminal does not interfere with sacsin domains proper folding. Minisacsin-V5 cDNA was therefore cloned into pcDNA3.1 plasmid, between CMV promoter and BGH polyadenylation signal for mammalian expression. The length of minisacsin-V5 coding sequence is 2.397 kb and with its regulatory elements is 3.346 kb (**Results Fig. 24a**, below).



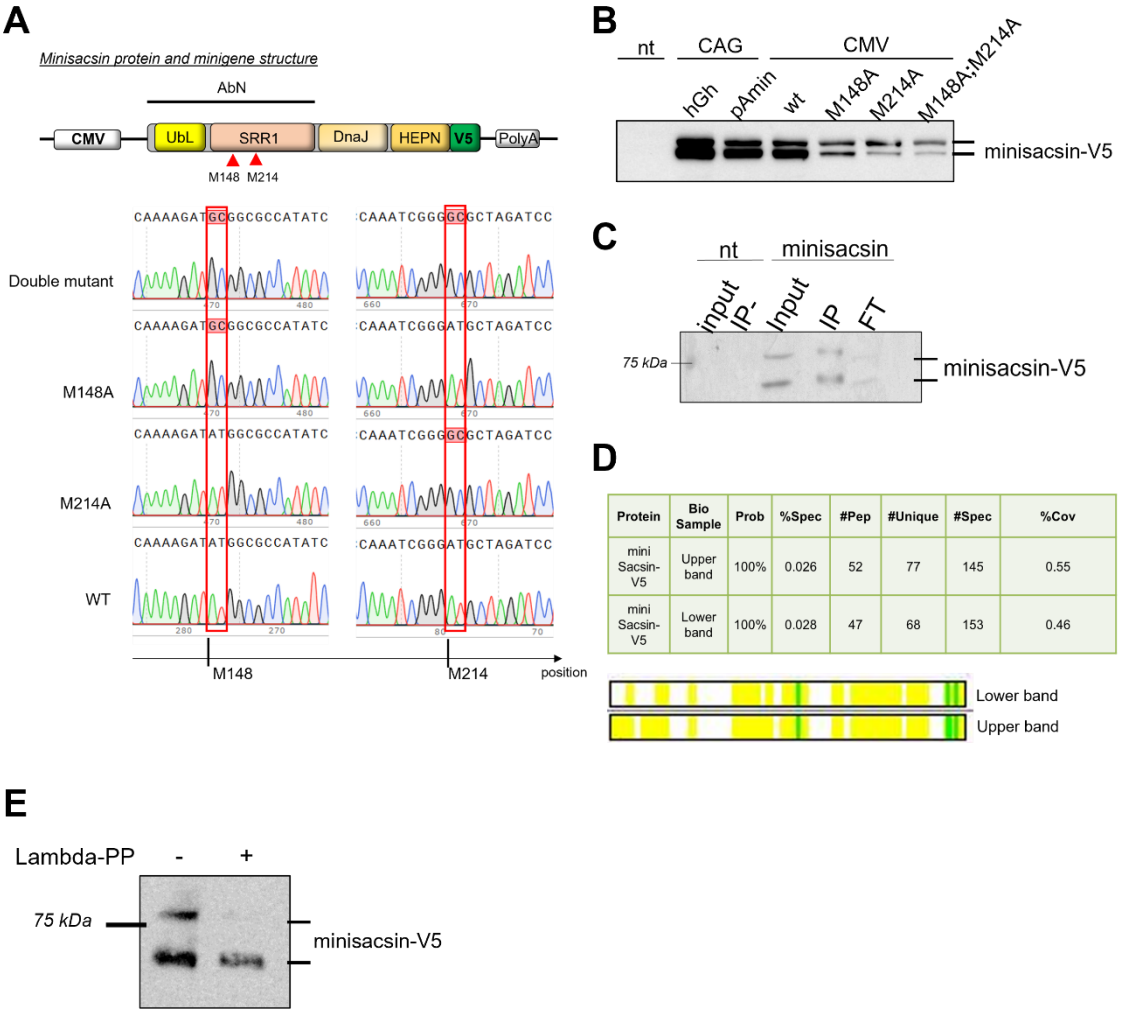
Results Figure 24 (from previous page). Minisacsin design and structure. *Above: schematics of sacsin full length structure and minisacsin cloning strategy. All sacsin domains, AbN and AbC epitopes are shown (see also Results Fig. 1). Grey bars represent sacsin regions whose cDNAs were cloned into minisacsin. GS represents flexible Gly-Ser encoding linker. Below: scheme of minisacsin protein and gene structure. NheI and XhoI sites were used for cloning into pcDNA3.1 between CMV universal promoter and polyadenylation signal (PolyA). Kozak sequence was put immediately before the ATG starting site and after NheI. GS-linker indicates a Gly-Ser spacer in frame between sacsin N- and C-terminal regions. Red arrows represent four primers used for sequencing. Abbreviations: AbN/C: N/C-terminal anti-sacsin antibody; UbL: Ubiquitin-Like domain; SRR: Sacsin Repeating Region; SIRPT: sacsin internal repeat; XPCB: Xeroderma Pigmentosus group C protein Binding domain; HEPN: Higher Eukaryotes and Prokaryotes Nucleotide-binding domain; bp: base pair; aa: amino acid; CDS: coding sequence. All aa sequences are from NP_014363.6*

Neuronal-like SH-SY5Y control cells and two different SH-SY5Y *SACS*$^{-/-}$ clones, were transfected with pcDNA3.1 plasmid carrying, to evaluate its expression by WB. Minisacsin lacks the epitope of the sacsin commercial antibody (AbC) (aa 4200-4300), but is still recognizable by the polyclonal AbN, which was originally designed against the N-terminal region of human sacsin (aa1-728) (see also **Results Fig. 1)**. In WB, a stable and intense double band was detected, only in transfected cells, both with the sacsin-specific AbN and with the C-terminal V5-tag Ab, at the same molecular weight with both antibodies (**Results Fig. 25a**). Both minisacsin bands ran in SDS-PAGE around 75 kDa, consistent with predicted molecular weight of 90 kDa. Also in immunofluorescence, both control and *SACS*$^{-/-}$ transfected cells shown stable and high expression of minisacsin, revealed with anti V5-tag Ab; in particular minisacsin was quite uniformly distributed in the cytosol, as expected from sacsin full length distribution and with a staining pattern similar to that of endogenous sacsin in primary PNs (as will be reported in **Results Section 3.3**). Furthermore, we did not detect abnormal subcellular localization in the nucleus, as it was observed for previously reported single sacsin J domain in the form of a cell membrane permeating peptide (Gentil *et al*, 2019). Finally, we did not detect aggregate formation upon minisacsin heterologous overexpression, at least at optical microscopy (**Results Fig. 25b**). These data indicate that minisacsin is stably expressed and not toxic in SH-SY5Y cells, and even the low number of transfected cells (transfection is a well-known limit in SH-SY5Y system) was comparable to that of control transfection with plasmid encoding V5-EGFP, confirming again no toxicity of this construct (**Results Fig 25c**).



Results Figure 25. Minisacsin is stably expressed in vitro. *A. WB analysis of minisacsin ectopic expression in SACS$^{+/+}$ and two different SACS$^{-/-}$ SH-SY5Y clones 48h after transient transfection, immunoblotted with sacsin-specific AbN (left) and V5-tag Ab (right) (samples were loaded in duplicate and the membrane was cut after blotting, so that in left and right proteins are at the same heights, to send both antibodies independently). Sacsin endogenous full length is recognized by AbN in control cells. Stars represent aspecific bands. IB=immunoblot; nt: not transfected. B. Representative images by widefield deconvolution microscopy (63X) of immunofluorescence with total NFH (red) and V5-Tag antibody (green) of minisacsin expression in control SH-SY5Y$^{+/+}$ cells 48h after transfection with minisacsin-V5 under CMV promoter in pcDNA3.1. DAPI was done as counterstaining. Rightmost inserts are magnified regions corresponding to white squares. Images are shown as max projections of z-stacks. C. Representative images as in B of same sample SH-SY5Y$^{+/+}$ cells transfected with V5-EGFP under CMV promoter; note similar number of cells transfected as with minisacsin-V5. B-C: scale bars = 20µm; Images taken with DeltaVision Ultra (G.E. Healthcare).*

These data confirm that minisacsin *per se* is stable and not toxic. However, by WB two bands were always detected, also upon transfection in different cell types, included HeLa cells (data not shown). Since both bands are detected both by the very N-terminal AbN and the very C-terminal V5-Tag Ab, no doubt is left on their specificity and that they are both in frame. Therefore, they could be isoforms due to in-frame alternative translation starting sites or to post-translational modifications. Translating from an internal ATG codon would produce a shorter isoform but still recognizable by the polyclonal AbN. To exclude this hypothesis, I mutagenized all ATG codons, placed in the corresponding AbN region in minisacsin, to alanine residues (ATG at codon 148 and ATG at codon 214) (**Results Fig. 26a**). Upon transfection in SH-SY5Y cells, the double band was still detected by WB with both mutant clones and even with double mutant clone combining both mutagenesis (**Results Fig. 26b**). In the same gel, lysates from cells transfected with plasmids in which minisacsin was cloned under different promoters were also loaded, further suggesting that double band expression was not due to regulatory elements. To further confirm the molecular identity of these bands, I immunoprecipitated minisacsin from lysates of transfected HeLa cells to perform MS analysis. HeLa cells were used as they are more efficient to transfect than SH-SY5Y cells and the aim of this analysis was independent from minisacsin function in more valuable SH-SY5Y tool; *SACS*$^{-/-}$ HeLa cells generated by CRISPR/Cas9 (see **Results Section 1.2**) were used to avoid any contamination from endogenous sacsin in control cells. Again, in this cell type minisacsin was expressed at high level with double bands, and both bands were efficiently immunoprecipitated with V5-Tag Ab, as revealed by WB (**Results Fig. 26c**). Each band was separately gel-excised and subjected to LFQ-MS/MS analysis. Minisacsin recombinant sequence was added manually to Uniprot database to compare with MS/MS spectra, and correspondence was detected, with 100% probability, for both the upper and the lower band, with almost identical peptide coverage and sequences, also upstream the previously mutagenized ATG putative starting sites (**Results Fig. 26d**). Finally, I took in consideration the hypothesis of post-translational modifications, starting from phosphorylation. Indeed, by digesting cellular lysates upon minisacsin transfection *in vitro* with phosphatase Lambda, the upper band disappeared almost completely in comparison to undigested lysate under the same conditions (**Results Fig. 26e**).



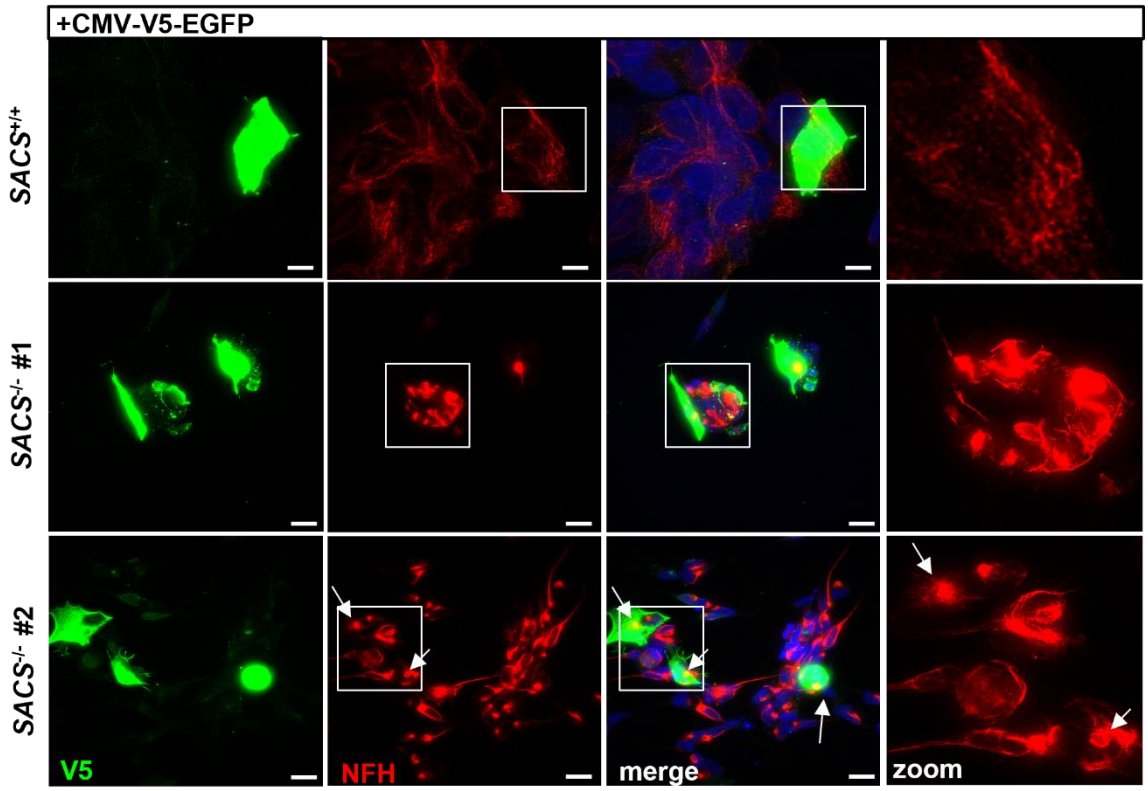
Protein	Bio Sample	Prob	%Spec	#Pep	#Unique	#Spec	%Cov
mini Sacsin-V5	Upper band	100%	0.026	52	77	145	0.55
mini Sacsin-V5	Lower band	100%	0.028	47	68	153	0.46

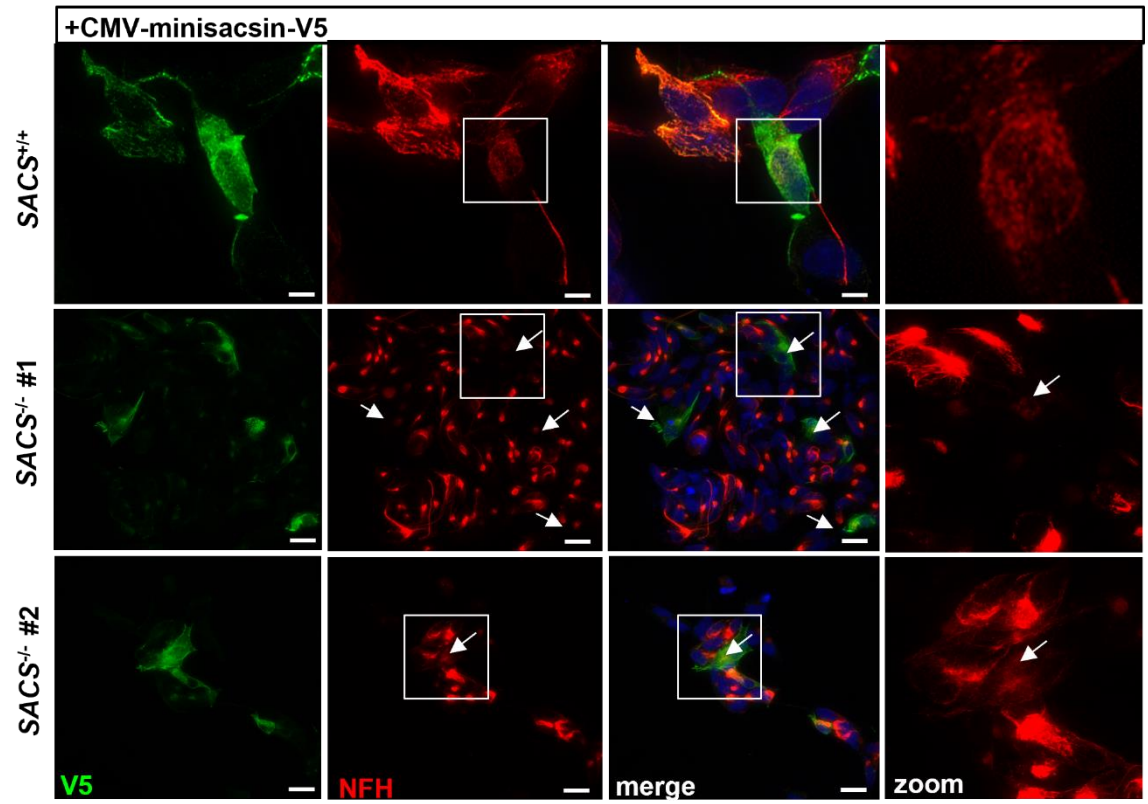
Results Figure 26. Analysis of minisacsin double band. *A. Above: Schematics showing internal in frame ATG sites encoding methionine (M) in the region which is recognized by AbN. Below: Sanger sequencing of original (wt) and minisacsin mutant clones with M148A, M214A and M148;M214A (double mutant) mutations. B. WB with V5-Tag antibody of minisacsin mutant clones as in A, cloned under CMV promoter in pcDNA3.1 plasmid and transfected in SH-SY5Y control cells. Nt = not transfected. Original minisacsin sequence was also cloned between CAG promoter and different polyA terminators (hGh or pAmin - see Results Section 3.3). CAG promoter consists of CMV enhancer with Chicken Beta Actin promoter and intron derived from human beta globin gene. C. IP of minisacsin with anti V5-tag antibody upon transfection in HeLa cells, revealed in WB by V5-tag antibody. Nt = not transfected; FT = flow through; IP- = immunoprecipitation with V5 antibody from nt cells. D. LFQ-MS/MS analysis and peptide coverage of upper and lower gel bands excised from minisacsin IP eluates loaded on gel. E. WB showing Lambda phosphatase treatment of lysate of HeLa cells transfected with minisacsin.*

3.2 – Minisacsin is functional and rescues NF bundling in vitro in SACS$^{-/-}$ SH-SY5Y neuronal cells

Next, I evaluated if minisacsin reverts NF bundling in *SACS*$^{-/-}$ SH-SY5Y cells, by immunofluorescence imaging of both V5-Tag and NFH subunit in widefield microscopy with deconvolution, 48 hours after transient transfection with plasmid encoding minisacsin. In two different *SACS*$^{-/-}$ clones, in most of cells transfected with control

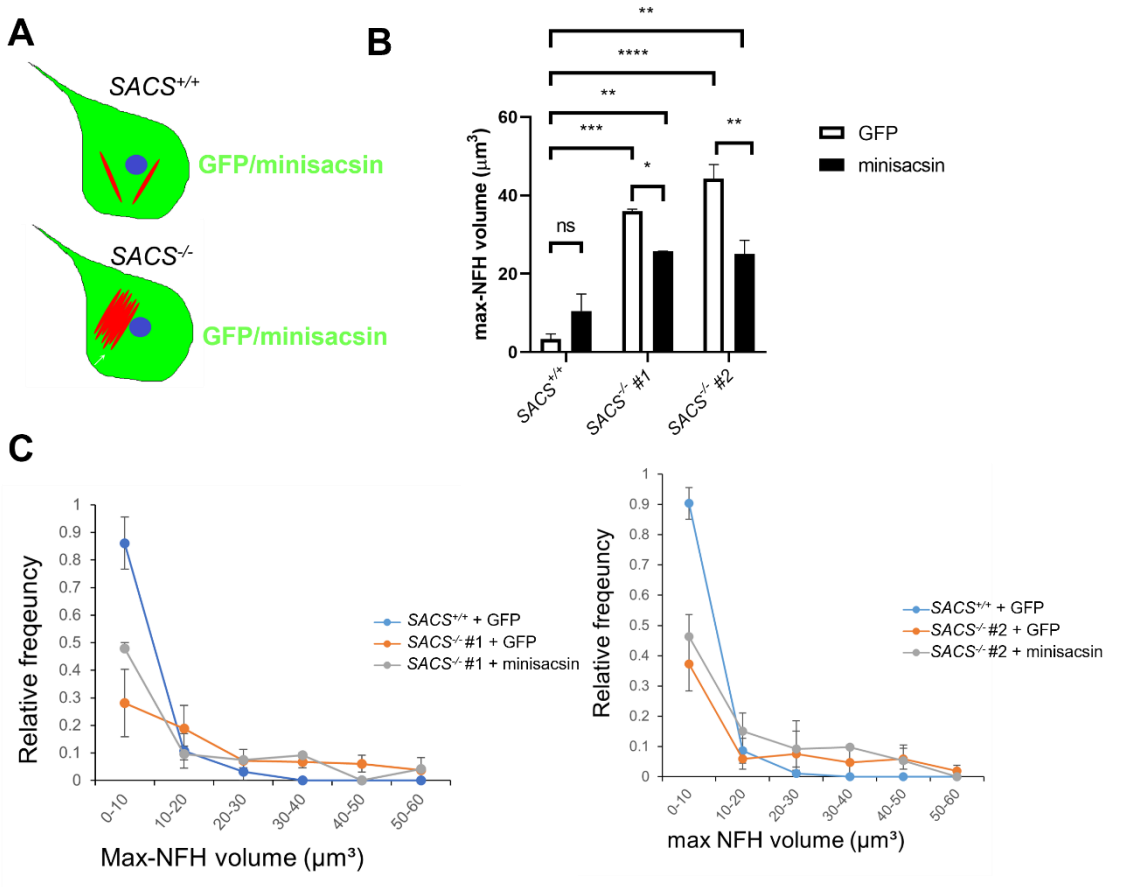
plasmid encoding V5-EGFP, NFH distribution was strikingly remodeled as expected, with perinuclear dense bundles (**Results Fig. 27**, above - white arrows). In contrast, many of the *SACS*$^{-/-}$ cells transfected with minisacsin had more filamentous NFH staining or decreased volume of the dense bundle; in some fields, almost all *SACS*$^{-/-}$ cells transfected with minisacsin had filamentous staining similar to what is observed in controls (**Results Fig. 27**, below **-** white arrows).


+CMV-V5-EGFP
SACS+/+
SACS-/- #1
SACS-/- #2
V5
NFH
merge
zoom


+CMV-minisacsin-V5
SACS+/+
SACS-/- #1
SACS-/- #2
V5
NFH
merge
zoom

Results Figure 27 (from previous page). Minisacsin significantly reduces NF bundling in SACS$^{-/-}$ SH-SY5Y cells. *Representative images by widefield deconvolution microscopy at 63X of immunofluorescence with total NFH (red) and V5 (green) of two different SACS$^{-/-}$ clones and SACS$^{+/+}$ control cells after 48h transfection with V5-EGFP (above) or minisacsin (below) cloned under CMV promoter in pcDNA3.1. CMV=cytomegalovirus universal promoter. White arrows indicate GFP transfected cells in which NF bundle is visible (above), or minisacsin transfected cells in which NF bundling has been reduced or completely resolved (below). Panels denoted with zoom are magnified regions corresponding to white squares showing NFH signal. DAPI was done as counterstaining. Images are presented as max projections of z-stacks. Note NF filamentous network in control cells compared to SACS$^{-/-}$ cells. Scale bars = 20μm. Images taken with DeltaVision Ultra (G.E. Healthcare).*

Quantification of max-NFH volume (see **Results Section 2.1**) was performed as already described by 3D-reconstruction of deconvoluted stacks and confirmed as expected significant increase in *SACS*$^{-/-}$ cells transfected with V5-EGFP compared to controls cells transfected with V5-EGFP, similarly to what reported at steady state conditions in **Results Section 2.1** (**Results Fig. 28a-b**, schematics and graphs). This analysis revealed that average max-NFH volume was significantly decreased in both *SACS*$^{-/-}$ SH-SY5Y clones transfected with minisacsin compared to V5-EGFP transfected cells (**Results Fig. 28b**). The reduction was 28.5% for *SACS*$^{-/-}$ #1 clonal cells (35.95±0.49μm^3 upon EGFP transfection vs 25.71±0.04μm^3 upon minisacsin transfection), and 25.2% in *SACS*$^{-/-}$ #2 clonal cells (44.28±3.61μm^3 vs 33.14±1.73μm^3). Qualitative analysis of frequency distribution of max-NFH volume, shown that in control *SACS*$^{+/+}$ sample transfected with EGFP most cells had NF structures lower than 10μm^3, whereas in *SACS*$^{-/-}$ clones transfected with EGFP this percentage was highly reduced, with many cells showing bundles much larger than 10μm^3; strikingly, this distribution was almost inverted in *SACS*$^{-/-}$ clone #1 transfected with minisacsin, while the percentage of cells with neurofilaments objects lower than 10 μm^3 increased also in *SACS*$^{-/-}$ clone #2 transfected with minisacsin (**Result Fig. 28c**). These data shown that minisacsin acts reproducibly on lowering NF bundling *in vitro* after 48 hours transient transfection, which is noteworthy due to very low transfection efficiency and given the high NF stability.



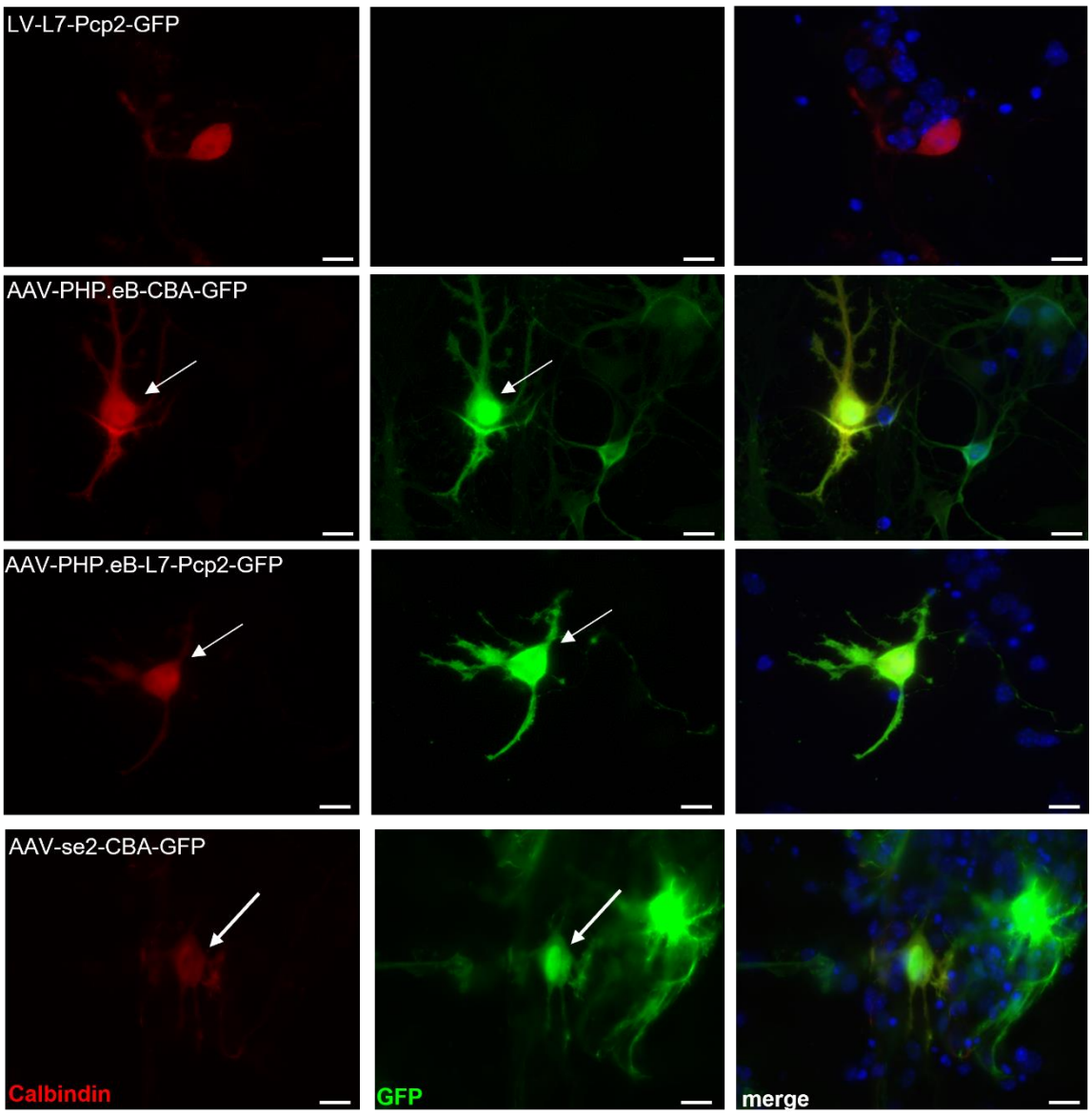
Results Figure 28. Quantification of NF bundling reduction in SACS$^{-/-}$ SH-SY5Y cells transfected with minisacsin. *A. Schematics of algorithm used for max-NFH volume quantification in each transfected cell, as in Results Fig. 12b. The pipeline has been modified to define cell object in 3D by thresholding green signal. B. Quantification of average max-NFH volume per cell after deconvolution and 3D-reconstruction using algorithm as in B, referred to Results Fig. 27. Data shown as mean±SEM; n=at least 3 biologically independent experiments; at least 20 cells quantified for each experiment; *p<0,05 **p<0,01 ***p<0,001 ****p<0,0001 (two-way ANOVA test with Tukey's test for multiple comparison). C. Relative frequency distribution of cells with max-NFH volume in the ranges specified by x-axis, for each sample i.e. SACS$^{-/-}$ #1 clone (left) and #2 clone (right) transfected with minisacsin and control cells (control cells + V5-EGFP).*

Finally, control cells transfected with minisacsin did not show any differences in respect to control cells in terms of NFH distribution and max-NFH quantification. Overall, this data confirm that minisacsin *in vitro* is not toxic, is functional and is able to act on NF reducing their bundle in the absence of sacsin.

3.3 – Minisacsin is stable ex vivo in PNs upon AAV-mediated delivery

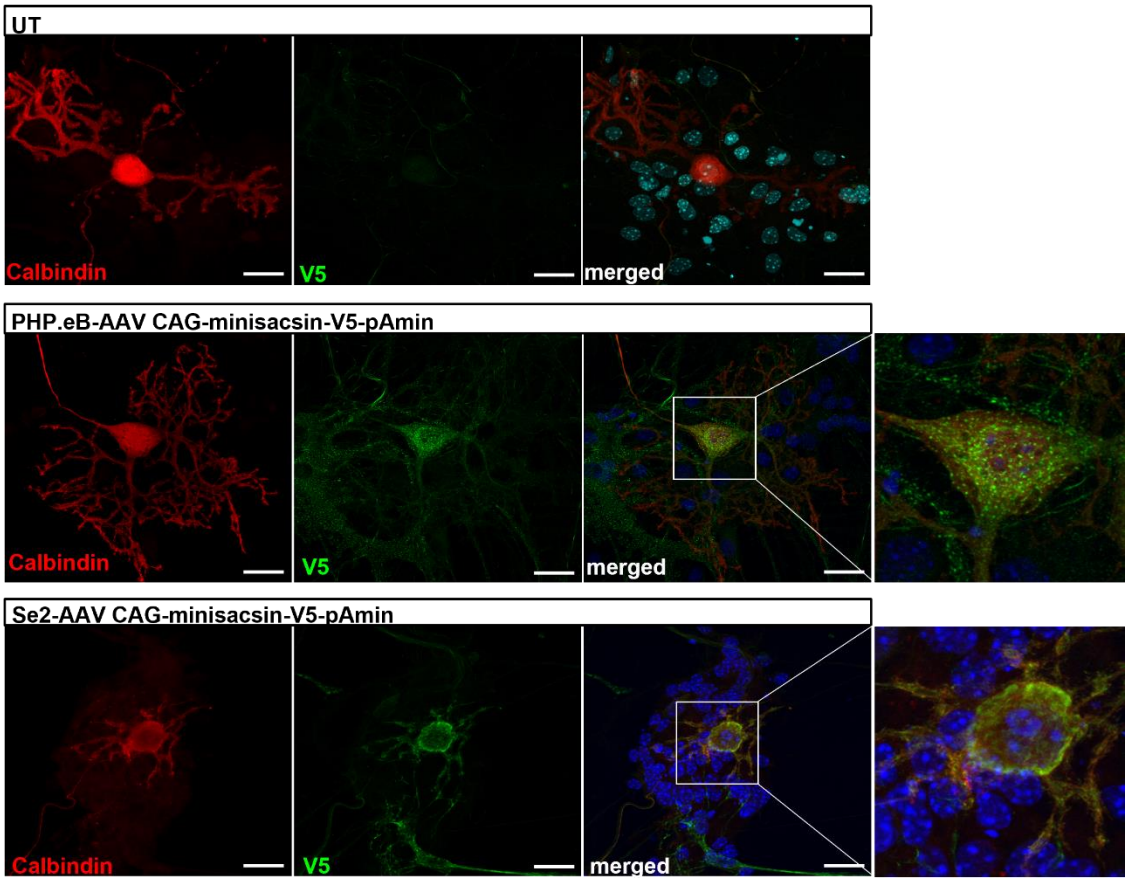
As a proof of concept of feasibility of AAV vectors for preclinical studies, we tested the ability of different capsids to transduce primary PNs (a data that was missing in literature). We used AAV PHP.eB capsid carrying V5-EGFP gene (a well-known recombinant capsid able to cross Blood Brain Barrier (BBB) in mice and to transduce CNS upon systemic injection (Chan *et al*, 2017; Morabito *et al*, 2017); and AAV-Se2

carrying V5-EGFP gene (a novel recombinant capsid patented by Vania Broccoli group at OSR Scientific Institute which is able, differently from PHP.eB, to cross the BBB also in non-human primates) (confidential information). GFP under universal CAG promoter (consistent of CMV enhancer followed by chicken β actin universal promoter and an intron derived from human β globin gene) shown very high expression upon AAV transduction at DIV0 with all AAV employed, and generally higher expression in PNs compared to other cells in cultures, such as astrocytes. We also produced a PHP.eB-GFP under a shorter, AAV-suitable, version of the PNs-specific L7-Pcp2 promoter, which also effectively and specifically transduced PNs (**Results Fig. 29**).



Results Figure 29 (from previous page). AAV are able to transduce primary PNs ex vivo. *Representative images at widefield epifluorescence (63X) of DIV11 control Sacs$^{+/+}$ PNs infected ad DIV0 with AAV PHP.eB-CAG-GFP or AAV Se2-CAG-GFP or AAV PHP.eB-L7-Pcp2-GFP, stained for PNs-specific marker calbindin (red). Infection with Lentivirus (LV)-L7-Pcp2-GFP was used as negative control, as they inefficiently transduce PNs ex vivo. White arrow indicates example of cell type other than PNs infected by AAVs with CBA promoter. Scale bars = 20µm.*

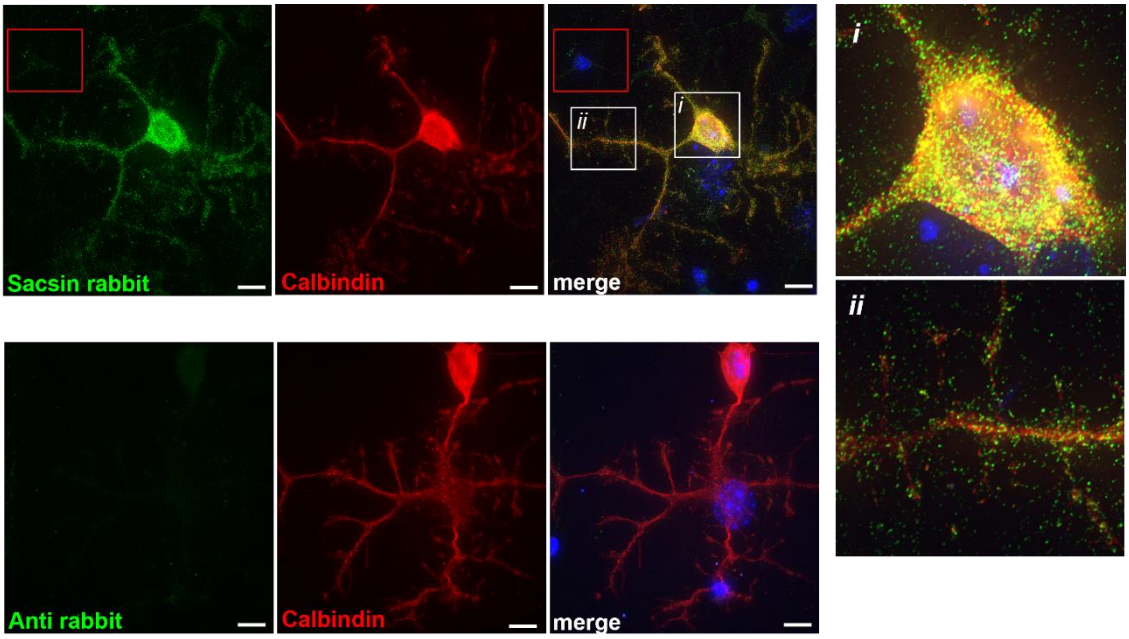
We next cloned minisacsin sequence into pAAV plasmids for AAV packaging and production. Minisacsin was put under strong universal CBA promoter. Two PolyA tail sequences for transcriptional termination were proofed: the terminator of human growth hormone (hGh terminator – 477 bp) and a much shorter terminator designed by the lab of Dr. Vania Broccoli at OSR scientific institute (pAmin terminator – 49 bp). *In vitro* expression of all minisacsin-carrying plasmids in immortalized human cells confirmed strong and stable expression of minisacsin, regardless of the nature of promoter and PolyA signal (see **Results Fig. 26b**). We therefore opted for the pAAV encoding minisacsin-pAmin for AAV production, as the shorter final sequence allows higher AAV production yield. This vector was used both to produce AAV-PHP.eB and AAV-Se2 capsids carrying CBA-minisacsin-V5-pAmin gene. As for V5-GFP previously shown, also minisacsin did transduced at high level primary *Sacs*$^{+/+}$ PNs in culture (**Results Fig. 30**).



Results Figure 30. Minisacsin is stable ex vivo in PNs upon AAV-mediated delivery. *Representative images at confocal microscopy (63X) of DIV11 control Sacs$^{+/+}$ PNs infected at DIV0 with 10^{10} vg of AAV PHP.eB-CAG-minisacsin or AAV Se2-CAG-minisacsin, stained for PNs-specific marker calbindin (red) and V5-Tag (green). Cells were counterstained with DAPI. Images are presented as max projections of z-stacks. Rightmost inserts are magnified regions corresponding to white squares. UT = untransduced; CAG = universal CAG promoter. Scale bars = 20µm. Images taken with Fluoview (Olympus).*

Minisacsin staining was similar to that of endogenous sacsin protein in control PNs cultures, where weak, but specific signal was detectable only in PNs after antigen unmasking retrieval. Sacsin staining shown a dotted pattern, diffused both in the soma and in proximal and distal dendrites of PNs, where it localizes also to dendritic spines as observed by colocalization with PNs-marker calbindin (**Results Fig. 31**). Noteworthy, other cells present in primary cerebellum cultures marked with DAPI did not show any endogenous sacsin expression, in agreement with specific very high expression in PNs in cerebellum (see **Introduction Section 1.2**); weak signal in PNs could be explained with low copy number of the protein in endogenous condition or with very low efficiency of the antibody in immunofluorescence, as indeed I was never able to detect endogenous sacsin *in vitro* in immortalized cells.

Therefore, minisacsin dotted and diffused staining was comparable to that of endogenous sacsin in control *Sacs*$^{+/+}$ PNs, again corroborating that minisacsin does not aggregate, mislocalize, nor its overexpression is toxic to PNs.

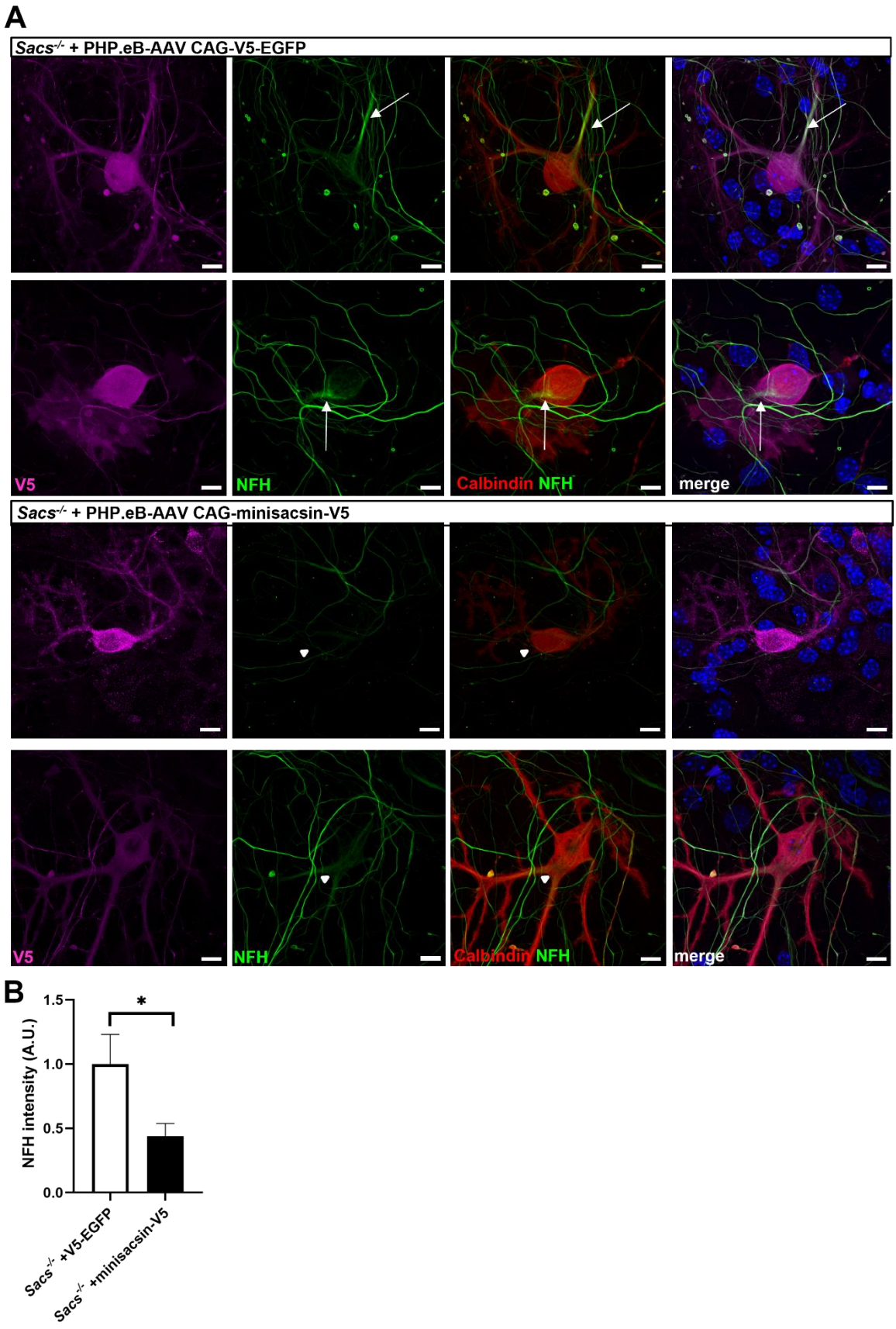


Results Figure 31. Sacsin endogenous distribution in PNs is similar to minisacsin. *Representative images at widefield deconvolution microscopy (63X) of immunofluorescence of endogenous sacsin (green) and PNs-specific marker (calbindin) on DIV15 control Sacs*$^{+/+}$ *PNs. Staining with secondary only antibody was used as negative control (antirabbit below); as internal control, note also that other cells marked by DAPI (red squares) do not have any sacsin signal at all. Inserts denoted with i and ii are magnified regions of corresponding white squares showing sacsin specific expression is both widely distributed in the soma and dendrites and dendritic spines. Dotted pattern is similar to minisacsin ectopic expression distribution. Images are shown as max-projections of z-stacks. Scale bars = 20μm. Images taken with DeltaVision Ultra (G.E. Healthcare).*

3.4 – Minisacsin is functional and rescues NF bundling ex vivo in Sacs$^{-/-}$ *PNs*

Finally, I evaluated if minisacsin is functional and reduces NF bundling *ex vivo* by confocal imaging of DIV15 *Sacs*$^{-/-}$ PNs infected at DIV0 with the same absolute amount of AAV as before (see **Results Fig. 30**). As a proof of concept, I delivered minisacsin with AAV-PHP.eB capsid. Again, minisacsin distribution (**Results Fig. 32a**, below - magenta) was uniformly diffused in *Sacs*$^{-/-}$ PNs soma and dendrites, which were fully mature and arborized as in *Sacs*$^{-/-}$ PNs with control V5-EGFP (**Results Fig. 32a**, above - magenta), confirming no toxicity. While *Sacs*$^{-/-}$ PNs infected with AAV-PHP.eB-CAG-V5-EGFP-hGh shown as expected intense bundles in proximal dendrites (**Results Fig. 32a**, above - white arrows), no such bundles were observed at all in *Sacs*$^{-/-}$ with minisacsin. Since *Sacs*$^{-/-}$ PNs may have more bundles and signal accumulations in each proximal dendrite (see **Results Fig. 13**) as opposed

to *SACS*$^{-/-}$ cells that show a single large perinuclear dense bundle, I quantitatively analyzed NFH signal plot profile for each proximal dendrite, rather than quantifying the volume of max-NFH per each cell; average peak NFH signal in proximal dendrites was significantly decreased by 56% upon minisacsin delivery (**Results Fig. 32b**). However, these data are preliminary as I need to increase the number of analyzed cells.


A
Sacs-/- + PHP.eB-AAV CAG-V5-EGFP
V5
NFH
Calbindin NFH
merge
Sacs-/- + PHP.eB-AAV CAG-minisacsin-V5
V5
NFH
Calbindin NFH
merge
B
NFH intensity (A.U.)
1.5
1.0
0.5
0.0
*
Sacs-/- +V5-EGFP
Sacs-/- +minisacsin-V5

Results Figure 32 (from previous page). Minisascin rescues NF bundling in Sacs$^{-/-}$ PNs. *A. Representative images of confocal microscopy (63X) of immunofluorescence with V5-tag antibody (colorized in magenta), calbindin (colorized in red) and total NFH (colorized in green) on DIV15 Sacs$^{-/-}$ PNs infected at DIV0 with 10^{10}vg of AAV-PHP.eB-CAG-V5-EGFP-hGh (above) or AAV-PHP.eB-CAG-minisacsin-V5-pAmin (below). White arrows above indicate examples of NF bundles in proximal dendrites; such bundles are not observed in Sacs$^{-/-}$ with minisacsin. White head arrows below indicate soma of PNs. Cells were counterstained with DAPI. Images are presented as max projections of z-stacks. CAG= universal CAG promoter; hGh and pAmin are polyA terminator signals (see Results Section 3.3). B. Quantification of average NFH intensity peak from plot profile along a line perpendicular to each proximal dendrite, showing significative reduction in Sacs$^{-/-}$ PNs with minisacsin. Data shown as mean±SEM; n=3 biologically independent experiments; at least 10 dendrites were quantified for each experiment; *p<0.05 (Student's t-test with Welch correction). Scale bars = 20μm. Images taken with Fluoview (Olympus).*

In conclusion, AAV-delivered minisacsin is not toxic in primary PNs and by preliminary data, AAV-PHP.eB delivered minisacsin was able to rescue NF bundling. Since in this case we did not observe any NF bundling in *Sacs*$^{-/-}$ PNs with minisacsin, further analysis is needed to conclude if the rescue is virtually total *ex vivo* and to test minisacsin delivery upon AAV systemic injection in *Sacs*$^{-/-}$ mice, to evaluate expression in cerebellum and PNs, npNFH bundling and loss of PNs and finally motor phenotypes assessment, in the light of preclinical translation of this novel gene therapy.

DISCUSSION

Parts of Discussion Section 1 were already published in our previous work, Longo, Fabiana, De Ritis Daniele et al. "Assessment of sacsin turnover in patients with ARSACS: Implications for molecular diagnosis and pathogenesis." Neurology 97.23 (2021): e2315-e2327.

With my work I have contributed to highlight many open issues in the study of ARSACS, giving information that were not present in the literature. In first two sections I will discuss these main issues that regarded mainly two aspects. (i) Genotype-phenotype correlation and the molecular consequence of missense mutations on sacsin protein, which are the most common mutations type in ARSACS (Xiromerisiou *et al*, 2020). (ii) Assessing the molecular function of sacsin in relation to the main ARSACS cellular phenotype known, i.e. NF remodeling. (iii) These studies ultimately rationalized gene therapy approach, which I will discuss in the third section on miniaturized sacsin protein (minisacsin).

1 – Assessment of sacsin turnover in patients with ARSACS

1.1 - Effect of missense mutations on sacsin protein level explains lack of genotype-phenotype correlation

We studied for the first time the effects of different ARSACS mutations on sacsin stability, at both mRNA and protein level, in patients' cells. The cohort of ARSACS patients that we analyzed encompasses a wide range of diverse types of *SACS* mutations localized in different regions of the gene. The main result we obtained is that sacsin is barely detectable in ARSACS patients, regardless of the nature or position of the mutation along the gene. Loss of protein was expected for patients carrying biallelic truncating mutations, as for patients carrying one monoallelic truncating mutation or large gene deletion, in which mRNA is unstable and likely degraded by nonsense mediated decay. However, loss of sacsin protein was not predicted for patients carrying missense mutations, especially biallelic missense mutations in compound heterozygosis. We indeed discovered that sacsin carrying missense mutations, in any site of its sequence, is cotranslationally ubiquitinated and degraded. Very low amount sometimes detectable in these patients by WB is likely due to protein chains that are able to escape cotranslational ubiquitination and to reach mature size with low frequency. We surmise that this mechanism prevents production of a huge misfolded protein like sacsin, that also is expected to dimerize in the cell, potentially highly prone to form toxic aggregates and inclusion bodies in the crowded cytosolic environment, which could be more dangerous than total loss

of function. Thus, similarly to nonsense mediated decay that prevents formation of truncated proteins, we believe that cotranslational degradation is a protective mechanism constitutively triggered by *SACS* missense mutations.

Since ARSACS presents high clinical variability, efforts have been dedicated to find a genotype-phenotype correlation, to better tailor a precision medicine approach, in terms of disease prognosis, family counselling and for future clinical trials. However, in previous systematic reviews, the effect of missense mutations was generally regarded to affect the function of the domain in which is localized, or to cause at some level protein instability and aggregation (Romano *et al*, 2013); moreover, the effect and pathogenicity of missense mutations was predicted by bioinformatic analyses (Xiromerisiou *et al*, 2020). Our data do not confirm these studies, since we demonstrated that loss of function in ARSACS is caused by loss/striking reduction of sacsin, independently of the mutation and therefore clinical severity and features cannot be correlated to the nature of the mutations. Excluding the Québec cohort, where the original c8844delT *SACS* mutation is highly prevalent, the 2020 worldwide ARSACS scenario shows that most mutations are missense, followed by small deletions, frameshift, nonsense and small insertions (Xiromerisiou *et al*, 2020). In our cohort of compound heterozygous patients, two of them carry biallelic missense mutations and five of them monoallelic missense, for a total of nine different missense changes analyzed. In all cases, the full-length protein is almost absent in patients with missense mutations (hitting different regions of the protein, from the N-terminus to the C-terminus) as well as in patients with truncating mutations. Only in one patient (PN5, see Results) a residue of sacsin was detected with both AbC and AbN antibodies, which is anyway about 20% of controls, whereas in another patient (PN9, who carries biallelic missense as well) sacsin is not detectable at all.

Other explanations for clinical variability in ARSACS: perspectives

While our study excludes the nature/position of the *SACS* mutation as a cause of the diverse ARSACS phenotype, further studies are needed to explain the pronounced clinical variability. The genetic background is certainly playing a role in this regard. In the genetically relatively homogeneous Québec population, ARSACS typically starts with ataxia and spasticity in the first decade of life, followed by neuropathy in the second decade, despite many different mutations have been identified (Thiffault *et al*, 2013). However, in other countries 20% of ARSACS patients show atypical presentations with disease onset after the age of 20, a Charcot–Marie–Tooth (CMT)-like disorder, or absence of one of the three defining clinical features, epilepsy or hearing loss (Vermeer *et al*, 2020; Baets *et al*, 2010; Synofzik *et al*, 2013;

Xiromerisiou *et al*, 2020). Both inter- and intra-familial heterogeneity of this complex clinical condition might be explained with the combined effect of modifier genes, risk alleles or multilocus variations (including mutations/copy number variants (CNVs) of other genes) that can modify the phenotype in terms of penetrance, expressivity and age of onset. The unexpected huge variation in the human genome on a population level indeed challenges the canonical Mendelian disease analysis, pointing to a more comprehensive model in which variants with different effect size and environmental factors contribute to determine the phenotype of the genetic disease. A genome wide screen in ARSACS patients, aggregated based on phenotypic similarities, may provide a more complete genetic view of the disease. This approach is already in place for other rare Mendelian diseases, such as CMTs and others (Posey *et al*, 2017; Karaca *et al*, 2018; Bis-Brewer *et al*, 2020; Miressi *et al*, 2020). Our findings are also supported by recently published *Sacs*^{R272C} knockin mouse model, which carries a human pathogenetic mutation localized in a highly conserved residue in the first SRR domain (Anderson *et al*, 2010; Larivière *et al*, 2019). This model presents a scarcely detectable sacsin protein in cerebellum lysate, despite showing stable mRNA level; accordingly, the phenotype of *Sacs*^{R272C} model phenocopies completely the one of the *Sacs*$^{-/-}$ knockout mouse (Larivière *et al*, 2015; Gentil *et al*, 2019). This data also indicate that cotranslational degradation of mutant sacsin occurs also in the cerebellum and is a universal mechanism. A striking reduction of sacsin was incidentally previously shown in at least two reports of ARSACS mutations in patient fibroblasts or lymphoblasts (Thiffault *et al*, 2013; Duncan *et al*, 2017); as for the published *Sacs*^{R272C} knockin mouse, also these findings were not provided with further mechanistic insights. In this work, we could not directly test RNA and protein levels in heterozygous parents of patients carrying missense mutations. However, sacsin protein is halved in the heterozygous *Sacs*$^{R272C/+}$ mouse (Larivière *et al*, 2019), supporting that sacsin carrying the R272C missense mutation likely undergoes co-translational degradation. Fifty percent of the amount of sacsin seems to be anyway sufficient to supply to cellular needs, as demonstrated by the fact that both *Sacs*$^{R272C/+}$ mice, as well as *Sacs*$^{+/-}$ mice, do not show any obvious phenotype, similarly to healthy human carriers. Indeed, *Sacs*$^{+/-}$ derived mouse embryonic fibroblasts (MEF) neither show vimentin bundling as *Sacs*$^{-/-}$ MEF; IFs bundling is indeed the main cytopathological hallmark of ARSACS, as shown in **Results Section 2** and as will be thoroughly discussed in next section.

1.2 – Cotranslational degradation as a novel pathophysiological general mechanism in protein quality control

Interestingly, we found that *SACS* mRNA is stable or even increased also in the ARSACS compound heterozygous patients carrying biallelic or monoallelic missense mutations, excluding mRNA degradation as the possible explanation for the absence of sacsin. The failure in rescuing full length sacsin upon the inhibition of all cellular degradative systems and all proteases' classes excluded faster post-translational degradation. Also, mRNA of sacsin turned out to be associated with polysomes in ARSACS patients as well as in controls, rejecting the hypothesis of defective translation. We instead discovered that sacsin nascent chains carrying missense mutations are cotranslationally ubiquitinated and degraded. To preserve proteostasis, eukaryotic cells must not only promote accurate protein folding, but also prevent the accumulation of misfolded species that may arise from inefficient folding, errors in translation, and aberrant/damaged mRNAs. A growing body of evidence indicates that large and multimodular proteins start folding cotranslationally. For such proteins, domain-wise cotranslational folding helps reaching their native states and may reduce the probability for off-pathways and aggregation-prone conformations (Liutkute *et al*, 2020; Pechmann *et al*, 2013; Waudby *et al*, 2019). Also, many studies indicate that a sizable portion of nascent chains are cotranslationally ubiquitinated and degraded by the proteasome in physiological conditions, both in yeast (Duttler *et al*, 2013; Willmund *et al*, 2013), and in mammalian cells (Wang *et al*, 2013). This likely applies to wild-type sacsin, a 520-kDa protein with a complex multimodular architecture containing repeated motifs, whose folding may take minutes to hours to complete. We hypothesize that cotranslational folding and degradation occur physiologically for sacsin as mechanisms of QC. In the case of sacsin carrying a missense mutation, after the unsuccessful attempts of chaperones to fold the nascent chain, the latter is constitutively ubiquitinated and degraded, preventing the synthesis of a misfolded full-length protein. This compartmentalized surveillance mechanism results in a loss-of-function, avoiding a potentially more dangerous toxic gain-of-function of mutant sacsin in the cytosol. Differently from pathogenetic missense mutations, missense variants present in healthy population probably do not impact the cotranslational folding of sacsin, but this hypothesis requires experimental validation. We provided the formal proof of cotranslational degradation of mutant sacsin with the IP with AbN in condition of proteasome inhibition, which revealed the presence of several specific ubiquitinated sacsin products at lower molecular weight compared to the full-length in ARSACS patients carrying missense mutations. The low residual amount of mutant

sacsin that is present in some patients (PN5 and PN7), even if barely detectable, may be due to a quote of mutant protein escaping from cotranslational degradation, because C-terminally localized mutations are presumably more permissive. Few studies observed cotranslational ubiquitination of mammalian proteins, although only in non-physiological conditions, i.e. *in vitro* translation, overexpression conditions or in the presence of artificial (non-pathogenic) mutations (Zhou *et al*, 1998; Müller *et al*, 2021). In cystic fibrosis (CF), this mechanism was observed for the CF transmembrane conductance regulator (CFTR), but only with the ΔF508 mutation (and not with other mutations) (Sato *et al*, 1998). Here we report *in vivo* the cotranslational degradation of a cytosolic protein (carrying any type of missense mutation) as the cause of a human disease. Preemptive mutant sacsin degradation in ARSACS may be a paradigmatic example of a mechanism which can potentially underlie many other genetic diseases with loss of function.

1.3 – Implications for ARSACS diagnosis and therapy

Our data identifies the lack of sacsin protein as unifying mechanism shared by different *SACS* mutations, with multiple important implications for ARSACS disease management. For the diagnosis, we propose that the evaluation of sacsin levels should be included in the clinical genetics practice to establish a definite ARSACS diagnosis, or even as pre-screening in high probable cases to avoid expensive next-generation sequencing panel analysis, and certainly to validate variants of uncertain clinical significance (VUS). In a previous report, it was suggested that mitochondrial network abnormalities in patient fibroblasts could be evaluated when *SACS* genetics and molecular results are difficult to interpret (Pilliod *et al*, 2015). However, this approach is experimentally complex and time consuming, compared to the evaluation of sacsin protein level that we propose here. We indeed found that sacsin is well detected in PBMCs at both RNA and protein levels, making feasible the development of a diagnostic approach for ARSACS aimed at testing sacsin amount in peripheral blood.

Understanding ARSACS molecular pathogenesis has great implications for providing rationales in therapy development, too. Indeed, cotranslational degradation of mutant sacsin makes unproductive any posttranslational approach at protein level. Moreover, we have demonstrated that ARSACS is not caused by misfolding and aggregation of sacsin, but it is caused by a pure loss-of-function molecular pathology mechanism. Thus, the most effective treatment would be to replace sacsin function, e.g. by means of gene therapy, rather than by clearing putative aggregates or downregulating abnormal gene products, as it is being

explored for other neurodegenerative diseases, included polyQ-expansion ataxia. In the next section I will provide several lines of evidence from results obtained and the literature regarding the molecular mechanisms underlying the primary cellular-molecular phenotype observed i.e. npNFH accumulation, and implications for ARSACS (gene) therapy.

2 – NFH accumulation in ARSACS and implications for ARSACS pathogenesis and therapy

Although previous papers documented of the npNFH bundles as a typical features of ARSACS (Larivière *et al*, 2015; Duncan *et al*, 2017; Larivière *et al*, 2019; Gentil *et al*, 2019), a detailed molecular characterization was not systematically done, especially in PNs. In this work, by integrating multiple approaches (*in vitro*, *in vivo* and *ex vivo* optical and electron imaging, biochemical and cross-species OMICS) we sought to address this unsolved issue. I have contributed to dissect the timing, the specificity and the molecular mechanism of NF bundling in the absence of sacsin. These studies shed light on sacsin molecular function, ARSACS pathogenesis and in careful assessment of *in vitro* and *ex vivo* models to test novel gene therapy that acts directly on the first main pathological event in ARSACS, NF bundling.

2.1 – NF remodeling in ARSACS is a primary event in the absence of sacsin

Neurofilaments impairment, which consists of dense bundles visible by optical microscopy, is a hallmark of ARSACS disease. It was reported at late stage by immunohistochemistry in post-mortem ARSACS brain autopsies and in 180 day-old-*Sacs*$^{-/-}$ brain sections. In particular, these bundles were observed in the neuronal cells in which sacsin is more expressed and that are linked to triad clinical phenotypes: namely in PNs and Layer V pyramidal cells of cerebral cortex (Larivière *et al*, 2015, 2019). NF perinuclear bundling was also reported in dissociated spinal cord motor neurons and DRG from *Sacs*$^{-/-}$ mice (Larivière *et al*, 2015; Duncan *et al*, 2017; Gentil *et al*, 2019). Here, we dissected NFH alteration and its timing in PNs, which are the neuronal types the selectively degenerate in ARSACS.

Increased npNFH signal by WB in cerebellum lysate is an early event, present already at P15 and consistent at timepoints of one and six months of age, with a constant fold change in respect to controls; this event occurs much earlier than PNs degeneration (which starts at P90 in the ARSACS mouse models) and is the primary event in the absence of sacsin investigated so far. Increased npNFH signal by WB on total cerebellum likely reflects npNFH increase specifically in PNs, due to high expression of this protein in PNs. Indeed, snRNAseq data, supports that *Nefh* gene is particularly highly expressed and abundant in PNs compared to all other neuronal types in the cerebellar cortex, strikingly similar to PNs markers such as *Pcp2* (Kozareva *et al*, 2021). At the protein level, NFH results highly expressed in PNs, as shown by immunofluorescence analysis in cerebellar slices (Demilly *et al*, 2011; White & Sillitoe, 2013). In general, we detect also high and specific NFH expression in primary PNs cultures. Data from another snRNAseq atlas of developing mouse

cerebellum from P0 to P10 also shown that *Nefh* changes its expression in PNs during early development and becomes detectable starting at P8 (Peng *et al*, 2019). Since we detected npNFH increase at P15, we hypothesize that in the absence of sacsin, NFH expression is not altered in respect to neurodevelopment, but NF impairment starts soon as *Nefh* is expressed in PNs, reflecting a primary role for sacsin in NF regulation in PNs. Indeed, we observe NF remodeling also by npNFH immunofluorescence in primary PNs from *Sacs*$^{-/-}$ cultures, that was visible already at DIV10 and DIV15 and presents with dense bundles both in the soma and proximal dendrites. Especially, large and long bundles are visible in proximal dendrites unlike the wild-type control.

PNs are characterized by extreme cellular morphology and dendritic arborization, that may explain their vulnerability to NF network disorganization, as NF cytoskeleton is important to confer structural and mechanical integrity (another vulnerability is also linked to organelle transport in such distal sites, which also interplays with NF; this will be discussed below). Although there is more abundant literature on the primary role of NF in axons and axonal radial growth, NF are highly present also in dendrites (Strack & Hell, 2008; Grant & Pant, 2000; Gentil *et al*, 2015; Yuan *et al*, 2012), where their transport and phosphorylation are specifically regulated. Neurofilaments dynamics in dendrites have also been linked to synaptic plasticity in pyramidal neurons, suggesting that they are not merely scaffolds (Hashimoto *et al*, 2000). Similar mechanisms may also be hypothesized in PNs. Interestingly, all NF subunits are detected in cerebellar PSD, both in our LFQ-proteomics dataset (see **Results Section 2.4**) and in published proteomics (Pandya *et al*, 2017), suggesting that NF are also associated with postsynaptic compartment in mouse cerebellum.

However, IF disorganization is a universal hallmark in the absence of sacsin in any cell type, thus corroborating that sacsin plays a primary role in IF regulation. Vimentin forming perinuclear dense bundles, was reported by us and our collaborator in ARSACS patients' fibroblasts (Duncan *et al*, 2017) and in *SACS*$^{-/-}$ HEK293 cells. Vimentin collapse and bundle identical to that observed in ARSACS fibroblasts was also observed in *SACS*$^{-/-}$ HeLa cells and undifferentiated *SACS*$^{-/-}$ SH-SY5Y cells that I had generated, by immunofluorescence both with antibodies against total NFH and npNFH. Finally, differentiated SH-SY5Y cells shown npNFH accumulation in soma and especially neurites, very similarly to bundles observed in primary PNs proximal dendrites.

A very important implication is that *SACS*$^{-/-}$ SH-SY5Y, despite being a relatively simple *in vitro* model, represents a valuable tool for testing and screening therapeutic

approaches directly aimed at reducing NF bundling in ARSACS. For this purpose, an essential requisite was also a simple but efficient quantitative setup to assess NF remodeling in an unbiased way, at least *in vitro*, which was not reported in precedent literature. This was done by quantifying bundle volume in cells after optical microscopy and 3D reconstruction, in the paradigm that the volume of these NF dense bundles observed at optical microscopy resolution is directly proportional do the degree of NF bundling. Ultimate definition of this quantitative model was allowed by a mechanistic dissection of NF bundling in PNs and several lines of evidence which I will discuss in the next section.

Finally, indeed using SH-SY5Y as *in vitro* tool, we were able to identify the interaction between sacsin and NF subunits in endogenous conditions, both by mass spectrometry and by co-IP. In particular, co-IP with sacsin and NFL was achieved from the NF cytoskeleton insoluble fraction, as described for other NFL interactors (Rao *et al*, 2002a), which was very difficult due the high molecular weight of both proteins and NFL stickiness. This interaction with the core component of NF fibers further supports that NF bundling is the primary cellular molecular phenotype in the absence of sacsin in neurons.

2.2 – Mechanistic explanation of NF remodeling in ARSACS

By optical microscopy, NF remodeling is observed as dense bundles in soma and neurites, detectable both by total NFH and npNFH antibodies. Whereas biochemically, by LFQ proteomics analysis the total level of all CNS-expressed NF subunits is not altered in the absence of sacsin in mouse cerebellum at late symptomatic stage. This was also confirmed by WB at late stage, that shows increased signal accumulation of npNFH only, but not of other NF subunits and in particular a slight decrease with pNFH antibody. Lowered mRNA expression of all NF subunits is indeed occurring in *Sacs*$^{-/-}$ cerebellum by bulk RNAseq. These findings suggest that dense bundles observed in optical microscopy and increased npNFH in WB are not caused by increased expression of NFH *per se*, followed by its aggregation; rather, in the absence of sacsin there is an imbalance in NFH phosphorylation. SMI32 antibody recognizes a KSP epitope site in the C-terminal tail of NFH (Morfini *et al*, 2006). Phosphoproteomics analyses confirmed quantitatively loss of phosphorylation at several C-tail KSP sites in NFH and NFM in *Sacs*$^{-/-}$ cerebellum. Previous literature did not investigate systematically if npNFH increase was due to impaired turnover of NFH subunits or imbalanced posttranslational modifications (Larivière *et al*, 2015; Gentil *et al*, 2019).

Also mature NF fibers assembly is not impaired *per se*. This was demonstrated again both by biochemical and imaging approaches. EM imaging in PNs in cerebellar sections did show normal 10-nm fibers that are more densely packed, with less interspace, in *Sacs*$^{-/-}$ in respect to wild-type. We hypothesize that reduced phosphorylation at C-tail KSP sites causes NF fibers compaction, as NFH phosphorylation in these sites is central on maintaining proper interspacing between NF mature fibers (Yuan *et al*, 2017). Biochemically, npNFH accumulation is also shown in the insoluble cytoskeletal fraction from mouse cerebellum in the absence of sacsin; this is the fraction which NF proteins enter after maturation into elongated mature fibers (Liu *et al*, 2004; Yuan *et al*, 2017; Yuan & Nixon, 2021). Altogether, this data suggests that NFH subunits are properly expressed, synthesized and assembled into mature triton-insoluble filaments, that eventually get or remain unphosphorylated, thus causing their abnormal bundling in PNs. This also allowed us to quantify NF remodeling in the absence of sacsin by taking as parameter the bundle volume in optical microscopy.

2.3 – Neurofilaments accumulation in ARSACS is different from other common neurodegenerative diseases

Accumulation of hyperphosphorylated NFH subunit is generally a hallmark of neurodegeneration (Grant & Pant, 2000; Didonna & Opal, 2019). Many neurodegenerative diseases (Alzheimer disease – AD - , Parkinson disease – PD -, PolyQ expansions, Amyotrophic Lateral Sclerosis – ALS - and tauopathies) are regarded as proteinopathies, characterized by inclusion body formation; these inclusion bodies are in generally caused by protein aggregation due to protein misfolding that generally starts the formation of amorphous aggregates that can then form amyloid-conformations. Structurally abnormal and phosphorylated NF subunits have been shown to be present in insoluble neurofibrillary tangles associated with AD disease by immunohistochemistry (Haugh *et al*, 1986; Didonna & Opal, 2019). NFM and NFH peptides highly phosphorylated in C-terminal tail KSP sites were also found by mass spectrometry analyses of insoluble neurofibrillary tangles, and all three NF subunits were detected (Rudrabhatla *et al*, 2011). NF were also discovered in Lewi bodies in dopaminergic neurons in PD as well as in other synucleinopathies (Goldman *et al*, 1983; Didonna & Opal, 2019). Thus, NF aggregation and hyperphosphorylation at KSP sites are usually associated to ongoing general neurodegeneration, and indeed NFL plasma and cerebrospinal fluid (CSF) concentration is being increasingly explored as biomarker of neurodegeneration (Yuan & Nixon, 2021). Inclusion bodies are observed also in motorneurons in ALS, usually made of aggregates of different

proteins, e.g. Superoxide dismutase 1 (SOD1), TAR DNA-binding protein 43 (TDP43) and FUS. NF aggregation is also a primary hallmark in ALS: ubiquitinated NF subunits and pNFH form or are enriched in perikaryal inclusion bodies and tangles in motorneurons and in axonal spheroids in ALS (Ross & Poirier, 2004; Blokhuis *et al*, 2013; Gentil *et al*, 2015). Also in ALS, NFM and NFH have been found to be abnormally hyperphosphorylated at their C-tails (Gentil *et al*, 2015).

NF remodeling observed in ARSACS is peculiar as there is no overexpression of NF subunits; there is neither misfolding nor abnormal assembly of NF fibers, as EM in *Sacs*$^{-/-}$ shown structurally normal 10-nm fibers. Also, inclusion bodies were never detected by EM. These results are confirmed independently also from other groups, that shown by EM similar orderly packed structures of IFs both in ARSACS patients' fibroblasts (Duncan *et al*, 2017) and in motorneurons from dissociated *Sacs*$^{-/-}$ mice DRGs (Gentil *et al*, 2019).

Phosphorylation is regarded as a general covalent mechanism that drives aggregation of proteins; indeed hyperphosphorylation in specific sites in synuclein and tau are being explored as primary drivers in related pathologies (Ross Poirier 2004); similarly, NFH and NFM hyperphosphorylation at KSP sites may be the main trigger of their aggregation and is robustly observed in neurodegeneration as already discussed (Grant & Pant, 2000; Sihag *et al*, 2007; Dale & Garcia, 2012; Rudrabhatla, 2014); consistently, imbalanced expression of PP2A and Cdk5 (two major phosphatase and kinase of NFH respectively) are associated with ageing and AD (Grant & Pant, 2000; Liu *et al*, 2004; Didonna & Opal, 2019). Very uncommonly, ARSACS manifests with hypophosphorylation of the same KSP sites, which is very uncommon for a neurodegenerative disorder.

Differences between ARSACS and NF metabolism disorders (examples from CMT and GAN)

ARSACS is different from other disorders in which NF metabolism is primarily affected. These disorders are generally caused by impaired turnover, folding or assembly of the NF fibers, which are usually associated with large structurally abnormal aggregates that are highly detrimental in peripheral neurons with large axons. Examples include Charcot-Marie Tooth (CMT) and Giant Axonopathy (GAN). Different CMT types (e.g. CMT2A and CMT1F) are caused by mutations in the *NEFL* gene, which cause abnormal NF assembly or transport, or increased stability of the fibers. Another form of CMT is caused by *HSPB1* gene encoding Hsp27 chaperone, that impairs NF assembly and results in NF perikaryal aggregates. Finally, CMT2CC is caused by mutations in the *NEFH* gene that make NFH protein prone to amyloid-

conformation (Rebelo *et al*, 2016). GAN is also caused by loss-of-function mutations in the gene encoding gigaxonin, an adapter of E3 ubiquitin ligase that specifically targets NF to degradation. GAN is much more severe than CMT as it causes very enlarged NF aggregates that swell axons throughout all PNS and CNS. As for GAN, alteration of other Ubiquitin Ligases specific for NF subunits, like TRIM2, are strictly associated with severe axonopathies. (Didonna & Opal, 2019; Gentil *et al*, 2015). Therefore, it is unlikely that sacsin may directly act as a chaperone on NF subunits, regulating their folding or assembly, or that it directly regulates NF degradation. In general, only slight turnover impairment was reported in ARSACS in motorneurons from dissociated DRGs (Gentil *et al*, 2019). However it is very hard to study NF turnover, as they are one the most stable proteins in the cell, with half-life up to 2.5 months (Yuan *et al*, 2009).

2.4 – Sacsin interacts with NF cytoskeleton linker proteins

We demonstrated defective localization of mitochondria and ER to distal dendrites in PNs and defective mitochondria anterograde trafficking in *Sacs*$^{-/-}$ cerebellar neurons. We hypothesize that defective trafficking is a consequence of npNFH bundling in soma and proximal dendrites of PNs and thus represents a secondary event to cytoskeleton remodeling occurring in the absence of sacsin. A very important piece of evidence was the identification of sacsin interactors in neuronally-differentiated SH-SY5Y cells. We used this tool to increase the chances to efficiently immunoprecipitate sacsin and getting cleaner results, taking the advantage of its validity as tool to model npNFH bundling seen *ex vivo* and *in vivo*. Most of the identified sacsin interactors were large cytoskeletal proteins, including NFL and NFM, while no mitochondrial proteins were detected as specific interactors. In addition to NFL, plectin and myosin Va were found to directly interact with sacsin. Plectin is a giant multifunctional protein (> 500 kDa) acting as a mechanical linker between IFs network and other cytoskeletal structures, as well as mitochondria and other organelles (Winter & Wiche, 2013). Class V myosins are actin-based motors that mediate the proper short-range intracellular transport of diverse organelles, mRNAs and proteins (Hammer & Wagner, 2013). Both plectin and Myosin Va (250 kDa protein) are expressed at high levels in PNs compared to other cell types in cerebellar cortex (Kozareva *et al*, 2021; Miyata *et al*, 2000). Strikingly, we were also able to confirm plectin interaction by co-IP in cerebellum, and NFL interaction in endogenous conditions in SH-SY5Y cells, as already discussed.

Thus, sacsin may form complexes with big cytoskeletal linkers that regulate organelle transport. Although mitochondrial transport is known to occur mostly on

microtubules and actin filaments, there is growing evidence that IFs contribute to mitochondrial localization and function in different cell types, including neurons (Schwarz & Leube, 2016); moreover, NF are especially important in mediating proper positioning of organelles and other structures (Yuan *et al*, 2017). NF impairment (in the form of aggregation) has been already associated to defective transport and mislocalization/soma retention of organelles, in particular mitochondria and ER, e.g. in CMT (Brownlees *et al*, 2002; Gentil *et al*, 2015; Didonna & Opal, 2019). Transgenic mouse models in which NF subunits are overexpressed or depleted show aberrant mitochondrial motility (Gentil *et al*, 2015; Israeli *et al*, 2016). Moreover, extensive dephosphorylation of NFH subunits affects their interaction with mitochondria leading to a reduced rate of mitochondrial motility (Wagner *et al*, 2003). Although we did not observe NF aggregation as in these disease models, is still likely that npNFH bundling leads to defective transport and mislocalization by steric hindrance or by dysregulation of cytolinker proteins or both. Indeed, also Myosin Va deficiency in PNs was associated to drastic organelle mislocalization defects, as demonstrated by ER missing specifically from dendritic spines (Wagner *et al*, 2011). Indeed, Myosin Va interacts with NFL in neurons, and this interaction is essential for proper ER distribution (Rao *et al*, 2002a; Yuan *et al*, 2017). Plectin deficiency was demonstrated to impact on mitochondrial shape and mostly on its transport (Valencia *et al*, 2021; Winter *et al*, 2015). Indeed, we observed biochemically plectin reduction in the soluble phase in ARSACS patients' fibroblasts and *SACS*$^{-/-}$ SH-SY5Y cells, and accumulation of both plectin and myosin Va in cerebellar insoluble fractions from *Sacs*$^{-/-}$ mouse. We also shown increased plectin signal in soma and proximal dendrites of PNs in cerebellar slices by immunofluorescence, which resembles NFH accumulation. This remodeling could represent the link between impaired NF and mitochondria mislocalization that was already reported in ARSACS (Duncan *et al*, 2017; Girard *et al*, 2012).

Cytoskeleton remodeling and sacsin function

If this cytoskeleton remodeling could reflect a direct role of sacsin on protein quality control of plectin and myosin Va, as well as NF, is to be clarified. As deeply discussed above, sacsin does not seem to be required at least for proper NF protein expression and assembly, which does not suggest a direct role as a molecular chaperone. Further biochemical and functional studies are needed to elucidate this point, which is anyway hard to be addressed *in vivo* considering the enormous size and stickiness of these cytoskeletal proteins. Since both plectin and Myosin Va interact also specifically with NF subunits (Rao *et al*, 2002a), we cannot exclude the hypothesis that plectin and Myosin Va get sequestered in the compacted npNFH

insoluble phase rather than being direct sacsin substrates and getting misfolded and aggregated *per se*. Again, aspecific aggregates were never observed in PNs in cerebellum by EM.

Further analyses are needed to analyze if sacsin exerts chaperone activity directly on these other interactors, or if they form a giant complex that coordinates NFH phosphorylation, spacing and organelle transport; specific kinases or phosphatases may be part or interact with such a big complex. Finally, we cannot also exclude the hypothesis that NF transport is impaired *per se* in the absence of sacsin. However, this last hypothesis seems unlikely, as NF transport is negatively regulated by NFH and NFM C-tail phosphorylation, and defective transport was demonstrated rather in the case of Cdk5-mediated hyperphosphorylation of NFH C-tail, which impairs proper binding with cytoskeletal motors that also are involved in NF assembly intermediates transport in neurons and again is associated with NF misfolding aggregation (Holmgren *et al*, 2013; Gentil *et al*, 2015; Didonna & Opal, 2019).

ARSACS pathogenetic cascade is caused by cytoskeleton remodeling

Cerebellum LFQ-proteomics at five months of age revealed that defective transport likely leads to deregulation of calcium homeostasis and synapse functionality. In a recent work form our lab (*Del Bondio, Longo, De Ritis et al., under revision*) we have dissected the pathogenetic cascade downstream of npNFH bundling that leads to PN degeneration. In this work, failure in calcium buffering was further demonstrated by calcium imaging and measuring in primary PNs upon depolarization induction. This is very likely the cause of PNs degeneration in ARSACS. Indeed impaired organelle transport depletes the synapses of ATP to sustain calcium-clearance systems of plasma membrane and ER, but also of the calcium-buffering capacity of the mitochondria and ER themselves. PNs would be more susceptible to this derangement, due to extremely developed and spiny dendritic arborization and huge number of glutamatergic postsynaptic sites. Moreover, defective organelle transport was indirectly seen also by cerebellar PSD proteomics in *Sacs*$^{-/-}$ mice, that revealed that even other organelles, like ribosomes and RNA granules, may be depleted and contribute to detriment synapses.

Finally, in this work it was also demonstrated that both *in vivo* in cerebellum and *ex vivo* in primary PNs, mitochondrial ultrastructure, functionality and bioenergetics are preserved in the absence of sacsin, contrary to what was reported *in vitro* cell models (Girard *et al*, 2012; Criscuolo *et al*, 2015; Bradshaw *et al*, 2016; Battaglini *et al*, 2022). Accordingly, mitochondrial ATP production was unaltered in *Sacs*$^{-/-}$ cerebellum, both at baseline and upon pyruvate stimulation. These experiments were

performed at five months of age, when neurodegeneration is ongoing in the ARSACS mouse model.

In conclusion ARSACS pathogenesis shows two main cellular pathological events, NF remodeling and organelle transport impairment; in particular the latter is secondary to cytoskeleton remodeling and leads to neurodegeneration ultimately impairing calcium buffering and synapses. On the other hand, mitochondria per se are not impaired. Inconsistence with previous literature may be reconciled with the fact that those experiments were performed *in vitro* in immortalized cells and that this ARSACS pathogenesis model would be highly cell autonomously starting from npNFH bundling specifically in PNs in cerebellum.

2.5 – NF remodeling in ARSACS and implications for therapy

ARSACS can be regarded as a NF-related pathology as it displays a very specific NF phenotype which is primary, early-onset and profoundly different from all other neurodegenerative disorders. This has profound impact on therapeutic approaches and possibly gene therapy. Previous studies suggested to modulate cellular chaperone systems in order to rescue IFs bundling in patients cells and neurons (Gentil *et al*, 2019; Nethisinghe *et al*, 2021; Gentil *et al*, 2019). However, there is no evidence that this bundling is indeed due to loss of chaperone functions by sacsin on NF, or that NF bundling in ARSACS is due to protein misfolding and aggregation. In the next section, I will discuss that gene replacement of sacsin function would be one of the most effective way to rescue NFH bundling in neurons, and that trying to act or modulate NF cytoskeleton pharmacologically would be much more difficult to test and achieve.

3 – Minisacsin gene therapy in ARSACS

ARSACS is a common genetic recessive cerebellar ataxia for which no cure is available, and no clinical trials are ongoing. Implications for therapy highlighted in previous sections, have explained the molecular basis of some limitations of other therapeutic approaches reported in the literature and demonstrated that ARSACS is suitable for gene therapy replacement strategy. In this section, I will discuss a minisacsin gene therapy approach to restore NF remodeling in neurons, which I have evaluated in different cellular models and quantitative phenotypic readouts.

3.1 – Minisacsin in the context of ongoing therapeutic approaches

Other pharmacological strategies are ongoing in our group. Deregulated calcium homeostasis in *Sacs*$^{-/-}$ PNs provided the rationale to test ceftriaxone efficacy in the ARSACS mouse model (*Del Bondio, Longo, De Ritis, manuscript in revision*). ceftriaxone is a repurposed antibiotic that has been shown to be successful in rescuing ataxia motor defects in a pre-clinical model of SCA28 cerebellar ataxia (Maltecca *et al*, 2015b). This drug limits glutamatergic stimulation, reducing post-synaptic calcium influx. ceftriaxone treatment was successful both in symptomatic and presymptomatic (at one month of age) *Sacs*$^{-/-}$ mice, in terms of calcium levels restoration and motor performance amelioration, with delayed PNs loss. However, ceftriaxone did not resolve npNFH bundling in *Sacs*$^{-/-}$ mice PNs. This findings would corroborate that calcium homeostasis dysregulation might be subsequent to impairment of organelle transport and synapse composition following NF cytoskeleton remodeling. However, we cannot exclude that ceftriaxone could target the earliest molecular mechanisms of ARSACS pathogenesis (i.e. npNFH bundling and/or others that may be still undefined), but it's possible that starting treatment at one month of age is too late, as these mechanisms are already active by then. Furthermore, few papers shown that ceftriaxone is able to resolve protein aggregates (Bachetti *et al*, 2010; Ho *et al*, 2018), again suggesting that npNFH bundling in ARSACS is likely due to different molecular mechanisms rather that protein aggregation. Therefore, gene therapy is being explored in the context of comprehensive strategies to target ARSACS molecular mechanisms in our group. Indeed, one main limitation of AAV-based therapy is that in clinical trials, transduction efficacy is dependent on previous exposure to natural occurring AAV capsids. The presence of AAV antibodies can occur in up to 60% of the population, from early age, and even low titers can reduce drastically therapeutic gene expression. AAV neutralizing antibodies can be produced following also long-term clinical trial; these neutralizing antibodies are highly cross-reactive to many different serotypes, making difficult to reinject patients or

impossible to treat in presence of high titers antibodies. Seropositive patients are excluded from clinical trials (Li *et al*, 2012; Sun & Liao, 2022; Earley *et al*, 2022; Schulz *et al*, 2023). On the other hand, one main limitation that gene therapy would overcome is the difficulty of modulating NF with small drugs, as NF subunits are among the most stable proteins in the cells, with a half-life up to 2.5 months (Yuan *et al*, 2009). An interesting proof of principle of the feasibility to modulate NF by gene therapy, comes from GAN, where AAV9-mediated delivery of human *GAN* gene in patients' fibroblasts and intrathecally in a mouse model of GAN reduced NF aggregates and ameliorated motor functions without showing toxicity (Didonna & Opal, 2019). A phase I clinical trial has been started with intrathecal treatment of one patient with this NF pathology (Bailey *et al*, 2018).

3.2 – Sacsin protein and miniaturized gene strategy

Gene replacement mediated by AAV vectors is gaining interest due to its safety profile, low immunogenicity, efficacy and long lasting transgene expression (Deverman *et al*, 2018; Hudry & Vandenberghe, 2019; Lee *et al*, 2017; Li & Samulski, 2020; Mendell *et al*, 2021; Tai, 2019). Currently, multiple clinical and preclinical trials are ongoing for the treatment of different neurodegenerative disease targeting neurons in the central nervous system; also the cerebellum is regarded as a suitable target, for the treatment of genetic ataxia, due to high tropism observed for different AAVs in this site and in particular in PNs (Borel *et al*, 2014; Chan *et al*, 2017; Deverman *et al*, 2018; Kaemmerer *et al*, 2000; Li *et al*, 2020; Morabito *et al*, 2017; Nitta *et al*, 2017). The main hurdle for translating this strategy to ARSACS is the huge dimension of sacsin protein. Indeed, coding sequence of sacsin is 13.73 kb, far away from the limit of packaging size of AAV, which is ~4.8 kb (Samulski & Muzyczka, 2014; Li & Samulski, 2020). For this reason, I designed and generated a miniaturized version of sacsin protein, by combining different sacsin domains. There are several papers attesting the efficacy of gene therapy with shortened versions of causal genes in inherited diseases (French *et al*, 2020; Tornabene & Trapani, 2020; Transl *et al*, 2021). This approach is novel in the ARSACS field, as previous reports have shown solely the effect of transfection of single sacsin domains (Gentil *et al*, 2019). This study from Gentil et al, was valuable in proving the ability of single sacsin domains to be functional and to modulate vimentin bundling in ARSACS patients' fibroblasts and NF bundling in *Sacs*$^{-/-}$ motorneurons from dissociated DRGs. However, different domains had differential ability to rescue NF network, e.g. SIRPT2 and SIRPT3 had no effect, HEPN domain had minor effect, UbL and SIRPT1 had a strong effect and finally J domain alone virtually rescued completely the bundling, restoring normal NF

network in all cells. Second issue of the study was that overexpression of single domains in control cells had different qualitative effects on proper NF network formation and maintenance (Gentil *et al*, 2019), ranging from complete NF dissolution to even formation of bundles and aggregates (see also **Introduction Section 6.2**). These findings indicate that sacsin's proper functioning relies on all of its domains. This is further supported by convergent evolutionary mechanisms that have brought together its unique combination of domains.

All sacsin domains with most experimental evidence were chosen and cloned together. Both Ubl, Hsp90-like ATPase region of SRR1, J and HEPN domains were individually crystallized and characterized biochemically (Ménade *et al*, 2018; Parfitt *et al*, 2009b; Kozlov *et al*, 2011); in two different works, the entire SIRPT1 or the N-terminal fragment containing both Ubl and SRR1 domains, were cloned and ectopically expressed (Anderson *et al*, 2010; Gentil *et al*, 2019). All these data demonstrate that single sacsin domains would retain their stability and molecular function. Although SRRs are only a portion of respective SIRPTs, the latter are too large to allow combination with other sacsin domains and addition of regulatory sequences suitable for AAV production. Moreover, other sub-repeats of SIRPTs other than SRR have never been further analyzed or associated to a particular biochemical function. Furthermore, we decided to include only the first SRR copy, as this is the most characterized and has been already cloned in different studies (Ménade *et al*, 2018; Anderson *et al*, 2010); also, SIRPT1 alone was the most effective SIRPT domain in restoring NF bundling (Gentil *et al*, 2019). The final construct, cloned between a universal CMV promoter and a terminator signal, has a length of ~3.3 kb, well suitable for AAV packaging and which allows the insertion of other regulatory sequences or other promoters, including the longer CAG universal promoter or longer PNs specific promoter derived from *Pcp2*-L7 (Nitta *et al*, 2017).

Recombinant minisacsin protein proved to be stable, highly expressed and not toxic *in vitro* and *ex vivo* by transfection in neuronal like SH-SY5Y cells and AAV-mediated transduction in *Sacs*$^{-/-}$ PNs. Minisacsin ectopic expression *in vitro* always presented with formation of two bands by WB analyses, which I have demonstrated to be phosphorylated isoforms of minisacsin. The molecular identity of each band was also demonstrated by IP followed by MS/MS analysis. One issue could be that heavy phosphorylation would interfere with minisacsin function or cause its aggregation. However, minisacsin had a subcellular localization and staining pattern similar to that of endogenous sacsin in PNs, with no suggestion of occurring aggregation; also I did not detect abnormal localization in the nucleus, as was observed for J domain -encoding permeating peptide previously reported to reduce NF bundling in DRG

neurons (Dabbaghizadeh *et al*, 2022). Minisacsin was also able to reduce NF bundling in transfected *SACS*$^{-/-}$ SH-SY5Y cells, demonstrating that it is functional, without showing altered NF distribution or network in control cells. Quantification of minisacsin effect shown that there is not a total rescue *in vitro*; however, although the low transfection rate may have been limiting for quantification analyses, we could still detect a reduction of 25-28% of max-NFH volume after 48 hours acute transfection, which is valuable due to very high stability of NF network. Preliminary results also shown that minisacsin conserves its function, reverts NF bundling and is not toxic in *Sacs*$^{-/-}$ PNs. These experiments, although still preliminary, provide for the first time the evidence of NF bundling reduction directly in the neurons specifically affected in ARSACS. Moreover, careful quantitative assessment of NF bundling reduction in human neuronal-like model *in vitro* was also achieved for the first time.

3.3 – AAV recombinant capsids for systemic gene therapy

One main issue regarding treatment of neurodegenerative disease is targeting the CNS and precise delivery of the transgene. While in many clinical trials, AAV9 parenchymal and stereotactic surgical injection have been used, systemic vascular injection would be less invasive and suitable to reach different neuronal population in the CNS. Sacsin is highly expressed in many neurons other than PNs, which show npNFH bundling as well (Larivière *et al*, 2015) and that are involved in ARSACS clinical features, included DCN and pyramidal neurons. AAV9-derived PHP.B and enhanced PHP.B (PHP.eB) recombinant vectors, selected by targeted evolution, are an established efficient tool for preclinical studies in mice, due to their ability to bypass the BBB and efficient transduction of the brain, especially PNs, by a single intra-venous tail injection (Chan *et al*, 2017; Morabito *et al*, 2017). To explore AAV PHP.eB use in ARSACS preclinical model and as a proof of concept of minisacsin efficacy, I have demonstrated also the ability of PHP.eB vectors to infect primary PNs, both carrying control EGFP gene and minisacsin, a data that was missing in literature. Strikingly, all lentiviruses tested were never been able to transduce PNs *ex vivo*, differently to what reported *in vivo* (Hirai, 2008; Nitta *et al*, 2017).

We are aware that one main limitation of PHP.B derived vectors is that when tested in non-human primates, they shown lower or poor transduction efficiency of the CNS than that observed in C57BL/6J-specific strain mice, highlighting inter-species differences in the BBB penetrance of this AAV serotype, likely residing on differentially expressed receptors (Liguore *et al*, 2019; Matsuzaki *et al*, 2018; Huang *et al*, 2019). Indeed, in ongoing collaboration with Dr. Vania Broccoli at OSR Milan, we are also investigating the use of a novel patented selected recombinant capsid, here called

Se2, which has been shown to have strong tropism for the cerebellum and PNs upon systemic intra-tail infusion, both in multiple mice strains and in a marmoset primate model. We cannot exclude also for the future the use of AAV9 in parenchymal injection both for preclinical and translational applications.

Perspectives

Future work is necessary to demonstrate feasibility to scale to clinical trials.

In the immediate future, I will carefully quantify the exact amount of NF bundling recovery in *Sacs*$^{-/-}$ PNs, both with PHP.eB and Se2 capsids. To this aim, I have recoded minisacsin cDNA sequence, to optimize stability and expression (Mauro & Chappell, 2014). Regarding minisacsin protein phosphorylation, I do not expect that it would be solved by codon optimization, as this of course does not affect aminoacidic sequence but only mRNA stability and translation; therefore, although I did not detect signs of aggregation by immunostaining, more specific studies will be done to exclude aggregate formation upon minisacsin transfection by WB analyses.

Secondly, I will test the functionality of minisacsin after recoding by codon-optimization to further improve its expression and stability *in vivo*. I will carry on a preclinical trial *in vivo* by injection of *Sacs*$^{-/-}$ and wild-type littermates at one month of age; then I will perform motor coordination tests and tissue and biochemical analyses at six months of age. Indeed, I have already injected wild-type mice with both PHP.eB and Se2 capsids carrying minisacsin or EGFP control gene, at one month of age with systemic intra-tail infusion of 10^{11} vg. Mice did not show any sign of toxicity and had normal weight course as monitored for one month of age after injection, suggesting that also *in vivo* in preclinical models minisacsin is not toxic (data not shown).

Another issue to study in the future, would regard the precise balance between tissue specificity and administration site. As vascular injection allows for reaching wider CNS populations neurons, it can also lead to transduction of other organs. Indeed, PHP.eB capsid carrying EGFP gene has been shown to target specifically PNs and not liver, heart and muscles upon systemic injection by using a PNs specific *Pcp2*-L7 promoter (Chan *et al*, 2017). As the entire *Pcp2*-L7 promoter would be too large for minisacsin, we have already tested *ex vivo* with PHP.eB capsid a shorter version that was already proved to work *in vivo* (Nitta *et al*, 2017). In alternative, preclinical studies can be carried by intraparenchymal injection of mice with capsid and promoter of choice. In conclusion, minisacsin small size allows us for high versatility in order to translate this approach to preclinical models.

MATERIALS AND METHODS

Methods relative to the Section 1 were followed exactly as published previously in our paper Longo, Fabiana, De Ritis Daniele et al. "Assessment of sacsin turnover in patients with ARSACS: Implications for molecular diagnosis and pathogenesis." Neurology 97.23 (2021): e2315-e2327.

1 – Sacsin protein level quantification and turnover assessment in ARSACS patients' cells (Results Section 1)

1.1 - Subjects' consent

Eleven subjects with the clinical and genetic diagnosis of ARSACS (table1) were retrospectively recruited among the cohort of spastic-ataxic patients referring to each center: Ospedale San Raffaele (Milan, Italy), IRCCS Stella Maris (Pisa, Italy) and VIB Uantwerp Center for Molecular Neurology (Uantwerp, Belgium). The selection of patients for this study was done based on the nature and position of *SACS* mutations, in order to have a comprehensive picture of ARSACS genetics, as detailed in the Results. All subjects included in the study gave their written informed consent according to protocols approved by the respective institutional human ethics review boards according to the Declaration of Helsinki.

1.2 - Human primary fibroblast derivation from skin biopsies

Patient-derived skin fibroblasts were obtained during diagnostic procedures by punch skin biopsy performed on distal leg, following standard protocols as described previously (Longo *et al*, 2020). In brief, the skin biopsy just picked up was gently transferred from a Falcon test tube in a T25 flask filled with 2ml of DMEM medium supplemented with 20% Fetal Bovine Serum (FBS), 1mM sodium pyruvate, 2mM L-glutamine and 100U/mL penicillin-streptomycin and daily monitored. After three weeks in culture, when the fibroblasts spreading from the biopsy were almost confluent, the first trypsin passage was performed, and then the cells were cultured until passage three, which provides fibroblasts suitable for experiments and freezing.

1.3 - Antibodies, drugs and reagents

Commercially available antibodies were used in Western blots (WB), for the detection of sacsin (Anti-sacsin AbC ab181190. Abcam, Cambridge, UK diluted 1:2500), spectrin (Anti-spectrin MAB1622 Merck Millipore, Burlington, MA, USA, diluted 1:10000), ubiquitinated proteins (Anti-ubiquitin ab134953, Abcam, diluted 1:1000), p62 (Anti-p62/SQSTM1 P0067 Merck Millipore, diluted 1:1000), LC3I-II (Anti-LC3A/B ab58610. Abcam, diluted 1:1000), HA (anti-HA Epitope Tag 16b12, Biolegend, San Diego, CA, USA, diluted 1:500). Secondary antibodies included HRP-

conjugated anti-mouse and anti-rabbit IgG (Amersham Bioscience, Buckinghamshire, UK, diluted 1:5000).

In vitro treatments were carried out with different compounds: 1 μM MG-132 24 hours or 3 hours (Merck Millipore), 20 μM Chloroquine (CQ) 24 hours (Merck Millipore) or together (0.25 μM MG-132 + 10 μM CQ, 18 hours); protease inhibitors (5 μM E64, 10 μM Bestatin, 5 μM Pepstatin, 48 hours (Merck Millipore)). After the treatments, cells were harvested and lysed for biochemical assays.

PBMCs proliferation was induced by treatment with phytohaemagglutin (Sigma L2769) at a concentration of 1-5 μg/mL.

1.4 - Anti N-terminal sacsin antibody (AbN) generation

We generated a new rabbit polyclonal anti-sacsin antibody recognizing the N-terminal portion of sacsin (ID Q9NZJ4 (SACS_HUMAN)). We decided to develop a new anti-sacsin antibody (AbN) raised against a polypeptidic region of sacsin including aminoacids from 1 to 728 (all the exons until the giant exon 10). The antibody was produced by the antibody production service of Biomatik (Cambridge, Ontario, Canada).

1.5 - SACS deletion by CRISPR/Cas9

Traditional 20 bp-NGG spCas9 gRNAs targeting *SACS* coding region were designed with CHOPCHOP web tool. The gRNA sequences were: gRNA-1 5' TGCTCCTGCGGTTATCAGTA 3'; gRNA-2 5' GTAGGCCATGCAATTCTCAT 3'. Oligos encoding the gRNAs were annealed and cloned into pCas-Guide-EF1a-GFP CRISPR/Cas9 plasmid (OriGene), according to the manufacturer instructions. To delete the *SACS* gene, HeLa cells and SH-SY5Y cells were transfected with CRISPR/Cas9 plasmid carrying gRNA-1 or gRNA-2. GFP positive cells were sorted by FACS Aria Fusion (Becton Dickinson), and plated at single cell density. Monoclonal cell lines were expanded from single colonies and sacsin KO was validated by immunoblot and by Sanger sequencing. Primers for gRNA-1 target region were: forward primer 5' AGCAAAAGGAGCAACGTCTG 3'; reverse primer 5' GCTCTTTTCCATCTCCAGACG 3'. Primers for gRNA-2 target region: forward primer 5' AGCCAAAACCCTCTTACTGG 3'; reverse primer 5' AGTGGCTCTCTTTGTCCTGA 3'.

Off-target effects were evaluated with CHOPCHOP web tool in order to avoid gRNAs with potential off targets with up to three mismatches.

1.6 – Standard WB analyses

For WB, tissues or whole cell pellets were homogenized in 100 mM Tris-HCl (pH 7.4), 1 mM EDTA (pH 8), 1% Triton X-100 and 150 mM NaCl supplemented with Protease Inhibitor Cocktail (PIC, Sigma-Aldrich, Merck KGaA) and Phosphatase

Inhibitor Cocktail (Merck KGaA) using a Dounce homogenizer and incubated for 30' on ice. Cell debris was discarded by centrifugation at 8000 g for 10' at 4°C. Samples from Triton-X100 soluble fractions were prepared in Laemmli buffer (5.8mM TrisHCl pH 6.8, 5% glycerol, 1,6% SDS, 0,1 M DTT, 0,002% bromophenol blue) and loaded in SDS-PAGE. SDS-PAGE gel were prepared by mixing acrylamide/bis-acrylamide solution (BioRad), Tris-HCl buffer, SDS, TEMED, and APS (Sigma).

1.7 - RNA extraction and Real Time-PCR (qRT- PCR)

Total mRNA from primary fibroblasts, or PBMCs was extracted and reverse-transcribed using standard procedures. From whole blood samples, RNA was extracted with ZR-Duet DNA/RNA MiniPrep plus kit (Zymo Research), quantified with Qubit® 2.0 fluorometer (Thermo Fisher Scientific) and checked for quality with Agilent 2100 Bioanalyzer RNA 6000 Nano Kit (Agilent Technologies). *GAPDH* primers: forward primer 5' CCACCCAGAAGACTGTGGAT 3'; reverse primer 5' GTTGAAGTCAGAGGAGACCACC 3'. qRT- PCR was performed based on SYBR Green chemistry (Light Cycler 480. SYBR Green I master, Roche). *SACS* primers for the analysis of total *SACS* mRNA levels in patients' and controls' samples were: forward primer 5' TTTTCAGTTGCGAGGGGTTG 3'; reverse primer 5' TCCTGGCTTGGGAGGTAAAG 3'.

To normalize *SACS* mRNA levels, we used TATA Binding Protein (*TBP*) mRNA levels. *TBP* forward primer 5' ACGCCGAATATAATCCCAAG 3'; reverse primer 5' GCACACCATTTTCCCAGAAC 3'.

1.8 - Aggregate detection methods (Results Fig. 5)

i) Soluble and insoluble fractions in SDS-PAGE

*Ultrasonication (**Results Fig. 5a**)*: Primary fibroblasts from controls and patients were lysed by using Dounce homogenizer in 100 mM Tris-HCl pH 7.4, 150 mM NaCl, 1 mM EDTA pH 8 and protease inhibitor cocktail (Sigma Aldrich), then passed through a syringe and centrifuged at 1000g x 10 minutes. Soluble fraction (post-nuclear supernatant (PNS)) was collected, and pellet (insoluble fraction) was resuspended in 500 µL lysis buffer and sonicated (20 seconds pulse-10 seconds stop; repeated twice). PNS and pellet were quantified, and equal amount (60 µg) were loaded on SDS-PAGE.

*Laemmli buffer resuspension (**Results Fig. 5b**)*: Equal number of primary fibroblasts from controls and patients were lysed by using Dounce homogenizer in 100 mM Tris-HCl pH 7.4, 150 mM NaCl, 1 mM EDTA pH 8 and protease inhibitor cocktail (Sigma Aldrich), then passed through a syringe and centrifuged at 1000g x 10 minutes. Separated soluble fraction (post-nuclear supernatant (PNS)) and pellet

(insoluble fraction) were directly resuspended in Laemmli sample buffer 1X and loaded on SDS-PAGE.

*ii) Total homogenates in agarose-acrylamide gel (**Results Fig. 5c**)*

Whole cellular pellets were lysed in Laemmli sample buffer 2X and sonicated to break the DNA as previously described in the ultrasonication method. Total homogenates were loaded onto acrylamide-agarose mixed-gels, which have much larger pores than pure acrylamide gels, allowing the passage and an acceptable resolution of large complexes (Weiss A, Klein C, Woodman B, Sathasivam K, Bibel M, Régulier E, et al. Sensitive biochemical aggregate detection reveals aggregation onset before symptom development in cellular and murine models of Huntington's disease. J. Neurochem. 2008). The stacking gel was prepared at 2% acrylamide concentration. The resolving gel was prepared at 2.7%. To the standard ingredients of an acrylamide gel a 0,5% agarose solution was added to the resolving gel. 0,1 mg of total protein was loaded per lane.

*iii) Urea solubilized-cell lysates (**Results Fig. 5d**)*

24 hours after the MG-132 treatment, total cellular pellets were lysed in 8 M Urea, 100 mM Tris HCl and ultrasonicated as previously described in the ultrasonication method. Homogenates were loaded onto two different acrylamide-concentrated gels (6% or 12%) in order to detect possible truncated sacsin proteins of any molecular weight. AbN was used to immunodecorate the membranes.

1.9 - Polysomal profile analysis

Polysomal fractions were derived from immortalized growing fibroblasts as described (Brina *et al*, 2015) and reverse transcription was performed. To analyze *SACS* mRNA, specific primers were used: forward primer 5' GGCAATTTTGTCCCCTTCTCC 3' reverse primer 5' GGTCTTCCTCGGGTTTGGG 3'. qRT-PCR for *TBP* was used as control of translation. For the analysis of targets from monosome and polysome fractions, the data were quantified as the percentage of expression in each fraction.

1.10 - Immunoprecipitation of N-terminal sacsin fragments

Immortalized fibroblasts (transfected for 16 hours with Ubiquitin-HA plasmid or not) were treated for 3 hours with 1 uM MG-132 and lysed in RIPA buffer. 700 ug of lysate was immunoprecipitated using Dynabeads Protein (#10002D Dynabeads Protein A, ThermoFisher Scientific) bound to AbN (6 µg of antibody per 700 µg of protein) following the manufacturer's instructions. Ubiquitin-HA plasmid was kindly provided by S. Polo's lab, IFOM, Milan.

1.11 - Peripheral blood mononuclear cells

Twenty mL of blood samples were collected from healthy people (one male and one female, respectively 56 and 55 years old) in Vacutainer™ EDTA blood collection tubes. Peripheral blood mononuclear cells (PBMCs) were isolated by density gradient centrifugation with Lymphoprep (STEMCELL Technologies). PBMCs where washed once in DBPS1X and then resuspended and cultured for 72-120 hours, using RPMI-1640 medium, and incubated at 37°C in a humidified, 5% CO_2; medium was added with Phytohaemagglutin at a concentration of 1-5 µg/mL. For WB analysis, PBMCs were pelleted and lysed in 1% Triton X-100.

1.12 – Statistical analyses

Continuous variables were summarized by their mean values and Standard Error of the Mean (SEM). Differences in protein levels between patients and controls were assessed by densitometric analysis of WB bands from at least three biologically independent experiments using ImageJ, followed by unpaired two-tailed Student's *t*-test analysis. The study employed a Student's t-test rather than ANOVA to evaluate the differences between each patient cell line with different genetic mutations and the control cells, rather than examining differences in protein levels between patients. Moreover, the primary objective was specifically to determine whether the treatments rescued or altered sacsin protein levels, therefore the statistical comparison was made within each patient cell line compared to patient untreated cells. The primary focus was not on comparing all patients, but rather on examining the differences within individual patient cell lines.

2 – NF molecular dissection in ARSACS (Results Section 2 and 3)

2.1 – Animals

Sacs$^{-/-}$ and wild-type littermates were obtained by breeding *Sacs*$^{+/-}$ male and female mice (C57BL/6). Experiments were performed in accordance with experimental protocols approved by the IACUC of San Raffaele Scientific Institute. Experiments were performed after sacrificing mice at five months of age, unless otherwise indicated; for cerebellar PSD extraction and LFQ proteomics, mice were sacrificed at one month of age.

Both males and females mice were equally used, except for RNA-seq in which only females *Sacs*$^{-/-}$ and controls were used.

2.2 - Antibodies used in WB

Commercially available antibodies were used for the detection of npNFH (SMI32 Calbiochem, Merck KGaA, diluted 1:1000), pNFH (SMI31, Biolegend, diluted 1:1000), NFM (Chemicon, diluted 1:2000), NFL(Santa Cruz, diluted 1:2000), total NFH (Millipore, diluted 1:1000), plectin, PSD95, sacsin, and vimentin (Abcam, diluted 1:2500), spectrin (Millipore, Merck KGaA, diliuted 1:10000), V5 tag antibody (Invitrogen, diluted 1:2000), calnexin and myosin Va (Sigma-Aldrich, Merck KGaA, diluted 1:1000). Secondary antibodies included Horseradish Peroxidase (HRP)-conjugated anti-mouse and anti-rabbit IgG (Amersham Bioscience, diluted 1:5000).

2.3 - Antibodies used in immunofluorescence

Primary antibodies: calbindin 28 kDa (Swant, diluted 1:300), calbindin (Synaptic System GmbH, diluted 1:300), chicken-IgY calbindin (Abcam, diluted 1:1000), OxPhos complex IV subunit I (Invitrogen), calreticulin (Sigma-Aldrich, Merck KGaA, diluted 1:500), npNFH (SMI32, Biolegend, diluted 1:150), total NFH (Millipore, diluted 1:250), vimentin (Abcam, diluted 1:1000), V5 tag antibody (Invitrogen, diluted 1:200), Tubulin (homemade, diluted 1:1000). Secondary antibodies conjugated with Alexa 488, Alexa 546 or Alexa 647 (Invitrogen, diluted 1:1000) were added in 5% goat serum and 0,2% Triton X-100 in PBS 1X solution (2h, RT). Phalloidin conjugated with AlexaFluor-647 (Life Technologies, diluted 1:1000) was used as secondary antibodies to stain F-actin.

2.4 – Primary PNs cultures preparation

Primary cerebellar cultures were prepared as described (Maltecca *et al*, 2015a). Briefly, the cerebellum from newborn mice was incubated in Hanks' balanced salt solution (HBSS) 1X (Invitrogen) containing 5 U/ml papain (Sigma-Aldrich), 50 mg/ml cystein-HCl, 0.1 mM EDTA, and 1 mg/ml DNase I (EMD Millipore) for 30 minutes at 37°C. Tissues were then dissociated by mechanical trituration. The reaction was

blocked with 10% horse serum, and samples were centrifuged at 100 *g* for 10 minutes. The cellular pellet was washed twice in HBSS 1X and resuspended in culture medium (herein PNs medium) containing Neurobasal (Gibco), B27 supplement (Gibco), 200 mg/mL D-glucose, 2 mM GlutaMax (Gibco), 1% U/ml PenStrep (Gibco), 1% horse serum (Gibco), 3 mM KCl, and 50 ng/ml NGF (Envigo B.5017). Cells were plated at a density of 1.5 × 104/cm2 on coverslips (13 mm in diameter) coated with Poly-L-Lysine (Sigma-Aldrich). *Sacs*$^{+/+}$ and *Sacs*$^{-/-}$ PNs were grown in the above-mentioned medium that was changed every two days. At DIV2, PNs were treated with 100 µM cytarabine (LGC standards) to avoid proliferation of fibroblasts.

2.5 - SH-SY5YS cells

SH-SY5Y cells were grown in SH-SY5Y medium (Dulbecco's modified Eagle medium – DMEM - (Gibco) supplemented with 10% fetal bovine serum (Gibco), 1% L-glutamine (Gibco), 1% sodium pyruvate (Gibco) and 1% penicillin-streptomycin (Gibco)) at 37°C in humidified atmosphere with 5% CO2. *For SACS*$^{-/-}$ SH-SY5Y clones generated by CRISPR/Cas9 genome editing see **Methods section 1.5**.

2.6 - SH-SY5Y differentiation (Results Fig 11, 14 and 18a-b)

SH-SY5Y were differentiated following protocol derived from (Agholme *et al*, 2010). Cells were cultured on Poly-L-Lysine (Sigma-Aldrich) coated plates, in DMEM 1% L-glutamine (Gibco), 1% sodium pyruvate (Gibco) and 1% penicillin-streptomycin (Gibco) supplemented with by all-trans retinoic acid (Sigma-Aldrich, Merck KGaA) 10 uM (7days), while downgrading FBS concentration from 10% to 0%. At this stage cells were collected for sacsin IP or further differentiated for imaging: medium was then changed with DMEM 1% L-glutamine, 1% sodium pyruvate and 1% penicillin-streptomycin suppelemented with BDNF (Sigma-Aldrich, Merck KGaA) 25ng/mL (for at least 3 days prior to fixation in paraformaldehyde 4%).

2.7 - Immunofluorescence in primary PNs and SH-SY5Y cells

Fixed cells were blocked and permeabilized with 10% goat serum and 0,5% Triton X-100 in PBS 1X solution (1h, RT), and then incubated in 5% goat serum and 0,2% Triton X-100 in PBS 1X solution with primary antibodies (over/night, 4°C). Secondary antibodies or phalloidin were added in 5% goat serum and 0,2% Triton X-100 in PBS 1X solution (2h, RT). Coverslips were mounted with FluorSave (Calbiochem).

2.8 - Cerebellar sections immunostaining (Results Fig. 19e)

Mice at five months of age were sacrificed in the presence of anaesthesia (2,2,2-Tribromoethanol, Sigma-Aldrich, Merck KGaA). Transcardially perfusion was performed and then the brain was isolated. Tissues were fixed in 4% paraformaldehyde (2h, 4°C), then dehydrated in 30% sucrose solution (over/night,

4°C) and finally embedded in OCT solution (Fisher scientific). Cryostat sagittal slices were cut at the thickness of 20µm and conserved at -80°C. Sagittal sections close to the midline cut through cerebellar vermis were used for plectin immunostaining; lobules III and IV/V were imaged. Immunofluorescence was performed as described for fixed primary PNs. Images were taken at FluoVIEW FV3000RS Confocal (Olympus) at 63X magnification and analyzed with FIJI. Antibodies used for immunostaining: plectin (Santa Cruz) and chicken-IgY calbindin (Biotechne).

2.9 - Cell imaging

Consecutive z-stacks images were taken at 0.1 µm intervals at 63X magnification. Either FluoVIEW FV3000RS (Olympus) or UltraView (Perkin Elmer) were used for confocal imaging; DeltaVision Ultra microscope (G.E. Healthcare) was used for widefield microscopy followed by deconvolution. Unless otherwise indicated, all z-stacks were subjected to max-projection with FIJI.

Analyses of soma, dendrite, mitochondria and ER volume were performed using Volocity 3D Image Analysis Software (version 5.5.1, PerkinElmer). For mitochondrial and ER volume evaluation, a region of interest (ROI) was drawn to cover the profile of each PNs (or dendrites only). A threshold for red signal (mitochondria and ER) and green signal (PNs) was set to exclude the background. We considered mitochondria/ER belonging to PNs those with red signal exclusively intersecting the green signal.

Images in **Results Fig. 10a** and **Results Fig. 29** were taken with Upright AxioImager Epifluorescence / Widefield Microscope (Zeiss).

2.10 - Mitochondrial live imaging in primary PNs cultures (Results Fig. 21)

Primary PNs cultures were obtained as described above. At DIV0, prior to plating, cells were mixed with lentivirus expressing mitoDsRed2 (Clontech, Mountain View, California, USA) at 1:200 concentration from $4.67*10^8$ U/mL (Tulli *et al*, 2019). Cells were plated on bottom-glass culture dishes (MatTek Corporation, Ashland, Massachusetts, USA). At DIV10, mitochondrial live imaging was performed in neurites with DeltaVision Ultra microscope (G.E. healthcare), acquiring in DsRed2 channel at 63X five stacks per minute, for 30 minutes, for a total of 31 timeframes. Images were deconvolved and max projection of z-stacks were taken for each timeframe. Kymographs were obtained with KimographClear plugin for FIJI, from time series of max-projections, according to user manual, where forward and backward motion correspond to anterograde and retrograde mitochondrial movement respectively.

2.11 - Pipeline for max-NFH quantification

Images acquired with G.E. healthcare DeltaVision Ultra microscope were deconvolved and 3D-reconstructed with Arivis 4D software; with a semiautomatic pipeline.

Pipeline ***Results fig. 10***

Nuclei signal was denoised; nuclei objects were identified as ROI; too large objects (>400µm³) were filtered out; dilated nuclei were identified as cell objects. Neurofilaments objects (npNFH or total NFH signal) were identified by signal thresholding and at least 80% overlapping with cell objects. Values of signal intensity and volume of all neurofilaments objects inside each cell object were calculated by 3D-reconstruction of z-stacks; the pipeline also returns the value of the largest NF object per each cell (referred as max-NFH volume). In post-analysis, only max-NFH volumes included between 0.1µm³ and 200µm³ were considered for statistical analysis.

Pipeline ***Results Fig. 28***

The pipeline has been slightly modified. Green signal (either V5-EGFP or minisacsin-V5) denoising and thresholding was performed to identify ROI (cell objects); only few identified cell objects were manually excluded as likely were dead cells. Neurofilaments objects (total NFH signal) were identified by signal thresholding and at least 80% overlapping with cell objects. Values of signal intensity and volume of all neurofilaments objects inside each cell object were calculated by 3D-reconstruction of z-stacks; the pipeline also returns the value of the largest NF object per each cell (referred as max-NFH volume). In post-analysis, only max-NFH volumes included between 0.1µm³ and 200µm³ were considered for statistical analysis.

2.12 - LFQ proteomics and Phosphoproteomics analyses

Three *Sacs*$^{+/+}$ biological replicates (two males and one female) and three *Sacs*$^{-/-}$ biological replicates (two females and one male) were used. Mouse cerebellum (at five months of age) were lysed in 8 M Urea, 100 mM Tris-HCl pH 8 and PIC in a Dounce homogenizer, then centrifuged 4000g for 20' at 4°C and quantified by Bradford analysis. Samples were digested and processed in technical replicates by MS/MS in collaboration with Cogentech proteomics facility (IFOM, Milan). Data from MS/MS were analyzed with MaxQuant ver. 1.6.0.16 (Cox & Mann, 2008; Cox *et al*, 2011, 2014) by the proteomics facility Cogentech (IFOM, Milan). LFQ intensities returned by MaxQuant were analyzed with Perseus ver. 1.6.2.3. Imputation was applied on missing numbers. To determine the significance of the differentially abundant proteins was used the cut-off determined by FDR < 0.05 (t-test,

permutation test). Proteins with significant changed abundance were submitted to GProfiler Enrichment analysis (https://biit.cs.ut.ee/gprofiler/gost).

Phospho peptides quantification was performed using the intensity columns contained on Phopho (STY)Sites table in Max quant results. Statistical analyses were done using the Perseus program (Version 1.5.1.6) in the MaxQuant environment with a p-value 0.05. Significative phosphopeptides were manually compared with respective proteins levels from proteomics to determine whether there are real differences between the two genotypes or changes can be attributed to variations in the protein levels.

2.13 - RNAseq analysis

Standard RNA sequencing analysis was performed on total RNA extracted from cerebellum with RNeasy kit (Qiagen). Libraries were prepared using True-Seq® stranded mRNA® for mRNA Sequencing (Illumina, San Diego, CA). Sequencing was performed on a NextSeq 500 machine (Illumina, San Diego, CA) obtaining 30 million single-end reads per sample on average. Only genes with a Counts per million (CPM) value higher than 1 in at least three samples were retained. Gene expression read counts were exported and analysed in R environment (v. 3.6.2) to identify differentially expressed genes (DEGs). The DEG analysis was performed with the package DESeq2 available in Bioconductor comparing different experimental groups. To determine the significance of the differential genes was used the cut-off determined by FDR filter < 0,1 (Adjusted p_value). The significant deregulated genes obtained with this algoritm were submitted to GProfiler Enrichment analysis.

2.14 - Sacsin immunoprecipitation and co-IP

SH-SY5Y cells were collected and freshly lysed in lysis buffer (5 mM EDTA pH 8.0, Triton X-100 0,1% in PBS1X and PIC (Sigma-Aldrich, Merck KGaA)) with a Dounce homogenizer. Total homogenate was centrifuged 8000 g for 10’ at 4°C to discard cell debris. 1 mg of total protein lysate was incubated 2h with magnetic Dynabeads Protein A (ThermoFisher Scientific) in a preclearing step; then 8 µg of Sacsin Abcam antibody was bound to Dynabeads and the Dynabeads-antibody complex was incubated with the precleared lysate over/night at 4°C on a wheel. After washes in lysis buffer, the antigen was eluted from the Dynabeads-antibody complex in Urea 8 M Tris-HCl pH 8 on rotation for 30’. Immunoprecipitated eluates were sent to Mass Spectrometry facility Cogentech (IFOM, Milan) for LC-MS/MS and/or loaded on SDS-PAGE for WB analysis.

2.15 - Interactomics

Proteins identified by LC-MS/MS in the immunoprecipitated eluates were considered as sacsin interactors if detected with at least two different peptides in *SACS*$^{+/+}$ SH-SY5Y samples and zero peptides in *SACS*$^{-/-}$ SH-SY5Y respective control samples. Interactors were analyzed with STRING web tool.

2.16 - Functional profiling and enrichments analyses (G-profiler, STRING, GSEA)

Functional profiling of proteomics data and RNAseq data were performed with web tool Gprofiler (version 2019) (https://biit.cs.ut.ee/gprofiler/gost), with statistical over-representation test and default Gprofiler multiple testing correction for significance threshold, which is refined for functional profiling analysis. For the analysis we used *Mus musculus* as organism, with only annotated genes, and for database source we used GO:BP and GO:MF without GO electronically inferred terms and with a maximum term size of 1000 and a minimum term size of 10 (Raudvere *et al*, 2019).

Protein-protein interaction network analysis of sacsin interactors were performed with STRING app for Cytoscape, using *Homo sapiens* (for sacsin IP experiment) as organism and a confidence cut-off of 0.400. For functional profiling provided by STRING, only GO:BP categories with an FDR < 0.05 and term size < 500 were considered (Doncheva *et al*, 2019; Szklarczyk *et al*, 2019).

GSEA analyses was done with WebGestalt online tool (http://www.webgestalt.org/) (Liao *et al*, 2019), ranking proteins by the $\log_2$ of foldchange of protein abundance level.

2.17 - PSD extraction and proteomics

PSD fraction were obtained from mouse cerebellum (at one month of age). Mouse cerebellum was homogenized in sucrose 0.32M, HEPES pH7.4 4mM with 20 strokes in Teflon-glass homogenizer and passed 20 times into a 25G syringe. Total Homogenates (TH) were centrifuged at 1000g 10 min at 4°C to pellet debris and nuclei. Supernatant (S1) was centrifuged at 10,000g 15min at 4°C to obtain synaptosomes (pellet) and S2:cytosol and light membrane fraction (surnatant S2). The pellet underwent an osmotic shock by resuspending in 4mM HEPES pH7.4 and rotating at 4°C for 30min. PSD fraction was recovered centrifuging at 25,000g for 20min at 4°C and resuspending the pellet in 50mM HEPES pH 7.4, 2mM EDTA, 0,5% Triton X-100 and rotating at 4°C 20min. Samples were centrifuged at 32,000g 20min at 4°C to generate triton-100 insoluble postsynaptic density-enriched fraction (PSD). PSD was resuspended in TrisHCl 100mM pH 8, Urea 8M for proteomics. Three *Sacs*$^{+/+}$

biological replicates and three *Sacs*$^{-/-}$ biological replicates were used for LFQ proteomics analysis described as in **Methods Section 2.12** in collaboration with Cogentech proteomics facility (IFOM, Milan). Differentially abundant proteins in *Sacs*$^{-/-}$ in respect to *Sacs*$^{+/+}$ samples were determined by t-test with permutation test (FDR<0.05) and were submitted to G:Profiler Enrichment analysis web tool. To perform GSEA analyses, all quantified proteins (3303) were submitted to WebGestalt online tool.

2.18 – EM analysis

EM analyses were done in collaboration with the Unit of Neuropathology of San Raffaele Institute as previously described (Maltecca *et al*, 2015). Electron Microscopy (EM) were done in collaboration with the Unit of Neuropathology of San Raffaele Institute. Isolated cerebellum was incubated in glutaraldehyde fixative to perform standard EM experiments. Several cells were evaluated in a single sample for a total 3 *Sacs-/-* versus 3 *Sacs+/+* tissues with a 150000X magnification.

2.19 - Insoluble fractions (Results Fig 17b; Results Fig. 19d)

To obtain Triton-X100 insoluble fractions, tissues were homogenized in high ionic strength buffer (0,05 M MOPS pH 6.8, 1% Triton X-100 and 0,6 M KCl) and then centrifuged at 15000 g for 5' at RT. The triton insoluble pellet was treated with 0,5 µg/ml DNase I in 10 mM $MgCl_2$ buffer for 30' at 37°C. After washing, the pellet was solubilized in urea buffer (8 M urea in 0,1 M MOPS).

2.20 – Total homogenates (Results Fig. 19c)

Whole cellular pellets were lysed in Laemmli sample buffer 2X and sonicated to break the DNA as previously described in the ultrasonication method. Total homogenates were loaded in acrylamide-agarose mixed-gels for WB analysis, which have much larger pores than pure acrylamide gels, allowing the passage and an acceptable resolution of large complexes (Weiss *et al*, 2008).

2.21 - Immunoprecipitation of endogenous NFL in SH-SY5Y cells (Results Fig. 18d).

Protocol was derived from (Rao *et al*, 2002). Briefly, SH-SY5Y cells were collected and lysed in TritonX100 1%, TrisHCl pH 6.8 50 m, NaCl 200mM, glycerol 20%, EDTA 1mM with Douncer homogenizer. Triton insoluble pellet was resuspended in Tris Buffered Saline and SDS 10%. To extract NF cytoskeleton, insoluble fraction was diluted 1:4 in NF extraction buffer (TrisHCl pH 7.4 60mM, NaCl 190mM, EDTA 6mM, Triton-X100 1.25%) and sonicated. 0.5 mg of total protein lysate, quantified with BCA protein assay kit (thermofisher), was incubated 2h with magnetic Dynabeads Protein G (ThermoFisher Scientific) in a preclearing step; then 2 µg of antibody was

bound to Dynabeads and the Dynabeads-antibody complex was incubated with the precleared lysate over/night at 4°C on a wheel. After washes in lysis buffer, the antigen was eluted from the Dynabeads-antibody complex in Laemmli buffer after rotation for 10' and incubation at 100°C for 5' and analyzed by WB. Antibodies used for IP: anti NFL-8A1 mouse IgG1 (Santa Cruz); mouse IgG1 isotype control (R&D Systems).

2.22 - Statistical analyses

Continuous variables were summarized by their mean values and Standard Error of the Mean (SEM). Differences in phenotypes between *Sacs*$^{-/-}$ cells or mice compared with wild-type controls were assessed by imaging as described above or by densitometric analysis of WB bands, from at least three independent experiments using ImageJ, followed by unpaired two-tailed Student's *t*-test analysis with Welch's correction. For quantification of phenotype through different *SACS*$^{+/+}$ and *SACS*$^{-/-}$ clones, ONE-WAY ANOVA was used with Tukey's correction for multiple comparison. Analyses were done with GraphPad Prism software, https://www.graphpad.com/scientific-software/prism/).

3 – Minisacsin molecular analysis (Results Section 3)

3.1 - Plasmid cloning and cell transfection

Minisacsin was cloned inside pcDNA3.1™ (+) (Invitrogene V790-20), between NheI and XhoI sites. Human cDNAs corresponding to sacsin human protein aa 1-508 and aa 4306-4579 (Uniprot Q9NZJ4) were cloned and linked together with a BamHI site in frame, which allowed also for the insertion of a GS-linker. V5 tag was cloned after codon 4579 before the STOP codon and the XhoI site. A 10 bp Kozak sequence was cloned between NheI and the first codon. Minisacsin-V5 was inserted into pAAV vectors by enzymatic digestions, between CAG universal promoter and either human growth hormone terminator sequence (hGh) or a shorter PolyA terminator signal (pAmin) designed by Dr. Vania Broccoli at OSR group. CAG promoter consists of CMV enhancer, Chicken β actin promoter and an intron derived from human β globin gene. The final constructs were all subjected to Sanger sequencing with primers spanning all the construct length. For WB analysis, SH-SY5Y cells or HeLa cells were transfected with using Lipofectamine3000 (Invitrogene L3000015) and collected after 48h; for immunfluorescence analysis, cells were transfected with either minisacsin-V5 pr GFP-V5 as control and fixed in 4% paraformaldehyde after 48h.

3.2 - Primers used for cloning, sequencing and mutagenesis

All primers are from 5' to 3'. Primers used for N-terminal portion cloning: FW AAGCTGGCTAGCGCCGCCGCGATCGCCATGGAGACCAAGGAGAACAGGTGG; REV cgcGGATCCCAGAGTAGCATAAGCTTTGGGG. Primers used for C-terminal portion cloning: FW cgcggatccATCTTAAAAGAAGTGACATCTGTGGTGG; REV TCTAGActcgagtcaCGTAGAATCGAGACCGAGGAGAGGGTTAGGGATAGGCTTACCCACTTTTTGTTGCATAAAATTTTCAAG.

Primers used for sequencing: T7 FW TAATACGACTCACTATAGG; BGH REV TAGAAGGCACAGTCGAGG; Internal REV TGGTGCAAACTGGTCTGAAAG; Internal FW CCCTCTTCGCCTACAACCTT.

V5 Tag sequence: GGTAAGCCTATCCCTAACCCTCTCCTCGGTCTCGATTCTACG.

M148A mutagenesis primers: FW cctgatatggcgccgcatcttttgaccaaagagtctctgttc; REV gaacagagactctttggtcaaaagatgcggcgccatatcagg. M214A mutagenesis primers: FW tgtttgatgaggatctagcgccccgatttggtcaccacta; REV tagtggtgaccaaatcggggcgctagatcctcatcaaaca.

3.3 - Minisacsin mutagenesis

ATG sites encoding M148 and M214 (in minisacsin aminoacidic position residues) were mutagenized using QuikChange Lightning Site-Directed Mutagenesis Kit (Agilent), according to manufacturer instructions.

3.4 - V5 immunoprecipitation

SACS$^{-/-}$ HeLa cells generated by CRISPR/Cas9 genome editing were transfected with pcDNA3.1 carrying minisacsin-V5; after 48 hours, transfected cells and untrasfected cells, used as negative controls, were collected and freshly lysed in 5 mM EDTA pH 8.0, Triton X-100 0,1% in PBS1X and PIC (Sigma-Aldrich, Merck KGaA) with a Dounce homogenizer. Total homogenate was centrifuged 8000 g for 10' at 4°C to discard cell debris. 1 mg of total protein lysate was incubated 2h with magnetic Dynabeads Protein G (ThermoFisher Scientific) in a preclearing step; then 8 µg of Mouse V5-Tag antibody (Invitrogen) was bound to Dynabeads and the Dynabeads-antibody complex was incubated with the precleared lysate over/night at 4°C on a wheel. After washes in lysis buffer, the antigen was eluted from the Dynabeads-antibody complex in Laemmli buffer incubating 100°C for 5'. Two aliquots from eluates samples were loaded on SDS-PAGE; half portion underwent WB, while the other was subjected to Coomassie staining O/N at 4°C and sent to proteomics facility Cogentech (IFOM, Milan). Gel bands corresponding to upper and lower minisacsin bands were excised and underwent LFQ-MS/MS as described above.

3.5 - Phosphatase lambda treatment

HeLa cells transfected with minisacsin for 48 h were collected and lysed in 1% TritonX-100. Triton-soluble surnatant was digested with PP-Lambda (NEB) according to manufacturer, incubating overnight at 30°C. Control sample was incubated as well overnight at 30°C with same saline buffer without addition of PP-Lambda.

3.6 - Minisacsin AAV production and purification (in collaboration with Dr. Vania Broccoli)

Recombinant AAV vectors were produced by transfection of HEK293T cells with pAAV plasmid encoding minisacsin under CAG promoter and with pAmin PolyA terminator. Plasmids, transfected using by polyethylenimine (PEI) (Polyscience) were three: the transgene-containing plasmid, the plasmid coding for the AAV packaging proteins, and the pHelper. Five days after cells were lysed in hypertonic buffer and the supernatant was concentrated (8% PEG8000). A discontinuous iodixanol gradient was prepared to isolate the viral particles. Upon ultracentrifugation, the purified library particles were aspirated from the layer containing 40% iodixanol and dialyzed against phosphate buffer solution (PBS). The virus titer was determined using AAVpro© Titration Kit Ver2 (TaKaRa).

3.7 - Primary PNs viral infection

Primary PNs were derived as already described above from P0 *Sacs*$^{+/+}$ and *Sacs*$^{-/-}$ mice pups. AAV PHP.eB vector carrying V5-EGFP under CAG promoter and hGh polyA

was derived as already described (Luoni *et al*, 2020). Lentiviral and AAV PHP.eB vectors carrying GFP under L7 promoter were produced by VectorBuilder.

All viruses were delivered to PNs at DIV0 prior to plating; a total amount of 10^{10} vg was delivered for each PNs preparation, in 500 µL final volume medium.

3.8 - Sacsin immunostaining in primary PNs

Immunofluorescence of sacsin and its interactors was performed in primary PNs as described above, with the addition of following steps for sacsin detection: after cell fixation, antigen retrieval was performed by incubating cells in Tris 10mM, EDTA 1mM, Tween-20 0.05% at pH 9.0 for 30' at 70-90°C; then cells were washed with DPBS1X and pre-blocked for 20' with 50mM glycine in DPBS1X; Bovine Serum Albumin 0.2% was added in blocking buffer. Antibodies used for IF: sacsin Abcam 181197 (diluted 1:25); Plectin and Myosin Va (Santa Cruz) and SMI32 (Biolegend); PNs were marked with chicken-IgY anti-calbindin (Abcam).

3.9 – Statistical Assessment of NF bundling recovery upon minisacsin delivery

In transfected SH-SY5Y cells, NF rescue was assessed by immunofluorescence, as described above, and applying pipeline2 for max-NFH volume parameter (see **Methods Section 2.11**). For quantification through different *SACS*$^{+/+}$ and *SACS*$^{-/-}$ clones after EGFP or minisacsin transfection, TWO-WAY ANOVA was used, with Tukey's correction for multiple comparison.

In infected primary PNs, NF rescue was assessed by immunofluorescence with ImageJ after max projection of z-stacks, applying plot profile built-in function along lines manually drawn transversal to each proximal dendrites of each PNs from three different cerebellar dissections (biologically independent experiments), followed by unpaired two-tailed Student's *t*-test analysis with Welch's correction. Analyses were done with GraphPad Prism software, https://www.graphpad.com/scientific-software/prism/).

REFERENCES

Agholme L, Lindström T, Kgedal K, Marcusson J & Hallbeck M (2010) An in vitro model for neuroscience: Differentiation of SH-SY5Y cells into cells with morphological and biochemical characteristics of mature neurons. *J Alzheimer's Dis 20(4), 1069-1082.*

Aida I, Ozawa T, Fujinaka H, Goto K, Ohta K & Nakajima T (2021) Autosomal Recessive Spastic Ataxia of Charlevoix-Saguenay without Spasticity. *Intern Med*: 1–5 60(24), 3963-3967.

Anantharaman V, Makarova KS, Burroughs AM, Koonin E V. & Aravind L (2013) Comprehensive analysis of the HEPN superfamily: Identification of novel roles in intra-genomic conflicts, defense, pathogenesis and RNA processing. *Biol Direct* 8(1), 1-28

Anderson JF, Siller E & Barral JM (2010a) The Sacsin Repeating Region (SRR): A Novel Hsp90-Related Supra-Domain Associated with Neurodegeneration. *J Mol Biol* 400: 665–674

Bachetti T, Di Zanni E, Balbi P, Bocca P, Prigione I, Deiana GA, Rezzani A, Ceccherini I & Sechi G Pietro (2010) In vitro treatments with ceftriaxone promote elimination of mutant glial fibrillary acidic protein and transcription down-regulation. *Exp Cell Res 16(13), 2152-2165*

Baets J, Deconinck T, Smets K, Goossens D, Van Den Bergh P, Dahan K, Schmedding E, Santens P, Rasic VM, Van Damme P, *et al* (2010) Mutations in SACS cause atypical and late-onset forms of ARSACS. *Neurology 75(13), 1181-1188.*

Bailey RM, Armao D, Nagabhushan Kalburgi S & Gray SJ (2018) Development of Intrathecal AAV9 Gene Therapy for Giant Axonal Neuropathy. *Mol Ther - Methods Clin Dev* 9: 160–171

Battaglini M, Carmignani A, Martinelli C, Colica J, Marino A, Doccini S, Mollo V, Santoro F, Bartolucci M, Petretto A, *et al* (2022) In vitro study of polydopamine nanoparticles as protective antioxidant agents in fibroblasts derived from ARSACS patients. *Biomater Sci* 10: 3770–3792

Bernal A & Arranz L (2018) Nestin-expressing progenitor cells: function, identity and therapeutic implications. *Cell Mol Life Sci* 75: 2177

Bis-Brewer DM, Fazal S & Züchner S (2020) Genetic modifiers and non-Mendelian aspects of CMT. *Brain Res* 1726, 146459.

Blokhuis AM, Groen EJN, Koppers M, Van Den Berg LH & Pasterkamp RJ (2013) Protein aggregation in amyotrophic lateral sclerosis. *Acta Neuropathol* 125: 777–

794

Bomont P (2021) The dazzling rise of neurofilaments: Physiological functions and roles as biomarkers. *Curr Opin Cell Biol* 68: 181–191

Borel F, Kay MA & Mueller C (2014) Recombinant AAV as a Platform for Translating the Therapeutic Potential of RNA Interference. *Mol Ther* 22: 692–701

Borruat FX, Holder GE & Bremner F (2017) Inner retinal dysfunction in the autosomal recessive spastic ataxia of Charlevoix-Saguenay. *Front Neurol, 8, 523.*

Bouchard JP, Barbeau A, Bouchard R & Bouchard RW (1979) Electromyography and Nerve Conduction Studies in Friedreich's Ataxia and Autosomal Recessive Spastic Ataxia of Charlevoix-Saguenay (ARSACS). *Can J Neurol Sci / J Can des Sci Neurol 6(2), 185-189.*

Bouchard JP, Richter A, Mathieu J, Brunet D, Hudson TJ, Morgan K & Melançon SB (1998) Autosomal recessive spastic ataxia of Charlevoix-Saguenay. *Neuromuscul Disord* 8: 474–479

Bouhlal Y, Amouri R, El Euch-Fayeche G & Hentati F (2011) Autosomal recessive spastic ataxia of Charlevoix-Saguenay: An overview. *Park Relat Disord* 17: 418–422

Bradshaw TY, Romano LEL, Duncan EJ, Nethisinghe S, Abeti R, Michael GJ, Giunti P, Vermeer S & Chapple JP (2016a) A reduction in Drp1-mediated fission compromises mitochondrial health in autosomal recessive spastic ataxia of Charlevoix Saguenay. *Hum Mol Genet* 25: 3232–3244

Brina D, Miluzio A, Ricciardi S, Clarke K, Davidsen PK, Viero G, Tebaldi T, Offenhäuser N, Rozman J, Rathkolb B, *et al* (2015) eIF6 coordinates insulin sensitivity and lipid metabolism by coupling translation to transcription. *Nat Commun* 6(1), 8261.

Brownlees J, Ackerley S, Grierson AJ, Jacobsen NJO, Shea K, Anderton BH, Leigh PN, Shaw CE & Miller CCJ (2002) Charcot-Marie-Tooth disease neurofilament mutations disrupt neurofilament assembly and axonal transport. *Hum Mol Genet* 11: 2837–2844

Chan KY, Jang MJ, Yoo BB, Greenbaum A, Ravi N, Wu W, Sánchez-guardado L, Lois C, Mazmanian SK, Deverman BE, *et al* (2017) t e c h n ic a l r e p o r t s Engineered AAVs for efficient noninvasive gene delivery to the central and peripheral nervous systems. 20(8), 1172-1179.

Cohlberg JA, Hajarian H, Tran T, Alipourjeddi P & Noveen A (1995) Neurofilament protein heterotetramers as assembly intermediates. *J Biol Chem* 270: 9334–

9339 doi:10.1074/jbc.270.16.9334 [PREPRINT]

Cox J, Hein MY, Luber CA, Paron I, Nagaraj N & Mann M (2014) Accurate proteome-wide label-free quantification by delayed normalization and maximal peptide ratio extraction, termed MaxLFQ. *Mol Cell Proteomics* 13: 2513–2526

Cox J & Mann M (2008) MaxQuant enables high peptide identification rates, individualized p.p.b.-range mass accuracies and proteome-wide protein quantification. *Nat Biotechnol* 26: 1367–1372

Cox J, Neuhauser N, Michalski A, Scheltema RA, Olsen J V. & Mann M (2011) Andromeda: A peptide search engine integrated into the MaxQuant environment. *J Proteome Res* 10: 1794–1805

Criscuolo C, Procaccini C, Meschini MC, Cianflone A, Carbone R, Doccini S, Devos D, Nesti C, Vuillaume I, Pellegrino M, *et al* (2015) Powerhouse failure and oxidative damage in autosomal recessive spastic ataxia of Charlevoix-Saguenay. *J Neurol. 262(12), 2755-2763.*

Dabbaghizadeh A, Paré A, Cheng-Boivin Z, Dagher R, Minotti S, Dicaire MJ, Brais B, Young JC, Durham HD & Gentil BJ (2022) The J Domain of Sacsin Disrupts Intermediate Filament Assembly. *Int J Mol Sci*, 23(24), 15742.

Dale JM & Garcia ML (2012) Neurofilament Phosphorylation during Development and Disease: Which Came First, the Phosphorylation or the Accumulation? *J Amino Acids* 2012: 1–10

Dantuma NP, Heinen C & Hoogstraten D (2009) The ubiquitin receptor Rad23: At the crossroads of nucleotide excision repair and proteasomal degradation. *DNA Repair (Amst)* 8: 449–460

Demilly A, Reeber SL, Gebre SA & Sillitoe R V (2011) Neurofilament heavy chain expression reveals a unique parasagittal stripe topography in the mouse cerebellum. *Cerebellum, 10, 409-421.*

Desserre J, Devos D, Sautière BG, Debruyne P, Santorelli FM, Vuillaume I & Defoort-Dhellemmes S (2011) Thickening of peripapillar retinal fibers for the diagnosis of autosomal recessive spastic ataxia of Charlevoix-Saguenay. *Cerebellum, 10, 758-762.*

Deverman BE, Ravina BM, Bankiewicz KS, Paul SM & Sah DWY (2018) Gene therapy for neurological disorders : progress and prospects, 17(9), 641-659.

Didonna A & Opal P (2019) The role of neurofilament aggregation in neurodegeneration: Lessons from rare inherited neurological disorders. *Mol Neurodegener* 14(1): 1–10

Doncheva NT, Morris JH, Gorodkin J & Jensen LJ (2019) Cytoscape StringApp: Network Analysis and Visualization of Proteomics Data. *J Proteome Res* 18: 623–632

Duncan EJ, Larivière R, Bradshaw TY, Longo F, Sgarioto N, Hayes MJ, Romano LEL, Nethisinghe S, Giunti P, Bruntraeger MB, *et al* (2017a) Altered organization of the intermediate filament cytoskeleton and relocalization of proteostasis modulators in cells lacking the ataxia protein sacsin. *Hum Mol Genet* 26: 3130–3143

Duttler S, Pechmann S & Frydman J (2013) Principles of cotranslational ubiquitination and quality control at the ribosome. *Mol Cell* 50: 379–393

Earley J, Piletska E, Ronzitti G & Piletsky S (2022) Evading and overcoming AAV neutralization in gene therapy. *Trends Biotechnol* xx: 1–10

Engert JC, Bérubé P, Mercier J, Doré C, Lepage P, Ge B, Bouchard JP, Mathieu J, Melançon SB, Schalling M, *et al* (2000a) ARSACS, a spastic ataxia common in northeastern Quebec, is caused by mutations in a new gene encoding an 11.5-kb ORF. *Nat Genet* 24: 120–125

Erlandsen H, Canaves JM, Elsliger MA, Von Delft F, Brinen LS, Dai X, Deacon AM, Floyd R, Godzik A, Grittini C, *et al* (2004) Crystal Structure of an HEPN Domain Protein (TM0613) from Thermotoga maritima at 1.75 Å Resolution. *Proteins Struct Funct Genet, 54(4), 806-809.*

French LS, Mellough CB, Chen FK & Carvalho LS (2020) A Review of Gene , Drug and Cell-Based Therapies for Usher Syndrome. 14, 183

Gandin V, Brina D, Marchisio PC & Biffo S (2010) JNK inhibition arrests cotranslational degradation. *Biochim Biophys Acta* 1803: 826–831

Garcia-Martin E, Pablo LE, Gazulla J, Vela A, Larrosa JM anue., Polo V, Marques ML & Alfaro J (2013) Retinal segmentation as noninvasive technique to demonstrate hyperplasia in ataxia of Charlevoix-Saguenay. *Investig Ophthalmol {\&} Vis Sci, 54(10), 7137-7142.*

Gentil BJ, Lai GT, Menade M, Larivière R, Minotti S, Gehring K, Chapple JP, Brais B & Durham HD (2019a) Sacsin, mutated in the ataxia ARSACS, regulates intermediate filament assembly and dynamics. *FASEB J* 33: 2982–2994

Gentil BJ, Tibshirani M & Durham HD (2015) Neurofilament dynamics and involvement in neurological disorders. *Cell Tissue Res* 360: 609–620

Girard M, Larivière R, Parfitt DA, Deane EC, Gaudet R, Nossova N, Blondeau F, Prenosil G, Vermeulen EGM, Duchen MR, *et al* (2012a) Mitochondrial dysfunction

and Purkinje cell loss in autosomal recessive spastic ataxia of Charlevoix-Saguenay (ARSACS). *Proc Natl Acad Sci U S A* 109: 1661–1666

Girard M, Larivière R, Parfitt DA, Deane EC, Gaudet R, Nossova N, Blondeau F, Prenosil G, Vermeulen EGM, Duchen MR, *et al* (2012b) Mitochondrial dysfunction and Purkinje cell loss in autosomal recessive spastic ataxia of Charlevoix-Saguenay (ARSACS). *Proc Natl Acad Sci U S A* 109: 1661–1666

Goldman JE, Yen SH, Chiu FC & Peress NS (1983) Lewy bodies of Parkinson's disease contain neurofilament antigens. *Science (80-)* 221: 1082–1084

Grant P & Pant HC (2000) Neurofilament protein synthesis and phosphorylation. *J Neurocytol* 29: 843–872

Greer PL, Hanayama R, Bloodgood BL, Mardinly AR, Lipton DM, Flavell SW, Kim TK, Griffith EC, Waldon Z, Maehr R, *et al* (2010) The Angelman Syndrome-associated ubiquitin ligase Ube3A regulates synapse development by ubiquitinating Arc. *Cell* 140: 704

Grynberg M, Erlandsen H & Godzik A (2003) HEPN: A common domain in bacterial drug resistance and human neurodegenerative proteins. *Trends Biochem Sci*, 28(5), 224-226.

Hammer JA & Wagner W (2013) Functions of class v myosins in neurons. *J Biol Chem* 288: 28428–28434

Hartmann-Petersen R & Gordon C (2004) Integral UBL domain proteins: A family of proteasome interacting proteins. *Semin Cell Dev Biol* 15: 247–259

Hashimoto R, Nakamura Y, Komai S, Kashiwagi Y, Tamura K, Goto T, Aimoto S, Kaibuchi K, Shiosaka S & Takeda M (2000) Site-specific phosphorylation of neurofilament-L is mediated by calcium/calmodulin-dependent protein kinase II in the apical dendrites during long-term potentiation. *J Neurochem* 75: 373–382

Haugh MC, Probst A, Ulrich J, Kahn J & Anderton BH (1986) Alzheimer neurofibrillary tangles contain phosphorylated and hidden neurofilament epitopes. *J Neurol Neurosurg Psychiatry* 49: 1213–1220

Hirai H (2008) Progress in transduction of cerebellar Purkinje cells in vivo using viral vectors. *Cerebellum* 7: 273–278

Ho Y, Weng J, Lin C, Shen M, Li H, Liao W, Tsai N, Hung C, Lai T & Lee I (2018) Ceftriaxone Treatment for Neuronal Deficits : A Histological and MEMRI Study in a Rat Model of Dementia with Lewy Bodies. 2018

Holmgren A, Bouhy D & Timmerman V (2012) Neurofilament phosphorylation and their proline-directed kinases in health and disease. *J Peripher Nerv Syst*, 17(4),

365-376.

Holmgren A, Bouhy D, De Winter V, Asselbergh B, Timmermans JP, Irobi J & Timmerman V (2013) Charcot-Marie-Tooth causing HSPB1 mutations increase Cdk5-mediated phosphorylation of neurofilaments. *Acta Neuropathol* 126: 93–108

Huang Q, Chan KY, Tobey IG, Chan YA, Poterba T, Boutros L, Balazs AB, Id RD, Id JMB, Seed C, *et al* (2019) Delivering genes across the blood-brain barrier : LY6A , a novel cellular receptor for AAV-PHP. B capsids. PLoS One, 14(11), e0225206.

Hudry E & Vandenberghe LH (2019) Review Therapeutic AAV Gene Transfer to the Nervous System : A Clinical Reality. *Neuron* 101: 839–862

Inada T (2017) The Ribosome as a Platform for mRNA and Nascent Polypeptide Quality Control. *Trends Biochem Sci* 42: 5–15

Israeli E, Dryanovski DI, Schumacker PT, Chandel NS, Singer JD, Julien JP, Goldman RD & Opal P (2016) Intermediate filament aggregates cause mitochondrial dysmotility and increase energy demands in giant axonal neuropathy. *Hum Mol Genet* 25: 2143–2157

Jung C, Yabe J, Wang F-S & Shea TB (1998) Neurofilament Subunits Can Undergo Axonal Transport Without Incorporation Into Triton-Insoluble Structures. *Cytoskeleton* 40: 44–58

Kaemmerer WF, Reddy RG, Warlick CA, Hartung SD, Mcivor RS & Low WC (2000) In Vivo Transduction of Cerebellar Purkinje Cells Using Adeno-Associated Virus Vectors. *Mol Ther* 2: 446–457

Kamionka M & Feigon J (2004) Structure of the XPC binding domain of hHR23A reveals hydrophobic patches for protein interaction. Protein science, 13(9), 2370-2377.

Karaca E, Posey JE, Coban Akdemir Z, Pehlivan D, Harel T, Jhangiani SN, Bayram Y, Song X, Bahrambeigi V, Yuregir OO, *et al* (2018) Phenotypic Expansion Illuminates Multilocus PathogenicVariation. *Genet Med* 20(12), 1528-1537.

Kocaturk NM & Gozuacik D (2018) Crosstalk Between Mammalian Autophagy and the Ubiquitin-Proteasome System. *Front cell Dev Biol,* 128

Kornreich M, Avinery R, Malka-Gibor E, Laser-Azogui A & Beck R (2015) Order and disorder in intermediate filament proteins. *FEBS Lett* 589: 2464–2476

Kozareva V, Martin C, Osorno T, Rudolph S, Guo C, Vanderburg C, Nadaf N, Regev A, Regehr WG & Macosko E (2021) A transcriptomic atlas of mouse cerebellar cortex comprehensively defines cell types. *Nature* 598: 214–219

Kozlov G, Denisov AY, Girard M, Dicaire MJ, Hamlin J, McPherson PS, Brais B & Gehring K (2011) Structural basis of defects in the sacsin HEPN domain responsible for Autosomal Recessive Spastic Ataxia of Charlevoix-Saguenay (ARSACS). *J Biol Chem* 286: 20407–20412

Larivière R, Gaudet R, Gentil BJ, Girard M, Conte TC, Minotti S, Leclerc-Desaulniers K, Gehring K, Mckinney RA, Shoubridge EA, *et al* (2015b) Sacs knockout mice present pathophysiological defects underlying autosomal recessive spastic ataxia of charlevoix-saguenay. *Hum Mol Genet* 24: 727–739

Larivière R, Sgarioto N, Márquez BT, Gaudet R, Choquet K, McKinney RA, Watt AJ & Brais B (2019a) Sacs R272C missense homozygous mice develop an ataxia phenotype. *Mol Brain* 12: 1–15

Lee CS, Bishop ES, Zhang R, Yu X, Farina EM, Yan S, Zhao C, Wu Y, Ho S, Athiviraham A, *et al* (2017) ScienceDirect Adenovirus-mediated gene delivery : Potential applications for gene and cell-based therapies in the new era of personalized medicine. Genes & diseases, 4(2), 43-63.

Li C, Narkbunnam N, Samulski RJ, Asokan A, Hu G, Jacobson LJ & Manco-johnson MJ (2012) Neutralizing antibodies against adeno-associated virus examined prospectively in pediatric patients with hemophilia. Gene therapy, 19(3), 288-294.

Li C & Samulski RJ (2020) Engineering adeno-associated virus vectors for gene therapy. *Nat Rev Genet*, 21(4), 255-272.

Li J, Zhu L, Su H, Liu D & Chen T (2020) Regulation of miR-128 in the nucleus accumbens affects methamphetamine-induced behavioral sensitization by modulating proteins involved in neuroplasticity. Addiction Biology, 26(1), e12881.

Li X, Ménade M, Kozlov G, Hu Z, Dai Z, McPherson PS, Brais B & Gehring K (2015) High-throughput screening for ligands of the HEPN domain of sacsin. *PLoS One, 10(9), e0137298.*

Liao Y, Wang J, Jaehnig EJ, Shi Z & Zhang B (2019) WebGestalt 2019: gene set analysis toolkit with revamped UIs and APIs. *Nucleic Acids Res* 47: W199–W205

Liguore WA, Domire JS, Button D, Wang Y, Dufour BD, Srinivasan S & McBride JL (2019) AAV-PHP.B Administration Results in a Differential Pattern of CNS Biodistribution in Non-human Primates Compared with Mice. *Mol Ther* 27: 2018–2037

van Lint M, Hoornaert K & ten Tusscher MPM (2016) Retinal nerve fiber layer thickening in ARSACS carriers. *J Neurol Sci, 370, 119-122.*

Liu Q, Xie F, Siedlak SL, Nunomura A, Honda K, Moreira PI, Zhua X, Smith MA & Perry G (2004) Neurofilament proteins in neurodegenerative diseases. *Cell Mol Life Sci* 61: 3057–3075

Liutkute M, Samatova E & Rodnina M V. (2020) Cotranslational Folding of Proteins on the Ribosome. *Biomolecules,* 10(1), 97

Longo F, Benedetti S, Zambon AA, Grazia Natali Sora M, Di Resta C, De Ritis D, Quattrini A, Maltecca F, Ferrari M, Carlo Previtali S, *et al* (2020) Impaired turnover of hyperfused mitochondria in severe axonal neuropathy due to a novel DRP1 mutation. *P share last Coauthorsh Hum Mol Genet* 29: 177–188

Luoni M, Giannelli S, Indrigo MT, Niro A, Massimino L, Iannielli A, Passeri L, Russo F, Morabito G, Calamita P, *et al* (2020) Whole brain delivery of an instability-prone Mecp2 transgene improves behavioral and molecular pathological defects in mouse models of Rett syndrome. *Elife* 9: 1–30

Maltecca F, Baseggio E, Consolato F, Mazza D, Podini P, Young SM, Drago I, Bahr BA, Puliti A, Codazzi F, *et al* (2015b) Purkinje neuron Ca2+ influx reduction rescues ataxia in SCA28 model. *J Clin Invest* 125: 263–274

Masciullo M, Modoni A, Tessa A, Santorelli FM, Rizzo V, D'Amico G, Laschena F, Tartaglione T & Silvestri G (2012) Novel SACS mutations in two unrelated Italian patients with spastic ataxia: clinico-diagnostic characterization and results of serial brain MRI studies. *Eur J Neurol* 19: e77–e78

Matsuzaki Y, Konno A, Mochizuki R, Shinohara Y, Nitta K, Okada Y & Hirai H (2018) Intravenous administration of the adeno-associated virus-PHP.B capsid fails to upregulate transduction efficiency in the marmoset brain. *Neurosci Lett* 665: 182–188

Mauro VP & Chappell SA (2014) A critical analysis of codon optimization in human therapeutics. *Trends Mol Med* 20: 604–613

Ménade M, Kozlov G, Trempe JF, Pande H, Shenker S, Wickremasinghe S, Li X, Hojjat H, Dicaire MJ, Brais B, *et al* (2018) Structures of ubiquitin-like (Ubl) and Hsp90-like domains of sacsin provide insight into pathological mutations. *J Biol Chem* 293: 12832–12842

Mendell JR, Al-zaidy SA, Rodino-klapac LR, Goodspeed K, Gray SJ, Kay CN, Boye SL, Boye SE, George LA & Salabarria S (2021) Current Clinical Applications of In Vivo Gene Therapy with AAVs. *Mol Ther* 29: 464–488

Michel AM, Fox G, M. Kiran A, De Bo C, O'Connor PBF, Heaphy SM, Mullan JPA, Donohue CA, Higgins DG & Baranov P V. (2014) GWIPS-viz: development of a ribo-seq genome browser. *Nucleic Acids Res*, 42(D1), D859-D864.

Miressi F, Magdelaine C, Cintas P, Bourthoumieux S, Nizou A, Derouault P, Favreau F, Sturtz F, Faye PA & Lia AS (2020) One Multilocus Genomic Variation Is Responsible for a Severe Charcot-Marie-Tooth Axonal Form. *Brain Sci* 10(12), 986.

Miyata M, Finch EA, Khiroug L, Hashimoto K, Hayasaka S, Oda SI, Inouye M, Takagishi Y, Augustine GJ & Kano M (2000) Local calcium release in dendritic spines required for long-term synaptic depression. *Neuron, 28(1), 233-244*

Morabito G, Giannelli SG, Ordazzo G, Bido S, Castoldi V, Indrigo M, Cabassi T, Cattaneo S, Luoni M, Cancellieri C, *et al* (2017) AAV-PHP . B-Mediated Global-Scale Expression in the Mouse Nervous System Enables GBA1 Gene Therapy for Wide Protection from Synucleinopathy. *Mol Ther* 25: 2727–2742

Morfini G, Pigino G, Szebenyi G, You Y, Pollema S & Brady ST (2006) JNK mediates pathogenic effects of polyglutamine-expanded androgen receptor on fast axonal transport. *Nat Neurosci* 9: 907–916

Morimoto RI & Cuervo AM (2014) Proteostasis and the aging proteome in health and disease. *J Gerontol A Biol Sci Med Sci* 69 Suppl 1: S33–S38

Müller JP, Scholl S, Kunick C & Klempnauer KH (2021) Expression of protein kinase HIPK2 is subject to a quality control mechanism that acts during translation and requires its kinase activity to prevent degradation of nascent HIPK2. *Biochim Biophys acta Mol cell Res*, 1868(1), 118894.

Naef V, Marchese M, Ogi A, Fichi G, Galatolo D, Licitra R, Doccini S, Verri T, Argenton F, Morani F, *et al* (2021) Efficient neuroprotective rescue of sacsin-related disease phenotypes in zebrafish. *Int J Mol Sci*, 22(16), 8401.

Nethisinghe S, Abeti R, Kesavan M, Wigley WC & Giunti P (2021) Hsp90 inhibition: A promising therapeutic approach for arsacs. *Int J Mol Sci*, 22(21), 11722.

Nitta K, Matsuzaki Y, Konno A & Hirai H (2017) Minimal Purkinje Cell-Specific PCP2 / L7 Promoter Virally Available for Rodents and Non-human Primates. *Mol Ther Methods Clin Dev* 6: 159–170

Pablo LE, Garcia-Martin E, Gazulla J, Larrosa JM, Ferreras A, Santorelli FM, Benavente I, Vela A & Marin MA (2011) Retinal nerve fiber hypertrophy in ataxia of Charlevoix-Saguenay patients. *Mol Vis, 17, 1871.*

Pandya NJ, Koopmans F, Slotman JA, Paliukhovich I, Houtsmuller AB, Smit AB & Li KW (2017) Correlation profiling of brain sub-cellular proteomes reveals co-assembly of synaptic proteins and subcellular distribution. *Sci Rep,* 7(1), 1-11.

Parfitt DA, Michael GJ, Vermeulen EGM, Prodromou N V., Webb TR, Gallo JM,

Cheetham ME, Nicoll WS, Blatch GL & Chapple JP (2009a) The ataxia protein sacsin is a functional co-chaperone that protects against polyglutamine-expanded ataxin-1. *Hum Mol Genet* 18: 1556–1565

Parkinson MH, Bartmann AP, Clayton LMS, Nethisinghe S, Pfundt R, Paul Chapple J, Reilly MM, Manji H, Wood NJ, Bremner F, *et al* (2018) Optical coherence tomography in autosomal recessive spastic ataxia of charlevoix-Saguenay. *Brain, 141(4), 989-999.*

Paulin D, Lilienbaum A, Kardjian S, Agbulut O & Li Z (2022) Vimentin: Regulation and pathogenesis. *Biochimie* 197: 96–112

Pechmann S, Willmund F & Frydman J (2013) The ribosome as a hub for protein quality control. *Mol Cell* 49: 411–421

Pedersen LC, Benning MM & Holden HM (1995) Structural Investigation of the Antibiotic and ATP-Binding Sites in Kanamycin Nucleotidyltransferase. *Biochemistry, 34(41), 13305-13311.*

Peng J, Sheng AL, Xiao Q, Shen L, Ju XC, Zhang M, He ST, Wu C & Luo ZG (2019) Single-cell transcriptomes reveal molecular specializations of neuronal cell types in the developing cerebellum. *J Mol Cell Biol* 11: 636–648

Pilliod J, Moutton S, Lavie J, Maurat E, Hubert C, Bellance N, Anheim M, Forlani S, Mochel F, N'Guyen K, *et al* (2015) New practical definitions for the diagnosis of autosomal recessive spastic ataxia of Charlevoix-Saguenay. *Ann Neurol* 78: 871–886

Posey JE, Harel T, Liu P, Rosenfeld JA, James RA, Coban Akdemir ZH, Walkiewicz M, Bi W, Xiao R, Ding Y, *et al* (2017) Resolution of Disease Phenotypes Resulting from Multilocus Genomic Variation. *N Engl J Med* 376: 21–31

Qiu XB, Shao YM, Miao S & Wang L (2006) The diversity of the DnaJ/Hsp40 family, the crucial partners for Hsp70 chaperones. *Cell Mol Life Sci* 63: 2560–2570

Ramnani N (2006) The primate cortico-cerebellar system: anatomy and function. 7: 511–522

Rao M V., Engle LJ, Mohan PS, Yuan A, Qiu D, Cataldo A, Hassinger L, Jacobsen S, Lee VMY, Andreadis A, *et al* (2002a) Myosin Va binding to neurofilaments is essential for correct myosin Va distribution and transport and neurofilament density. *J Cell Biol* 159: 279–289

Raudvere U, Kolberg L, Kuzmin I, Arak T, Adler P, Peterson H & Vilo J (2019) G:Profiler: A web server for functional enrichment analysis and conversions of gene lists (2019 update). *Nucleic Acids Res, 47(W1), W191-W198.*

Rebelo AP, Abrams AJ, Cottenie E, Horga A, Gonzalez M, Bis DM, Sanchez-Mejias A, Pinto M, Buglo E, Markel K, *et al* (2016) Cryptic Amyloidogenic Elements in the 3' UTRs of Neurofilament Genes Trigger Axonal Neuropathy. *Am J Hum Genet* 98: 597–614

Rezende Filho FM, Bremner F, Pedroso JL, de Andrade JBC, Marianelli BF, Lourenço CM, Marques-Júnior W, França MC, Kok F, Sallum JMF, *et al* (2021) Retinal Architecture in Autosomal Recessive Spastic Ataxia of Charlevoix-Saguenay (ARSACS): Insights into Disease Pathogenesis and Biomarkers. *Mov Disord*: 1–10

Ricca I, Morani F, Bacci GM, Nesti C, Caputo R, Tessa A & Santorelli FM (2019) Clinical and molecular studies in two new cases of ARSACS. *Neurogenetics, 20, 45-49.*

Riedhammer C, Halbritter D & Weissert R (2016) Peripheral Blood Mononuclear Cells: Isolation, Freezing, Thawing, and Culture. *Methods Mol Biol* 1304: 53–61

Romano A, Tessa A, Barca A, Fattori F, Fulvia de Leva M, Terracciano A, Storelli C, Santorelli FM & Verri T (2013a) Comparative Analysis and Functional Mapping of SACS Mutations Reveal Novel Insights into Sacsin Repeated Architecture. *Hum Mutat* 34: 525–537

Ross CA & Poirier MA (2004) Protein aggregation and neurodegenerative disease. *Nat Med* 10: S10

Rudrabhatla P (2014) Regulation of neuronal cytoskeletal protein phosphorylation in neurodegenerative diseases. *J Alzheimers Dis* 41: 671–684

Rudrabhatla P, Jaffe H & Pant HC (2011) Direct evidence of phosphorylated neuronal intermediate filament proteins in neurofibrillary tangles (NFTs): phosphoproteomics of Alzheimer's NFTs. *FASEB J* 25: 3896–3905

Samulski RJ & Muzyczka N (2014) AAV-mediated gene therapy for research and therapeutic purposes. *Annu Rev Virol* 1: 427–451

Sato S, Ward CL & Kopito RR (1998) Cotranslational ubiquitination of cystic fibrosis transmembrane conductance regulator in vitro. *J Biol Chem* 273: 7189–7192

Schulz M, Levy DI, Petropoulos CJ, Bashirians G, Winburn I, Mahn M, Somanathan S, Cheng SH & Byrne BJ (2023) Binding and neutralizing anti-AAV antibodies : Detection and implications for rAAV-mediated gene therapy. *Mol Ther* 31: 1–15

Schwarz N & Leube RE (2016) Intermediate filaments as organizers of cellular space: How they affect mitochondrial structure and function. *Cells*, 5(3), 30.

Shimazaki H, Takiyama Y, Sakoe K, Ando Y & Nakano I (2005) A phenotype without spasticity in sacsin-related ataxia. *Neurology* 64: 2129–2131

Sihag RK, Inagaki M, Yamaguchi T, Shea TB & Pant HC (2007) Role of phosphorylation on the structural dynamics and function of types III and IV intermediate filaments. *Exp Cell Res* 313: 2098–2109

Snider NT & Omary MB (2014) Post-translational modifications of intermediate filament proteins: Mechanisms and functions. *Nat Rev Mol Cell Biol* 15: 163–177

Srivastava M, Duan G, Kershaw NJ, Athanasopoulos V, Yeo JHC, Ose T, Hu D, Brown SHJ, Jergic S, Patel HR, *et al* (2015) Roquin binds microRNA-146a and Argonaute2 to regulate microRNA homeostasis. *Nat Commun* 6: 1–13

Strack S & Hell JW (2008) Postsynaptic targeting of protein kinases and phosphatases. In *Structural And Functional Organization Of The Synapse, 459-500*

Sun K & Liao MZ (2022) Clinical Pharmacology Considerations on Recombinant Adeno-Associated Virus – Based Gene Therapy. 62, S79-S94.

Synofzik M, Soehn AS, Gburek-Augustat J, Schicks J, Karle KN, Schüle R, Haack TB, Schöning M, Biskup S, Rudnik-Schöneborn S, *et al* (2013) Autosomal recessive spastic ataxia of Charlevoix Saguenay (ARSACS): Expanding the genetic, clinical and imaging spectrum. *Orphanet J Rare Dis* 8(1), 41

Szklarczyk D, Gable AL, Lyon D, Junge A, Wyder S, Huerta-Cepas J, Simonovic M, Doncheva NT, Morris JH, Bork P, *et al* (2019) STRING v11: Protein-protein association networks with increased coverage, supporting functional discovery in genome-wide experimental datasets. *Nucleic Acids Res* 47: D607–D613

Tai PWL (2019) Adeno-associated virus vector as a platform for gene therapy delivery. *Nat Rev Drug Discov*, 18(5), 358-378

Terracciano A, Casali C, Grieco GS, Orteschi D, Di Giandomenico S, Seminara L, Di Fabio R, Carrozzo R, Simonati A, Stevanin G, *et al* (2009) An inherited large-scale rearrangement in SACS associated with spastic ataxia and hearing loss. *Neurogenetics* 10: 151–155

Thiffault I, Dicaire M, Tetreault M, Huang K, Demers-Lamarche J, Bernard G, Duquette A, Larivière R, Gehring K, Montpetit A, *et al* (2013) Diversity of ARSACS mutations in french-canadians. *Can J Neurol Sci, 40(1), 61-66.*

Tornabene P & Trapani I (2020) Can Adeno-Associated Viral Vectors Deliver Effectively Large Genes ? 31: 47–56

Toscano Márquez B, Cook AA, Rice M, Smileski A, Vieira-Lomasney K, Charron F, McKinney RA & Watt AJ (2021) Molecular Identity and Location Influence Purkinje Cell Vulnerability in Autosomal-Recessive Spastic Ataxia of Charlevoix-

Saguenay Mice. *Front Cell Neurosci, 485*

Transl J, Lee JA, Cho A, Huang EN, Xu Y, Quach H, Hu J & Wong AP (2021) Gene therapy for cystic fibrosis : new tools for precision medicine. *J Transl Med*: 19, 1–15

Tsuchiya H, Ohtake F, Arai N, Kaiho A, Yasuda S, Tanaka K & Saeki Y (2017) In Vivo Ubiquitin Linkage-type Analysis Reveals that the Cdc48-Rad23/Dsk2 Axis Contributes to K48-Linked Chain Specificity of the Proteasome. *Mol Cell* 66: 488-502.e7

Tulli S, Del Bondio A, Baderna V, Mazza D, Codazzi F, Pierson TM, Ambrosi A, Nolte D, Goizet C, Toro C, *et al* (2019) Pathogenic variants in the AFG3L2 proteolytic domain cause SCA28 through haploinsufficiency and proteostatic stress-driven OMA1 activation. *J Med Genet* 56: 499–511

Valencia RG, Mihailovska E, Winter L, Bauer K, Fischer I, Walko G, Jorgacevski J, Potokar M, Zorec R & Wiche G (2021) Plectin dysfunction in neurons leads to tau accumulation on microtubules affecting neuritogenesis, organelle trafficking, pain sensitivity and memory. *Neuropathol Appl Neurobiol* 47: 73–95

Vermeer S, Warrenburg BP van de, Kamsteeg E-J, Brais B & Synofzik M (2020) ARSACS. *GeneReviews®*

Vill K, Müller-Felber W, Gläser D, Kuhn M, Teusch V, Schreiber H, Weis J, Klepper J, Schirmacher A, Blaschek A, *et al* (2018) SACS variants are a relevant cause of autosomal recessive hereditary motor and sensory neuropathy. *Hum Genet* 137: 911–919

Vingolo EM, di Fabio R, Salvatore S, Grieco G, Bertini E, Leuzzi V, Nesti C, Filla A, Tessa A, Pierelli F, *et al* (2011) Myelinated retinal fibers in autosomal recessive spastic ataxia of Charlevoix-Saguenay. *Eur J Neurol, 18(9), 1187-1190.*

Wagner OI, Lifshitz J, Janmey PA, Linden M, McIntosh TK & Leterrier JF (2003) Mechanisms of mitochondria-neurofilament interactions. *J Neurosci, 23(27), 9046-9058.*

Wagner W, Brenowitz SD & Hammer JA (2011) Myosin-Va transports the endoplasmic reticulum into the dendritic spines of Purkinje neurons. *Nat Cell Biol, 13(1), 40-48.*

Wang F, Canadeo LA & Huibregtse JM (2015) Ubiquitination of newly synthesized proteins at the ribosome. *Biochimie* 114: 127–133

Wang F, Durfee LA & Huibregtse JM (2013) A cotranslational ubiquitination pathway for quality control of misfolded proteins. *Mol Cell* 50: 368–378

Waudby CA, Dobson CM & Christodoulou J (2019) Nature and Regulation of Protein Folding on the Ribosome. *Trends Biochem Sci* 44: 914–926

Weiss A, Klein C, Woodman B, Sathasivam K, Bibel M, Régulier E, Bates GP & Paganetti P (2008) Sensitive biochemical aggregate detection reveals aggregation onset before symptom development in cellular and murine models of Huntington's disease. *J Neurochem* 104: 846–858

White JJ & Sillitoe R V. (2013) Postnatal development of cerebellar zones revealed by neurofilament heavy chain protein expression. *Front Neuroanat,* 7, 9.

Willmund F, Del Alamo M, Pechmann S, Chen T, Albanèse V, Dammer EB, Peng J & Frydman J (2013) The cotranslational function of ribosome-associated Hsp70 in eukaryotic protein homeostasis. *Cell* 152: 196–209

Winter L, Kuznetsov A V, Grimm M, Zeöld A, Fischer I & Wiche G (2015) Plectin isoform P1b and P1d deficiencies differentially affect mitochondrial morphology and function in skeletal muscle. *Hum Mol Genet, 24(16), 4530-4544.*

Winter L & Wiche G (2013) The many faces of plectin and plectinopathies: Pathology and mechanisms. *Acta Neuropathol, 125, 77-93.*

Xiromerisiou G, Dadouli K, Marogianni C, Provatas A, Ntellas P, Rikos D, Stathis P, Georgouli D, Loules G, Zamanakou M, *et al* (2020) A novel homozygous SACS mutation identified by whole exome sequencing-genotype phenotype correlations of all published cases. *J Mol Neurosci* 70: 131–141

Yabe JT, Chan WKH, Wang FS, Pimenta A, Ortiz DD & Shea TB (2003) Regulation of the transition from vimentin to neurofilaments during neuronal differentiation. *Cell Motil Cytoskeleton* 56: 193–205

Yu-Wai-Man P, Pyle A, Griffin H, Santibanez-Korev M, Rita Horvath R & Chinnery PF (2014) Abnormal retinal thickening is a common feature among patients with ARSACS-related phenotypes. *Br J Ophthalmol, 98(5), 711-713.*

Yuan A & Nixon RA (2021) Neurofilament Proteins as Biomarkers to Monitor Neurological Diseases and the Efficacy of Therapies. *Front Neurosci*, 15, 689938.

Yuan A, Rao M V., Veeranna & Nixon RA (2012) Neurofilaments at a glance. *J Cell Sci* 125: 3257–3263

Yuan A, Rao M V, Veeranna & Nixon RA (2017) Neurofilaments and neurofilament proteins in health and disease. *Cold Spring Harb Perspect Biol, 9(4), a018309.*

Yuan A, Sasaki T, Rao M V., Kumar A, Kanumuri V, Dunlop DS, Liem RK & Nixon RA (2009) Neurofilaments form a highly stable stationary cytoskeleton after reaching a critical level in axons. *J Neurosci* 29: 11316–11329

Zhang Q, Fan L, Hou F, Dong A, Wang YX & Tong Y (2015) New Insights into the RNA-Binding and E3 Ubiquitin Ligase Activities of Roquins. *Sci Rep*, 5(1), 1-13.

Zhou M, Fisher EA & Ginsberg HN (1998) Regulated Co-translational ubiquitination of apolipoprotein B100. A new paradigm for proteasomal degradation of a secretory protein. *J Biol Chem* 273: 24649–24653



Milan 27/03/2023

APPENDIX 1

Publications

Longo, Fabiana, et al. "Assessment of sacsin turnover in patients with ARSACS: Implications for molecular diagnosis and pathogenesis." Neurology 97.23 (2021): e2315-e2327.

Longo, Fabiana, et al. "Impaired turnover of hyperfused mitochondria in severe axonal neuropathy due to a novel DRP1 mutation." Human Molecular Genetics 29.2 (2020): 177-188.

APPENDIX 2

Code

Pipeline used in Methods Section 2.11


```
<!--Created by Vision4D 3.6.2 tags/3.6.2-release^0@838752f415aef9ef579861100d12e0175eb51f32-->
<pipeline version="3.6" created="0001-01-01T00:00:00" modified="2022-11-27T12:00:06.3206587+01:00">
  <operations>
    <operation type-id="arivis.analysis.selection" id="arivis.analysis.selection1">
      <outputs>[{"Channels":[{"v":1,"id":"arivis.analysis.selection1.0.0","p":null,"n":"435 nm","a":true},{"v":1,"id":"arivis.analysis.selection1.0.1","p":null,"n":"525 nm","a":true},{"v":1,"id":"arivis.analysis.selection1.0.2","p":null,"n":"597 nm","a":true}]},{"Channels":[]},{"ObjectTags":[]}]</outputs>
      <settings>{"Document":"E:\\Maltecca\\deritis\\analisi-arivis-SH-NF-new\\exp-1\\ko1-sacs-_01_D3D.sis","ScopeID":"0","PixelSize":{"X":0.10830499976873398,"Y":0.10830499976873398,"Z":0.20000000298023224},"PixelType":1,"ChannelCount":3,"Bounds":"0, 0, 1914, 1914","Channels":"1-3","Planes":"1-15","Frames":"1","SelectionHint":3,"Zoom":1.0,"ZoomXYOnly":false,"CropToBounds":false,"LegacyMode":false}</settings>
    </operation>
    <operation type-id="arivis.analysis.voxel.Denoising" id="arivis.analysis.voxel.Denoising2" name="Denoising GREEN">
      <inputs>[{"Channels":[{"v":1,"id":"arivis.analysis.selection1.0.1"}]}]</inputs>

<outputs>[{"Channels":[{"v":1,"id":"arivis.analysis.voxel.Denoising2.0.0","p":"arivis.analysis.selection1.0.1","n":"525 nm","a":true}]}]</outputs>
      <settings algorithmId="arivis.analysis.imagetoimage.denoising.DiscreteGaussian" version="1.0" OutputMode="1" OutputFile="" CreateNewChannels="False" NewChannelNamePattern="$o ($n)">
        <strategy planewise="False" />
        <filter>{"UseLegacyMode":false,"Diameter":5.4152499884366989}</filter>
      </settings>
    </operation>
    <operation type-id="arivis.analysis.filter.Enhancement" id="arivis.analysis.filter.Enhancement1" name="Enhancement Filter-Red">
      <inputs>[{"Channels":[{"v":1,"id":"arivis.analysis.selection1.0.2"}]}]</inputs>

<outputs>[{"Channels":[{"v":1,"id":"arivis.analysis.filter.Enhancement1.0.0","p":"arivis.analysis.selection1.0.2","n":"597 nm","a":true}]}]</outputs>
      <settings OutputMode="1" OutputFile="" CreateNewChannels="False" NewChannelNamePattern="$o ($n)">{"FilterId":"arivis.itkbridge.filters.SharpeningFilter","Properties":[]}</settings>
    </operation>
    <operation type-id="arivis.analysis.voxelresult" id="arivis.analysis.voxelresult1">

<inputs>[{"Channels":[{"v":1,"id":"arivis.analysis.selection1.0.0"},{"v":1,"id":"arivis.analysis.voxel.Denoising2.0.0"},{"v":1,"id":"arivis.analysis.filter.Enhancement1.0.0"}]}]</inputs>

<outputs>[{"Channels":[{"v":1,"id":"arivis.analysis.voxelresult1.0.0","p":"arivis.analysis.selection1.0.0","n":"435 nm","a":true},{"v":1,"id":"arivis.analysis.voxelresult1.0.1","p":"arivis.analysis.voxel.Denoising2.0.0","n":"525 nm","a":true},{"v":1,"id":"arivis.analysis.voxelresult1.0.2","p":"arivis.analysis.filter.Enhancement1.0.0","n":"597 nm","a":true}]},{}]</outputs>
      <settings mode="1" useForAnnotations="false" filename="" scopename="" autochannels="true" />
```

```
      </operation>
      <operation                              type-id="arivis.analysis.segmentation.SimpleWatershed"
id="arivis.analysis.segmentation.SimpleWatershed1" name="NEUROFILAMENT">
        <inputs>[{"Channels":[{"v":1,"id":"arivis.analysis.voxelresult1.0.2"}]}]</inputs>

<outputs>[{"ObjectTags":[{"v":1,"id":"arivis.analysis.segmentation.SimpleWatershed1.0.0","p":null,"n"
:"NEUROFILAMENT","a":true,"cm":2,"c":"#00D800"}]}]</outputs>
        <settings object-name-pattern="$t #$I ($o)" version="1.0">
          <strategy planewise="False">
            <restrictor />
            <preparer />
          </strategy>

<labeler>{"ObjectBased":true,"Bright":true,"Threshold":15376.0,"MaximumDistance":1.5162699967622757,"
LimitToMaxKernelRadius":false,"Level":0.033816217132353887,"MinimumIntensity":0.0,"MaximumIntensity":
65535.0,"Connectivity":2}</labeler>
          <creator useholes="True" />
          <merger>
            <overlapping />
            <validator />
          </merger>
          <filter />
          <publisher />
        </settings>
      </operation>
      <operation                              type-id="arivis.analysis.segmentation.SimpleWatershed"
id="arivis.analysis.segmentation.SimpleWatershed2" name="Watershed">
        <inputs>[{"Channels":[{"v":1,"id":"arivis.analysis.voxel.Denoising2.0.0"}]}]</inputs>

<outputs>[{"ObjectTags":[{"v":1,"id":"arivis.analysis.segmentation.SimpleWatershed2.0.0","p":null,"n"
:"Watershed","a":true,"cm":2,"c":"#D88B00"}]}]</outputs>
        <settings object-name-pattern="$t #$I ($o)" version="1.0">
          <strategy planewise="False">
            <restrictor />
            <preparer />
          </strategy>

<labeler>{"ObjectBased":true,"Bright":true,"Threshold":12000.0,"MaximumDistance":12.94244747236371,"L
imitToMaxKernelRadius":false,"Level":0.11864548602612575,"MinimumIntensity":3.0,"MaximumIntensity":63
242.0,"Connectivity":1}</labeler>
          <creator useholes="False" />
          <merger>
            <overlapping />
            <validator />
          </merger>
          <filter />
          <publisher />
        </settings>
      </operation>
      <operation                                  type-id="arivis.analysis.volume.FeatureFilter"
id="arivis.analysis.volume.FeatureFilter2" name="CELLULE VERDI">
```

<inputs>[{"ObjectTags":[{"v":1,"id":"arivis.analysis.segmentation.SimpleWatershed2.0.0"}]}]</inputs>

<outputs>[{"ObjectTags":[{"v":1,"id":"arivis.analysis.volume.FeatureFilter2.0.0","p":null,"n":"CELLUL
E
VERDI","a":true,"cm":0,"c":"Cyan"},{"v":1,"id":"arivis.analysis.volume.FeatureFilter2.0.1","p":null,"
n":"not CELLULE VERDI","a":false,"cm":0,"c":"Cyan"}]}]</outputs>

<settings>{"FilterParts":[{"Mode":0,"Feature1":{"FeatureId":"arivis.analysis.features.volume","ValueI
ndex":0},"Feature2":null,"Comparison":1,"CompareValue1":3.0000000000000004E-
16,"CompareValue2":1.0,"CompareString":""}]}</settings>
</operation>
<operation type-id="arivis.analysis.volume.Compartmentalization"
id="arivis.analysis.volume.Compartmentalization2" name="Neuro in CELL VERDI">

<inputs>[{"ObjectTags":[{"v":1,"id":"arivis.analysis.volume.FeatureFilter2.0.0"},{"v":1,"id":"arivis.
analysis.segmentation.SimpleWatershed1.0.0"}]}]</inputs>

<outputs>[{"ObjectTags":[{"v":1,"id":"arivis.analysis.volume.Compartmentalization2.0.0","p":null,"n":
"Neuro in CELL
VERDI","a":true,"cm":0,"c":"Cyan"},{"v":1,"id":"arivis.analysis.volume.Compartmentalization2.0.1","p"
:null,"n":"NEUROFILAMENT in CELLULE
VERDI","a":false,"cm":4,"c":"Cyan"},{"v":1,"id":"arivis.analysis.volume.Compartmentalization2.0.2","p
":null,"n":"CELLULE VERDI with NEUROFILAMENT","a":false,"cm":4,"c":"Cyan"}]}]</outputs>
<settings
version="2.0">{"NodeLevels":[1,2],"NodeSettings":[{"ProvideAsFilteredOutputForParent":false,"Filtered
OutputForParentName":"CELLULE
VERDI","Modes":3,"Overlap":0.8,"MaximumDistance":0.0,"ProvideAsOutput":false,"OutputName":"CELLULE
VERDI","ProvideOverlapAsFeature":false,"ProvideDistanceAsFeature":false,"ProvideModeTags":false},{"Pr
ovideAsFilteredOutputForParent":false,"FilteredOutputForParentName":"CELLULE VERDI with
NEUROFILAMENT","Modes":3,"Overlap":0.8,"MaximumDistance":0.0,"ProvideAsOutput":false,"OutputName":"NE
UROFILAMENT in CELLULE
VERDI","ProvideOverlapAsFeature":false,"ProvideDistanceAsFeature":false,"ProvideModeTags":false}]}</s
ettings>
</operation>
<operation type-id="arivis.analysis.store.ExportAnnotation"
id="arivis.analysis.store.ExportAnnotation2" name="Neuro in CELLULE VERDI-excel">

<inputs>[{"ObjectTags":[{"v":1,"id":"arivis.analysis.volume.Compartmentalization2.0.0"}]}]</inputs>
<settings
version="3.1">{"File":"E:\\user\data.xlsx","Features":[{"FeatureId":"arivis.analysis.features.tags","
ValueIndex":0},{"FeatureId":"arivis.analysis.features.scope","ValueIndex":0},{"FeatureId":"arivis.ana
lysis.features.children-names","ValueIndex":0},{"FeatureId":"arivis.analysis.features.parent-
names","ValueIndex":0},{"FeatureId":"arivis.analysis.features.intensities[1]","ValueIndex":2},{"Featu
reId":"arivis.analysis.features.intensities[2]","ValueIndex":2},{"FeatureId":"arivis.analysis.feature
s.volume","ValueIndex":0},{"FeatureId":"2279815c-a767-417a-92a5-
682725c802bf","ValueIndex":0},{"FeatureId":"2279815c-a767-417a-92a5-
682725c802bf","ValueIndex":1},{"FeatureId":"2279815c-a767-417a-92a5-
682725c802bf","ValueIndex":2},{"FeatureId":"2279815c-a767-417a-92a5-
682725c802bf","ValueIndex":3},{"FeatureId":"2279815c-a767-417a-92a5-
682725c802bf","ValueIndex":4}],"Details":null,"Mode":3}</settings>
</operation>
<operation type-id="arivis.analysis.store.StoreAnnotation"
id="arivis.analysis.store.StoreAnnotation1">

<inputs>[{"ObjectTags":[{"v":1,"id":"arivis.analysis.segmentation.SimpleWatershed1.0.0"},{"v":1,"id":"arivis.analysis.volume.FeatureFilter2.0.0"},{"v":1,"id":"arivis.analysis.volume.Compartmentalization2.0.0"}]}]</inputs>
<settings version="V_2_12_5">{"NamePattern":"$n","TagPattern":"$n","TagsToAdd":null,"TagsToDelete":["Watershed"],"PreserveAllTags":false,"KeepOnUndo":false}</settings>
</operation>
<operation type-id="arivis.analysis.endOfPipeline" id="arivis.analysis.endOfPipeline1">
<settings />
</operation>
</operations>
<layout>
<entry name="_viewpartstates">arivis.analysis.voxelresult1=collapsed
arivis.analysis.segmentation.SimpleWatershed1=advanced
arivis.analysis.segmentation.SimpleWatershed2=advanced
</entry>
<entry name="arivis.analysis.segmentation.SimpleWatershed1">{"Labeler.Threshold":{"pixeltype":"UInt16","minimum":"0","maximum":"65535"}}</entry>
<entry name="arivis.analysis.segmentation.SimpleWatershed2">{"Labeler.Threshold":{"pixeltype":"UInt16","minimum":"0","maximum":"63242"}}</entry>
<entry name="arivis.analysis.store.StoreAnnotation1">[]</entry>
</layout>

<features><![CDATA[{"Version":"3.1","Features":[{"FactoryId":"arivis.analysis.features.intensities","Id":"arivis.analysis.features.intensities[1]","Name":"Intensities #2","Parameter":"{\"Channel\":1}"},{"FactoryId":"arivis.analysis.features.intensities","Id":"arivis.analysis.features.intensities[2]","Name":"Intensities #3","Parameter":"{\"Channel\":2}"},{"FactoryId":"arivis.objectstore.features.groupstatistics","Id":"2279815c-a767-417a-92a5-682725c802bf","Name":"VOLUME","Parameter":"{\"FeatureId\":\"arivis.analysis.features.volume-without-holes\",\"Value\":0,\"Tag\":null,\"Subgroups\":false,\"ObjectType\":null}"}]}]]></features>
</pipeline>



Milan 27/03/2023